Environmental Impact Assessment and Process Simulation of the Tidal Current Energy Resource in the Strait of Messina

Tarek Mohamed Ahmed El-Geziry

Thesis submitted for the degree of Doctor of Philosophy

The University of Edinburgh

2010

Abstract

Interest in exploring renewable energy resources has increased globally, especially with recent worldwide intentions to maintain the global climate. Looking at the oceans as a vast sustainable clean energy resource to satisfy present high humankind energy demands has been strongly recommended. Several types of renewable energy resources exist in the oceans: waves, tides, thermal and salinity variations, currents, and offshore winds. Exploiting tidal currents is considered one of the most effective approaches to the generation of electricity. Tidal turbines are deployed beneath the sea surface to transfer the kinetic energy in tidal currents to mechanical energy suitable for ongoing conversion to electricity and subsequent transmission. However, choosing a suitable site to deploy these turbines is not a trivial process. Various constraints must be satisfied subject to basic criteria dependent upon local factors, technology limitation and economic consideration. In addition, an important issue to consider is taking care to harness energy from tidal currents with minimum possible impact on the surrounding environment.

The present study justifies the nomination of the Strait of Messina as an exceptional tidal current energy resource within the Mediterranean Sea basin. The maximum tidal current velocity at spring peak tide through the Strait may exceed 3 m/s. This mainly results from the tidal phase-difference (180°) between the northern (Tyrrhenian Sea) and southern (Ionian Sea) tips of the Strait, associated with a difference of 0.27 m in tidal wave amplitudes. In addition, the complex coastline configuration of the Strait plays an important role in enhancing tidal current velocities. Therefore, the Strait of Messina fulfils the basic criterion (2 m/s tidal current velocity) to be considered as a valid tidal current energy resource. This massive tidal current energy resource is assessed in the present study.

A detailed full desk-based Environmental Impact Assessment (EIA) study is performed using the interactive matrix approach in order to investigate the anticipated environmental impacts on the marine ecosystem of the Strait of Messina resulting from the harnessing of energy from its tidal currents. Through the EIA study the different environmental components, both biotic and abiotic, which may be affected by the energy extraction process, are explained. In addition, the proposed key project activities are listed; the likelihood of occurrence and the magnitude of

impact interaction with the environmental components are evaluated. The final judgment matrix guides to make a right decision on the proposed project. From the resulted matrix, the major impacts do not exceed 10% of the total anticipated effects. The positive point is that all the expected impacts, including the majors, can be controlled and minimised to the lowest possible limits by applying a good monitoring programme.

The University of Edinburgh "Tidal Flow Development (TFD)" numerical model is used to mimic the tidal environment of the Strait of Messina in different cases. The model successfully simulates the tidal flow regime within the Strait under some exceptional conditions. Modifications to the main numerical code and coefficients were necessary in the present research to adjust the model according to each case study. In the three different cases of simulation, using these exceptional coefficients, the model simulates the main tidal characteristics of the tidal flow within the Strait. According to the results of the numerical simulation process, tidal currents are more intensive close to the eastern coast of the Strait of Messina near to Punta Pezzo. This area is far from any ferry route between Italy and Sicily. The best location to deploy tidal turbines for the energy extraction process is therefore recommended to be within these surroundings.

Finally, a physical (laboratory) model is used to simulate the flow regime within the Strait of Messina. The Particle Image Velocimetry (PIV) technique was applied in the flow-table tank at the University of Edinburgh. The physical model simulates the flow behaviour within the Strait of Messina to a satisfactory degree. The cyclonic and anti-cyclonic motions observed at the southern extremity of the Strait are also very well simulated.

The results of the present study assure confidence in the use of tidal currents within the Strait of Messina as a renewable energy resource. The safety of the environment must be ensured by following environmental guidelines, respecting the energy extraction limits and by applying an effective monitoring programme. The later is strongly recommended to be an adaptive one in which higher environmental authorities are able to watch, revise and control the environmental team within the project. These authorities are also able to postpone the project in case of any severe environmental case. The simulation processes emphasize the effect of morphometry

and topography in enhancing tidal currents in the Strait of Messina. Moreover, numerical simulation assures that the complex morphometry and bathymetry, in addition to the open boundaries of the Strait of Messina, are challenging issues for modellers in order to mimic the real tidal current resource in the case of the Strait of Messina. The study also strongly recommends applying a more effective numerical model than TFD to assess the tidal hydrodynamical environment before and after any proposed energy extraction process. This will certainly, with the EIA of the marine ecosystem, help to make a right decision about the proposed project in order to achieve the goal of using clean and clear renewable energy resources while maintaining both natural and hydrodynamical environments to the most possible safest degree.

Declaration

I, hereby, declare that this thesis is entirely my own work and that, except where indicated to the contrary, the research documented is also entirely my own.

Tarek M. El-Geziry

Acknowledgements

All praise is due to ALLAH, Lord of the Worlds, by whose grace this work has been completed.

I would like to express my deep and sincere appreciation to my direct supervisor, *Prof. Ian Bryden*, for his kind and effective supervision of this thesis, for the fruitful discussions and for the constant support throughout the study period.

I am grateful to my second supervisor, *Dr. Tom Bruce*, for his invaluable comments and cooperation throughout the time of the present study.

My endless thanks are due to *Dr. Scott Couch*, for his constructive comments, his invaluable suggestions and for all the time he spent helping me during the numerical simulation part in the present work.

I would sincerely like to acknowledge the sponsorship and the financial support of the *Ministry of Higher Education and State for Scientific Research* in my home country, *Egypt*, during the whole study period.

Thanks are also due to *Mr. Neil Wood and Mr. Kevin Anderson* for their sincere and effective help during the time of the physical experiment.

Words, however special, cannot express my love, respect and appreciation to *my mother, sisters, brothers-in-law, nephew and nieces*, who are always in my thoughts. During three years of work, my family gave me endless love, support, encouragement and help.

Above all, I feel a deep sense of gratitude for my late father, *Mohamed*, to whom I owe much of my success in both my private and practical lives. I trust he would so much have liked to have seen the completion of this piece of work.

My acknowledgments will certainly be incomplete if I would forget to thank my beloved wife, *Rania*, for her love, support and patience during the PhD period. Having been simultaneously proceeding for her PhD research, she spared no effort to encourage me to achieve my own target.

List of Figures

List of Tables

Contents

CHAPTER 1
INTRODUCTION

An Overview

Chapter one serves as an introduction to the present study. This chapter consists of five sections, the first of which is a brief introduction to renewable energy. Section two discusses the concepts of tides. Section three focuses on the different renewable resources, which can be exploited from the oceans. The different technologies used to exploit each of these oceanic resources and the expected environmental impacts associated with this exploration are briefly discussed. The objectives of the thesis and its structure are pointed out in sections four and five, respectively.

1.1 Introduction to renewable energy

In recent times there has been a considerable increase in worldwide interest in exploring renewable resources, especially with current targets to maintain the global climate. Renewable energy may be defined as power generated from a renewable resource such as winds and tides. When the energy is exploited, the resource itself is replenished naturally and can either be managed so that it lasts forever or its supply is so enormous humans can never meaningfully deplete it [1]. In addition to this important sustainability feature, renewable energy resources do not release carbon dioxide as a by-product into the atmosphere. Hence, they are considered as environment-friendly resources. Despite this advantageous feature and compared to the use of fossil fuels, harnessing energy from renewable resources for mass consumption is still limited. In the year 2006, 79% of the global final energy consumption came from fossil fuel, 3% from nuclear power and 18% from renewable resources of which large hydropower represented 3% [2]. This limited use of renewables may be due to the high capital cost needed to exploit these resources, which in turn affect the cost of the final product. However, advances in technology can result in the real costs of such technologies decreasing considerably over time [3].

The examples of renewable energy include: wind power, solar power, bio-fuels, geothermal energy and ocean energy. A comparison between the fundamentals of the different global energy resources [4] is summarised in Table (1.1).

	Renewable Resource	Low capital cost	Low running cost	Minimal environmental impact	Predictable	Minimal visual impact	Modular
Fossil	x	✓	x	x	✓	x	x
Nuclear	x	x	✓	x	✓	x	x
Wind	✓	x	✓	✓	x	x	✓
Solar	✓	x	✓	✓	x	x	✓
Hydro (tides)	✓	x	✓	x	✓	x	x
Waves	✓	x	✓	✓	x	✓	✓
Currents	✓	x	✓	✓	✓	✓	✓

Table 1.1: Comparison between global energy resources [4]

Large hydropower resources, i.e. ocean resources, have been of special interest in the last few decades. These resources contributed 15% to the global electricity production for the year 2006 [2]. Consequently, a better understanding of the nature of these resources and how we may benefit from them in order to satisfy the high energy demands of humankind is of paramount importance. In particular, the examination of the exploitation of tidal currents will be the main goal of the present research. Hence, it is worth starting with a brief introduction to the main concepts of oceanic tides in order to highlight their main features and behaviour. This introduction is presented in section 1.2.

1.2 Concepts of tides

Tides can be defined as the periodic rise and fall of a body of water resulting from gravitational interactions between the Sun, Moon and Earth [5]. The relative positions of these three celestial bodies produce the most observed variations in the magnitude of tides.

The tidal producing forces are the result of interaction between the gravitational forces of the three bodies. These producing forces may be categorised into two systems: the Earth-Moon system and the Earth-Sun system. The latter, even though the mass of the Sun is greater than that of the Moon, is the weaker force due to the greater distance between the Earth and the Sun.

1.2.1. Tidal producing forces in the Earth-Moon system

If (R) denotes the distance between the centres of the Earth and the Moon and (a) denotes the Earth's radius (Fig. 1.1), then the tidal producing forces (TPF_E) affecting a point E that lies on the line joining the two centres, i.e. in the equatorial plane, using the Newtonian law of attraction may be given by:

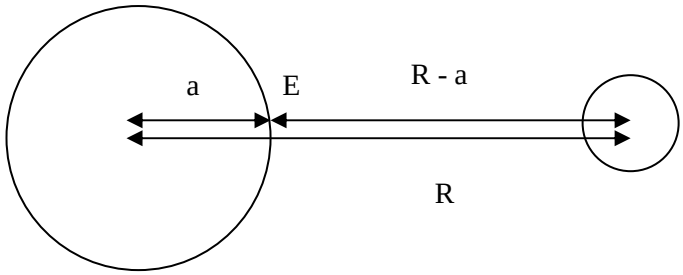

Figure 1.1: Tidal producing forces in the Earth-Moon System (Equatorial Plane)

TPF_E = attraction force of the Moon – centrifugal force of the Earth

$$= [G M m / (R - a)^2] - [G M m / R^2] \quad (1.1)$$

$$= [G M m a (2 R - a)] / [R^2 (R - a)^2] \quad (1.2)$$

As the radius of the Earth (a) is much smaller than the distance between the centres of the two planets (R), then equation (1.2) may take the form:

$$TPF_E = 2 G M m a R / R^4 \quad (1.3)$$

$$= 2 G M m a / R^3 \quad (1.4)$$

where,

G is constant; M is the Earth's mass; and m is the Moon's mass

For a point (P) that does not lie in the plane of the equator or the poles (Fig. 1.2), the gravitational force affecting the point P is given by

$$F_g P = G M m / (R - a \cos \psi)^2 \quad (1.5)$$

where, ψ is the angle with the equatorial line that joins the two planets' centres.

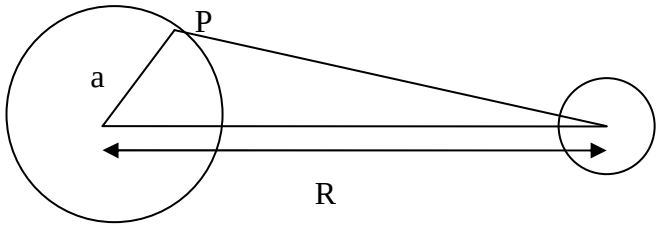

Figure 1.2: Tidal producing forces in the Earth-Moon System (Non-Equatorial Plane)

The tidal producing force at P is hence given by

$$TPF_P = G\,M\,m / (R - a\cos\psi)^2 - G\,M\,m / R^2 \quad (1.6)$$

$$= G\,M\,m\,[R^2 - (R - a\cos\psi)^2] / (R - a\cos\psi)^2\,R^2 \quad (1.7)$$

$$= G\,M\,m\,a\cos\psi\,(2R - a\cos\psi) / (R - a\cos\psi)^2\,R^2 \quad (1.8)$$

As the radius of the Earth (a) is much smaller than the distance between the centres of the two planets centres (R), then

$$TPF_P = G\,M\,m\,2\,a\,R\cos\psi / R^4 \quad (1.9)$$

$$= G\,M\,m\,2\,a\cos\psi / R^3 \quad (1.10)$$

There are two lunar behaviour of significant effect on the behaviour of the observed tide. These are the Moon's declination and the Moon's elliptical orbit.

The Moon's declination, which is 28° to the equatorial plane, results both in diurnal and semidiurnal tide cycles and in tidal inequalities all over the Earth's surface. On the other hand, the Moon's elliptical orbit, in which the Earth represents one of its two foci, results in the relative differentiation of the Moon's location to the Earth in the equatorial plane (Fig. 1.3). When the Moon is in its nearest location to the Earth, we get what is called the perigee, in which the tidal producing force increases up to 20% above the average value [6]. The interval between two successive perigees is 27.5 days [6, 7]. When the Moon is at its furthest location from the Earth, we get what is called the apogee, in which the tidal producing force is reduced to 20% below the average value [6, 7].

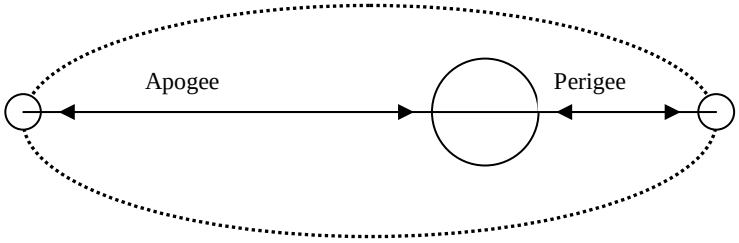

Figure 1.3: Apogee and Perigee lunar tides

1.2.2. Tidal producing forces in the Earth-Sun system

The magnitude of the solar tide producing force is 0.46 of that of the Moon [6]. This is due to the greater distance of the Sun from the Earth than that of the Moon; 360 times. The solar tide has a semidiurnal period of 12 hours. According to the position of the Earth in its elliptical orbit in which the Sun represents one of its two foci, two tidal phenomena are defined: the perihelion tide at the nearest distance and the aphelion in the furthest one (Fig. 1.4). The difference between the perihelion and the aphelion is 4% compared to 13% difference between the perigee and the apogee [6].

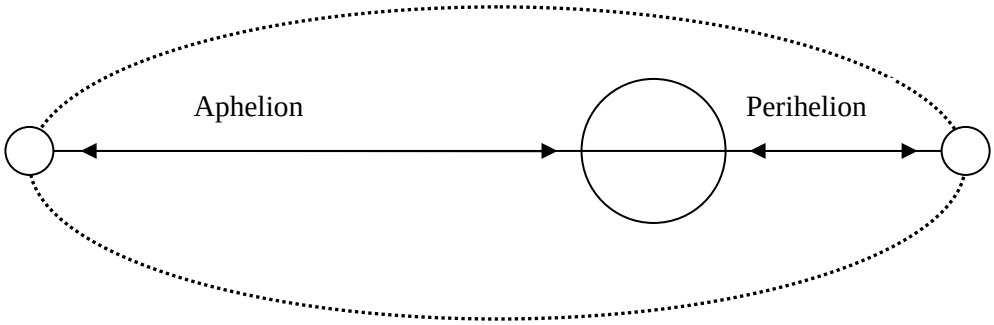

Figure 1.4: Perihelion and Aphelion solar tides

The two most extreme tidal phenomena are the spring and the neap tides. These tides result mainly from the combined gravitational effects of the Sun and the Moon. When the Moon's trajectory is aligned with that of the Sun (new and full Moon), the extreme gravitational force between the two celestial bodies is extracted and results in the spring tide. The neap tide, on the other hand, results when the Moon's trajectory is normal to that of the Sun (1^{st} and 3^{rd} quarters). The highest high tides and lowest low tides are recorded during spring tides while neap tides have lower high tides and higher low tides. Hence, the difference in water level between high

and low tides, known as tidal range, is much larger in a spring tide than in a neap tide. The spring and the neap tides are schematically shown in Figure 1.5.

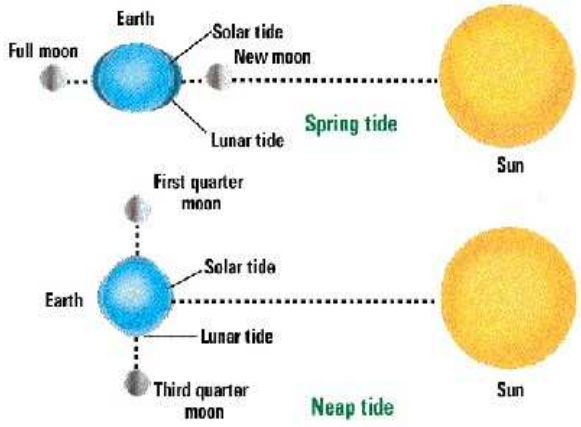

Figure 1.5: Spring and Neap tides (www.jochemnet.de/fiu/tide2.jpg)

The following terms are usually associated with the study of tides and are important; they should always be considered in order to fully understand the tidal phenomenon for any given area:

The datum is defined as a base elevation used as a reference from which to reckon heights or depths [5]. It is called a tidal datum when defined in terms of a certain phase of the tide. A tidal datum is regional. Such a datum is referenced to fixed points known as bench marks.

The duration of one complete tidal cycle; i.e. the time between two successive highs or lows, is called the tidal time period [5].

An amphidromic system is the result of the combination of the ocean basin geometry and configuration and the influence of the Coriolis force [6, 7]. The amphidromic point is a point of zero amplitude of the observed tide, i.e. water is always at the same level [5, 6].

The co-tidal lines are curved lines on a chart that pass through places having the same tidal phase [5, 7]. The centre of these lines is always an amphidromic point. The co-tidal ranges, on the other hand, are isolines on charts joining places of the same tidal ranges [6]. The co-tidal range isolines are normal to the co-tidal lines.

1.2.3. Types of tides

Broadly speaking, there are three types of tides (Fig. 1.6):

1. Semidiurnal tides, in which two high and two low waters occur daily, with relatively small differences in the respective highs and lows.
2. Mixed tides, in which the oscillations of both semidiurnal and diurnal tides may be observed. There are usually two highs and two lows per day in this type of tide.
3. Diurnal tides, in which a single high and a single low water occurs each day.

The type of a tidal cycle may be determined using the following constituent factor [8]:

F = (main diurnal components) / (main semidiurnal components)

$$F = (H_{O1} + H_{K1}) / (H_{M2} + H_{S2}) \quad (1.11)$$

where,

H_{O1} is the tidal height of the principal lunar diurnal constituent;

H_{K1} is the tidal height of the luni-solar diurnal constituent;

H_{M2} is the tidal height of the principal lunar semidiurnal constituent; and

H_{S2} is the tidal height of the principal solar semidiurnal constituent

According to the value of the factor F the type of a tidal cycle may be defined as follows [8]: if F ranges between 0 and 0.25 then a semidiurnal cycle results; if F ranges between 0.25 and 1.25 then a mixed mainly semidiurnal tide occurs; if F ranges from 1.25 to 3 then a mixed mainly diurnal tide occurs and finally a diurnal tide results for F values great than 3.

1.2.4. Tidal constituents

The tidal signal experienced at any location is a composite of multiple partial tides called tidal constituents [9]. Approximately 390 tidal constituents have been defined [10], the most significant of which are formed by the gravitational attraction between the three celestial bodies: Earth, Moon and Sun. The principal constituents and their periods are listed in Table (1.2). In modelling applications the following constituents have particular importance: K_1, O_1, P_1, Q_1, M_2, S_2 and K_2. This stems from the fact that these constituents are significant for any tidal signal and that they are sufficient to calculate the variations in tidal level and currents [9].

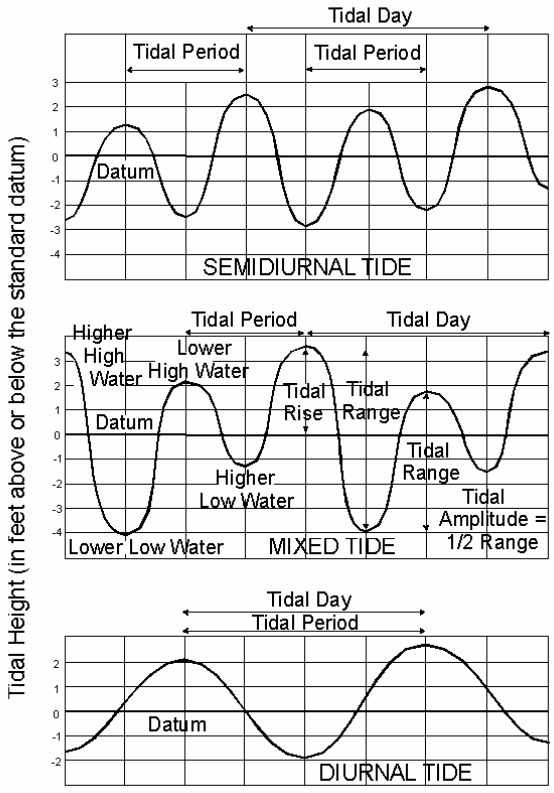

Figure 1.6: The three types of tides found in the global oceans (www.fhwa.dot.gov/engineering/hydraulics/images/h25_b6.jpg)

Accordingly, tidal elevations can be expressed as the sum of all the harmonic components [11]:

$$\eta(t) = \Sigma A_n \cos([2\pi/T_n]\, t + \varphi_n) \qquad (1.12)$$

where,

$\eta(t)$ is the tidal elevation as a function of time (m); A_n is the amplitude of harmonic component (m); T_n is the period of a harmonic component (s); $[2\pi/T_n]$ is the tidal angular velocity (rad/s); t is the time (s); and φ_n is the tidal phase of the harmonic component

The largest recognised tidal constituent is known as the principal lunar semidiurnal tide component M_2. The tidal producing force of this tidal component is twice as strong as that for the K_1 tide, the major diurnal constituent [7]. The distribution of tidal amplitudes and phases in the global oceans, based on Topex/Poseidon satellite observations and on global numerical models, has been adequately summarized [12].

A description of global tides and the global distributions of the main tidal amplitudes and phases are given in detail and discussed [7, 8 and 13].

Tides spread in the form of long waves, the movement of which is associated with what are called tidal currents. These may be defined as the horizontal movement of water caused by gravitational interactions between the Sun, Moon and Earth [5]. Large amounts of power and energy can be extracted from these currents when they are of sufficient velocity.

Name	Symbol	Period (Solar hr.)
Principal lunar	M_2	12.42
Principal solar	S_2	12.00
Larger lunar elliptic	N_2	12.66
Luni-solar semidiurnal	K_2	11.97
Larger solar elliptic	T_2	12.01
Smaller solar elliptic	L_2	12.19
Lunar elliptic second order	$2N_2$	12.91
Larger lunar evectional	ν_2	12.63
Smaller lunar evectional	λ_2	12.22
Variational	μ_2	12.87
Luni-solar diurnal	K_1	23.93
Principal lunar diurnal	O_1	25.82
Principal solar diurnal	P_1	24.07
Large lunar elliptic	Q_1	26.87
Smaller lunar elliptic	M_1	24.84
Small lunar elliptic	J_1	23.10
Lunar fortnightly	Mf	327.86
Lunar monthly	Mm	661.30
Solar semi-annual	Ssa	2191.43

Table 1.2: Principal tidal constituents and their periods [14]

1.3 Ocean Energy

The oceans cover 71% of the Earth's surface. They contain enormous renewable energy resources that can be exploited, contributing to the increasing global energy demand in a sustainable manner. In fact, oceans represent an energy resource that is theoretically far larger than the entire human race could possibly use, although, in practice most of this huge resource is inaccessible [15]. The different oceanic renewable energy resources include: waves, thermal energy, tides and marine currents. Marine currents themselves comprise many forms: wind driven currents, thermohaline currents, geostrophic currents and tidal currents. The last are the main focus of the present study. The main features and characteristics of the first three mentioned oceanic resources are summarised in sections (1.3.1-1.3.3), while section 1.3.4 gives a detailed description of tidal currents.

1.3.1. Wave energy

Ocean waves result from the direct effect of winds blowing on the ocean surface. These waves propagate from the fetch area, the origin of the wave generation, everywhere in the ocean with a speed proportional to the wave length. The size of a propagating wave is determined by the wind speed, the length of the fetch area, the water depth and the topography of the sea over which the wave propagates. Waves can be found superficially as well as in deep waters, though they are higher in the former as the wave height diminishes exponentially with depth.

Waves form a potentially large worldwide resource estimated at more than 2 terawatts (TW) [16]. There are several regions around the world with high incident wave power levels which are particularly well situated to the exploitation of this renewable resource.

Although wave energy is usually spread out along thousands of kilometres of shoreline, in some coastal areas the "energy density" is enough to produce electricity economically [17]. Wave energy is unequally distributed all over the world as shown in Figure 1.7. Between 30° and 60° latitudes of both hemispheres, the highest wave energy densities are located due to the characteristics of the dominant west winds of these areas [17]. The most irritating point about wave energy exploitation is that waves are not predictable. However, wave power at a given site is available for up to 90% of the time compared to only 20-30% of availability for wind and solar powers

[18]. England and Japan were the first to develop methods to capture the power of waves [19]. Nowadays, companies are building installations that convert the energy of the waves into electricity in many countries such as Scotland, Portugal, Norway, the United States, Australia, India and China [20]. Various methods exist to harness energy from ocean waves. These include the Tapered Channel System; the Salter Duck Wave Energy Conversion Device and the Oscillating water column system [19]. The accessible resource of wave energy depends on [21]:

1. The length of the coastline or offshore regions exposed to the waves.
2. The size of the area over which the winds blow to generate waves (the fetch area).
3. The strength of the winds generating the waves.

Basically, wave energy converters depend on the oscillating motion of waves to generate electricity. The energy extraction process may either be from surface waves or from pressure fluctuations below the water surface. Some systems of energy extraction are fixed in position, while others move with the propagating waves.

Wave energy can be harnessed by using either onshore or offshore technologies. Each type of technology has its advantages and disadvantages [17, 22, 23]:

- Advantages and disadvantages of onshore wave technology:
    1. The general reduction in the capital costs of installation.
    2. The rigidity of fixation using the strong onshore seabed structure.
    3. The reduced final consumption cost due to the shorter extended cables.
    4. Low operating and maintenance costs.
    5. Lower energy near the coast compared to the open ocean.
    6. Major engineering structures may affect the coastline activities: e.g. tourism and wildlife.
- Advantages and disadvantages of offshore wave technology:
    1. There are more places to harness wave energy in the open seas.
    2. Higher power is available offshore than onshore.
    3. Higher operating and maintenance costs.
    4. Collision risks with ships and marine species.
    5. High costs of cable and grid connection, which will affect the price of the final product.

6. Ocean storm may affect the technology.
7. Negative effect on shipping and fishing activities.

Examples of technologies used to harness energy from waves in the global oceans comprise the 20 megawatt (MW) wave-hub off the north coast of Cornwall, England (Fig. 1.8); the 7 MW Wave Dragon device (Fig. 1.9); the 3 MW Pelamis device (Fig. 1.10) and the 2 MW Oyster-1 (Fig. 1.11) in Orkney, off northern Scotland; the 1 MW Swedish AquaBuOY device (Fig. 1.12); the 500 kilowatt (kW) LIMPET (Land Installed Marine Power Energy Transformer) shoreline device on Isle of Islay, Scotland (Fig. 1.13) and 1 MW MRC1000 ORECon device developed by Plymouth University (Fig. 1.14).

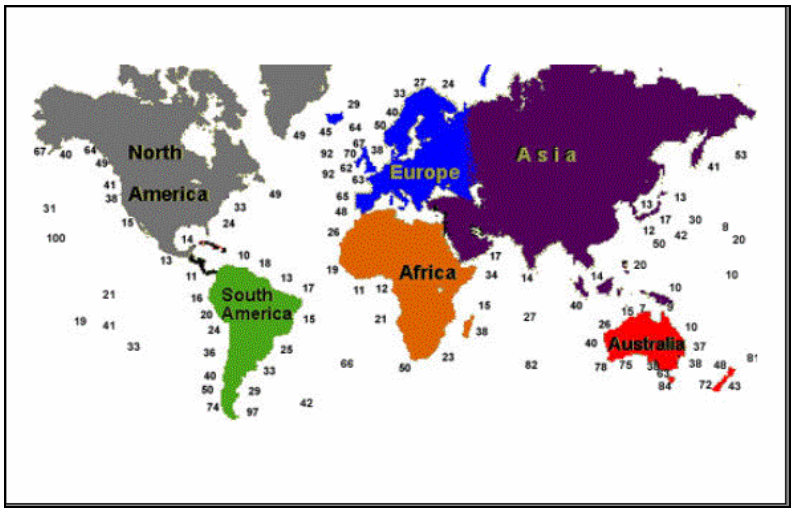

Figure 1.7: Global relative wave energy density (kW/m)
(http://www.dpenergy.com/marine/images/wavephotos/image006s.jpg)

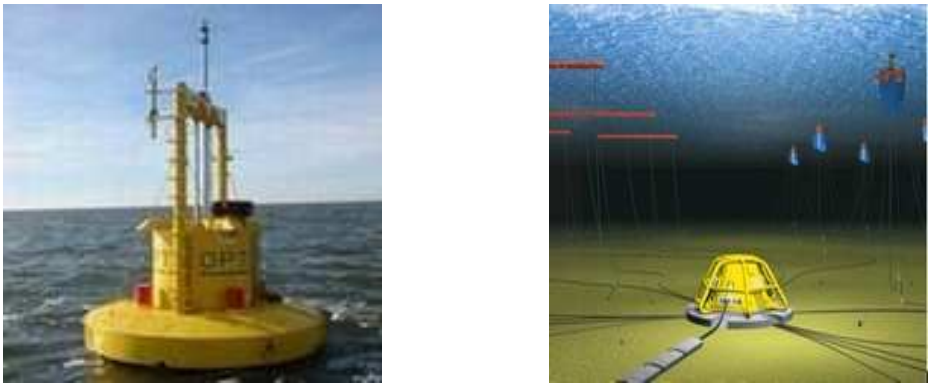

(a) **(b)**

Figure 1.8: (a) The buoy of the wave-hub device and (b) An artist's impression of the converter resting on the seabed (www.reuk.co.uk/Grant-for-Wave-Hub-Wave-Farm.htm)

Figure 1.9: The floating Wave Dragon device (www.wavedragon.net)

Figure 1.10: Pelamis device (www.waveenergy.ie/)

Figure 1.11: Oyster-1 device (http://www.aquamarinepower.com/technologies/oyster-1/)

Figure 1.12: AquaBuOY wave converter (tradenetholdings.com/aquawaveText.htm)

Figure 1.13: LIMPET plant (www.renewscotland.org/sea/wave.html)

Figure 1.14: MRC1000 ORECon device (www.orecon.com)

Environmentally, wave energy systems provide clean energy and have a very minimal effect on the marine environment [24]. In addition, wave energy devices may have a positive impact on the surrounding ecosystem: floating buoys may serve as artificial reefs that attract fish and may serve as nursery areas for some fish species. The onshore devices may help to reduce the effect of erosion and hence

protect the coastline. The following table may be regarded as a summary of the expected levels of environmental impact of wave energy.

Environmental effects	Shoreline	Near-shore	offshore
Land use/Sterilization	L		
Construction/Maintenance	L		
Recreation	L	L	
Coastal erosion	L	L - M	L - M
Sedimentary flow patterns		L	L
Navigation hazard		L	L
Fish and marine biota	L	L	L
Acoustic noise	L		
Working fluid loss		L	L
Endangered species	L	L	
Device/mooring damage		L - M	L - M

(L: Low, M: Medium)

Table 1.3: Environmental impact of wave energy devices [24]

1.3.2. Ocean Thermal Energy Conversion (OTEC)

Ocean Thermal Energy Conversion (OTEC) is a means of converting the temperature difference between surface water of the oceans in tropical and sub-tropical areas and water at a depth of approximately 1000 m, from Polar Regions, into useful energy [25]. The main problem with this type of renewable oceanic energy resource is the conditional thermal difference of 20° C between hot and cold reservoirs, which is viable only in tropical seas during the whole year [3]. 99 nations and territories have been listed [26] with access to OTEC thermal resources. There are 15 listed as “Americas-Mainland”, 23 as “Americas-Island”, 18 as “Africa-Mainland”, 5 as “Africa-Island”, 11 as “Indian/Pacific Ocean-Mainland” and 27 as “Indian/Pacific Ocean-Island”. The best-known example of an OTEC plant is that located on the Kona Coast of Hawaii, USA (Fig. 1.15).

The main advantages and disadvantages of OTEC systems [17, 27] are:

1. The possibility to be used for the desalination process of sea water.
2. OTEC is based on established turbine and refrigeration technologies.

3. OTEC readily produces, as side benefits, considerable quantities of fresh water, sea foods, and marine-life-based industrial products, as well as chill-water for air conditioning and cold-bed agriculture.

4. An OTEC facility requires a substantial initial capital expenditure (in the range of $50 to $100 million for a “small” ten-megawatt plant).

5. OTEC has not been demonstrated on a large scale over a prolonged period with integrated power, mari-culture, fresh-water, and chill-water production.

6. OTEC is only feasible at relatively isolated sites (deep tropical oceans); from such sites, the power and marine products must be transported to market. (In general, the fresh water and certainly the chill-water cannot be transported more than a few miles economically.)

7. Higher costs of operation and maintenance as compared to other energy resources.

Figure 1.15: Land based view of the 210 kW OTEC Experimental Plant, Hawaii (www.rise.org.au/info/Tech/otec/image007.jpg)

Environmentally, OTEC may potentially have an effect on the oceanographic properties of the sea water. However, the rigid plant structures may provide a positive artificial reef for fish breeding and a safe pathway for fish migration. Also,

OTEC is non-polluting; in fact it enriches nutrient-poor surface water and tends to "sink" carbon [27].

1.3.3. Tides

Tides have the distinct advantage of being highly predictable, compared to solar, wind and wave energy [3]. Tidal energy itself has been used since the 11th century when small dams were built along ocean estuaries and small streams in order to turn water wheels used in the milling of grains [28]. In the modern age, tides are used to drive turbines to produce electricity. The main concept is to use the rise and fall of tide, i.e. the potential energy in tides, to extract energy. The scheme is dependent on the use of a tidal barrage to control the natural flow from the tidal range. The barrage has gates that allow water to pass through. The gates are closed when tides have stopped coming in, trapping the water within the basin or estuary and creating a hydrostatic head. As tides ebb out the barrage, gates in the barrage that contain turbines are opened; the hydrostatic head causes the water to pass through these gates, thus driving the turbines and generating power. The principle of this barrage system, therefore, depends on using the tidal range between high and low tides to drive turbines to get the required energy. This tidal range potentially controls the available energy at any location. The main requirement for extracting cost-effective electric energy from the tide is to have as wide tidal range as possible. This range has been identified to be at least 5 m [6, 15, 20, 23, 29]. This, therefore, restricts suitable places for such energy extraction to a few locations scattered around the world. Table (1.4) shows the highest tidal ranges in the world.

The total worldwide potential of tidal-range energy scheme is estimated to range between 500 and 1000 Terawatt-hour per year (TWh/yr), though only a fraction of this figure is actually exploited due to economic considerations [30]. Currently, there are four tidal barrage plants which are actually working and producing energy, Table (1.5). Figure 1.16 shows La Rance plant, the first active tidal plant in the world that uses the tidal range to produce 240 MW of electricity.

Country	Site	Tidal range (m)
Canada	Bay of Fundy	16.2
France	Port of Ganville	14.7
England	Severn estuary	14.5
Russia	Penzhinskaya Guba	13.4
Argentina	Puerto Rio Gallegos	13.3
Russia	Bay of Mezen	10

Table 1.4: Highest tides of the global ocean [31]

Country	Site	Starting year	Basin area (km^2)	Given power (MW)	Mean tidal range (m)
France	La Rance	1967	22	240	8.55
Russia	Kislaya Guba	1968	1.1	0.4	2.3
Canada	Annapolis	1984	15	18	6.4
China	Jiangxia	1985	1.4	3.9	5.08

Table 1.5: Existing tidal power plant [31]

The use of tidal barrage schemes is presently limited. This is a result of the very large capital costs of such systems, the long construction period and the fear of the severe associated environmental impact. The large capital cost will, no doubt, affect the final product cost, e.g. the estimated capital cost of the proposed tidal station at the Severn Bay in England would be in the range of $15 billion [13]. The time taken to build a barrage system is long, e.g. the La Rance plant took about 7 years to build. During the construction period there is no benefit from any outcome from the barrage plant, which in turn affects the final consumers and the cost of the generated power.

However, once built, a tidal barrage has a very long lifetime. It has been estimated that the barrage structure will last for 120 years and the equipment for 40 years [22]. Environmentally, barrage systems have an impact on the coastal processes, on the sediment motion and on the creatures in the area of the basin. On the other hand, one advantage of using a barrage system is that the barrage itself may act as a storm surge barrier, which protects the coastline from erosion.

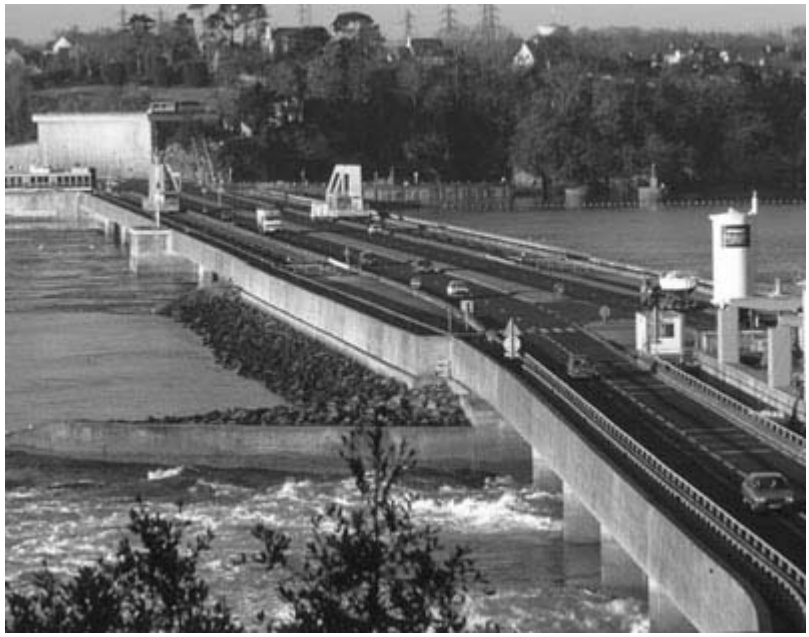

Figure 1.16: La Rance tidal plant, France (www.rise.org.au/info/Tech/tidal/image020.jpg)

1.3.4. Tidal currents

Tidal currents are the horizontal component of the water motion associated with the propagating tidal wave [5]. The speed of tidal currents is not necessarily proportional to the range of the tide, i.e. the vertical variation in the sea level. In general, tidal current speeds are low, but these may be modified by local topography and by coastline configuration. The velocity can be greatly enhanced and magnified, particularly in straits between islands or between islands and the mainland [21]. A tidal stream technology aims to produce electricity from the kinetic energy in the flowing tidal currents. The kinetic energy in these flows can readily be harnessed using turbines using principles similar to those of wind turbines [32]. It has been estimated that the yearly potential electricity that could be generated from tidal

currents is 80 x 10^3 TWh, i.e. more than five times of the World annual demand, which is roughly 14 x 10^3 TWh [4].

A location that has been proposed for the harnessing of tidal current energy has to practically fulfil three basic criteria [33]:

1. The local water depth: this should range between 25 and 45 m to suit the installation of existing device technologies. This depth range may be modified for the new generations of tidal current energy converters and technologies. The depth will also affect the choice of the rotor diameter of tidal turbine as shown in Table (1.6).

Water depth	**Rotor diameter** **(assuming no shipping exclusion)**	**Rotor diameter** **(assuming shipping exclusion)**
< 20 m		10 m
20-25 m	5 m	12 m
25-40 m	10 m	20 m
> 40 m	20 m	20 m

Table 1.6: Influence of water depth on maximum permitted turbine size [34]

2. The distance of the location to the nearest grid connection: this connection has to be easily accessed to be economically feasible in order to minimise the capital cost of power generation and accordingly minimise the final consumption cost per kW.

3. An energetic and persistent resource: this criterion is the basis of choice as the mean spring and neap tide velocities in the chosen locality must be as high as possible. This velocity should preferably not drop below 3 m/s [23, 33]. Other authors lower this limit to 1 m/s [17] or 2 m/s [6, 15].

It is important to realise that the extraction of energy from a tidal environment will modify that environment. Even though the marine biota may not be harmfully affected, the sedimentation and seabed processes as well as the hydraulic nature itself may be severely affected if considerable care is not taken. So, it is highly recommended to assess the environmental impacts that may result from harnessing energy using tidal currents in any location proposed to deploy tidal devices. It would be better to perform such an assessment both before and after the operation; hence the recommendation to apply a suitable effective monitoring programme is of high concern. For this reason a detailed desk-based Environmental Impact Assessment

(EIA) study for the tidal resource in the Strait of Messina, the present area of investigation, is introduced in chapter three of this thesis.

The greatest advantage of using tidal currents to generate electricity is that tides are driven by regular astronomic mechanisms; hence they may be well predicted. The energy flux density in many of the most attractive sites is formidable, offering the prospect of large-scale generation using relatively compact technology [35].

Theoretically, the maximum power available by using a tidal turbine is jointly proportional to the water density and the velocity of the tidal flow cubed. As the density of sea water is 800 times greater than that of air, the same amount of energy generated by a wind can be extracted by a relatively much slower water movement using smaller diameter turbines [23, 29]. 4 kW/m^2 power may be achieved with a water flow of 2 m/s velocity, while the same energy amount would require a wind speed of 18 m/s [32]. The available power in tidal currents may be mathematically expressed [11, 15, 17, 23, 30, 33-36] using the following equation:

$$P = \tfrac{1}{2}.\rho.U^3.A \qquad (1.13)$$

where,

P is the Kinetic Energy flux in the tidal stream (W); ρ is the water density (kg/m^3);
U is the current speed (m/s); and A is the cross sectional area (m^2)

1.3.4.1. Significant Impact Factor (SIF)

To control the limits of extraction from the total available energy in the tidal currents and to eliminate the negative environmental impact, which may result from the harnessing process, it is worth introducing a controlling factor in equation (1.13). This factor is called the Significant Impact Factor (SIF). This factor gives the significant energy percentage, which can be safely extracted from the total energy in the flow. It would not be possible to extract the total available energy in the tidal flow from both engineering and environmental points of view. This could negatively affect the efficiency of tidal turbines, the hydrodynamical environment of the flow and also the marine ecosystem itself. Therefore, SIF is recommended to range between 10-20% of the energy contained in the tidal current [17, 23, 37, 38]. Accordingly, equation (1.13) may take the form:

$$P = \tfrac{1}{2}.\rho.U^3.A.SIF \qquad (1.14)$$

The tidal current velocity U may be predicted using the following equation [15]:

$$U = [K_0 + K_1 \cos(2\pi t / T_1)] \cos(2\pi t / T_0) \quad (1.15)$$

where,

K_0 and K_1 are constants determined from the mean spring peak and the ratio between the mean spring peak and the mean neap peak currents; T_1 is the spring neap period, normally of 353 hrs; and T_0 is the diurnal tidal period (12.4 hrs)

To harness energy from tidal currents, different types of turbines have been developed for a submerged installation in suitable locations [17]. When designing a tidal turbine, the following must be taken into consideration [39]:

1. The turbine machinery must be as simple as possible as the turbine will be working in a submarine environment.
2. The strong currents experienced during installation and maintenance.
3. A compromise must be found between the capital cost and the yearly energy production.
4. The interaction of waves with the currents must be considered.

There are four developed types of tidal turbines:

- Horizontal axis turbines
- Vertical axis turbines
- Variable foil systems, and
- Venturi systems.

1. Horizontal axis turbines

For this type of tidal turbine, the rotational axis of the turbine is parallel to the direction of flow [23]. These turbines look similar to wind turbines and can be installed either seabed-mounted or hanging from floating platforms [17]. The main operating principle of a horizontal axis turbine is to transfer the hydrodynamic force component normal to the blades rotation plane along a shaft to drive a generator in order to produce electricity. The technology of this type of tidal turbine is presently very well developed. This is represented in the SEAFLOW turbine (Fig. 1.17), a well-applied 300 kW horizontal axis turbine installed in the Bristol Channel between England and Wales, and in the SeaGen tidal converter which produces 1.2 MW from the tidal current resource in Strangford Lough, Northern Ireland.

Figure 1.17: The SEAFLOW horizontal axis tidal turbine risen for maintenance
(www.marineturbines.com/mct_image_files/Seaflow_raised_16_jun_03b.jpg)

2. Vertical axis turbines

In this type of turbine the flow is perpendicular to the rotational axis [17]. The key feature of a vertical axis turbine is the cross-flow design [40], where the blades and rotor transmission shaft are parallel to one another and are both normal to the incoming current flow. This allows the rotor to rotate in the same direction regardless of the flow direction [40]. Vertical axis tidal turbines may be classified, according to the blade shape, into two sets: rectilinear-blade turbines and helicoidal-blade turbines. An example of the former is the Kobold Turbine (Fig. 1.18), part of the ENERMAR project in the Strait of Messina, and an example of the latter is the Gorlov helical turbine rotor, deployed in Korea (Fig. 1.19 a & b). The main advantage of the rectilinear blade turbine is that the shaft power is taken out perpendicular to the flow, which lends itself to having a drive train either on the seabed or in a surface vessel [15]. However, its main disadvantage is that its rectilinear blade produces efficient but is highly unstable and has a high tendency to rupture due to vibrations [17]. Using helicoids turbines, the vibration problem is resolved and hence the rupture problem is as well. Another advantage of the helicoids Gorlov turbine is the amount of energy extracted from the tidal stream

(35%) compared to 23% from the rectilinear turbine and 20% from the conventional horizontal axis turbines [17].

Figure 1.18: A schematic of the Kobold turbine (www.turbosquid.com)

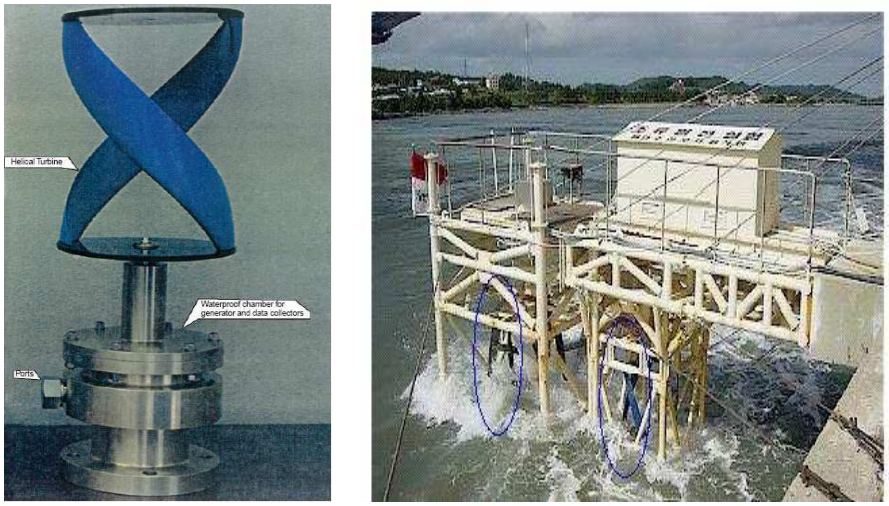

(a) **(b)**

Figure 1.19: The Gorlov turbine in Korea: (a) different parts of the converter on land (b) the converter in the field
(www.pugetsoundtidalpower.com/Technology/gorlov_turbine.htm)

3. Variable foil systems

This type of tidal turbine is not as widely applied as the horizontal and vertical axis types. A well-known example of this type is the ‘Stingray’ turbine [41], developed to produce 150 kW of electricity using tidal currents, and has been tested in Yell Sound in Shetland, which lies to the north of Scotland and the Orkney Islands [42, 43] (Fig. 1.20).

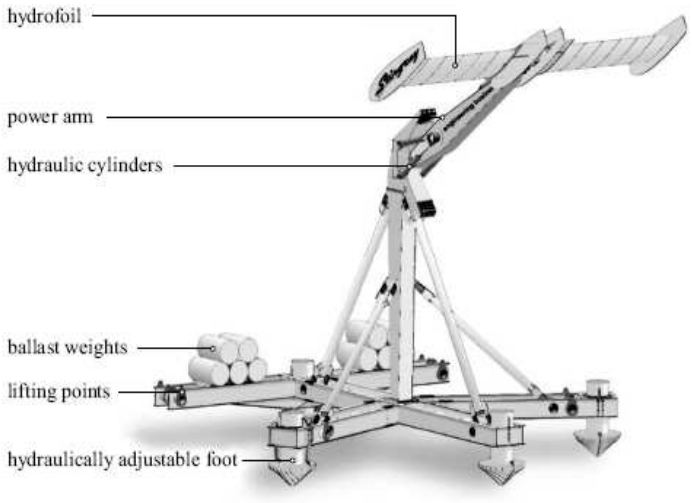

Figure 1.20: Stingray device [13]

‘Stingray’ differs from other proposed devices in that it uses an oscillating motion rather than rotation to harness the energy from the tidal flow. ‘Stingray’ consists of a hydroplane which has its attack angle relative to the approaching water stream varied by a simple mechanism [41]. The combination of lift and drag force causes the arm of ‘Stingray’ to oscillate vertically. A hydraulic cylinder attached to the main arm is forced to alternately extend and retract, producing high-pressure oil, which is delivered to the hydraulic motor driving the generator, thus producing electricity [44]. The whole system is fully submerged and rigidly fixed to the seabed. The key specification parameters of ‘Stingray’ are defined in Table (1.7). The main characteristic of this technology is its large wing-like hydroplane, which can be pitch-controlled, oscillating up and down and compressing oil for a hydraulic power converter [17].

Maximum height	23.6 m with hydroplanes in highest position
Maximum width	15.5 m
Arm length	11 m
Arm operating angle	± 35 degrees
Hydroplane actuation angle	Relative to arm ± 90 degrees
Rated power	150 kW at 3 knots and above

Table 1.7: The key specification parameters of 'Stingray' [44]

4. Venturi based systems

This system of tidal current energy converter uses pressure changes in a flow contraction to drive secondary extraction hydraulics or pneumatics [43]. The two well-known systems based on this principle are the GENTEC venturi developed by Greenheat Systems Ltd and the Rochester venturi developed by HydroVenturi (Fig. 1.21), both in the UK.

Figure 1.21: HydroVenturi Rochester Venturi for Tidal Power

(http://www.ambafrance-uk.org/local/cache-vignettes/L283xH212/Mathieu-RV-f1feb.jpg)

1.3.4.2. Design of Support Structures

The most difficult technical problem is to install a marine current turbine rotor securely enough to resist the large forces that it will be subjected to, and, in a manner which is not so costly as to make the system uneconomic [32]. Therefore, it is

important to focus attention on the different methods used to fix the rotating blades (main component in any tidal energy converter) and their shafts in the ocean. This is done through support structures installed in the desired location. These installations may take different forms as shown in Figure 1.22. The structures must be heavy and strong enough to overcome the strong currents, wave conditions, storms and any unexpected difficult conditions that may occur in the field.

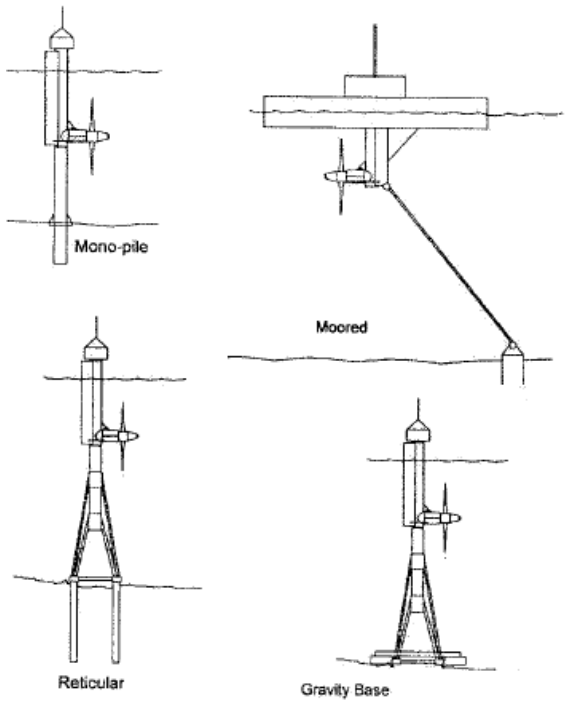

Figure 1.22: Types of support structure technology [35]

In the monopile structure, a vertical steel or concrete bar is cemented in the desired location after drilling a suitable hole for fixation. The proportion of the drilled hole to the total bar length has to be well-considered for stability purposes. In this type of support structure, the energy capture device must be raised to the surface for maintenance [35]. For the moored support structure, the structure itself is moored to the seabed with strong anchors or chain-lines with the major support body floating on the surface. It is only convenient to use this type of supporting structures with small prototype devices. As the device is relatively free to move on the mooring lines, there may be issues with device safety in high-turbulence and fast currents [35]. The reticular support structure resembles the mono-pile already described with the

exception of being supported by two main vertical bars drilled deeper into the stratum. Lastly, the gravity base support structures are held on position depending on their weight and on the force of the gravitational attraction. The weight is either self-included in the body itself or added using rock ballast after deploying the body in place. Due to the large forces needed to install, move and maintain this type of support structure, large crane barges are required [35].

The following discussion illustrates some of the main points that must be taken into consideration when designing and using a tidal turbine.

The power coefficient of a real tidal turbine (C_p) is a function of the ratio between the speed of the turbine tip and the flow speed, which is commonly known as the tip speed ratio (λ) [34]. The actual relationship depends on the blade form and number (Fig. 1.23). Geographic factors that affect the development of a tidal turbine include water depth, the natural cyclic behaviour of the tidal current and the desired location of the turbine installation. The costs of hardware, installation, operation and maintenance are also important factors which should be carefully considered when designing a tidal turbine.

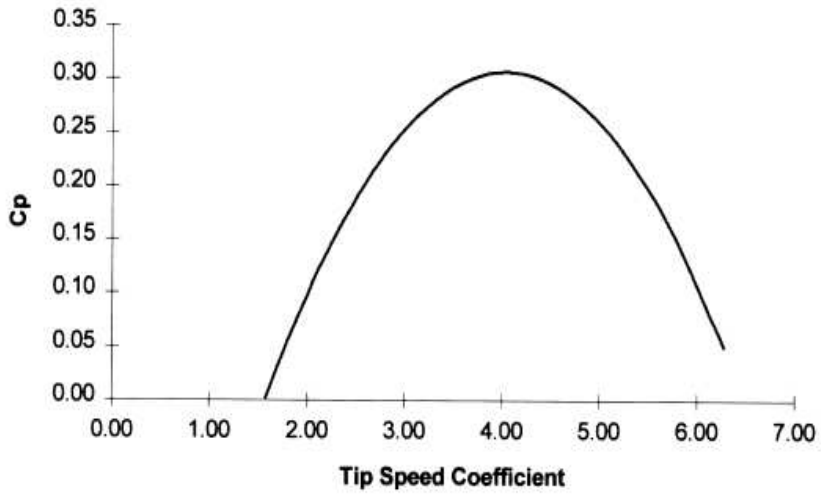

Figure 1.23: Sample Cp-λ curve for a four-bladed turbine [34]

1.4 Objectives of the thesis

The objectives of the present study may be summarised by the following points:

1. To review the principal physical oceanographic features of the Mediterranean Sea and its major straits; in order to assess specifically the choice of the Strait of Messina as an exceptional tidal resource within the Mediterranean whose tidal currents can be exploited.
2. To assess the anticipated environmental impacts that may result from the energy extraction process from the Messina resource in order to determine to what extent the marine ecosystem may be affected by such a process.
3. To propose an applied monitoring programme to control and minimise the expected environmental impacts.
4. To examine the simulation process of the tidal current regime within the Strait of Messina using both numerical and physical models.
5. To propose, using the outcomes of the tools used in this study: the environmental assessment, the numerical and the physical simulations, the suitable location within the Strait of Messina where tidal turbines may be deployed. Also, to suggest the most effective technology which best suits the situation in the Strait.

1.5 Thesis outline

The thesis consists of seven chapters. A total of 115 Figures and 33 Tables are used as illustrations within the text. The chapters are followed by the attachment of any necessary appendices and a list of references.

Chapter one is an introduction to the present study, in which the concepts of tides are given. The fundamentals behind and the main terms used in the study of global tides are explained. Different types of ocean renewable energy resources: waves, OTEC, tides, and tidal currents are briefly introduced. For each of these energy resources the concept, the technology applied and the expected impacts on the marine ecosystem are highlighted. More details are given for tidal currents being the main resource of interest in the present work. The conditional criteria for a selected area in which to

deploy tidal turbines, as well as the different technologies of those turbines, are also introduced.

Chapter two highlights the basic environmental characteristics of the Mediterranean Sea. The main biological and physical features of the Mediterranean basin are introduced. In addition, attention is focused on some major straits (Bosphorus, Dardanelles, Messina, Sicily and Gibraltar) within the Mediterranean basin and on their basic hydrological and tidal characteristics. The aim is to examine the suitability of any location within the Mediterranean Sea basin to be considered as a renewable energy resource using tidal currents. Literature reviews and results of previous surveys reveal that both tidal ranges and currents are weak enough within the Mediterranean that the whole basin has to be excluded from any energy plan. Nowhere within the Mediterranean basin satisfies the main principle criterion of tidal current velocity. This is true except at the Strait of Messina, where tidal currents are reasonably strong enough to be appreciated as a massive tidal current resource to harness energy. The discussion in this chapter justifies the choice of the Strait of Messina to be selected as an area of investigation.

Chapter three deals with the area of interest in the present study: the Strait of Messina. The given characteristics (morphometry and tidal behaviour) of the Strait explain its exceptional potential within the Mediterranean basin as a massive renewable energy resource using tidal currents. In addition, this chapter focuses on the environmental impacts that may result from the process of energy extraction using tidal currents. This is performed through a detailed desk-based Environmental Impact Assessment (EIA) study, using the interactive matrix approach. Through the EIA study the European Union (EU) environmental legislation, the interactive matrix method and a monitoring programme are detailed.

Chapter four introduces the concepts and meaning of ocean numerical modelling, their importance and their practical use. The basic Navier-Stokes equations are briefly introduced. This chapter also summarises the results of the numerical modelling studies carried out in order to simulate the circulation pattern of the

Mediterranean Sea and briefly discusses the results. In addition, the major numerical models used to simulate the global tides are introduced. Tides within the Mediterranean basin are omitted from these studies because of the naturally very low tidal characteristic of the Sea.

Chapter five discusses the numerical simulation of the tidal current regime within the Strait of Messina. This chapter initially focuses on the results of some previous attempts to simulate tidal currents within the Strait. Then, the Tidal Flow Development (TFD) numerical model and its basic structure are introduced and briefly discussed. After that, the Strait of Messina is simulated numerically in different cases. The simulation process assures the effect of morphometry on tidal currents within the Strait of Messina and declares how the coastline configuration enhances tidal current velocities. The out-of-phase characteristic between the two extremities of the Strait and its effect in enhancing the tidal current velocity along the main channel of the Strait is confirmed and simulated to a satisfactory degree. However, the applied numerical model required modifications to the main code in order to mimic the Strait of Messina with its real configuration. These modifications are stated and justified in this chapter.

Chapter six presents the physical simulation of the tidal flow regime in the Strait of Messina. This chapter starts with a general introduction to physical models, followed by an explanation of the Particle Image Velocimetry (PIV) technique. Using the tidal flow-table tank facility at the University of Edinburgh with a waterproofed plywood frame, the Tyrrhenian southward flow in the Strait of Messina is physically simulated. The present physical model confirms the effect of the constriction at the sill area in enhancing tidal currents in the Strait of Messina. In addition, gyre features at the southern region of the Strait of Messina are successfully simulated.

Finally, chapter seven presents the results of the study in hand. This chapter begins with a discussion of each point examined in the thesis, followed by a set of conclusions and recommendations. This chapter ends with a set of points of the further work, which can be based on the present study.

1.6 Chapter Conclusion

Different types of renewable energy resources exist in global oceans: waves, tides, offshore winds and currents. Studies and research have proven that the two most environment-friendly resources mentioned in the list above are waves and tidal currents. The latter are the resource of interest in the present study. To harness energy from tidal currents, different types of tidal turbines are deployed beneath the sea surface to convert the kinetic energy in the flowing currents into mechanical energy. A site suitable for the deployment of tidal turbines must satisfy three basic criteria: a water depth of between 25 and 45m, an appropriate distance to a near-by grid and, most importantly, a tidal current velocity which, according to the majority of studies, must not fall below 2 m/s in order to be economically feasible for the energy extraction process. The tidal current energy resource in the Strait of Messina is investigated in the present study through a full Environmental Impact Assessment (EIA) study, in addition to simulations for the tidal flow regime within the Strait using both a numerical and a physical model.

CHAPTER 2
ENVIRONMENT OF THE MEDITERRANEAN SEA

An Overview

This chapter focuses on the environment of the Mediterranean Sea: its morphometry, biological features and physical properties. In addition, the main characteristics of some major straits within the Mediterranean basin are briefly discussed.

The morphometry of the Mediterranean Sea is described in section 2.1. Section 2.2 focuses on the biology of the Sea. The physical parameters and the water masses of the Mediterranean Sea, its circulation pattern and its tidal behaviour are discussed in sections 2.3, 2.4 and 2.5, respectively. Finally, some major straits within the Mediterranean basin and their main characteristics are introduced in section 2.6.

2.1 Morphometry of the Mediterranean Sea

The Mediterranean Sea extends between latitudes 30º 00.00' and 45˚ 00.00' N and longitudes 06˚ 00.00' W and 35˚ 00.00' E. Figure 2.1 shows the geography of the Mediterranean Sea and the nomenclature of its major sub-seas. The Mediterranean basin is a large semi-closed basin, connected, at its western extremity, to the Atlantic Ocean through the Strait of Gibraltar. It is connected to the Black Sea by the Dardanelles/Marmara Sea/Bosphorus system. The shelf of the Mediterranean Sea is narrow and, in the north, is mostly bordered by mountain chains, e.g. the Sierra Nevada, Alps, Dinaric Alps, sloping steeply into the Sea, resulting in a narrow littoral zone and small drainage basin [45]. The Mediterranean Sea covers an approximate surface area of 2.5×10^6 km^2 [46]. This is equal to only 0.82% of the surface area of the world oceans [47] and to 0.32% of the world water volume [14]. The coasts of the Mediterranean Sea extend for about 46×10^3 km and its average depth is 1.5 km. The greatest measured depth in the Mediterranean Sea is 5.1 km in the Ionian Sea [48]. The Sicilian-Tunisian sill, at a depth of 400 m, divides the Mediterranean basin into two distinct sub-basins: the western and the eastern basins, and acts as a geographical and hydrological frontier [49]. The western basin covers a surface area of 0.85×10^6 km^2 while the eastern basin covers 1.65×10^6 km^2 [50].

Figure 2.2 shows the topographic features and the bathymetry of the entire Mediterranean Sea basin.

The western basin of the Mediterranean Sea comprises of the Alboran Sea in the extreme west between Spain and Morocco and the Balearic Sea off the Algerian coasts extending to the north to the Gulf of Lions. It also includes the Ligurian and the Tyrrhenian Seas to the north and the east of this western basin, respectively. The continental shelves of the western basin are generally narrow except along the coasts of the Gulf of Lions [51]. The Tyrrhenian Sea is the easternmost and deepest part (3500 m) of this western basin, and joins the rest of the western basin to the south in a wide opening between Sardinia and Sicily [51, 52].

The eastern basin of the Mediterranean Sea is more complicated than its western counterpart. Four sub-sea basins may be identified there: the Ionian, the Levantine, the Aegean and the Adriatic Seas. The Ionian Sea lies between Italy and Greece to the north, and Libya and Tunisia to the south, with a maximum depth of 5000 m south of Greece [45]. The Levantine Sea has depths of about 2500-3000 m in the centre of the basin and a maximum depth of 4500 m in a depression located southeast of Rhodes Island [51]. The Aegean Sea joins the Levantine through several passages located between Greece, Turkey, Crete and Rhodes. Its maximum depth is about 1500 m and it has very irregular coastlines and topography [53]. The Adriatic, the most continental basin in the Mediterranean Sea, is enclosed between two mountain chains, the Apennine and the Balkans, and is elongated latitudinally [54]. It is connected to the Ionian Sea by the Strait of Otranto, whose width is about 75 km and whose sill depth is about 800 m [52].

The Mediterranean Sea is used by humans for domestic and industrial waste disposal, plant cooling, marine mining, tourism and recreation, fishing, shipping and also for marine aquaculture [50].

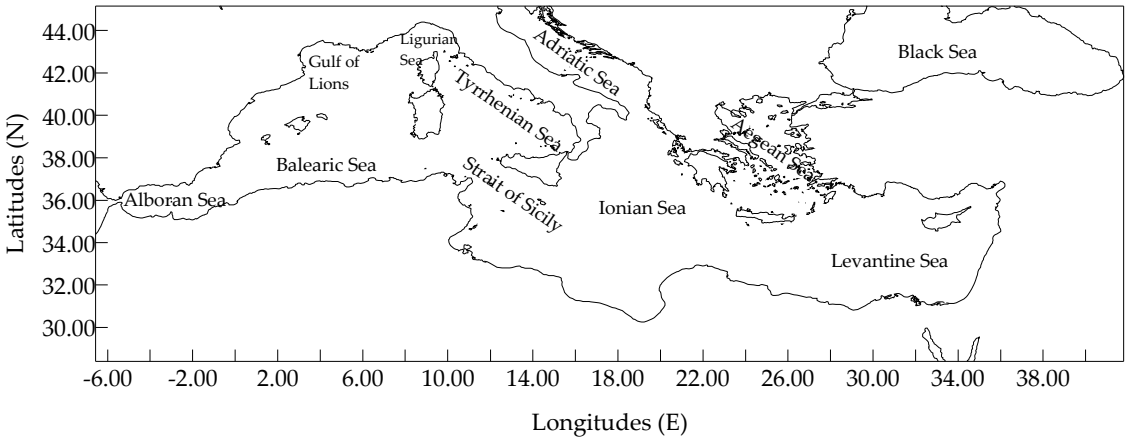

Figure 2.1: Geographic features of the Mediterranean Sea

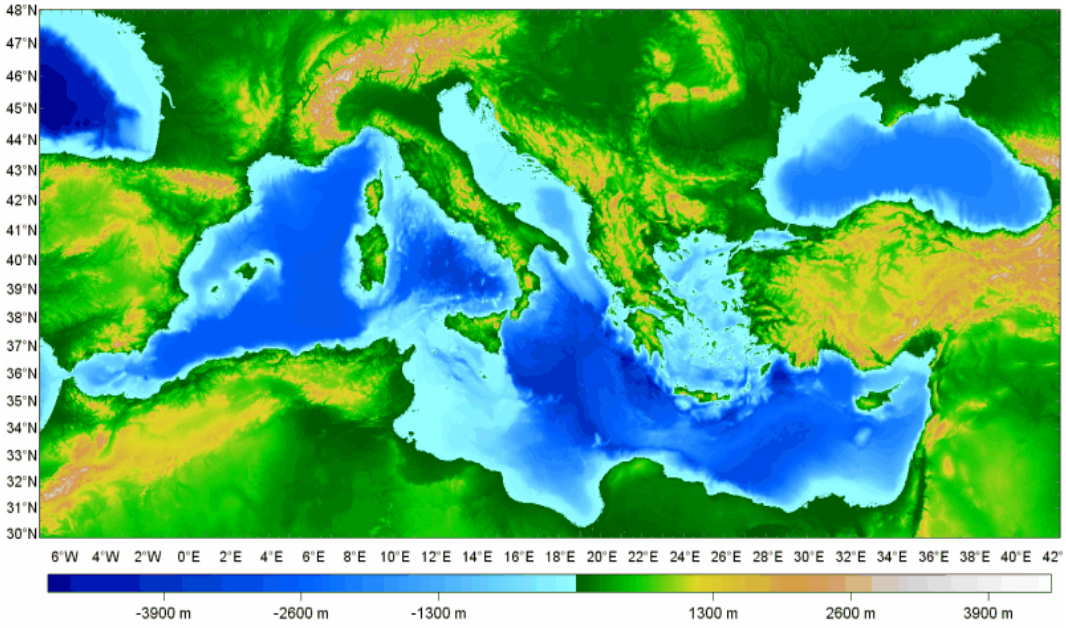

Figure 2.2: Topographic and bathymetric map of the whole Mediterranean basin (www.unipv.it/cibra/MedBathy%20800.gif)

2.2 On the biology of the Mediterranean Sea

It is evident that the present marine biota of the Mediterranean Sea belongs to several bio-geographic categories [47]:

1. Temperate Atlantic - Mediterranean.
2. Cosmopolitan - Panoceanic.
3. Paleo - Neoendemnic.
4. Subtropical Atlantic.

5. Boreal Atlantic.
6. Red Sea migrants, and
7. Eastern Atlantic migrants.

Compared with the Atlantic Ocean, the Mediterranean marine communities have more species with generally smaller individuals of shorter life cycles [55]. The Mediterranean Sea is considered to be oligotrophic; i.e. it is rich in oxygen content and poor in nutrients [49]. The Adriatic Sea, the Gulf of Lions and the Northern Aegean Sea are areas with relatively higher mean nutrient concentration, higher primary and secondary productivity and sometimes with local algal blooms [56]. Eutrophication; i.e. an excess of nutrients and depletion of oxygen, may be observed in some near-shore areas and enclosed coastal bays along the Mediterranean coasts [57]. Figure 2.3 shows the areas along the Mediterranean coast where this phenomenon has been reported. These areas are influenced by direct river inputs and domestic sewage. The highest levels of productivity are also observed there. The major rivers that discharge waters into the Mediterranean basin and their average discharge [58] are: the Rhone (France; 1721 m^3/s), the Po River (Italy; 1569 m^3/s), the River Nile (Egypt; 1542 m^3/s between 1912 and 1982, and 873 m^3/s between 1973-1982) and the Ebro River (Spain; 416 m^3/s).

Figure 2.3: Mediterranean Sea areas where eutrophication has been reported [57]

The Mediterranean fauna and flora have evolved over millions of years into a unique mixture of temperate and subtropical elements, with a large proportion (28%) of species of economic values [59]. The flora and fauna of the Mediterranean Sea consist of sea-grass, pelagic and demersal species that are spread over the whole Mediterranean basin. More than 8000 species of macroscopic marine animals have been roughly estimated [47] to live in the Mediterranean (Table 2.1). The existence of this large number of species was explained by two facts:

1. The Mediterranean Sea is older than almost any other global sea. Hence, it is more intensively studied than other oceans.
2. The complex ecology of the Mediterranean Sea.

The rapid changes in the Mediterranean biodiversity due to climate change and human impact have been alerted and pointed out [47, 59]. The most typical Mediterranean fauna and flora occur in the central parts of the Sea, especially in the central western basin [47].

Extensive sea grass beds lie in a fringe along the major part of the Mediterranean coastline with maximum abundance found in the Gulf of Gabes off Tunisia and the Gulf of Sirte off Libya [60]. These areas of sea grass are important locations for spawning, nursery and first feeding stages of many pelagic species in the Mediterranean.

With respect to fish groups and fisheries, the Mediterranean Sea may be considered as one of the most diverse ecosystems in terms of groups of inhabiting species and total catch [61]. Herrings, sardines and anchovies represent 38%, coastal fishes 18% and molluscae 16% of the total Mediterranean catch [61]. From an economic point of view, Tuna and Swordfish, though being migratory fishes through the Mediterranean, are the most economically valuable fisheries in the Mediterranean basin [60].

Taxa	World	Mediterranean	Med. /World (%)
Red algae	5250	867	16.5
Brown algae	1500	265	17.7
Green algae	1200	214	17.8
Sea grass	50	5	10.0
Total plants	**8000**	**1351**	**16.9**
Sponges	5500	600	10.9
Cnidarians	11000	450	4.1
Bryozoans	5000	500	10.0
Annelids	8000	777	9.7
Molluscs	32000	1376	4.3
Arthropods	33600	1935	5.8
Echinoderms	6500	143	2.2
Tunicates	1350	244	18.1
Other invertebrates	~ 13550	~ 550	4.1
Total invertebrates	**~ 116500**	**~ 6575**	**5.6**
Cartilaginous fishes	850	81	9.5
Bony fishes	11500	532	4.1
Reptiles	58	5	8.6
Mammals	114	21	18.4
Total vertebrates	**12522**	**639**	**5.1**
Grand total	**~ 137000**	**~ 8565**	**6.3**

Table 2.1: Numbers of species of macroscopic marine organisms in the world ocean and in the Mediterranean Sea [47]

Species of marine mammals in the Mediterranean Sea include cetaceans (whales and dolphins) and seals [62]. Eight species of cetaceans are dominant in the Mediterranean: bottlenose dolphins, striped dolphins, fin whales, sperm whales, Risso dolphin, common dolphins, long-finned pilot whales and Cuvier's beaked

whale [63-65]. The first seven species are cited as observed between 1986 and 1989 in order of a decreasing frequency [63]. The last is the only species of beaked whale commonly found in the Mediterranean Sea [66]. The best-known species of Mediterranean seals is the Monk seal, which is one of the ten most threatened mammal species in the World [60]. Three turtle species are found in the Mediterranean Sea, two of which dominate the Mediterranean basin while the third is a visitor from the Atlantic Ocean [67].

As the Mediterranean Sea is a high-diversity ecosystem, it is highly affected by any external pressure on its environment. Such pressures [57] include: pollution, over-fishing, habitat erosion, climate change, industrial activities and ferry routes. All are man-made effects. Briefly: mass tourism causes enormous changes in the Mediterranean Sea area leading to soil erosion, increasing discharge into the Sea and the destruction of natural habitat. Blue Plan scenarios show that the number of tourists is expected to increase along the Mediterranean coasts from 135 x 10^6 in 1990 to 235-353 x 10^6 tourists in 2025 [68]. This increase will, no doubt, have an impact on the Mediterranean ecosystem.

Fishing, during the 1990s, in the whole Mediterranean basin has increased by 12% with high exploitation of Tuna, Swordfish and many invertebrate species [69]. Apart from the legal fishing processes, thousands of cetaceans are killed every year in the Mediterranean [49]. The use of cetacean meat for human consumption has been widely documented by surveying reports in Italy and Spain [70].

The maritime traffic and its related hazards also affect the Mediterranean Sea environment. A sinking tanker could cause an ecological catastrophe. There are many industrial and large commercial harbours distributed over the two basins of the Mediterranean Sea, e.g. Alexandria, Port Said, Sfax, Cagliari, Marseille, etc. These harbours are being affected by different types of toxic pollutants that, in some cases, may totally destroy the marine environment.

In order to protect the environment of the Mediterranean Sea, several conventions and action plans have been signed, for example:

- Action plan for the conservation of Mediterranean marine turtles [71].
- 112 designated Specially Protected Area (SPA) sites in the Mediterranean Sea under the UNEP-Protocol [72], 47 of which cover marine areas.

- Action plan for the conservation of cetaceans in the Mediterranean Sea [73, 74].
- Action plan for the conservation of marine vegetation in the Mediterranean Sea [75].

Unfortunately, despite these conventions and protocols, human activities continue to have a great effect on the marine environment of the Mediterranean Sea. The following actions are recommended for further protection for the Mediterranean ecosystem biodiversity [57]:

- Development of more national and Mediterranean-wide coordinated environmental plans.
- Introduction of effective measures for environmental protection from increasing sea-transport, coastal-works and sea-exploitation activities.
- Promotion of the biodiversity conservation convention comes in force.
- Promotion of the existing action plans for species protection in the Mediterranean environment.
- Increase in protection of the remaining pristine areas.

2.3 Physical properties and water masses in the Mediterranean Sea

A broad view on the physical characteristics of the Mediterranean waters leads to the following deductions:

Hydrographically, in winter, the upper 400 m in the Mediterranean Sea are characterized by temperatures between 15.0˚ C and 17.0˚ C and a maximum salinity of 38.90 - 39.20 practical salinity unit (psu), whilst, in summer, the warming effect increases the temperature of the surface water (30 - 50 m) up to 28.0˚ C and a strong thermocline is developed [45]. The maximum salinity layer varies between 38.80 - 39.20 psu. For the layer between 50 and 100 m, the temperature and the salinity range between 17.0˚ C and 22.0˚ C and between 38.60 and 38.80 psu, respectively, identified as the Atlantic water mass [76]. Below this Atlantic layer, intermediate water exists with a temperature ranging between 15.0˚ C and 17.0˚ C, and a salinity of 38.90 – 39.10 psu. Moving towards the bottom, i.e. below 1000 m depth, the water temperature and the salinity values fluctuate between 13.3˚ - 13.5˚ C and between

38.68 - 38.75 psu, respectively [77]. Figure 2.4 is a satellite image taken in January 1988 (winter season) for the surface temperatures of the Mediterranean Sea. The temperature values in the image range from about 18º C (red, eastern basin), to 15-16º C (orange-yellow, near Gibraltar) to ~ 13º C (light blue, Ligurian sub-basins) to ~10º C or less (dark blue, Adriatic Sea) [78]. In the figure, $\sum A_E$, $\sum L_W$ and $\sum L_E$ are areas where eddies accumulate in the east Algerian basin, western and eastern Levantine sub-basins, respectively. Using Extended Bathy-Thermograph (XBT) data, the temporal and spatial variability of temperature files was found to be significantly different in the Western and Eastern Mediterranean [79]. In the Western Mediterranean, the winter cooling leads to a loss of thermal stratification. In the Eastern Mediterranean, on the other hand, the stratification is always detected although varying with the seasons and strongly affected by the gyres. The results of analysing data from satellites and using field data revealed a general increase in the Mediterranean surface temperature by 0.6˚ C in the last two decades [80]. The same trend of temperature increase, extended to sub-layers of the Mediterranean has been confirmed through a thermohaline investigation, between 2000 and 2006 [81]. Examining the evaporation process, which is a main cause in the general increase in Mediterranean salinity, the annual evaporation in the Mediterranean Sea is found to generally exceed the rainfall and the river runoff [57]. The Adriatic Sea, which receives a large amount of fresh water from the River Po, is the only part of the Mediterranean Sea that receives more fresh water than it loses through evaporation [60].

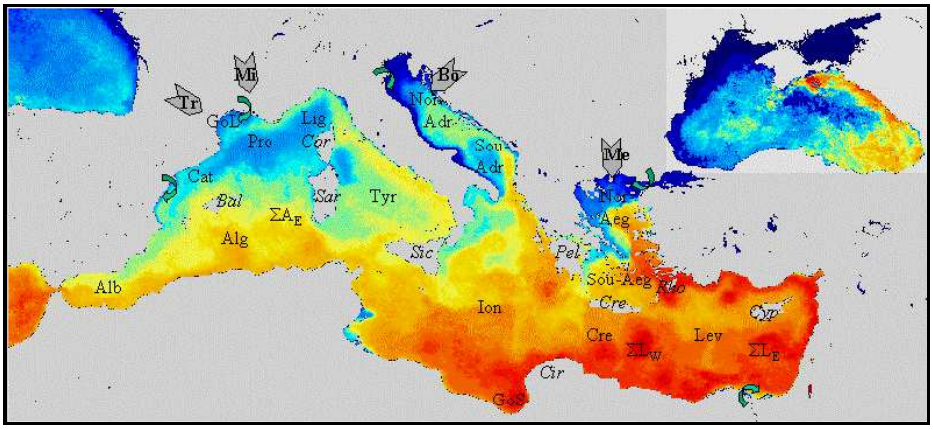

Figure 2.4: Satellite image of surface temperatures of the Mediterranean Sea in winter, January 1998 (the Black Sea has its own colour scale) (www.ifremer.fr/lobtln/OTHER/Millot_TL_fig1.gif)

Within the Mediterranean Sea, three main water masses can be distinguished:

1. Surface water, also known as the Atlantic inflow. This invades the Mediterranean through the Strait of Gibraltar and extends from the surface to a depth of about 150 m.
2. Intermediate water, lying to the south of Turkey, is formed by cooling and evaporation processes during the winter. This layer extends from 150 to 600 m depth, and flows at this depth out through the Strait of Gibraltar into the Atlantic Ocean. The region of formation of this water mass and its dependence upon the deviation of the heat budget from the long term average of the cold period of the year has been studied [82]. It is concluded that the formation of this water mass takes place in the Levantine Sea everywhere except in its southern and extreme eastern parts.
3. Deep water, found below a depth of 600 m and formed by strong winter cooling and wind mixing processes south of France and in the Adriatic.

All these water masses are closely related, and it is supposed that any significant modification involving a single water mass may propagate its effects to the others [83]. The observational evidence [83] shows that significant anomalies at the sea surface in the Eastern Mediterranean may have an effect on the deep layer of the adjacent basin.

2.4 The general circulation pattern in the Mediterranean Sea

The Mediterranean Sea is one of the few locations in the world where deep convection and water mass formation take place and as such, it may be used to study the interaction of physical and dynamical processes [84]. The Mediterranean is also an important marginal basin to the North Atlantic producing very saline waters, the outflow of which through the Strait of Gibraltar may play an indirect role in the deep circulation of the North Atlantic [85]. The Mediterranean Sea acts like an ocean system in which several temporal and spatial scales (basin, sub-basin and mesoscale) interact to form a highly complex and variable circulation [86]. The circulation pattern and the hydrography of the Mediterranean Sea are driven by the surface energy and heat exchange with the atmosphere and by the salinity and heat exchange through the Strait of Gibraltar [87]. The inflowing waters are altered by an excess of

evaporation over precipitation and slight cooling within the Mediterranean basin during their 100-year-long journey before returning back to the Atlantic [84]. The general circulation in the Mediterranean Sea is composed of sub-basin gyres: a cyclonic motion dominates the northern part of the basin and an anticyclonic motion in its southern part [88]. The earliest robust circulation descriptions of the Mediterranean Sea [89-92] were from basin-wide and low-resolution measurements. The Mediterranean Sea is now known to have a very high spatial and temporal variability at all scales, from small turbulences to basin scale processes [79].

The modern research on the general circulation within the Mediterranean Sea as well as its thermohaline pattern and its variability, and the identification and qualification of critical processes relevant to ocean and climate dynamics involves several issues. This research includes [45, 76-78, 82, 93-110] and others. Consideration of such research reveals that the three distinguished water masses mentioned in section 2.3 are found in the two basins of the Mediterranean. These water masses flow independently in a special flow regime. The circulation pattern of these three water masses, together, gives the general circulation pattern of the Mediterranean Sea.

2.4.1. The surface water

The circulation of the surface (Atlantic) water, shown in Figure 2.5, enters the Mediterranean through the Strait of Gibraltar. The topographic stress could be a significant factor driving the circulation in the whole Western Mediterranean at both basin and sub-basin scales [87]. Accordingly, in the extreme western basin of the Mediterranean Sea, the Atlantic inflow is first directed north-eastward due to the orientation of the Strait of Gibraltar then, due to the effect of Coriolis force, describes a clockwise gyre in the east of the Alboran Sea between Spain and Morocco and spreads toward the African coast. Later on, this superficial flow starts to separate to the along slope current of modified Atlantic water (lighter surface water) and the Algerian current (denser lower water). Due to complex hydro-dynamical processes, baroclinic and barotropic instability mainly, the Atlantic water current generally develops meanders from about 0-1º E, creating an upwelling and another two clockwise gyres, of approximately 100 km in radius are formed in front of the Algerian coasts [106]. These eddies can last for many months or even years [105].

It is stated that: “These eddies play a major role in the configuration of the general circulation and the distribution of the water masses and biogeochemical parameters in the Algerian Basin” [106].

The surface current at this stage is 100 - 200 m thick and its maximum speed is of several tens of cm/s [45].

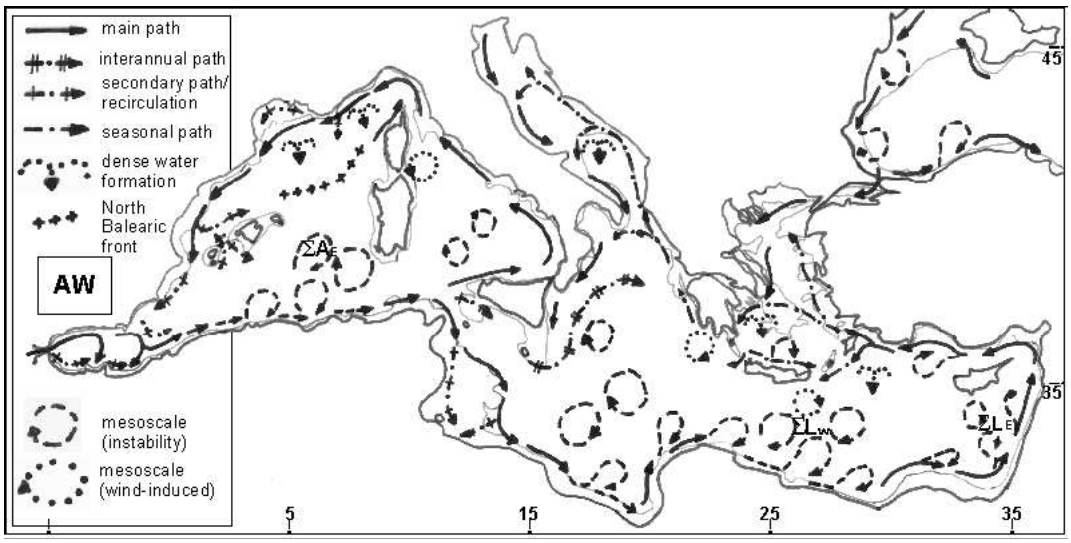

Figure 2.5: The surface Atlantic water circulation in the Mediterranean basin (www.ifremer.fr/lobtln/OTHER/terminology_currents.gif)

At the entrance to the Strait of Sicily, the Algerian current splits into two branches: a northern flow branch enters the Tyrrhenian Sea and a southern flow branch enters the Strait of Sicily itself. Observations show that 2/3 of the Atlantic waters enters the Strait of Sicily while 1/3 flows into the Tyrrhenian Sea [111]. This latter flow takes its pathway and branch flows anticlockwise around the Tyrrhenian Sea along Sicily and the Italian Peninsula before entering the Channel of Corsica. It then joins the west-Corsica branch so that the flow of Atlantic water reorganises itself again as the western basin gyre. This gyre continues along in the Ligurian Sea up to the Algerian and the entrance of the Alboran Seas where it closes. In the Ligurian Sea, the northern current is characterized by a maximum speed of tens of cm/s at its core, a width of a few tens of kilometres and a thickness of a few hundreds meters [45]. Since the Atlantic water is denser at this northern location than in the south, the northern current is narrower and deeper than the Algerian current [95]. However, it displays a marked seasonal variability, being more intense, narrower and deeper in winter [101]. The Gulf of Lions is a semi-circular continental shelf so that most of

the northern current flows as a major vein along the upper part of the continental slope, i.e. along its diameter [95]. Where the Atlantic surface water closes its western gyre [45], i.e. along the Spanish coast near the border between the Alboran and the Algerian Seas, the old water that has skirted the whole basin encounters the water that has just flowed in. Hence, large horizontal gradients occur there. The various islands in the western Mediterranean basin and their associated shelves have significant effects on the circulation of the surface Atlantic water within the basin. The Algerian eddies, blocked by the Sardinian and Tunisian converging shelves, often force the Atlantic waters southwards off western Sardinia, while the Atlantic waters released by the decaying of eddies in the north, is constrained to flow northwards off western Corsica [103].

Some 2/3 of the Atlantic surface water enters the eastern Mediterranean basin through the Strait of Sicily [111]. Within the Strait itself, the circulation is rather complex due to the complexity of the topography with numerous islands and banks, and to the large width of the Strait. At the exit of the Strait of Sicily, the eastern gyre starts to split into several components [45]: one is a north-eastward spreading branch, the second is the generation of mesoscale eddies that tend to drift in the central part of the Ionian Sea and the third is the regular flow along the Tunisian coast flowing eastward. A general cyclonic circulation pattern was proposed in the Levantine Sea as well as in the Ionian basin [97]. The geostrophic circulation of the central and eastern Mediterranean waters is stable in winter and autumn and is mainly characterized by a vast cyclonic gyre in the Levantine Sea and an anti-cyclonic gyre near the Egyptian coast [77].

2.4.2. The intermediate Mediterranean water

Moving eastward to enter the Eastern Mediterranean basin, the surface Atlantic water is affected by the increasing rate of evaporation. Consequently, it becomes denser and starts to sink in the Levantine basin. This denser water, at 150 – 600 m depth, has a westward flow. The Levantine Intermediate Water (LIW) is believed to be formed mainly south-southeast of Rhodes [45]. Figure 2.6 shows the circulation of LIW in the Mediterranean Sea basin. This water mass is the warmest and saltiest water formed in the whole basin and can easily be tracked up to Gibraltar just below the inflowing surface Atlantic water. The importance of this intermediate water mass

lies in the fact that during its spreading phase it reaches the basin's deep water formation areas and, being extremely saline (39 psu), helps in the preconditioning of the water column [112]. In the northern part of the Levantine basin, the intermediate water flows along the coasts of Crete and Rhodes, mainly due to the effect of the Coriolis force. This water then continues to flow from the Ionian Sea to the Western Mediterranean basin through the Strait of Sicily, over its sill, at 400 m depth [45]. Within the Strait of Sicily, the LIW flows along the Sicilian slope to strike Sicily, and then the circulation takes place around the Tyrrhenian Sea at 200-600 m [113]. The flow is still affected by the Coriolis force, so that it makes its way along the Italian Peninsula and south to the European coasts. When the LIW leaves the Strait of Sicily, it turns right along the Sicilian coasts and flows towards The Strait of Gibraltar along an anticlockwise pathway [94]. However, it has been reported [114] that there is a straight LIW flow from Sicily Strait toward the Sardinian Channel before this water reaches The Strait of Gibraltar. By taking the 1000 dbar surface as the level of no motion, the geostrophic current velocity ranges between 5-10 cm/s in the south Ionian Sea, 15-25 cm/s near the Egyptian coasts, between 35-40 cm/s in the eastern part of the Levantine Sea and 15-30 cm/s at the Strait of Crete [115].

The LIW appears to play a major role in the functioning of the Mediterranean Sea [45]: firstly, because it is the warmest and saltiest Mediterranean water formed with the largest volume. Secondly, because it mainly flows along the northern continental slopes of both basins just below the Atlantic water thus being involved there in the offshore formation of all deep Mediterranean waters. The circulation of the intermediate water masses remains close to that of the surface layers [77]. The Levantine Intermediate Water formed in the Levantine basin is involved in the Levantine cyclonic gyre, and in the Aegean Sea, the intermediate water moves through the eastern Strait of Crete. In the centre of the basin, this water is carried northwards by the cyclonic gyre of the Ionian Sea, while the south Ionian (Libyan) anti-cyclonic moves intermediate water westward.

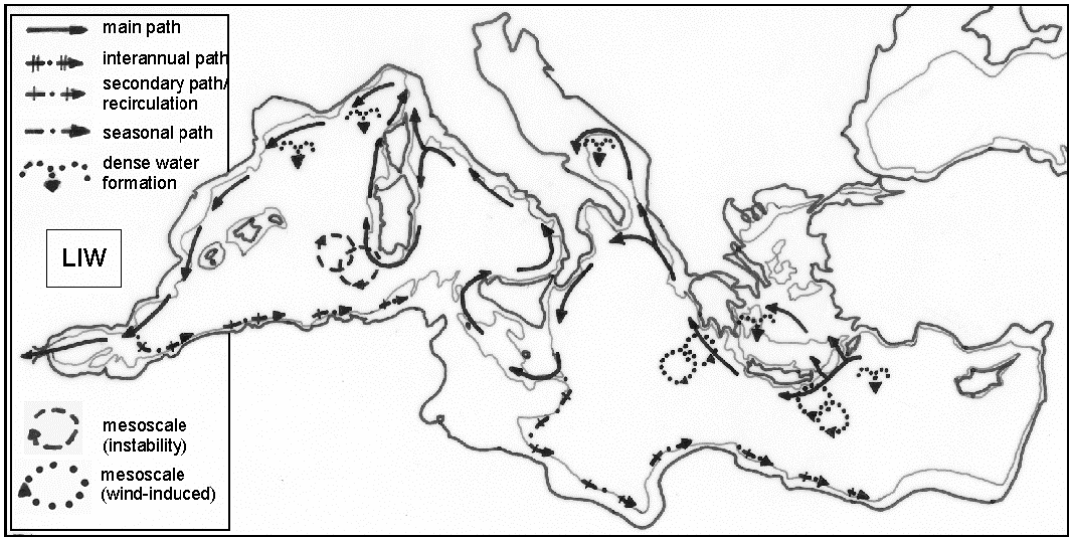

Figure 2.6: The Levantine Intermediate Water (LIW) circulation at 500 m depth in the Mediterranean basin [45]

2.4.3. The deep Mediterranean water

The dynamics of the Mediterranean regional seas e.g. the Adriatic and the Aegean Seas, associated with their transport through their relatively shallow and narrow straits e.g. Gibraltar and Sicily, are of primary importance for the circulation variability observed in the deep parts of the Mediterranean Sea [116]. Actually, the deep waters within the Mediterranean basin have two sources: eastern and western. The former comes from the Aegean and the Adriatic deep waters to form the Eastern Mediterranean Deep Water (EMDW). The latter comes from the Tyrrhenian and the Gulf of Lions deep waters, which together form the Western Mediterranean Deep Water (WMDW). The two water sources for the EMDW are formed over troughs at the depth of 1000-1500 m in the southern Aegean and southern Adriatic, respectively, before out-flowing through the different openings to fill the total depth of the eastern Mediterranean basin of 4000-5000 m [117]. The circulation pattern of these deep water masses is shown in Figure 2.7. In this figure AeDW, AdDW, TDW and WMDW denote the Aegean, Adriatic, Tyrrhenian and Western Mediterranean Deep Waters, respectively. Field experiments conducted in the early 1980s within the international co-operative research POEM programme (Physical Oceanography of the Eastern Mediterranean) demonstrated that a single homogeneous deep water body filled the entire Eastern Mediterranean below a depth of about 1200 m [104]. It is concluded that the deep water column is characterised by potential temperature and salinities slowly decreasing with depth, which implies a very low static stability.

Taking the upper boundary of the deep regime as 1200 m, the renewable period of the Mediterranean deep waters has been calculated to be approximately 126 years [118]. The deep waters from the Aegean and Adriatic Seas flow at the deepest point of Sicily Strait to the western Mediterranean basin. These waters are denser than the resident deep Tyrrhenian water, so they flow underneath and mix with these waters to form the Tyrrhenian deep water found at 2000-3500 m [45]. The Gulf of Lions deep waters are formed at 2000-2500 m depth and mix with the Tyrrhenian deep water flow as a continuation of the basin wide gyre in the Catalan, the Alboran and the Algerian areas [45]. These waters end their journey by flowing from the Mediterranean basin to the Atlantic Ocean through the Strait of Gibraltar.

The influence of the Mediterranean Sea circulation pattern extends out of its proper basin with its two wings. The impact on the global oceanic circulation is more significant than previously realized due to its appreciable contribution to the North Atlantic bottom water thermohaline cell [119]. Moreover, it has been hypothesized that the climate of the entire North Atlantic and Labrador Sea areas is controlled by the intensity of the Mediterranean water outflow [120].

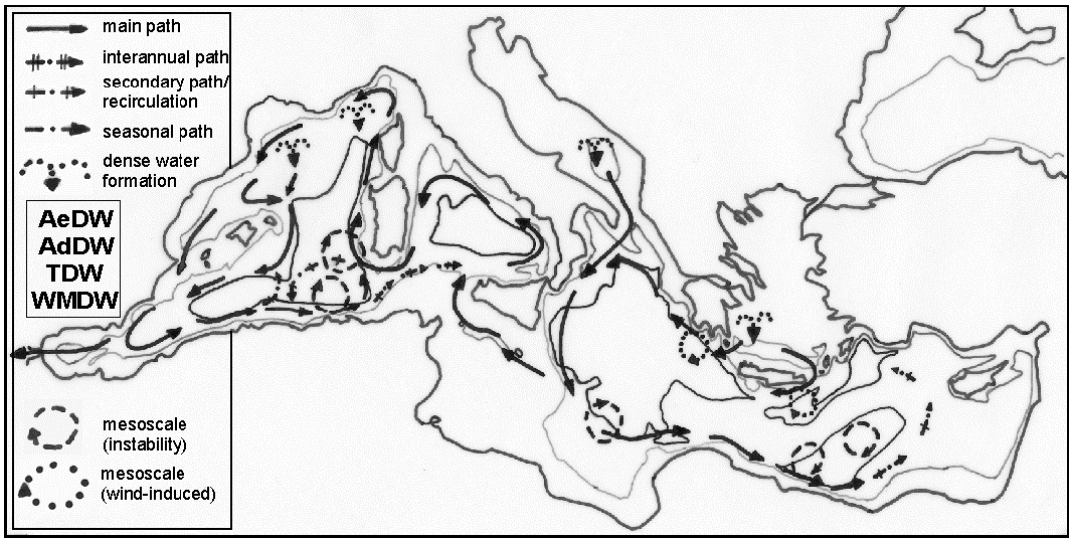

Figure 2.7: The deep water circulation in the Mediterranean basin [45]

2.5 Tidal behaviour of the Mediterranean Sea

Tides in the Mediterranean Sea are of the order of a few centimetres. Hence, Mediterranean tides have not been as intensively studied as other oceans and seas. Tides in the Mediterranean Sea are mainly of semidiurnal type. The tidal amplitudes

are of a few centimetres except in some places, such as the Adriatic Sea, the Aegean Sea and the Gulf of Gabes where resonance phenomena act to amplify the heights of the tides [14]. The tides in the Mediterranean Sea have been presented [14] as two standing waves, one covers its western basin and the other covers its eastern basin.

Generally speaking, two main theories are proposed to describe the tidal motion in the whole basin of the Mediterranean Sea. The first describes tides in the Mediterranean Sea as an independent tide that only depends on the relative motion of the Sun, Moon and Earth, i.e. the Mediterranean tides are purely astronomic tides [121]. The second theory, on the other hand, describes tides in the Mediterranean as a result of two contributing factors: the independent astronomical tide and the effect of the Atlantic tidal wave (co-oscillating tide), which enters the Mediterranean through the Strait of Gibraltar and affects the Mediterranean tidal phenomenon at both basins of the Sea [14].

Using numerical models to explain tides in the Mediterranean Sea, a problem arises when trying to explain the effect of the Atlantic tidal wave on the Mediterranean tide. The effect of the closure of The Strait of Gibraltar on the Mediterranean tides has been examined [122]. Results reveal small differences in the tidal behaviour; hence it has been concluded that tides in the eastern Mediterranean basin are mainly astronomic. However, while the main impact of the Atlantic tidal wave may apparently be just on the Western Mediterranean basin, it has been found that the M_2 amplitude in the Aegean Sea is doubled upon the closure of The Strait of Gibraltar [123], hence the broad effect of the Atlantic tidal wave on the Mediterranean tides in its two basins has been confirmed.

What is mostly accepted by many oceanographers and researchers is that the whole Mediterranean basin is affected in a relative manner by both independent and co-oscillating tides: the Western Mediterranean basin is affected by both independent and co-oscillating tides [7, 14, 124, 125], whereas the Eastern basin is affected mainly by the independent one. The effect of the co-oscillating tides is large enough in extent to be observed in the Sicily and Messina Straits. The combined effect of both independent and co-oscillating tides appears in the Strait of Sicily where complicated tidal processes may be observed. These processes appear in the M_2

amplitude height (~ 1m) in the Gulf of Gabes off Tunisia and the amphidromic point off Cap Bon on the Sicilian coast [125].

The semidiurnal M_2 amplitudes in the Mediterranean basin are, in general, less than 10 cm [124]. These amplitudes increase in 3 defined areas: the Gulf of Gabes, the northern Aegean Sea and the northern Egyptian coasts.

Broadly speaking, the investigations of the tidal behaviour of the Mediterranean Sea and its environment reveal that both tidal ranges and currents all over the Sea basin are weak enough to be excluded from any considered plan to use this natural phenomenon as a renewable resource to extract energy. This fact may have some exception due to the irregularities in the coastlines of the Mediterranean which may give a chance for tidal current velocities to be enhanced, especially at the constrictions in the straits and the estuarine regions. The total average energy dissipation for the Mediterranean is estimated to be about 8×10^8 W [126]. The available energy source in the Mediterranean rises from the independent tidal signal, i.e. excluding the Atlantic tidal effect, as 94% of the Atlantic wave is reflected at the entrance of the Strait of Gibraltar [121]. The results of the model [124] reveal that 40%, 20%, 5% and 9% of the energy in O_1, K_1, M_2 and S_2 constituents, respectively; entering the eastern Mediterranean basin from the west passes through the Strait of Sicily. When the Strait of Gibraltar was closed, only the independent tidal force is considered, and the Western basin provides energy to the Eastern basin at all the frequencies involved.

Having discussed the general tidal behaviour of the Mediterranean Sea, it is important to examine this within some straits throughout the Mediterranean basin. This is in order to examine whether any location within the basin may be suitable enough to be considered as a renewable tidal energy resource using tidal currents.

2.6 Some Straits within the Mediterranean Basin

Due to its irregular coastlines and its complex morphometry, the Mediterranean basin contains many straits. These straits play an important role in controlling both the general and the thermohaline circulations in the Mediterranean Sea [112]. Examples of such straits in the Mediterranean Sea include: Bosphorus, Dardanelles, Messina, Sicily and The Strait of Gibraltar s, covering the basin of the Mediterranean Sea from

east to west. In the following sub-sections, the main characteristics of each of the mentioned straits will be briefly discussed.

2.6.1. The Bosphorus Strait

The Bosphorus Strait occupies the area between latitudes 41˚ 00.00' and 41˚ 15.00' N and longitudes 29˚ 00.00' and 29˚ 09.00' E. Figure 2.8 shows the Strait of Bosphorus and its borders. The Bosphorus presents a long narrow channel of 30 km length and is known as the narrowest strait in the World where the narrowest section is only 698 m at Kandilli-Rumelihisari-Bebek [127]. The maximum width of the Strait is 4.7 km in its northern entrance; while its southern entrance width is only 2.5 km [127]. The depth within the strait does not exceed 110 m [128]. There are two sills in the Strait: one, near the southern entrance, is 34 m deep and the other, near the northern entrance, is 60 m deep [129]. The Strait connects the Black Sea (North) to the Marmara Sea (South). Historically, the Bosphorus has a strategic importance since it is the only maritime route for the five neighbouring Black Sea states (Ukraine, Romania, Georgia, Bulgaria and Russia) and the Central Asian Turkish Republics [127].

Four factors control the water circulation in the Bosphorus Strait: the geographic structure (coastlines and constrictions), the salinity difference between the Black and Marmara Seas, the evaporation process and the wind regime. The general flow pattern in the Strait of Bosphorus is mainly hydrological depending on the haline differentiation between the water layers [130]. It consists of two layers of oppositely flowing currents. The upper layer current is coming from the Black Sea (north) towards the Marmara Sea (south) with a salinity ranging from 18 to 20 psu and a velocity of 0.5 - 1.0 m/s [131]. The lower layer current is running in the opposite direction from the Marmara Sea to the Black Sea, with a salinity ranging between 36 and 38 psu and a velocity ranging from 0.3 to 0.7 m/s. Using the average salinity, the mass flux of the upper flow within the Strait was found to be twice as big as that of the lower one [132], i.e. there is a net flux of about 300 km^3/year from the Black Sea to the Mediterranean Sea. Local topographic features have a significant influence on the flow and determine its detailed structure [133]. Observations suggest increased entrainment south of the contraction (upward) and past the northern sill (downward) in the Black Sea [130]. Generally speaking, the hydrological current speed within the

Bosphorus does not exceed 1.75 m/s [130]. The Bosphorus currents have a rapid response to sea level differences between the Black and the Mediterranean Seas. In the Bosphorus tides are mainly of diurnal type with a spring tidal range of 2.5 cm [134, 135]. With respect to atmospheric pressure changes, the tidal levels in the Strait show a range in sea level of ΔZ varying between 0.2 m to 0.45 m [133]. The Bosphorus Strait is one of the heaviest sea-traffic regions in the World despite its extremely irregular coastline [127].

From an energy-aspect point of view, discussing the determination of the appropriate energy policy for Turkey, the following is stated [136]:

"In Turkey, the use of tidal energy is not possible. Also the sea traffic in Canakkale (Dardanelles) and Istanbul Bosporus obstructs use of sea flows".

Figure 2.8: The Strait of Bosphorus (www.encarta.msn.com)

2.6.2. Dardanelles Strait

The Dardanelles Strait, shown in Figure 2.9, is a narrow strait in the northwest of Turkey. It connects the Aegean Sea to the Sea of Marmara and is located at approximately 40˚ 13.00' N and 26˚ 26.00' E. The Strait is of 61 km long, 1.2 to 6 km wide, with an average depth of 55 m and a maximum depth of 105 m in its narrowest central section [137]. As with the Bosphorus Strait, the Dardanelles Strait separates Europe from the mainland of Asia. The Strait is an international waterway, and along with the Bosphorus Strait, it connects the Black Sea to the Mediterranean Sea to create what is known as the Turkish Straits Systems [135]. Water flows

superficially along the Strait, from the Sea of Marmara to the Aegean Sea and in the opposite direction via an undercurrent. This is mainly a hydrological current regime that is mainly due to the haline difference between waters of Marmara and Aegean Seas.

Tides in the Dardanelles Strait are mainly of a semidiurnal type [134]. The mean spring tidal ranges in the Strait of Dardanelles are 19 and 5.5 cm for central and northern parts, respectively [138]. The mean tidal current velocity in the Strait is 0.25 m/s [137]. As with the Bosphorus, the same conclusion may be reached for the Strait of Dardanelles concerning its suitability as a place to harness energy using tidal currents. Apart from the massive maritime traffic passing through the Dardanelles Strait [136], the tidal current velocity is completely inconvenient for the process.

Figure 2.9: The Strait of Dardanelles linking the Marmara Sea (North) to the Aegean Sea (South) (www.encarta.msn.com)

2.6.3. The Strait of Messina

The Strait of Messina is considered to be an exception within the Mediterranean basin with its well-known, strong tidal currents. The Strait presents a vital water passage, between the Italian Peninsula and the Island of Sicily. The maximum tidal current velocity along the main axis of the Strait varies between 1.8 m/s to more than 3 m/s [139-141]. Therefore, the Strait is chosen to be the area of investigation in the present study. The main characteristics and properties of the Strait of Messina are given in detail in chapter three of this thesis to justify the choice of the Strait as a convenient tidal resource within the Mediterranean basin.

2.6.4. The Strait of Sicily

Figure 2.10 shows the Strait of Sicily. The Strait extends between latitudes 36˚ 30.00’ and 38˚ 00.00’ N and longitudes 11˚ 00.00’ and 15˚ 00.00’ E. The Strait separates Sicily Island from the Tunisian coast, and the Western Mediterranean basin from its Eastern one. Two sills are present at the eastern and western extremities of the Strait. The maximum sill depths are about 400 – 500 m, whilst the depth in the interior basin of the Strait can reach 1400 m [142]. The minimum width of the Strait coincides with the western sill and is of about 140 km. Most of the studies that have examined the Strait of Sicily and its region have focused on specific processes based on cross-section, time series, coastal and surface observations. The behaviour of circulation in the Strait has its special complex dynamics. The flow pattern in the Strait of Sicily may be described best as a two-layer flow system. In the Strait, the surface Atlantic water of lower density flows into the Eastern Mediterranean Sea, while the denser Levantine Intermediate Water enters the Western Mediterranean [143]. Additional intrusions of waters from the Ionian Sea of intermediate properties between the Atlantic and the Levantine also occur, and result in important horizontal and vertical mixing processes [144]. The modelled [112] maximum exchange through the Strait is from November to February, with a volume transport of almost 2 Sv. This is in good agreement with the *in situ* [114] measurements. The Levantine Intermediate Water leaves the Strait of Sicily to turn right along the Sicilian coasts and follows a cyclonic path from the Strait of Sicily to the Strait of Gibraltar [94]. However, it has been reported [114] that there is a direct path for this water mass from the Strait of Sicily to the Sardinian Channel.

Tides in the Strait of Sicily are of semidiurnal type [145, 146] with an amphidromic point within the Strait [124, 145]. The cross transect component of tidal current velocity at 8 sections within the Strait of Sicily has been computed [147]. The velocity ranged between 0.20 to 0.55 m/s. Investigating the tidal current pattern in the Strait of Sicily, the maximum value of the current has been about 20 cm/s along the western sill of the Strait [142]. Along the eastern sill, on the other hand, this maximum velocity does not exceed 10 cm/s, as observed on Malta Plateau. The barotropic tidal energy budget reveals that 61% of energy dissipation occurs in the Gulf of Gabes, 13.6% of the total Strait domain, while the energy loss due to bottom

friction in the total domain of the Strait reaches 79% [146]. The Strait of Sicily does not fulfil the main condition of tidal current velocity [33] in order to be chosen as a tidal resource within the Mediterranean basin.

Figure 2.10: The Strait of Sicily and its surrounding lands (www.encarta.msn.com)

2.6.5. The Strait of Gibraltar

The Strait of Gibraltar is located between the southern coast of Spain and the northern coast of Morocco as shown in Figure 2.11. The Strait extends between latitudes 35˚ 45.00’ and 36˚ 10.00’ N and longitudes 05˚ 20.00’ and 06˚ 00.00’ W. The width of the Strait ranges from 44 km (west section) to 14 km (Tarifa-Punta Cires section, or Tarifa narrows). The bathymetry of the Strait is very irregular with a minimum depth of about 300 m in the Punta Paloma-Punta Malabata section [148]. The Sill divides the main channel of the Strait in two regions:

1- The west region with a maximum depth of 630 m NE of Tangier, and
2- The east region, known as Gibraltar Basin, with a mean depth exceeding 700 m south of Punta del Acebuche.

The Strait of Gibraltar is the single connection between the Atlantic Ocean and the Mediterranean Sea. The water body in the Strait and its approaches consists of a deep layer of saltier Mediterranean water and an upper layer of less dense Atlantic water [149]. The mean flow is composed of two counter-flowing layers: the surface layer flows eastward towards the Mediterranean Sea (Alboran) and the lower layer flows westward towards the Atlantic Ocean [150]. This current system in the Strait of

Gibraltar results mainly from the variations in temperature and salinity [151] and is modulated by the predominant semidiurnal tidal current [149]. Due to the complexity of its northern coastline and the presence of numerous islands, many small eddies and other local currents form an essential part of the general circulation in the Gibraltar area [152].

The exchange across the Gibraltar sill is found to be due in nearly equal parts to the mean currents and to the tidal fluctuations [153]. The water mass exchange in the Strait caused by the main semidiurnal tidal component M_2 has been estimated [153] as 2.3 Sv. (incoming flow towards the Mediterranean) and 1.3 Sv. (outgoing flow towards the Atlantic).

Tides in the Strait of Gibraltar are mainly of a semidiurnal type. The tidal flow in the area of the Strait is mainly driven by tidal differences between the Gulf of Cadiz in the western side and the Alboran Sea in the eastern side [154]. The two independent tides, one from the Atlantic and the other from the Mediterranean, drive water interchange between both seas and give rise to seemingly irregular currents in the Strait [152]. Two effects have been reported [150] for the effect of tides in the Strait of Gibraltar: the generation of strong surface currents through the Strait and the presence of internal waves with higher amplitude in its southern area. Tidal currents in the Strait of Gibraltar, generally, fluctuate between 60 cm/s and 1 m/s [155]. The highest intensity of tidal flows occurs in the Main Sill area because it is the minimum hydraulic section, and the lowest intensity occurs at the west and east ends of the Strait [156]. The maximum M_2-tidal current velocity at the sill is 1.2 m/s [153]. The same conclusion may be reached for the Strait of Gibraltar as an unsuitable place to be chosen for an energy extraction process using tidal currents in the Strait.

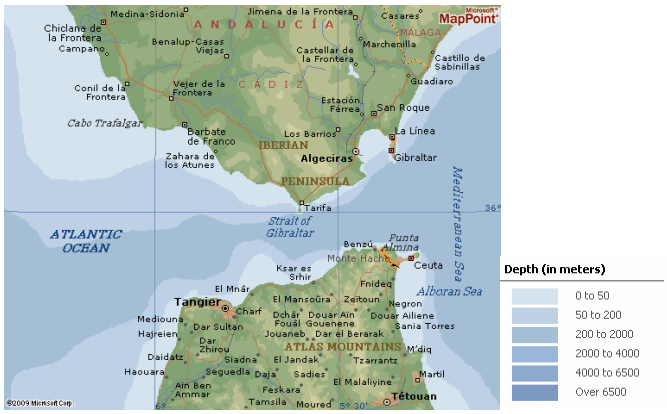

Figure 2.11: The Strait of Gibraltar (www.encarta.msn.com)

2.7 Chapter Conclusion

The Mediterranean Sea basin is a large (2.5×10^6 km^2), semiclosed basin connected to the Atlantic Ocean through the Strait of Gibraltar in its western extremity. The Mediterranean is one of the most researched sea basins in the world from all oceanographic points of view: physical, biological, chemical and geological. Three water masses: surface, intermediate and deep occupy the whole Mediterranean basin, strongly related to each other and circulate in a very well-studied pattern. The Mediterranean tides are of semidiurnal type and have not been intensively studied. This is mainly due to the centimetre order of tidal ranges within the whole Mediterranean basin. The associated Mediterranean tidal currents are also of a few cm/s velocities even when enhanced by the natural coastline configuration in the system of straits within the Mediterranean basin. This system includes: Bosphorous, Dardanelles, Messina, Sicily and The Strait of Gibraltar s. Investigations reveal that both tidal ranges and currents all over the Mediterranean basin are weak enough to be excluded from any tidal energy plan. The Strait of Messina is an exception with its reasonable strong tidal current velocities. The Strait is, therefore, selected as area of investigation in the present work.

CHAPTER 3
THE STRAIT OF MESSINA

An Overview

As mentioned in the previous chapter, the Strait of Messina is chosen as the area of investigation in the present study. In this chapter, the Strait will be examined in details. Recalling both the facts about tidal currents in the Mediterranean Sea and its major straits and the main tidal current velocity criterion [33] that should be satisfied by a tidal current resource, the whole Mediterranean basin should be excluded from any proposed tidal energy plan. However, the discussion which follows will demonstrate how the Strait of Messina is an exception and will justify its use as a tidal current energy resource. The Strait, where the maximum spring peak tidal currents may reach 3 m/s, can be proposed as a massive tidal resource for the exploitation of tidal currents to generate electricity.

Chapter three consists of five sections, the first of which is a description of the morphometry of the Strait of Messina. Section two focuses on the Strait's biological structure. The physical properties and the circulation pattern within the Strait of Messina are presented in section three and its tidal features are discussed in section four. As our aim is to harness energy from tidal currents in the Strait of Messina, it is important to examine the effect of such an energy extraction process on the surrounding ecosystem. Therefore, a detailed desk-based Environmental Impact Assessment study is given and discussed in section five.

3.1 Morphometry of the Strait of Messina

Figure 3.1 represents the geographical position and features of the Strait of Messina. The Strait is a narrow passage of water, which separates the main Italian Peninsula from the Island of Sicily and joins the Tyrrhenian Sea (north) to the Ionian Sea (south). The fit of the two bordering coastlines of the Strait, united as they were in the remote past, is still now perceivable [141]. The Strait of Messina extends between latitudes 37˚ 35.00' and 38˚ 18.00' N and longitudes 15˚ 06.00' and 15˚ 42.00' E. The main axis of the Strait of Messina is oriented NE - SW in its northern part and N - S in its southern part. The width of the Strait decreases from 30 km

between C.S. Alessio and C. Armi (south) to 4 km between Ganzirri and Punta Pezzo (north) [157]. The narrowest width within the Strait is 3 km and the smallest cross-sectional area is 0.3 km^2 in the sill region where the mean water depth is 80 m [158]. From the sill, the bottom slopes downward in the form of valleys on both sides. The natural constriction in the Strait extends uniformly for about 7 km and represents a barrier separating the Ionian and the Tyrrhenian Seas [140]. In the southern part of the Strait the water depth rapidly increases to reach more than 800 m depth 15 km south of the sill, while in the northern part it increases more gently to reach 400 m depth 15 km north of the sill [159]. The sill region in the Strait of Messina represents the junction point between two basins (Tyrrhenian and Ionian) of different physico-chemical properties mainly due to the effects of the Atlantic and the LIW water masses [141, 160].

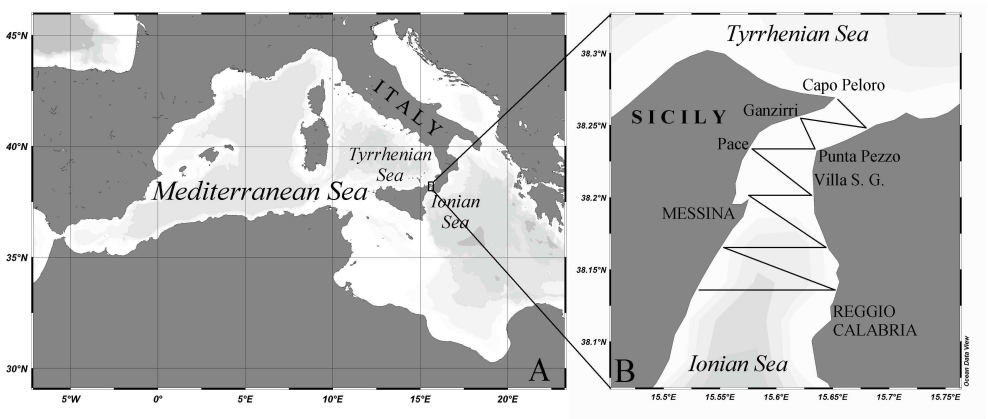

Figure 3.1: Geographical position and features of the Strait of Messina [161]

On both sides of the Strait of Messina, the coasts are lined with beaches, bands of gravel and sand, which end towards the 100 m bathymetric contour where bare rock is exposed [162]. The seabed of the Strait of Messina (Fig. 3.2) is extremely non-homogeneous comprising different types of strata distributed randomly along the axis of the Strait. It can be geologically classified as gravely sandy rocky. The sill of the Strait is of an erosive nature. Small sediment dunes to the north and south of the sill, where velocities decrease due to the enlargement of the cross-sectional width, are made up of eroded materials from the sill region [160]. The seabed of the whole Strait may, therefore, be divided into the northern section to the north of the sill known as Scilla Submarine Valley and the section south of the sill known as the

Southern Messina Valley. Sand waves have commonly been observed along the seabed of the Strait. This phenomenon is an important oceanographic characteristic and has been the subject of many research studies, e.g. [160, 163, 164]. The importance of these waves stems from their high speed of propagation that may affect any submerged structure, cables and pipelines [160]. The bathymetry of the main body of the Strait of Messina is shown in Figure 3.3, based on data extracted from Admiralty Chart [165].

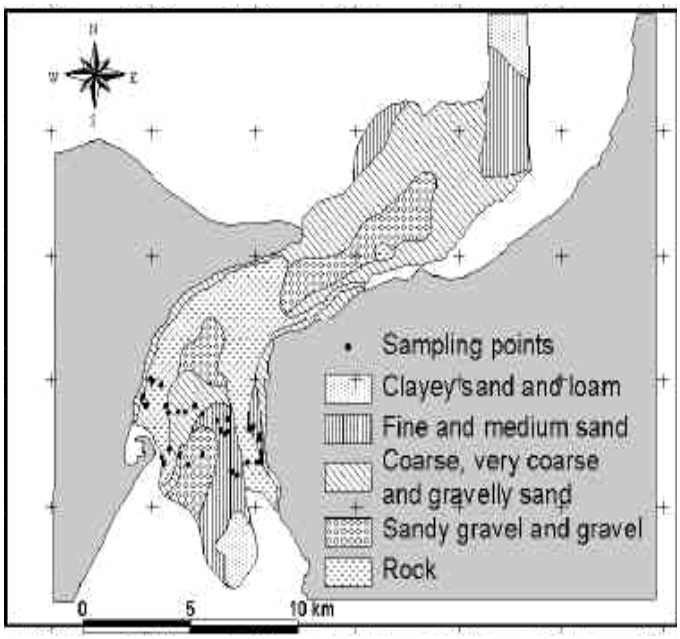

Figure 3.2: Seabed structure of the Strait of Messina [160]

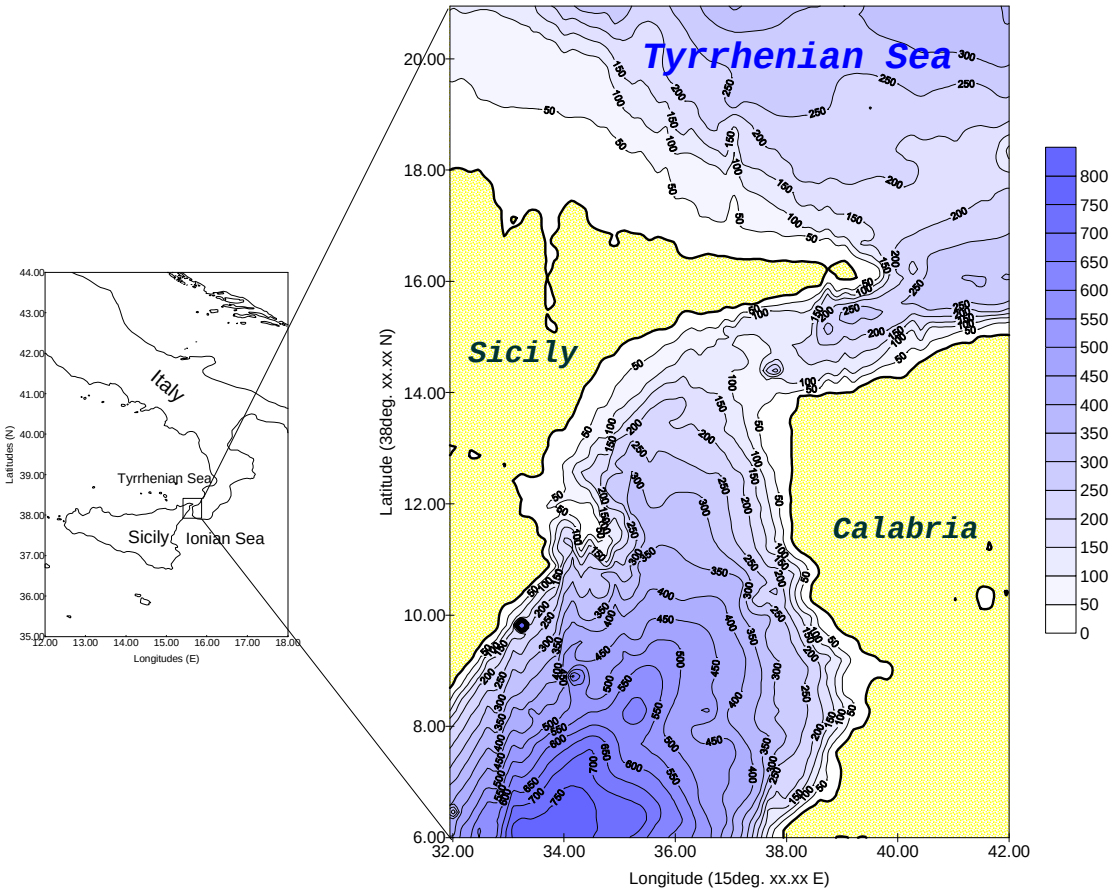

Figure 3.3: Bathymetric chart of the main body of the Strait of Messina based on data extracted from Admiralty Chart [165]

3.2 On the biology of the Strait of Messina

The Strait of Messina may be considered one of the richest biological habitats within the whole basin of the Mediterranean Sea. The biological structure of the Strait consists of both marine biota (fauna and flora) and bird communities. The latter may be readily observed within the aerial domain of the Strait.

The hydrographic, physico-chemical properties as well as the biological processes in the Strait of Messina have remarkable effects on both the abundance and the structure of its planktonic, pelagic and benthic communities, making this ecosystem unique in the Mediterranean Sea with regard to biodiversity [166]. Due to the Strait's turbulence, many organisms are found at a greater depth than in any area of the Mediterranean Sea [166].

The abundance of phytoplankton in the Strait of Messina is affected all the year round by variations in nitrate and salinity levels and seasonally by variations in the temperature [161]. As the whole southern area of the Strait of Messina is characterized by its upwelling process, an increase in the primary productivity of about 10 times compared to the Tyrrhenian waters is found there [167]. Hence, this southern tip of the Strait is considered to be the richest biologically due to the abundance of the first contributor in the oceanic food chain. The zooplankton communities in the Strait of Messina are mainly affected by both the upwelling phenomenon and by the current regime within the Strait [168, 169]. The vertical migration of the planktonic communities in the Strait of Messina is mainly affected by the day-light period.

The marine macro-biota in the Strait of Messina comprises both of pelagic and of benthic species. However, the latter are rarely found in the Strait [166]. For pelagic species, the Strait of Messina is their principal habitat, a spawning and breeding area or a migratory route.

Euphasiids (Krill) are a group of pelagic, shrimp-like crustaceans that play an important role in the marine food chains. The presence of this crustacean group and its abundance in the area of the Strait of Messina were reported by meso- and bathy-pelagic stranded organisms [170], by studies on the feeding behaviour of the most common meso-pelagic fishes of the Strait of Messina [171] and by pelagic trawling nets and visual observations [172]. Recently, 12 out of 13 Mediterranean euphasiids species were found to live in the Strait of Messina [172]. The spawning areas of the European eel could be found close to the Strait of Messina [173]. Early evidence for this was provided [174]. 50 mm European eel larvae were discovered in the Strait [174]. The presence of adult eels in the Strait has also been reported [175, 176]. The Strait of Messina is also the breeding-ground for the Swordfish found in the Mediterranean Sea. The spawning season of this species in the Strait of Messina extends from the end of spring until the end of summer [177].

The Mediterranean Spearfish is one of the small size billfish species, which inhabits the upper water layers of the Strait of Messina [178]. This is mainly due to the upwelling phenomenon that enriches these layers with nutrients. For this species, the Strait is a good place for spawning [179]. Eggs and larvae of Spearfish were found in

the early 1970s in the plankton samples collected along the main axis of the Strait [180]. The average size of the Spearfish in the Strait of Messina ranges between 79 and 193 cm, while the weight ranges between 1.4 and 36 kg [179]. This species is a common catch in the Strait during the period July – September [181]. Luminescent fish species also inhabit the Strait of Messina. These species are responsible for the luminescence of the water of the Strait beneath the superficial water layer. These species are mainly characterised by their vertical migration in the water column, which is controlled by the photoperiod cycle. Three luminescent species were observed [182] during initial research into the abundance and behaviour of these fish-species within the Strait: *Argyroprlrus hemigymnus*, myctophids and *Cyclothone braueri*. The first species was encountered between 180 and 500 m depth, the second from the surface to 550 m depth and the third between 330 and 530 m depth. Since those observations, these three species remain dominant in the Strait. Cetacean mammals are of special importance within the Strait of Messina, and the Strait is characterised by several species. They comprise sperm whales, Cuvier's beaked whale, striped dolphins and bottlenose dolphins. Fin whales, on the other hand, use the Strait of Messina as a migration route between the Ionian and the Tyrrhenian Seas [63]. Tunas also use the Strait of Messina as the main migratory passage between the Western and Eastern Mediterranean basins [183]. Blue-fin Tunas are one of the most important Mediterranean commercial species found along the main axis of the Strait and are caught using purse seines, long-lines, hand lines, harpoons and driftnets [183].

In addition to the aquatic biology, the Strait of Messina is an important European site for resident and migratory birds. The Strait is an important migration route for five bird species [184]. Since 1984, 40 resident species of raptors have been recorded in the area of the Strait [185]. In addition, Seagulls and ducks may be widely observed on the western coast of the Strait near Ganzirri [184].

3.3 Physical properties and circulation pattern in the Strait of Messina

To the knowledge of the author, the recorded data files of the basic physical parameters (water temperature and salinity) in the Strait of Messina and its vicinity

are scarce. This may result from the complicated dynamics of the Strait created by the strong current regime and turbulence that exists there. The most relevant data available for these two important oceanographic parameters come from field work [139, 141]. Tables (3.1) and (3.2) show, respectively, the recorded water temperature and the salinity in the vicinity of the Strait of Messina. The parameters are measured on a layer basis from the surface to the allowed depth at the field stations shown in Figure 3.4. The anchored currentmeters record temperatures and salinities simultaneously with current speed and direction.

The water circulation system in the Strait of Messina is the result of two dynamical effects, which take place in the Strait: hydrological and tidal effects. The former is considered as the usual classical effect observed in any strait due to the vertical haline structure and density differences between water layers. The latter, on the other hand, is of special concern in the case of the Strait of Messina.

Waters in the Strait of Messina have two sources: the Tyrrhenian Sea (north) and the Ionian Sea (south). The hydrological current of the two-layer structure in the Strait of Messina (Fig. 3.5) results from the difference in the vertical haline structure between the water masses of the superficial lighter Tyrrhenian Sea (~ 38.00 psu) and the denser Ionian Sea (~ 38.80 psu). In addition, when the waters of the two seas meet in the Strait of Messina, the water of the Ionian Sea, due to the large upwelling process in the southern extremity of the Strait, is colder and denser than that of the Tyrrhenian Sea [182]. Consequently, the two-layer flow system is established along the Strait of Messina, in which the Tyrrhenian water flows southward occupying the superficial layer to a depth of 30 m [48, 182] and the Ionian water flows northward in the lower layer from 30 m to the bottom. This system may occasionally be reversed due to changes in the salinity distribution, as was recorded on 24 and 25 October 1995 when a reverse flow system occurred contrary to the usual situation [159]. The longitudinal velocity component of this hydrological current is much more important than the transversal one [139].

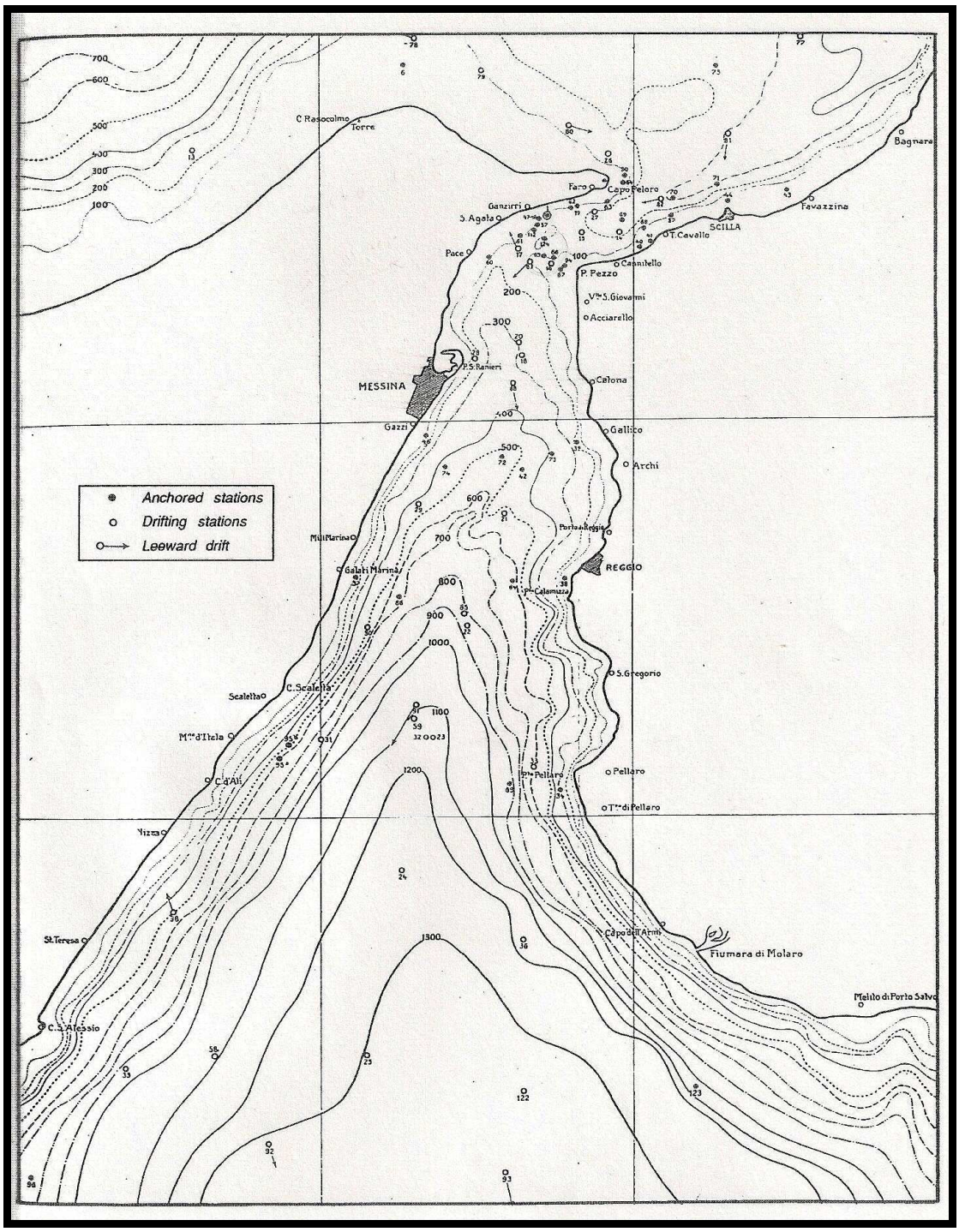

Figure 3.4: Measurement stations in the Strait of Messina and its vicinity where water temperature and salinity were recorded [186]

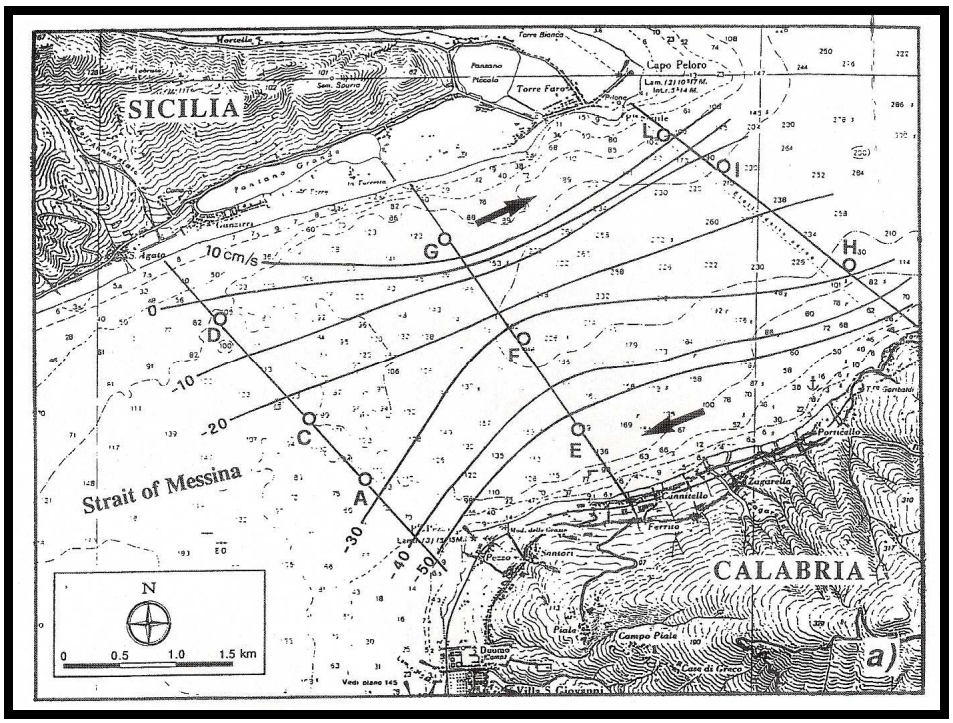

(a)

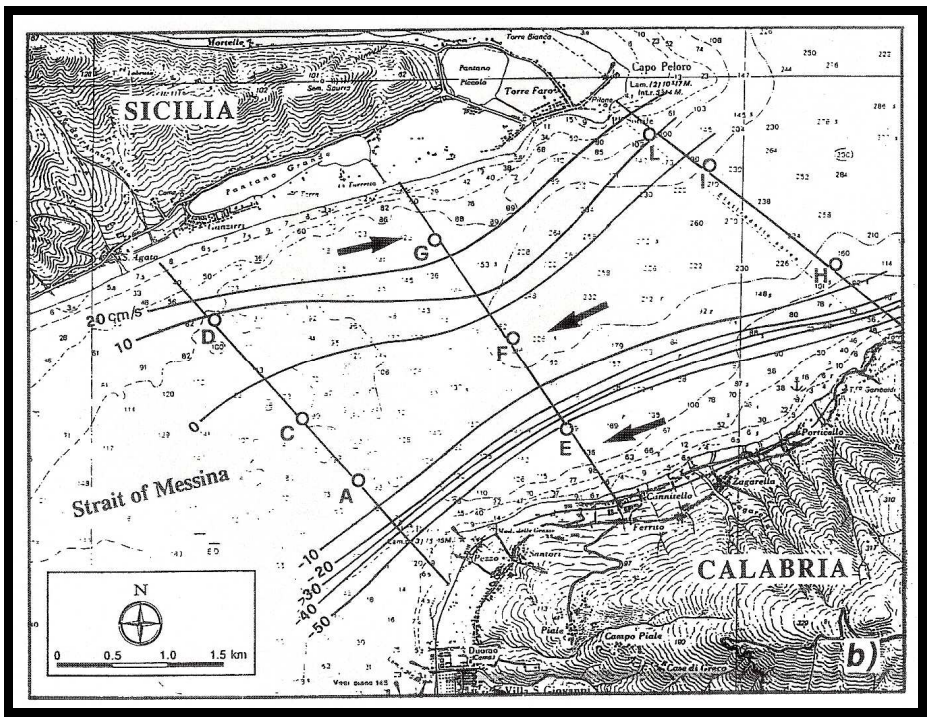

(b)

Figure 3.5: Behaviour of Temperature and Salinity variations resulting in (a) surface current from the Tyrrhenian Sea towards the Ionian Sea and (b) subsurface current in the reverse direction [186]

Depth (m)	Mar.	Apr.	May	June	Jul.-Aug.	Sept.	Oct.
0	13.0-13.5	14.5-14.8	17.9-20.9	18.2-23.5	21.6-27.1	23.3-24.0	20.1-21.0
5	13.5-13.9	14.4-14.8	17.6-18.9	17.0-23.0	21.4-25.5	23.3-23.7	19.9-20.7
10	13.5-13.8	14.3-14.4	14.5-17.8	15.0-22.0	20.8-25.5	22.3-23.7	19.8-20.7
20	13.5-13.7		14.1-15.9	14.5-20.5	20.6-25.3	19.5-23.2	19.2-20.7
25			13.8-15.8	13.8-19.0	19.7-22.0	18.0-22.7	19.1-20.7
50	13.6-13.7	13.6-14.2	13.7-15.6	13.7-17.8	14.8-16.6	15.5-16.3	17.1-20.5
75	13.6-14.1	13.6-14.2	13.6-14.1	13.6-15.0	14.2-15.1	14.6	15.9-16.7
100	13.6-14.2		13.6-14.1	13.6-14.3	13.6-14.7	14.3	15.4
150			13.7-14.1	13.7-14.3	13.7-14.3	14.3	
200			13.7-14.1	15.7-14.5	13.7-14.3		14.7
250			13.8-14.1		13.8-14.3	14.3	
350			13.9-14.1		13.9-14.3		

Table 3.1: Recorded water temperature range (℃) in the Strait of Messina in the vicinity of the Tyrrhenian Sea [186]

Depth (m)	Ionian Sea	Tyrrhenian Sea
0	38.06 – 38.22	37.50 – 38.10
30	38.17 – 38.57	37.70 – 38.30
100	38.30 – 38.62	37.70 – 38.46
200	38.64 – 38.68	38.26 – 38.62
500	38.66 – 38.75	38.66 – 38.70
1000	38.66 – 38.78	38.50 – 38.58

Table 3.2: Recorded salinity range (psu) in the vicinity of the Strait of Messina [186]

The hydrological current in the Strait of Messina has a velocity of ~ 0.13 m/s in its lower layer and a maximum velocity of ~ 0.10 m/s in its superficial layer [48, 187]. These velocity magnitudes may increase to 50 cm/s under the influence of wind and the upwelling process [140]. This means that the exchange flow can strongly fluctuate depending on wind and air pressure changes [158].

Beside this hydrological current regime, tides have strong effects on the circulation dynamics within the Strait of Messina. Strong tidal currents, which dominate the Strait, are mainly due to tides in the Tyrrhenian and Ionian Seas whose phase is almost opposite, approximately 180° [48, 139, 140, 159]. This tidal phase difference is associated with an amplitude range of 0.27 m between the two extremities of the Strait [140, 161, 187]. In general, the flood stream occurs when the current is directed toward the Tyrrhenian Sea, and the ebb stream occurs when the flow is towards the Ionian Sea [167, 188]. Due to this phase and amplitude differences between the two extremities of the Strait, in addition to the natural morphometry of the coastlines, the velocities of tidal currents in the Strait of Messina are intensive and have extreme values in the context of the Mediterranean Sea. The highest velocity value is recorded at the sill region where its topography together with the natural morphometric constriction in the Strait's borders, play an important role in increasing and enhancing the flow. The maximum velocities recorded in the sill region vary between 1.8 m/s to more than 3 m/s [139, 141, 158, 167, 189]. The M_2, S_2 and K_1 components are the major harmonic tidal constituents [190], with a maximum total velocity value of around 2.30 m/s [160]. Such high velocities demonstrate the potential of the Strait of Messina for consideration as a renewable energy resource using the tidal current phenomenon.

Eddies are another oceanographic feature associated with the current pattern in the Strait of Messina. The different characteristics of these eddies have been specified and their cause has been referred to the shear instabilities between surface and bottom waters [157].

3.4 Tides in the Strait of Messina

It is obvious now that the tidal phenomenon is of special importance in the Strait of Messina. Indeed, tides may be considered as the main driving force for the intensive currents seen and measured along the Strait. Due to this fact, the physical tidal phenomenon in the Strait of Messina and the tidal harmonic constituents have been the subject of research and study since early days.

Tides in the Strait of Messina are of a semidiurnal type. The importance of tides in the Strait of Messina derives not only from being a main driving force for the current

there but also from the fact that Messina is an amphidromic point for the tides of the two main basins of the Mediterranean Sea [191, 192]. Figure 3.6 is a schematic representation of the amphidromic point in the Strait of Messina.

The initial attempt to explain the tidal dynamics in the Strait of Messina was through a proposed scheme of tidal oscillations generated by the M_2 tide [193]. This scheme gave numerical solutions to the linear tidal equations. The Darwin method was applied [139] and successfully led to obtaining some tidal harmonic components for one of the 100 stations which were distributed all over the area of the Strait. At this station, which was located near the northern tip of the Strait (38° 15.15' N; 15° 37.15'E), the current meter was moored for 15 consecutive days [192]. The computed harmonic components [139] are: M_2, M_4, S_2, N_2, K_2, K_1, P_1 and O_1 (Tables 3.3 and 3.4). From this analysis, the M_2 component appears to be of particular importance in the Strait of Messina. The theoretical results [139] were later confirmed by experimental work [194]. This agreement between field and experimental results confirms that tides are the basic components of currents along the Strait of Messina. The linear and the non-linear tidal components in the sill region have been investigated [140]. Results confirm the outcomes [139] and show the importance of tidal currents in the Strait of Messina. These results also reveal a true thermocline at the depth of 20 m, which was not obvious in any previous study. This thermocline surprisingly occurs at this depth even with the apparent turbulent superficial tidal current in the Strait of Messina. This has been analytically explained [140] by the exceeded effect of nonlinear terms over the linear one at that depth, and the confirmed strong influence of astronomical factors on the thermal water regime. Therefore, this is considered as a mathematical thermocline rather than an observational one. The data sets and the results [139] have been appropriately studied and displayed [191]. In addition, a numerical model to discuss the tidal phenomenon in the Strait of Messina has been represented.

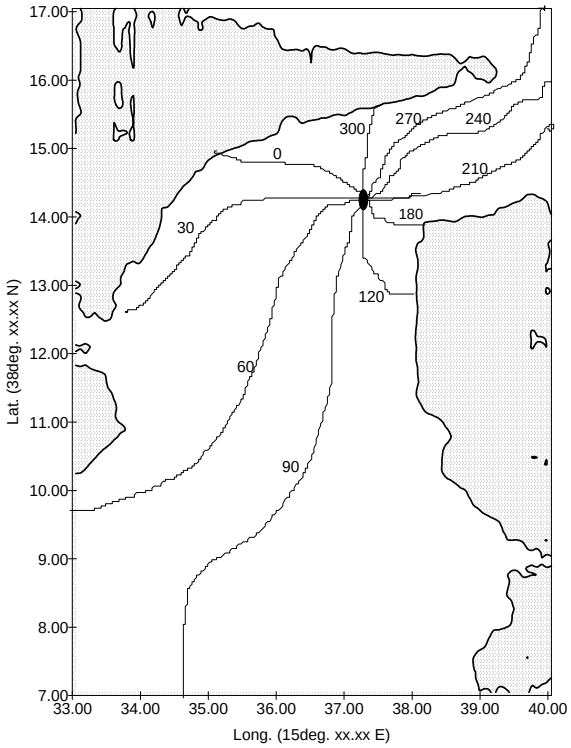

Figure 3.6: A schematic representation of the amphidromic point in the Strait of Messina

Depth (m)	M_2	M_4	S_2	N_2	K_2	K_1	P_1	O_1
5	131	11	35	20	10	34	10	14
10	126	11	34	19	9	29	10	11
20	124	13	30	19	8	29	10	11
30	116	10	35	17	10	30	10	13
50	115	9	36	17	10	29	10	15
90	107	8	31	16	8	31	10	13

Table 3.3: Tidal harmonic constituent velocities (cm/s) at station No. 1 in Vercelli's work [191]

Depth (m)	M_2	M_4	S_2	N_2	K_2	K_1	P_1	O_1
5	131	86	148	125	148	74	74	58
10	130	79	150	124	150	74	74	73
20	130	76	150	124	136	73	73	91
30	129	60	139	123	139	64	64	97
50	129	32	132	123	132	59	59	100
90	130	0	137	124	137	66	66	100

Table 3.4: Tidal harmonic constituent phases (ϑ) at station No. 1 in Vercelli's work [191]

Having discussed the tidal behaviour in the Strait of Messina (phase, velocity and intensity), by recalling the facts about the other major straits within the Mediterranean Sea that have been discussed in chapter two of this thesis and by fulfilling the basic criterion of tidal current velocity required to consider a tidal current resource to harness energy, it is now convenient to choose the Strait of Messina as an exceptional suitable place within the Mediterranean basin to be used to harness energy from tidal currents. However, it is not sufficient just to select a place for the energy extraction process using tidal currents. The process of harnessing energy by deploying tidal turbines in the marine environment will, to some extent affect the surrounding environment. Therefore, it is important to evaluate and assess the expected impact on the ecosystem prior to any actual work in order to highlight the mitigation process and to propose an applied monitoring program to be in-force during the project operation. A full desk-based Environmental Impact Assessment (EIA) study is carried out for the case of the Strait of Messina in order to benefit from its massive tidal currents for the extraction of energy with the least possible impact on the surrounding environment. This is discussed in detail in the next section.

3.5 Environmental Impact Assessment (EIA) of the tidal current energy resource in the Strait of Messina

In the following discussion, a desk-based Environmental Impact Assessment (EIA) for the tidal current energy resource in the Strait of Messina is presented in detail. For any actual project, the points discussed in this EIA should be examined practically for the specified site of work prior to carrying out any work. In the following sub-sections the aims of the EIA, the European Union (EU) environmental legislation, the environmental keys assessment and a monitoring programme are discussed.

3.5.1. Tidal energy and its development

Tidal power is one of the earliest renewable energy forms used by man. Tidal power has been used since the 11^{th} century when small dams were built along ocean estuaries and small streams [28]. However, the earliest-known tide mill, which is located in London on the River Fleet, may date back to Roman times, and the earliest

excavated tide mill, dating from 787, is the Nendrum Monastery mill on an island in Strangford Lough in Northern Ireland [195]. The difference in water level was used to drive wheels to mill grains and, in the modern age, to drive turbines to produce electricity. This has come to be known as “tidal barrage” technology. The main requirement for cost-effective electric energy using this approach is to have a high tidal range. This range has been reported [15, 20, 29] to be at least 5 m. Tidal barrage development is presently limited because of the high capital costs of such systems, the long construction time and environmental impact concerns [196].

In the last few decades, technology to exploit the kinetic energy in regions of extreme tidal currents has also been considered. Pre-commercialisation examples of this technology [197-199] are now undergoing full scale testing, and the future for this technology approach appears bright. It has been well documented that tidal currents throughout Europe and the UK represent a significant sustainable energy resource and it is widely accepted that tidal current power could supply energy to the EU and the UK [200, 201].

Two principal types of tidal currents energy converters are presently the target of research to produce electricity. The first type uses tidal currents to rotate blades attached to vertical structures, similar to the way in which wind-energy is harnessed by turbines. The second type uses tidal currents to create an oscillatory motion of hydroplanes.

The technologies proposed for harnessing energy from tidal currents to generate electricity will not directly produce any carbon emissions or any harmful by-product that may affect the resource itself or the surrounding environment. This is of major significance given the need to reduce carbon emissions reflected in various EU carbon reduction targets. Technically, it is possible to extract energy from tidal currents with no pollution during operation and with a presumed low environmental impact [31]. However, this cannot be a one hundred per cent guaranteed because anything which is introduced to the marine ecosystem will potentially affect its balance. Generally speaking, the environmental impacts from tidal turbines are believed to be limited [196, 233, 234]. The main effects may be on shipping, navigation and fishing. Additionally, harnessing energy from tidal currents will reduce the local current velocity and hence impact on the local ecology and the

sediment transport processes [22, 23, 34, 35]. So even, a ‘renewable’ energy concept with all its socio-environmental benefits in terms of sustainability, local security of supply and low carbon footprint still has to undergo rigorous environmental assessment.

3.5.2. Aim of the Environmental Impact Assessment

An Environmental Impact Assessment (EIA) may be defined as the examination of the likely impacts on the surrounding environment that will result from any proposed project prior to that project being started.

EIA, according to legislation, is a process required under the terms of EU Directive 97/11/EC, which amends the terms set out in Directive 85/337/EC on the assessment of the effects of certain public and private projects on the environment [200]. An EIA can accordingly be considered as a process of identifying, getting and predicting information on the potential impacts of a proposed action or development on the environment and to propose the measures to address and mitigate these impacts.

Paragraph 2 (C) of the second schedule of the 1989 European Regulations outlines the following headings as specified information which shall be included in the environment assessment [202]:

“A description of the likely significant effect, direct and indirect, on the environment of the development, explained by relevance to its impacts on human beings, flora, fauna, soil, water, air, climate, material, landscapes and the cultural heritage”.

Thus, we can specify the aim of our EIA in the following two points:

1. To assess the environmental impacts associated with exploitation of a tidal current energy system.
2. To set up a programme to quantify their importance practically.

3.5.3. The European Union (EU) Environmental Legislation

It is widely accepted that tidal current power can generate an efficient and consistent energy supply, especially with the continuing research and development efforts in the EU. However, a principal barrier that inhibits this development is the environmental uncertainty issue related to the tidal current technology and how it may affect the marine environment.

Tidal current energy appears to have the least environmental impacts among other renewables although most, if not all, of the renewable energy resources developed so far have some adverse impact to some degree [203]. For tidal current energy to be

economically efficient, it is envisaged that devices will need to be deployed in clusters or ‘farms’. This centralisation has the potential for adverse environmental impact [200].

There have been a few generic studies investigating the topic of the environmental impacts of marine renewable energy. Environmental aspects of tidal barrage schemes have been evaluated [204-206]. However, there has, as yet, been no specific study into the impact of tidal-current energy schemes [206].

There are eleven principles listed in the first EU environmental programme released in the year 1972. These principles are basics that are always present even with any changes and modifications in acts, codes and laws. These principles [207] are:

1. Prevention is better than cure. This principle was taken up again under the 4th environmental action programme.
2. Environmental Impact Assessment should be considered at the earliest stage in decision-making.
3. Exploitation of nature which causes significant damage to the ecological balance must be avoided.
4. Scientific knowledge should be improved to enable action to be taken.
5. The ‘polluter pays’ principle, i.e. polluter should pay for repairing any environmental damage.
6. Activities in one Member State should not have detrimental effects on the environment in another.
7. Environmental policies in all member countries must take into account the interests of the developing countries.
8. The EU and its member countries should promote international and worldwide environmental protection through international organizations.
9. Environmental protection is everyone’s responsibility and therefore education is necessary.
10. Environmental protection measures should be taken at the most appropriate level taking into account the type of pollution and the action needed.
11. National environmental programmes should be co-ordinated on the basis of a common long term concept and national policies should be harmonised within the EU community.

The 5th environmental action programme for sustainable development within the EU covered the period 1992-2000 [208]. This action programme focused on reducing pollution levels, implementing legislation that would benefit EU citizens and integrating the environmental dimension into all areas of commission policies. The programme, also aimed at achieving a better environmental protection, has two main terms [56]:

1. Defining the term of sustainable development as “development which meets the needs of the present without compromising the ability of future generations to meet their own needs”.
2. Measuring the environmental degradation.

The programme targets five sectors:

1. Energy.
2. Transport.
3. Tourism.
4. Agriculture.
5. Manufacturing industry.

Article 130r in title VII/part II of the treaty of Rome 1958 identifies three objectives in relation to the environment. These are:

1. The preservation, protection and improvement of the quality of the environment.
2. To contribute towards protection of human health.
3. Ensure a prudent and rational usage of natural resources.

Regarding the Aquatic Environment, the EU environmental legislation may be set in three broad categories [207]. These are:

1. Regulations setting water quality objectives for various uses.
2. Directives to limit or prohibit discharges of dangerous substances into waters by industrial plants.
3. Provisions on marine pollution, which aim to put an end to marine pollution in order to protect the North Sea, the Baltic and the Mediterranean, in addition to prevent pollution in these aquatic environments from land-based sources.

What is of concern in our case study is Category 3, which conserves the marine environment from any type of pollution resulting from any source or due to the use of any technology.

The main codes dealing with this case are:

Council Decision 75/437/EEC [209] aimed at preventing marine pollution from land-based sources (i.e. that emanating from watercourses, underwater pipelines and ports) in the northeast Atlantic and Arctic Oceans, the North and Baltic Seas and parts of the Mediterranean. This was extended in 1986 to cover marine pollution by emissions into the atmosphere. A proposal on the introduction of emergency procedures to combat marine pollution by oil and other pollutants following accidents has been under consideration since 1983, but a set of measures has yet to be agreed by the Council of Ministers for the Environment. In 1990 it was agreed to impose a total ban by 1993 on the dumping of industrial waste in the North Sea though it was permitted to dump PCBs until 1999.

Directive 96/61/EC on INTEGRATED POLLUTION CONTROL [210] aims to modify and supplement existing Community legislation concerning the prevention and control of pollution from industrial plants in order to achieve an integrated approach to pollution prevention so as to preserve and improve the quality of the environment, protect human health and to ensure a rational utilisation of natural resources. It lays down the criteria by which Member States will grant operating licences to a range of industries and processes which come within its scope. The impacts of emissions to all media (air, water and soil) have to be taken into consideration and minimised in an integrated fashion, without placing an undue pollution-load on any medium.

Dealing with the conservation and protection of living organisms from any external effect, the following legislation were set by the EU:

Council directive 78/659/EEC (FRESH WATER FOR FISH) [211]: the aim of this Directive is to set quality objectives for fresh waters so as to protect fish life from the discharge of pollutant substances into waters. The Directive laid out sampling and monitoring procedures and definitions of conformity between Member States. Under the Directive, Member States must designate fresh waters needing protection in order to support fish life.

Council Directive 79/923/EEC (Quality of Shellfish Waters) [212] is intended to protect and improve the quality of coastal and brackish waters (again designated by Member States) for shellfish growth.

Council Regulation EEC/348/81 (CETACEANS) [207] requires a licence for imports of whale parts and products and prohibited the issue of such a licence for products used for commercial purposes after January 1982.

Council Regulation EEC/3418/83 [207] sets out requirements for a uniform system of permits and licensing governing import and export of specimens listed under the Convention on Trade in Endangered Species.

The definition of renewable energy resources used in the EU legislation may be found in **EU Directive 2001/77/EC** [213], as follows:

2 (a) Renewable energy resources shall mean renewable, non-fossil energy sources (wind, solar, geothermal, waves, tidal, hydropower, bio-mass, landfill gas, sewage treatment plant gas and bio-gas)

For tide, wave and wind power generation, the EU [214] set the following directives:

European Legislation	Provisions
98/352/EC Decision concerning a multi-annual programme for the promotion of renewable energy sources in the Community.	Encourages Member States to increase renewable share of energy supply from 4% to 8% by 2005.
Directive 2001/77/EC of the European Parliament and of the Council of 27 September 2001 on the promotion of electricity produced from renewable energy sources in the internal electricity market.	A proposal for a directive on the promotion of electricity from renewable energy sources has been unveiled aiming to double 'green' energy. The non-binding indicative national target for renewable sources for the UK is from 1.7% in 1997 to 10% in 2010. The Scottish Government has set the target for energy production from renewable sources at 18% by 2010.

Table 3.5: European legislation for tide, wave and wind power generation

In January 2008, a new EU directive on the use of energy from renewables was approved. The new plan targets an increase in the level of the EU power generated from renewables by 2020 to 20% [215]. This proportion is proposed to increase to reach 50% and more by 2040/2050 [216].

3.5.4. Factors affecting the choice of location of a tidal turbine

There are several factors which must be taken into account when considering the assessment of the tidal current energy resource in the Strait of Messina. These factors will affect not only the choice of the mooring location and fixation of the turbine but they will also affect the surrounding environment during long-term operation of the turbine. These factors include:

3.5.4.1. The tidal resource itself

Operation of a tidal turbine is dependent on the nature of marine currents in which it is situated. Tidal currents are stronger where the flow is constrained by topographic features, e.g. sills, estuaries and irregular coastlines. Areas where significant tidal currents exist are generally found in regions around headlands and narrow straits. It has been suggested that turbines need a mean spring peak tidal current velocity of at least 2 m/s in order to operate effectively. Higher velocities are more desirable and have more potential for economic operation. Underlying the tidally driven flow in the Strait of Messina, there exists a persistent density driven flow. This hydrodynamical current is a two-layered current system in which the lighter Tyrrhenian waters occupy the superficial layer and the denser Ionian waters fill the lower layer. This density-current flows with a velocity of order of magnitude of 10 cm/s in both layers and this may increase to 50 cm/s under the influence of wind and the upwelling process [140]. This means that exchange flows can strongly fluctuate depending on wind and air pressure changes [158].

Tidal hydrodynamics have significant impacts on flow development within the Strait of Messina. The strong tidal current that dominates the Strait is mainly due to the tides in the Tyrrhenian and Ionian Seas, which are almost totally out-of-phase [48, 139, 140, 159]. This phase difference is associated with a maximum amplitude range of 0.27 m that occurs between the two extremities of the Strait [140, 161]. In general, the flood is directed toward the Tyrrhenian Sea, and the ebb towards the Ionian Sea [188]. The highest speed is recorded at the sill region, where the natural topographic constriction in the Strait's borders enhances flow velocities through the passage. The maximum velocities recorded in the region vary between 1.8 m/s to more than 3 m/s [139, 141, 158, 167, 189]. The M_2, S_2 and K_1 components are the major harmonic tidal constituents with maximum total velocity value around 2.30 m/s [160]. Such

high velocities demonstrate the potential of the Strait of Messina for consideration as a renewable energy resource using the tidal current phenomenon. It should, however, always be appreciated that high tidal current speeds represent a necessary but not sufficient indicator of potential for energy extraction.

3.5.4.2. Water depth

First-generation tidal turbine concepts that have reached the stage of full-scale pre-commercialisation testing tend to have specific depth requirements and have to be fixed in water of a depth ranging between 20 m and 45 m [33, 200, 217]. This limitation is generally related to operational constraints regarding the installation and continuing maintenance of the proposed device concepts. Second generation technologies may overcome this constraint.

In the Strait of Messina, this constraint restricts potential locations for tidal turbines to particular near-shore coastal areas where the tidal currents reach suitable velocities and the water depth does not exceed 45 m.

3.5.4.3. Distance from the coast

This factor may affect the turbine location in two ways:

1. Economically: the shorter the distance from the coast, the shorter the cables needed to connect the turbine to the electricity-grid on land. This means a reduction in capital costs relating to the construction of the farm of devices.
2. Operationally: moving far offshore generally reduces the tidal currents.

Care must be taken not to affect other coastal human activities with the choice of the suitable distance to allocate the turbine.

As the Strait of Messina is an important area for maritime navigation and leisure activities, this may also impose a further constraint on the location of the farm.

3.5.4.4. Wave conditions

As tidal turbines operate totally beneath the water surface, the wave action will have only limited influence on its operation, although it is acknowledged that this is a subject of ongoing research [218]. The Strait of Messina is known for both surface and internal wave propagation. Surface waves, as shown in Figure 3.7, generally propagate southward, following the hydrological current scheme in the Strait. Internal waves, as shown in Figure 3.8, appear to follow two propagation patterns within the Strait: the first propagates northward with an average speed of 1 m/s and

the second propagates southward with an average speed of 0.90 m/s [158]. These waves are observed at the northern and southern extremities of the Strait [219, 220]. As the recommended location for the deployment of a turbine is near the sill at the Strait's main constriction, where tidal current is enhanced to reach its peak velocity (~ 3 m/s), it is likely that the influence of waves on the location of tidal turbines within the Strait itself will be minimal.

Figure 3.7: Surface wave propagation in the Strait of Messina (http://earthobservatory.nasa.gov/Newsroom/NewImages/Images/messina_ast_2003223_lrg.jpg)

Figure 3.8: Propagation of internal wave sets in the Strait of Messina viewed by ERS-1 [158]

3.5.4.5. Seabed configuration and dredging areas

The seabed configuration affects the choice of the location of the installation of tidal plants. It is generally preferable to have bedrock, or at least a stable bed material to

allow the safe installation of the body of the support structure of the turbine. Additionally, it is preferable if the seabed is flat in order to facilitate positioning of the device and to limit local three-dimensional flow structures. The turbidity resulting from flow irregularity may increase the load on the turbine and, hence, affect its performance.

The bed of the Strait of Messina is defined as gravely sandy rocky, and is generally well suited for the siting of turbines. However, an important bed feature in the Strait of Messina is propagation of sand waves. The locations and the behaviour of these waves have been extensively investigated, e.g. [160, 163, 164]. Results reveal that these waves are present at the northern and southern extremities of the Strait and rarely found within its central area. Hence, the location of the tidal turbines in the narrows region of the Strait will not be affected by this phenomenon in any way.

3.5.4.6. Navigation

The location of the tidal turbine farm needs to be chosen to avoid major shipping and navigation routes. The farm may not, on the other hand, affect the movement of small leisure crafts.

The Strait of Messina is the main route used to link the Italian Peninsula (Villa San Giovanni and Reggio Calabria) to Sicily (Messina) via ferry transport. Care must be taken to site the farm in a location that does not interfere with the well defined ferry routes (Fig. 3.9). The size of the rotor of the deployed turbine, according to the navigation activity and water depth, has to be carefully determined. The top of the rotor needs to be at the lowest astronomic tide (LAT) minus 1.5 m for the lowest negative storm surge, minus 2.5 m for the trough of a 5 m wave and minus a further 5 m to minimise the potential for damage from shipping and waves [34].

Navigation between the Tyrrhenian Sea (north) and Ionian Sea (south) along the main axis of the Strait is difficult due to the harsh conditions resulting from the currents and winds that dominate the area. As the areas with the greatest tidal currents, in the sill region of the Strait and its surroundings, are of most interest for siting any farm of devices, there appears to be very limited conflict of interest with major shipping in this instance, as the navigation channels avoid the shallower, extreme current regions.

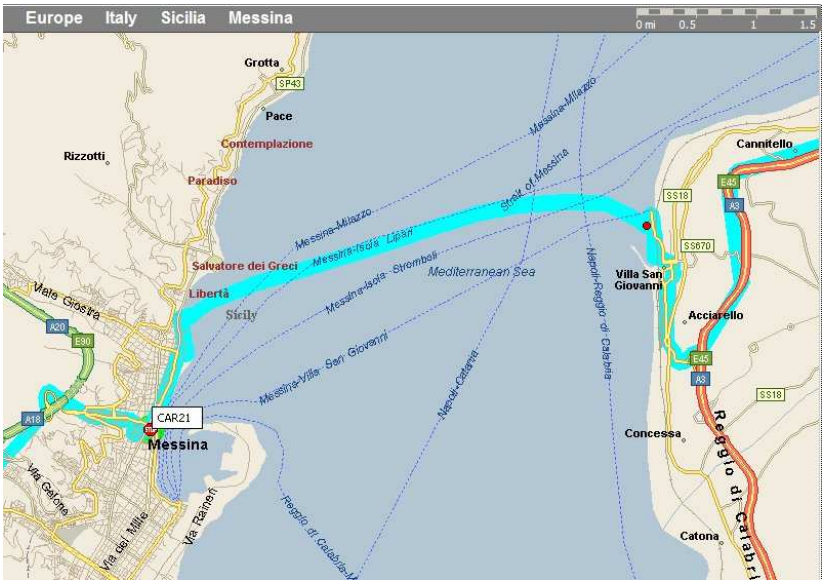

Figure 3.9: The ferry routes between Italy and Sicily (www.v-sol.co.uk/gumball3000/imagesmaps/Messina%20Ferry.jpg)

3.5.4.7. Fishing and Biomass

Even though the allocation of tidal turbines in the marine environment may not affect the fisheries themselves, it may have an impact on the fishing processes. Care must be taken to choose a place as far as possible from the major fishing areas. However, as farm placement potentially creates a fisheries exclusion zone in the vicinity, there is potential that this exclusion zone could provide a haven for local fish populations and hence enhance fish species in the Strait.

Having discussed the factors affecting the choice of location of tidal turbines, it is now possible to identify and assess the environmental impacts expected from harnessing energy from the tidal current in the Strait of Messina. The advocated methodology [221] has been applied. This method consists of the identification of the key environment and project interactions using a simple check-list structure to construct an interaction matrix. The latter may be defined as a semi-quantitative method to identify the main components of the ecosystem and to assess the interactions among them [222]. The interaction matrix applied in this study is extended to incorporate all aspects of the EIA process. The likelihood and the interaction magnitudes are all considered using an interaction matrix model. This approach is used in many environmental research studies, e.g. [200, 221-224].

3.5.5. Identification of key project activities

The key project activities for the four phases of the project are given in Table (3.6).

Transportation	• Movement of installation equipment • Transportation of device components (e.g. foundations, towers, nacelles, blades… etc.)
Installation	• Physical presence of installation equipment • Piling foundations (if required) • Grouting/cementing of material during installation • Disposal of spoil from drilling • Jack-up crane Barges • Barge installation cables • Power Cable installation • Construction activities
Operations and Maintenance (O&M)	• Overall structure presence • Rotor effects • Extraction of tidal current energy • Routine maintenance/emergency repairs • Physicality of grid connections • Overall generation of electricity
Decommissioning	• Physical removal of device etc. • Disposal • Presence of decommissioning Vessels

Table 3.6: Key Project Activities

3.5.6. Identification of environmental impacts

The impacts of installation, O&M and decommissioning processes on the different environmental variables are shown in the matrix (3.7). This matrix may be considered as a conceptual model of the environmental evaluation. In this study, the

different ecological parameters that may be affected during each operation phase, as hypothetically proposed by the author in this case, are listed. These may vary from one assessor to another, depending on the area of the study and its environment.

	Tidal current	Wave climate	Noise	Sedimentation	Seabed	Turbidity	Coast	Benthos	Pelagic organisms	Sea birds	Cetaceans	Fishing	Navigation	Cables	Tourism	Grid infrastructure	Local infrastructure	Employment	Energy
Installation phase																			
Physical installation					•			•	•		•	•	•	•	•	•	•	•	
Piling foundation			•	•	•	•		•	•		•	•	•	•	•	•	•	•	
Cementing				•		•		•	•		•	•	•	•	•	•	•	•	
Jack up Barges			•	•	•	•		•	•		•		•		•			•	
Structure installation			•	•	•	•	•	•	•		•	•	•	•	•	•	•	•	
Cables installation			•	•	•	•	•	•	•		•	•	•	•	•	•	•	•	
Land based activities			•	•			•	•	•	•					•	•	•	•	
Operation phase																			
O & M			•	•		•		•	•	•	•	•	•	•	•	•	•	•	•
Rotor effect	•	•	•	•	•	•	•	•	•	•	•	•	•		•	•	•	•	
Decommissioning																			
Vessels			•		•					•	•	•	•		•	•	•	•	
Structure removal	•		•	•	•	•	•	•	•	•	•	•	•		•				
Disposal							•								•			•	

Table 3.7: Conceptual model of the environmental evaluation

3.5.7. The significance of the environmental impacts

Tables (3.8) and (3.9) represent the degree of likelihood of occurrence and the level of magnitude of the environmental impacts, respectively. The combination of both tables, according to the author's point of view, appears in matrix (3.10). This matrix assists in decision-making and the assessment of the impact of the project on the marine environment. The expected major impacts in the case of harnessing energy from tidal currents in the Strait of Messina, according to Table (3.10), based on the author's point of view, does not exceed 10% of the total expected impacts.

Occurrence	Level
Continuous	5
High	4
Moderate	3
Minimum	2
One-off event	1

Table 3.8: Degrees of likelihood of impact occurrence

Magnitude level	Definition
Major	Impacts are severe. They may have an effect on internationally or nationally protected species, designated sites or habitats Possible effect may be on infrastructure and local residences. These are difficult to restore.
Moderate	Impacts leading to short-term damage with recovery expected within 2 years. May have an effect on protected locally-important sites. Mitigation and remedy possible with consultation.
Minor	Changes caused by impact are within the scope of natural variability. They have little effects on the surrounding environment.
Positive	These impacts may enhance the area either biologically or socio-economically, i.e. they benefit the local, regional and national economy or increase tourism etc.

Table 3.9: Levels of impact magnitudes

	Tidal current	Wave climate	Noise	Sedimentation	Seabed	Turbidity	Coast	Benthos	Pelagic organisms	Sea birds	Cetaceans	Fishing	Navigation	Cables	Tourism	Grid infrastructure	Local infrastructure	Employment	Energy
Installation phase																			
Physical installation					1			2	1		3	1	3	1	1	1	1	1	
Piling foundation			1	1	1	1		1	1		1	1	1	1	1	1	1	1	
Cementing				1		1		1	1		1	1	1	1	1	1		1	
Jack up Barges			1	1	1	1		1	1		1		1		1	1	1	1	
Structure installation			1	1	1	1	1	1	1	1	1	1	1	1	1	1	1	1	
Cables installation			1	1	1	1	1	1	1		1	1	1	1	1	1	1	1	
Land based activities			1	1			1	1	1	1					2	1	2	2	
Operation phase																			
O & M	4		3			3	2	2	3	3	3	3	3	3	3	2	3	3	4
Rotor effect	5	5	5	5	5	5	5	2	3	3	3	3	3		2	2	3	3	
Decommissioning																			
Vessels			1		1						1	1	1	1	1	1	1	1	
Structure removal	1		1	1	1	1	1	1	1	1	1	1	1		1	1	1	1	1
Disposal							1								2			1	

Table 3.10: Judgment matrix of the Environmental Impact Assessment (EIA) according to the author's point of view

3.5.8. Principal Environmental Impacts

The main sources of the observed environmental impacts may be classified into four categories [206]:

1. Kinetic Energy removal
2. Rotor and Support structure
3. Noise levels
4. Installation/Decommissioning disturbance

These sources have direct/indirect impacts on the following components of the marine environment:

1. Tidal current velocity
2. Tidal current dynamics

3. Waves
4. Sedimentation and seabed
5. Turbidity and water quality
6. Marine ecology

3.5.8.1. Impact of the Kinetic Energy removal

Harnessing energy from tidal flows passing within the domain of the turbine blades will affect the complex interaction dynamics between tidal flows and suspended matters in the region. Extracting energy will potentially modify the flow speed and, possibly, its direction. When the flow velocity is reduced, the deposition process of the suspended particles in the domain will be affected and the rate of deposition will be dependent on the particle sizes. Consequently, other environmental impacts will be associated with kinetic energy removal: deposition, turbidity and water column quality. The process of deposition will affect the benthic habitat of the area and may, if prolonged, modify the local water depth. In order to control the effect of Kinetic Energy removal and to diminish its impacts on the marine environment, it is important to restrict the harnessed energy to certain limits. Some researchers [23, 37, 217] have recommended this extraction does not exceed 10-20% of the flux. However, increasing understanding of the resource and the realisation that the kinetic flux is only part of the available energy has suggested to some that the available extraction can exceed the apparent kinetic flux. The ultimate extractable resource can be shown to be a function of the undisturbed kinetic flux and the geography of the site under investigation [43] and that, under some conditions, the available energy for artificial extraction can exceed the kinetic flux considerably. The clue for this logical exclamation lies in the fact that the tidal flow posses potential energy beside its kinetic one. Therefore the total energy flux is the sum of the two existing energies. In principle at least it should be possible to restrict the extraction of energy so that flow speed reductions are kept below predefined limits for environmental acceptability [225] and that this limit is a function of local hydrographic conditions as well as the undisturbed flow patterns. For the Strait of Messina, the situation will not be an exception. Care must be taken not to exceed the proposed limits of harnessing Kinetic Energy from the passing tidal flow, in order to protect the marine environment from the problem of accelerated rate of deposition.

3.5.8.2. Rotor and Support structure

The water column will be affected by the rotor movement, which results in the generation of vortices, turbulence in the water column, and an increase in the turbidity and possibly also in sedimentation. The biological habitat is also of high concern. Sea birds, even though they are not a part of the aquatic system may mistakenly judge shadowing when identifying fish shoals [200]. Fish species, and especially marine mammals, might face the danger of collision with active rotors. However, it is assumed that the fluid dynamics of the rotor may aid in protection from such collision risk [206]. For instance, the local pressure gradients set-up around a tidal device would be felt by fish and marine mammals, while the interpretation of such pressure gradients is an important part of their sensory and movement interaction. The Strait of Messina is known as a rich biological habitat; hence it would be of great interest to monitor any variation in the biological structure of the Strait during rotor operation in this early stage of development and deployment of full scale technology in the open sea environment.

The support structure of a rotor fixes the turbine in the correct position in terms of elevation from the seabed and orientation [226]. As with any structure submerged in the aquatic environment, this support structure will impact local flow dynamics in the surrounding domain. The impact from such a structure will appear in the reduction of current speed, the formation of vortices in front of the structure, the formation of lee-wake behind the structure, the generation of turbulence, the refraction of waves and the possible redistribution of erosion and deposition locations. The latter may, in the very long term, lead to alteration of the dominant seabed habitat.

On the other hand, the rotor support structure may serve as an artificial nursery and breeding ground. It has been documented [227] that offshore oil and gas structures can attract motile species such as fish. Also, the study performed to test the Vindeby offshore wind farm on the Danish coast revealed that test fishing conducted before and after installation of rotors and support structures found that fish yields increased and that fauna and flora generally improved [228]. This issue needs be tested in the Strait of Messina.

3.5.8.3. Noise levels

All gears and hydraulic systems will generate some noise and badly designed ones can generate considerable amounts [229]. Noise, which may result from using tidal current turbines, has two sources; the first comes during the installation phase with the associated construction processes: vessels' engines, propellers, drilling and piling. This will be a one-off source. The second source concerns noise emissions during the operation phase itself. This has to be tested and reduced to a minimal level as continuous noise may affect pelagic organisms. For instance, the noise levels of the SeaFlow tidal turbine have been assessed and been found to be insignificant [230, 231]. A similar acoustic test must be carried out for the deployed turbine in the case of the Strait of Messina especially with the abundance of the marine mammals that exist in the Strait. Generally speaking, seabed effects will depend on the intensity of vibrations and the nature of the bed and sediment characteristics, while mammals will be particularly affected by noise resulting from installation and operation. The Strait of Messina is famous for the different marine species inhabiting, migrating and spawning there. These include sperm and fin whales, dolphins, Tunas and Swordfish [166, 183, 232]. Whales and dolphins depend on sound for many vital functions and, therefore, are likely to be affected by the resulting noise. They differ in their sensitivity to noise levels and have different adaptations to overcome the extensive ambient noise. The degree to which noise may affect whale and dolphin communities, especially breeding, communication and survival has to be fully assessed and reviewed. This remains a significant research question. For Tunas and Swordfish, the Strait of Messina is an important location for spawning and migration. The noise may not affect the species directly but may affect their spawning areas within the Strait and the period and routes of migration.

A biological assessment of the chosen location would be preferred prior to any installation to get a real picture of marine biota.

3.5.8.4. Installation/Decommissioning disturbances

The installation/decommissioning of tidal turbines will affect the biomass, the seabed, the water column turbidity, the tidal velocity and the tidal dynamics.

Both installation/decommissioning will result in a general redistribution of benthic communities due to disturbance of the seabed by any of these two operations. Even

though the risk of direct mortality of demersal species is high in many chosen places, the Strait of Messina is not rich in such species [166]. This may not therefore be of high concern, and can be mitigated by observation of the chosen location for such species in any pre-development environmental baseline study. For the pelagic habitat, the impact of installation/decommissioning disturbance may be evident in the disturbance of spawning and breeding grounds.

Attention has to be given during the installation or the removal of tidal turbines to ensure that service vessels do not leak fuel or oil. Such a leakage may affect the chemical composition of the marine environment in the surrounding area and a serious problem of contamination might easily occur. Ultimately man himself, through feeding on species affected by this contamination may well be affected!

3.5.9. Monitoring Programme

In order to extract energy safely from the tidal current in the Strait of Messina, a monitoring programme must be set for each phase of the desired project: installation, O&M and decommissioning.

3.5.9.1. During the Installation Phase

A baseline survey has to be conducted to record all the biota in the chosen farm-location and along the intended cable route. If the chosen location is far to the northern or to the southern tip of the Strait, the sand waves and their propagation have to be studied prior to any development to avoid any effect they may have on the structure of the plant or on cable routing.

Care should be taken not to dump any harmful materials while fixing the support structure of the turbine blades, either from the service vessel (oil/fuel leakage) or from the installation process itself (any construction materials).

3.5.9.2. Operation and Maintenance (O&M) Phase

A log-book to record any emergency or abnormal situations and the action taken to resolve it must always be held in the management office of the project. Knowing, understanding and following the codes and laws set to conserve the marine environment are essential.

Even though with the large rapid dilution process due to the extreme tidal flow, it is recommended that a water column analysis should be performed periodically to

detect any harmful changes (oil leak, iron, copper…etc) in the composition of the water quality in the environment surrounding the tidal plant.

3.5.9.3. Decommissioning Phase

The same level of care taken while installing the plant has to be taken in the decommissioning phase too. Specifically this includes care regarding dumping of harmful materials and leaking of chemical substances from the decommissioned plant and decommissioning vessels. It also requires consideration of the impact on living communities (benthic and pelagic) present in the vicinity of the decommissioned structures.

3.5.10. Conclusion of the Environmental Impact Assessment

The belief that renewable energy has no environmental impact is not one hundred per cent correct. Even with all its socio-environmental benefits in terms of sustainability, local security of supply and a low carbon footprint, a renewable energy resource still has to undergo rigorous environmental assessment. In the present work, the conceptual model matrix showing the interaction between the different project phases and the environmental parameters is shown. It is necessary during any applied (actual) project, to magnify the likelihood of occurrence of the expected impacts in order to make the right decision and to judge the case accurately. In the case of the Strait of Messina the major impacts which may result from exploiting its tidal currents, according to the authors' judgment matrix, does not exceed 10% of the whole expected impacts. This percentage results from weighing the major impacts in this matrix to the total anticipated effects on the marine ecosystem in the Strait. The fulfilment of and respect to the environmental legislation and rules is also a must. The most positive point in the present study is that all expected impact can be minimised and limited by applying a meticulous monitoring programme during each phase of project, such as that described in the present study. It is strongly recommended in such type of projects to follow an adaptive monitoring scheme in which controlling the environmental quality comes not only from the environmental manager in the project team but also from some higher authorities that are able to detect, control and act in any emergency case or serious situation. Moreover, these authorities must have the right to postpone the project in case the managerial administration does not follow the environmental legislation as it should be. This

way the ecosystem is strictly secured and safe to the highest degree. The final intention of deploying and operating a clean sustainable renewable-energy technology making a sustainable contribution to the future energy-mix is significant enough to merit such an intensive monitoring programme. In addition, we should not allow our care and deep environmental concern stagnate promising technologies and possibilities in order to get sustainable and clean energy.

3.6 Chapter Conclusion

The Strait of Messina is a long (32 km), narrow (3-4.2 km) channel, which separates the main Italian peninsula from the Island of Sicily. The Strait connects the Tyrrhenian Sea (north) to the Ionian Sea (south). In this chapter a detailed bathymetric map is built for the Strait of Messina based on data extracted from Admiralty Chart [165]. Unlike elsewhere in the Mediterranean Sea basin, massive tidal currents exist along the Strait of Messina. These mainly result from the out-of-phase tidal characteristic between the Tyrrhenian and Ionian Seas, associated with a tidal range of 0.27 m between these two extremities. Tidal current velocities at spring peaks in the Strait of Messina vary between 1.8 to more than 3 m/s. In this chapter, the massive renewable tidal current resource in the Strait of Messina is environmentally assessed by using the interactive matrix approach. The expected major impacts in the case of harnessing energy from tidal currents in the Strait of Messina do not exceed 10% of the total expected impacts. In addition, a monitoring programme is proposed at the end of the EIA study in order to highlight the main points to be considered during each phase of energy extraction process. An adaptive monitoring system is strongly recommended for the marine renewable projects.

CHAPTER 4
OCEAN MODELLING

An Overview

Chapter four consists of five sections, the first of which is a general introduction to numerical modelling and explains how this can be a useful tool for the investigation of different topics in oceanography and engineering. Section two briefly highlights the basic hydrodynamical equations used in numerical modelling. Some numerical trials simulating the circulation pattern in the Mediterranean Sea are discussed in section three. Sections four and five deal with tidal models. The first is a discussion of some worldwide tidal models, while the second briefly covers the few numerical trials which simulate tides in the Mediterranean Sea.

4.1 Introduction

Theory, observation and numerical modelling are three distinct approaches used to study and describe the dynamics of the oceans. Practically, none of them is sufficient on its own. Because ocean processes are actually non-linear, theory has to be simplified to a large extent in order to describe the dynamics of these complicated phenomena. Meanwhile, observations are somehow limited in time and space. They cannot be carried out smoothly whenever or wherever required. Consequently, they provide only a rough description of the average time flow and many processes may be poorly observed. Numerical models can overcome the shortcomings of these two approaches as they include much more realistic theoretical ideas and may help to interpolate oceanic observations in time and space. Numerical models may also be effectively used to forecast and predict the future status of the oceans. By combining theory and observation in numerical models, difficulties associated with the individual approaches may be overcome and to a large extent, avoided. This combination also leads to new ways and methodologies to study and perform oceanography and marine engineering.

The basic advantages which accrue from using numerical models can be summarised in the following points [233]:

1. Numerical models include the influence of non-linear dynamical terms, which are avoided as much as possible in theories.
2. Numerical models interpolate between sparse observations of the ocean produced by expeditions and satellites. Hence, their final result may give a more realistic picture of the studied phenomenon.
3. The real coastal features and seabed configuration may be easily represented in numerical models. This gives more realistic flow schemes.
4. Numerical models can be used to predict the possible future status of the oceans and suggest different scenarios to deal with any particular case.

However, numerical models should not be considered as ideal solutions to everything. Some problems may arise while using such models [233, 234] due to:

1. Turbulence terms and their complex calculations.
2. The complexity of the real field of work, oceans, which cannot be easily simulated using the simplicity and assumptions of the models.
3. Errors that may arise in codes and programmes.

A numerical model is constructed in four basic steps:

1. Definition of the full set of equations that govern the system.
2. Definition of the boundary conditions used to simplify the set of governing equations.
3. Constructing a scheme e.g. an explicit finite difference scheme, to convert the mathematical equations to numerical ones.
4. Writing a computer programme to calculate the unknown variables and to visualise the results.

A hydrodynamical model must examine the variations in the oceanic processes with respect to the different forces acting on the water body, e.g. Coriolis force, pressure gradient…etc, and at the same time to apply some boundary and initial conditions according to the case being studied in order to simplify the process of examination. It is an established fact that hydrodynamical models have considerably evolved since the early days. The present generation of time-dependent, three-dimensional primitive equation models have reached a stage of full development which satisfies their routine application to the study of marine environmental dynamics [235].

4.2 The basic hydrodynamical equations

The basic hydrodynamical equations are a set of mathematical equations, which are solved simultaneously to give numerical solutions to any fluid flow problem. These governing equations are based on the conservation laws of mass and of momentum [236]. These two principles allow one to develop the governing equations of fluid motion known as the continuity and momentum equations, respectively [237]. The hydrodynamical equations are fairly used, and models differ from each other only in the expressions and values of parameters appearing in the closure scheme of the model used [235]. In the case of the ocean, there will usually be four variables in the system of equations: the water elevation η and the water velocity components u, v and w in the X, Y and Z Cartesian directions, respectively.

There are many hydrodynamics and oceanographic text books, which give a detailed explanation and methodology of the derivation of these governing equations, e.g. [236, 238, 239].

In the present work, just a brief description of this derivation is given below:

Consider a cubic parcel of fluid of dimensions Δx, Δy and Δz in Cartesian coordinate planes X, Y and Z as shown in Figure 4.1. If this fluid parcel has a density of ρ and velocity components of u, v and w in the X, Y and Z directions, respectively, then the net mass flux of the considered cube to move in a time interval Δt will be given by

$$-\left(\frac{\partial \rho u}{\partial x}+\frac{\partial \rho v}{\partial y}+\frac{\partial \rho w}{\partial z}\right)\Delta x\,\Delta y\,\Delta z\,\Delta t \qquad (4.1)$$

and the net mass increase due to the movement in the same temporal interval will be given by

$$\frac{\partial}{\partial t}\left(\rho\,\Delta x\,\Delta y\,\Delta z\right)\Delta t \qquad (4.2)$$

Equating equations (4.1) and (4.2) to satisfy the law of conservation of mass, we get

$$\frac{\partial \rho}{\partial t}=-\left(\frac{\partial \rho u}{\partial x}+\frac{\partial \rho v}{\partial y}+\frac{\partial \rho w}{\partial z}\right) \qquad (4.3)$$

Equation (4.3) is known as the continuity equation of flow.

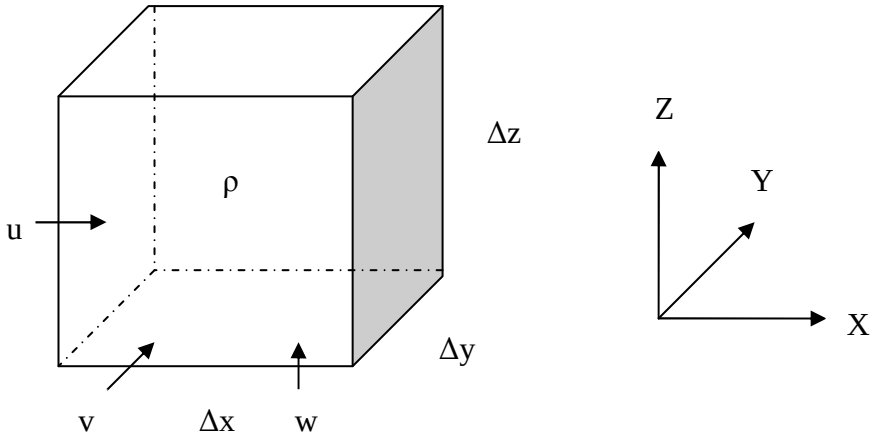

Figure 4.1: A cubic parcel of fluid in XYZ Cartesian plane

For incompressible fluids, such as ocean waters, the density ρ is considered to be constant. Consequently, equation (4.3) may be written as

$$\frac{\partial u}{\partial x}+\frac{\partial v}{\partial y}+\frac{\partial w}{\partial z}=0 \qquad (4.4)$$

The principle of the conservation of momentum may be stated as:

The rate of change of momentum with respect to time equals the sum of the acting forces on the fluid. This, in fact, is Newton's second law of motion.

Since the momentum = mass * velocity

Then,

$$\frac{d}{dt}(momentum)=\frac{d}{dt}(mass*velocity)=\sum F \qquad (4.5)$$

where, F is the forces acting on the fluid

If M denotes the fluid mass and V denotes the fluid total velocity, then equation (4.5) takes the form

$$M\frac{dV}{dt}+V\frac{dM}{dt}=\sum F \qquad (4.6)$$

According to the conservation of mass principle dM/dt = 0, then equation (4.6) becomes

$$M\frac{dV}{dt}=\sum F \qquad (4.7)$$

i.e. the rate of change of fluid acceleration equals the sum of the forces acting on the fluid.

Claude-Louis Navier and George Stokes were the first to give the description of the motion of a fluid and derived the full mathematical form of the fluid momentum equations. Hence, the following expressions are known as Navier-Stokes equations:

Briefly, for a unit volume of fluid, i.e. $\Delta x\, \Delta y\, \Delta z = 1$, equation (4.7) takes the form

$$\rho\left(\frac{dV}{dt}\right)=\sum F \qquad (4.8)$$

The acceleration term in equation (4.8) in an Eulerian system is in fact the sum of two terms: the local acceleration term $\left(\frac{\partial V}{\partial t}\right)$ and the advective acceleration term $(V.\nabla V)$; then equation (4.8) becomes

$$\rho\left(\frac{\partial V}{\partial t}+(V.\nabla V)\right)=\sum F \qquad (4.9)$$

The right-hand side in equation (4.9) is the sum of the acting forces on the fluid. These comprise the pressure gradient force (∇P), the viscosity gradient force (∇T) and any other force (Q) e.g. the Coriolis force due to the earth rotation.

Accordingly, equation (4.9) may take the form:

$$\rho\left(\frac{\partial V}{\partial t}+(V.\nabla V)\right)=-\nabla P+\nabla T+Q \qquad (4.10)$$

Hence, the derivatives for each component in Navier-Stokes equation system may be written as follow

$$\rho\left(\frac{\partial u}{\partial t}+u\frac{\partial u}{\partial x}+v\frac{\partial u}{\partial y}+w\frac{\partial u}{\partial z}\right)=-\frac{\partial P}{\partial x}+\mu\left(\frac{\partial^2 u}{\partial x^2}+\frac{\partial^2 u}{\partial y^2}+\frac{\partial^2 u}{\partial z^2}\right)+Q_x \qquad (4.11)$$

$$\rho\left(\frac{\partial v}{\partial t}+u\frac{\partial v}{\partial x}+v\frac{\partial v}{\partial y}+w\frac{\partial v}{\partial z}\right)=-\frac{\partial P}{\partial y}+\mu\left(\frac{\partial^2 v}{\partial x^2}+\frac{\partial^2 v}{\partial y^2}+\frac{\partial^2 v}{\partial z^2}\right)+Q_y \qquad (4.12)$$

$$\rho\left(\frac{\partial w}{\partial t}+u\frac{\partial w}{\partial x}+v\frac{\partial w}{\partial y}+w\frac{\partial w}{\partial z}\right)=-\frac{\partial P}{\partial z}+\mu\left(\frac{\partial^2 w}{\partial x^2}+\frac{\partial^2 w}{\partial y^2}+\frac{\partial^2 w}{\partial z^2}\right)+Q_z \qquad (4.13)$$

Equations (4.11, 4.12 and 4.13) are the general form of the hydrodynamical governing equations. This form changes by assumptions, boundary conditions and controlling forces from one case to another. To simulate any hydrodynamical process

in the oceans mathematically, the described equation set has to be solved numerically using any numerical scheme such as explicit finite difference, implicit finite difference or elementary analysis.

As the Mediterranean Sea basin is the vast area of interest in the present study, it is worth focusing on some numerical attempts to simulate its circulation pattern. This is presented in the following section.

4.3 Some numerical attempts to simulate the circulation pattern in the Mediterranean Sea

Several numerical attempts have been made to reproduce, simulate and understand the Mediterranean Sea circulation pattern and its variable dynamical processes. Authors of this research used different general circulation and hydrodynamical models with different grid resolutions considering the different acting forces. The results of these studies explain the circulation regime of the three distinct water masses within the Mediterranean Sea basin and have added to the understanding of their characteristics. In addition, the results emphasise the importance of the different gyres found in the two basins of the Mediterranean Sea. Moreover, the results of the simulation processes confirm that the inter-annual variability of the external atmospheric forces, more specifically anomalies in the winter wind stress and heat fluxes, could account for some of the large changes in the circulation regime observed from year to year in the Mediterranean Sea. According to the author's knowledge, attempts to simulate the Western Mediterranean basin numerically considerably outnumber similar attempts for the Eastern Mediterranean basin.

Some of the numerical simulation studies carried out on the circulation regime within the Mediterranean basin can be easily accessed through the following bibliography:

The Geo-Hydrodynamical and Environmental Research (GHER) 3D model, developed at the University of Liege (Belgium) and its application in the western Mediterranean Sea has been briefly described and applied [231, 235, 240, 241, 242].

In an attempt to discover the main driving forces for the circulation in the Eastern Mediterranean basin, an extensive and thorough series of numerical experiments using a multilevel model of circulation have been carried out [100]. Using the Bryan-Cox model, the effect of using different initial and boundary conditions in several

numerical simulations was examined [243]. The steady seasonal circulation of the Eastern Mediterranean Sea has been determined [244]. The relationship between bottom topography and circulation pattern in the Western Mediterranean, which is known as the Neptune effect (eddy-topography interaction), has been studied [87]. The Geophysical Fluid Dynamics Laboratory (GFDL) model has been examined and applied [88, 245, 246]. Also, the Princeton Ocean Model (POM) [247], developed for coastal and open sea applications, was applied to simulate the Mediterranean flow structure and physical properties [52, 107, 112, 248, 249]. The GFDL model updated to the Modular Ocean Model (MOM) version has been used in order to reproduce the principle water masses and water pathways in the Mediterranean Sea [84, 116, 250].

A review of the recent changes in the deep water formation in the eastern Mediterranean Sea has been made [251, 252]. The general Mediterranean Sea circulation pattern by a review and summary of the results of the previous studies (observations and simulations) has been described [253]. The points of agreement and disagreement between these studies have been discussed. The seasonal and interannual variabilities in the circulation within the Mediterranean basin and the main driving forces affecting each of them have also been discussed.

The DieCast model has been used [86] in the Mediterranean Sea in order to:

1. Test the model to judge its ability to reproduce the general circulation features and seasonal cycles as produced by other models.
2. Determine if interannual variability induced by realistic behaviour of fronts and eddies may be obtained in model simulations.

A new Mediterranean circulation model has been described [254] in which, for the first time, an implicit free surface is considered. This enabled the simulation of sea height variations. The model solves the basic hydrodynamic primitive equations using the spherical coordinates (λ, φ, z), where λ denotes the longitude, φ denotes the latitude and z denotes the depth.

There is a great need for precise and accurate tidal models for many applications: oceanography, geophysics, engineering, investments and even space technology. Accordingly, it is convenient to focus on some numerical models developed to simulate the tidal behaviour on both Global and Mediterranean Sea scales. These are presented in sections 4.4 and 4.5, respectively.

4.4 Some worldwide numerical tidal models

The development of the well-known numerical models to simulate the ocean tides began in the 1980s. The first, being [255-257] whose importance stems from the fact that it was used as the standard global tidal model for so many years. The model is based on the basic hydrodynamical governing equations, with a 1° x 1° grid resolution and uses an interpolation scheme to fit the tide gauges. Only the M_2 constituent is given in this model due, apparently, to the weak velocities of the other components. The CEFMO code (Code d'Elements Finis pour les Marées Océaniques) has been developed and tested [258] on a limited area: the Northeast Atlantic. The results of this model for the M_2 and S_2 tidal components are in a good agreement with the theoretical and observed data sets of their area of investigation.

Later on, with the development of satellite altimetry, tidal models developed rapidly. A global program was in early 1990s to combine the available *in situ* data sets from different tide gauges and data from satellite altimetry missions (Geosat, ERS1, TOPEX/POSEIDON) for use in hydrodynamical numerical models. An Atlas of the main tidal components has been produced [259] using a finite element hydrodynamical model, Finite Element Solution (FES94.1), based on nonlinear shallow water equations. The *in situ* data sets from the International Hydrographic Bureau (IHB) and the altimetry of ERS1 and TOPEX/POSEIDON were used. The behaviour of the four larger tidal components (M_2, S_2, K_1 and O_1) was presented. The results over the deep oceans fitted the observations within a few centimetres but were less accurate over the shelves. This is due to the increase in amplitude of the tidal waves [259]. Using a 12 months altimetry TOPEX/POSEIDON data set, a harmonic analysis on the captured data has been performed [260]. The aim was to qualify the data of TOPEX/POSEIDON and to explain the differences between the tidal models [255-257, 261].

CSR3 and CSR4 are long wavelength adjustments of FES94.1 using TOPEX/POSEIDON data and are given on a ½° x ½° grid. Unfortunately, these two models have spurious grid cells over lands that have been removed using the grid of GOT00.2 model as a mask. The latter, which uses ERS1/2 data for assimilation, has been used to add extra tidal values in the Weddell and Ross Sea in the Antarctic. For

the other tidal values below and above 66° S and 66° N latitudes (the limits of the TOPEX/POSEIDON satellite), these models become equal to FES94.1 [262].

A two-year altimetry data set from TOPEX/POSEIDON has been used [263] to numerically investigate the global tide. The model has a 0.5° x 0.5° grid resolution and delivers a numerical solution for eight major tidal constituents: M_2, S_2, N_2, K_2, K_1, O_1, P_1 and Q_1. The obtained results were verified using two field data sets: tide gauge data and Super-Conducting Gravimeter (SCG) data. The results actually give a more accurate output than do the models [255-257, 261]. This refers to the higher resolution applied as well as the accuracy and availability of large reference data sets.

It is pointed out [264] that FES95.2 is a numerical upgrade of the numerical tidal model FES94.1. In this upgrade, tides in the Arctic were improved and TOPEX/POSEIDON data has been used to adjust the long wavelength behaviour of FES94.1. The resolution of the model is ½º x ½º. The outcomes simulated six major tidal components: M_2, S_2, N_2, K_1, O_1 and Q_1. The performance of the model was evaluated by comparing tidal predictions with observations at 59 sites distributed over the world oceans and by looking at the level of variance of sea surface as observed by TOPEX/POSEIDON altimeter. In general, the results of the model are in very good agreement with both data-sets.

FES98 is also a purely hydrodynamic model to simulate the global ocean tides [265]. The model has a ¼º x ¼º grid resolution and incorporates a set of about 700 selected tide gauges. FES98 differs than other FES tidal models in two ways:

1. It is verified using only data sets of the selected tide gauges with no altimetry techniques.
2. It is characterised by its global ocean grid, as opposed to other models that compute tides in a few ocean basins separately and then amalgamate the output.

The FES98 model simulates eight tidal constituents: M_2, S_2, N_2, K_2, 2 N_2, K_1, O_1 and Q_1.

The results of a global tidal model (NAO.99b) to derive a regional one around Japan (NAO.99Jb) has been discussed [266]. The global model runs to simulate 16 major tidal constituents developed by assimilating about five years of TOPEX/POSEIDON altimeter data. The regional model, on the other hand, assimilates both altimeter and

regional tide gauge data sets. The dissipated energy for the major tidal constituents in the Japanese region, location and amount, has also been highlighted. For the M_2 constituent, the energy is intensive in the Yellow Sea and the Sea of Okhtosk regions at a mean rate of 155 gigawatts (GW) and 55 GW, respectively. For the K_1 constituent, the energy is mainly dissipated in the Sea of Okhtosk, with an average rate of 89 GW.

A ¼º x ¼º grid model has been developed [267] using inverse theory and assimilated both tide gauge and TOPEX/POSEIDON data. This model finds the optimum balance between observations and hydrodynamics.

FES99 [268] is a size model which upgrades the FES98 model. FES99 depends not only on tide gauge data sets for verification, but also uses TOPEX/POSEIDON data assimilation.

4.5 Mediterranean Sea tidal models

The hydrodynamical characteristics and circulation pattern of the Mediterranean Sea have been intensively studied using different numerical models. However, as mentioned previously, tides in the Mediterranean Sea are nearly absent from such numerical modelling processes except in some limited case studies. This is mainly due to the fact that tides in the Mediterranean Sea do not exceed a few centimetres in the spring phase. Hence, the Mediterranean Sea may be considered as one of the oceanic areas which are missed in the global ocean tide models (Fig. 4.2). In addition, there is a conflict between the researchers in determining the main tidal force within the Mediterranean basin, whether it is the equilibrium tide resulting from the gravitational force between the celestial bodies: Earth, Moon and Sun or the tidal wave which enters the basin through the Strait of Gibraltar.

The trials of simulating the tidal phenomenon in the Mediterranean Sea, successfully found for the present work, comprise the following:

The M_2-tidal component has been simulated in the Mediterranean Sea [122] using a ⅓° resolution model. The effect of the closure of the Strait of Gibraltar on the Mediterranean tides was examined and small differences in tides prior to and after the closure process were found. Hence, it is concluded that tides in the Eastern Mediterranean basin are mainly astronomic in origin.

Data sets from both tide gauges and altimeteric observations over the Mediterranean basin have been used [269], excluding the Aegean Sea, to run a numerical model. The model has a resolution of ½ ° degree.

A two-dimensional numerical model of Hansen type, i.e. solved by boundary-values method, has been used [270] to investigate the M_2 tides in the Mediterranean Sea. The driving forces for the model were both equilibrium and external tides. The effects of topography and coastal configuration on the tidal motion were also considered. The obtained results were generally in good agreement with observations. However, in some locations there was deviation in phase and amplitudes between simulation and observations. This may be due to the coarse resolution of the model (1° x 1°).

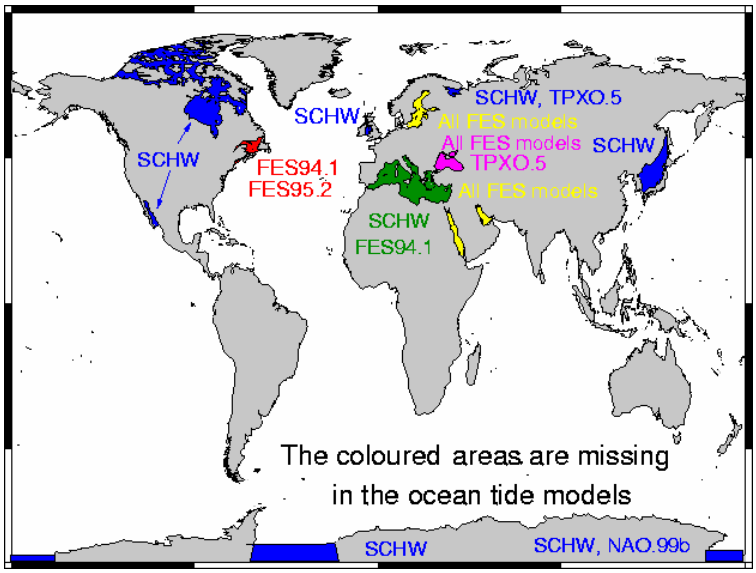

Figure 4.2: Water masses that are missed in the global ocean tide models (http://geodac.fc.up.pt/loading/tidemodels.html)

A numerical model was developed [271] to investigate the M_2-tidal component in the Mediterranean basin. The whole basin was assumed to be a closed basin, i.e. only the equilibrium gravitational tide has been investigated. Two cases were proposed:

1. Two connected rectangular sub-basins with a constant depth of 500 m, using a resolution of 1° x 1°.
2. Almost realistic coastal and bottom configuration using resolutions of 1° x 1° and ¼° x ¼ °.

It is concluded that boundaries have a minor influence on the M_2-tidal component in the Mediterranean basin, while the dimensions of the basins have a significant impact on the tidal pattern.

The M_2 tides were reinvestigated in the Mediterranean basin [272] using a ¼° x ¼° resolution and real open boundaries. The effect of the Gibraltar tidal oscillation is found to be more effective in the Western Mediterranean basin than in the Eastern one. The water exchange process between the different basins in the co-oscillating condition is successfully simulated.

The developed model [272] was used [273] to investigate the influence of friction on the tidal motion in the Mediterranean Sea. The Sea was assumed to be of rectangular shape and was investigated in two cases:

1. The whole basin is divided into two closed rectangular sub-basins, which are separated by a barrier at the Strait of Sicily.
2. The whole basin is divided into two rectangular sub-basins connected to each other through an opening of 2° width.

The results reveal that friction affects both amplitudes and phase distributions all over the Mediterranean basin. It is also concluded that, with large depths, the effect of the Coriolis parameter may be ignored.

A two-dimensional hydrodynamical model forced by both the equilibrium tide and the incoming tidal wave from the Strait of Gibraltar has been presented [124]. The model grid is 1/12° x 1/12°, ignores the atmospheric forces affecting the Mediterranean basin and is solved by an explicit finite difference method. The model outputs confirm the existence of an amphidromic point in the Strait of Sicily and appreciate the concept of the apparent effect of both independent (astronomic only) and co-oscillating (Atlantic tidal waves) tides in the western Mediterranean basin.

4.6 Chapter Conclusion

Numerical models are frequently applied in many fields as tools that aid decision making prior to the intention of any actual work. A hydrodynamical model is used to propose different scenarios and examine variations in the complex oceanic processes with respect to different forces acting on the water body. The governing equations in a hydrodynamical model are known as the Navier-Stokes system of equations in

which assumptions, boundary conditions and controlling forces alter from one case to another. This system of equations results from the application of the principles of conservation of mass and of momentum. Numerical simulation processes have been extensively applied to simulate and study ocean circulation patterns in the global oceans including the circulation pattern in the Mediterranean Sea. Examples of these studies are discussed in the present chapter. Unlike the hydrography and circulation patterns, tides in the Mediterranean Sea basin are rarely simulated numerically. This is mainly due to the fact that tides in the Mediterranean basin do not exceed a few centimetres in spring phase nor the associated tidal currents.

CHAPTER 5
NUMERICAL ASSESSMENT OF THE STRAIT OF MESSINA

An Overview

The numerical simulation of the tidal flow regime in the Strait of Messina is discussed in the present chapter. The chapter consists of three sections. Section one is a brief introduction to the Shallow Water Equations (SWE), followed by a brief description of the Tidal Flow Development (TFD) numerical model used to simulate the Strait of Messina. Section two discusses some previous trials to simulate the Strait of Messina. The simulation of tidal currents within the Strait of Messina in the present study is discussed in section three. The Strait is simulated in different cases and modifications to the TFD model are discussed for each case.

5.1 Introduction to Shallow Water Equations (SWE)

Shallow Water Equations (SWE) describe a thin layer of inviscid fluid with a free surface [274]. They are a set of depth-averaged integrated partial differential equations mainly derived from the basic equations of conservation of mass and momentum (Navier-Stokes equations). SWE are based on the premise that the horizontal scale is much larger than the vertical scale and that the flow is nearly horizontal [237]. SWE can be used in the following cases [236, 237, 274]:

1. When the fluid density is homogeneous.
2. When the flow is approximately hydrostatic, i.e. $\frac{\partial P}{\partial Z} = -\rho g$, where P is the pressure, Z is the fluid depth, ρ is the fluid density and g is the acceleration due to the Earth's gravity.
3. When the depth is small enough compared to the horizontal distance. The use of shallow water equations has been restricted to cases where the depth is less than 20 times the wave length [275].
4. In coastal and estuarine areas.
5. To reduce the complicated three-dimensional problems to two-dimensional ones.

Consequently, the places in which the use of these equations is convenient may be specified as: weakly stratified or non-stratified flows in estuaries, bays, coastal areas and harbours, and in places where the wind shear stress is relatively small.

Generally speaking, the equation of conservation of mass (continuity equation) in the shallow water case takes the form:

$$\frac{\partial \eta}{\partial t} + (\nabla . HV) = 0 \qquad (5.1)$$

where,

η is the free surface elevation (m) and H is the total fluid depth (m), which is the sum of the free surface elevation and the mean water depth (h) in the location of investigation, i.e. H = η + h

$$\nabla = \left(\frac{\partial}{\partial x} + \frac{\partial}{\partial y} \right) \qquad (5.2)$$

V is the total flow velocity (m/s), which is essentially horizontal in the case of shallow water equations.

The equation of conservation of momentum in the shallow water case are given by

$$\frac{D(Hu)}{Dt} - fv = -g \frac{\partial \eta}{\partial x} + F_x \qquad (5.3)$$

$$\frac{D(Hv)}{Dt} + fu = -g \frac{\partial \eta}{\partial y} + F_y \qquad (5.4)$$

where,

$$\frac{D}{Dt} = \frac{\partial}{\partial t} + \nabla .(VHV) \qquad (5.5)$$

f is the Coriolis force parameter; u and v are the horizontal components of the flow velocity (m/s) in X and Y planes, respectively; g is the acceleration due to the Earth's gravity (m/s^2) and F_x and F_y are the acting forces on the fluid in X and Y directions, respectively.

For a detailed derivation of the above equations the reader may refer to many text books, e.g. [238, 276-278].

The final equations of the shallow water equations set, which will be used in the Tidal Flow Development (TFD) model in the present study take the following form:

$$\frac{\partial \eta}{\partial t} + \frac{\partial (uH)}{\partial x} + \frac{\partial (vH)}{\partial y} = 0 \qquad (5.6)$$

$$\frac{\partial uH}{\partial t}+\frac{\partial uuH}{\partial x}+\frac{\partial uvH}{\partial y}=fvH-gH\frac{\partial \eta}{\partial x}-gn^2\frac{u\sqrt{u^2+v^2}}{H^{1/3}}+\frac{\rho_a}{\rho_w}C_wW_x\sqrt{W_x^2+W_y^2}+$$
$$+\left(\frac{k\sqrt{gn}\sqrt{u^2+v^2}H^{5/6}}{6}\right)\left(2\frac{\partial^2 uH}{\partial x^2}+\frac{\partial^2 uH}{\partial y^2}+\frac{\partial^2 vH}{\partial x\partial y}\right) \quad (5.7)$$

$$\frac{\partial vH}{\partial t}+\frac{\partial uvH}{\partial x}+\frac{\partial vvH}{\partial y}=-fuH-gH\frac{\partial \eta}{\partial y}-gn^2\frac{v\sqrt{u^2+v^2}}{H^{1/3}}+\frac{\rho_a}{\rho_w}C_wW_y\sqrt{W_x^2+W_y^2}+$$
$$+\left(\frac{k\sqrt{gn}\sqrt{u^2+v^2}H^{5/6}}{6}\right)\left(2\frac{\partial^2 vH}{\partial y^2}+\frac{\partial^2 vH}{\partial x^2}+\frac{\partial^2 uH}{\partial x\partial y}\right) \quad (5.8)$$

where,

n is the Manning (roughness) coefficient (s/m^3); ρ_a is the air density (kg/m^3); ρ_w is the water density (kg/m^3); C_w is the wind drag coefficient; W_x and W_y are the wind velocity components (m/s) in X and Y directions, respectively and k is the eddy viscosity coefficient (kg/ms)

Equation (5.6) is the shallow water continuity equation and equations (5.7) and (5.8) are the shallow water momentum equations in the X and Y directions, respectively.

This set of equations is a two dimensional set in which three unknowns, averaged-depth velocity in X and Y directions (u, v) and surface elevation (η) can be calculated using three equations. The equations (5.6 - 5.8) present an Initial Value Problem. These equations may be solved using various numerical techniques. The three most widely accepted and applied techniques [240] are:

1. The method of characteristics.
2. The finite element method, and
3. The finite difference method.

Of these methods, the solution of problems involving fluid dynamics has been dominated by the use of the finite difference method [279]. Either the explicit approach or the implicit approach may be applied to get numerical solutions using the finite difference method. The major difference between the two approaches is the stability condition, which should and must be fulfilled when applying the explicit approach. The stability condition is known as Courant-Friedrich-Levey (CFL) condition, which is the ratio of the celerity of propagation in the analytical to that in the numerical solutions.

$$CFL = \frac{\sqrt{gh}}{\Delta x / \Delta t} \leq 1, \; i.e. \; \frac{\Delta x}{\Delta t} \rangle \sqrt{gh} \qquad (5.9)$$

where,

$\sqrt{gh}$ is the field tidal long wave propagation velocity (m/s); Δx is the distance interval in the numerical domain (m); and Δt is the time step of simulation in the numerical domain (s)

If CFL is less than the unity, then the stability criterion is fulfilled and the stable solution may be explicitly calculated.

There are three finite difference methods used to solve the equations explicitly:

1. The forward-difference method,
2. The backward-difference method, and
3. The central-difference method.

Though the last may appear to be the best from amongst the three, it cannot be applied in the field of Computational Fluid Dynamics (CFD) as it is unsuitable for the simulation of the important convection term [237]. To deal with the convection term it is essential to have a method, which satisfies the stability condition and, simultaneously, be simple to use. Fortunately, finite difference methods based upon the 3rd order upwinding have been found to offer good accuracy, inherent numerical stability and relative computational simplicity [237].

5.2 The Strait of Messina: Some previous simulation attempts

The complexity of the morphometry of the Strait of Messina, combined with the strong non-linearity of its tidal phenomena, complicate the simulation process of the Strait [280]. However, attempts to simulate the tidal features in the Strait of Messina numerically have been proposed and applied in research studies since the early 1900s. The first investigation of the tidal phenomena in the Strait of Messina [193] was made in order to explain its tidal dynamics. The behaviour of the M_2-semidiurnal tidal constituent was simulated using a numerical solution for one-dimensional linear tidal dynamics equations.

A barotropic model was used [281] to study tides in the Strait of Messina. The step-integration method of one-dimensional, non-viscous, linearised barotropic equations of motion was applied. The results allocated an amphidromic point within the Strait

just over the sill, where the tidal heights decrease from 10 cm in the Ionian Sea to zero cm. These heights then rise again towards the Tyrrhenian Sea to reach 16 cm as shown in Figure 5.1. This explains the intensive current (>2 m/s) observed and calculated [139].

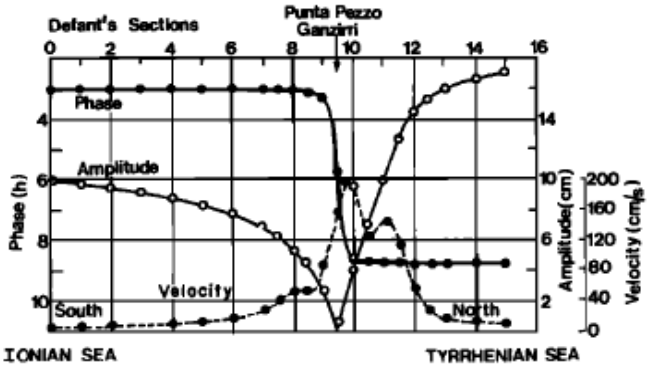

Figure 5.1: The distribution of the main tidal features in the Strait of Messina over a semidiurnal tidal cycle [293] as shown in [192]

The central finite-difference method has been applied [187] in order to solve the equations for a two-dimensional numerical model. The time evolution of the interface between the Tyrrhenian and the Ionian water masses in the sill region of the Strait of Messina has been investigated as a practical case study. The results of this research reveal large vertical oscillations between the surface and the bottom in the Strait, and they are in reasonable agreement with the field data [139]. The model is verified to be capable of reproducing the general features of the circulation pattern of the Strait of Messina [187].

Using the least square minimization technique a two-layered model was developed [192], in which the Coriolis force and the lateral dimension are neglected. To run the model, the data set of the field first station [139] was used, where the currentmeter was moored for 15 consecutive days. Both wind and seabed shear stresses were also neglected in this simulation study by omitting the very near surface and deep records. The results [192] give a reasonable picture of the tidal behaviour in the Strait of Messina. The outputs are in agreement with those previously computed [139, 140] and are also in a reasonable agreement with the results of the model study [187].

The boundary value problem of shallow water equations has been transferred [282] from a Cartesian coordinate system to a curvilinear coordinate system and been

solved using a half time-step difference scheme. The Strait of Messina was taken as a case study with a curvilinear grid resolution of 16 x 27. The behaviour of the M_2-tidal component in the Strait has been successfully deduced as well as its energy balance.

A rectangular domain has been created [280] for the Strait of Messina with two opposite open boundaries, in a 2D curvilinear coordinate system. The barotropic approximation was considered and the following targets were successfully achieved:

1. The computation of the averaged tidal amplitudes and phases due to tidal motion within the Strait of Messina (Table 5.1). A comparison of the simulated figures with the observations showed a very good agreement.

	Locality	S_2		K_1		O_1	
		Record	Calculate	Record	Calculate	Record	Calculate
Amplitudes (cm)	Ganzirri	1.6	1.3	1.4	0.9	0.5	0.3
	Faro	2.2	2.6	2.1	2.5	0.8	0.9
	P. Pezzo	0.6	0.8	0.9	2.4	1.6	0.6
	Reggio	3.0	3.3	1.6	2.0	0.8	0.9
	Villa S.G.	1.3	1.3	1.2	2.1	0.2	0.6
	Messina	2.8	2.7	0.9	1.2	0.9	0.7
	Scylla	3.2	3.5	2.8	3.2	0.9	0.7
Phases (°)	Ganzirri	354	8	242	239	214	280
	Faro	307	318	229	235	217	232
	P. Pezzo	137	135	236	124	235	98
	Reggio	100	95	57	67	50	52
	Villa S.G.	104	115	48	113	–	84
	Messina	98	69	290	8	65	12
	Scylla	295	304	220	225	136	226
χ (cm)	Ganzirri	0.33		0.36		0.33	
	Faro	0.43		0.33		0.17	
	P. Pezzo	0.14		2.02		1.47	
	Reggio	0.29		0.36		0.07	
	Villa S.G.	0.18		1.36		–	
	Messina	0.98		0.95		0.57	
	Scylla	0.43		0.34		0.81	

Table 5.1: Observed and computed amplitudes and phases of the main tidal components in the Strait of Messina [280]

2. The construction of M_2 tidal wave chart within the Strait of Messina, where the amphidromic point is precisely determined (Fig. 5.2) and the behaviour of this main tidal constituent is simulated and found to be in good agreement with the classical observations (Table 5.2).
3. The calculation of the energy dissipation in the Strait of Messina over a tidal cycle, which is found to be averaged with a value of 0.77×10^7 W. They referred this small value to the fact that strong tidal currents are only found in the sill area while, in the rest of the Strait, the tidal current velocities are much weaker.

4. The calculation of the nonlinear tidal components within the Strait of Messina: M_4, M_6 and M_8.
5. The fields of vortices (gyres) generated by the main tidal constituents in the Strait of Messina were precisely determined.

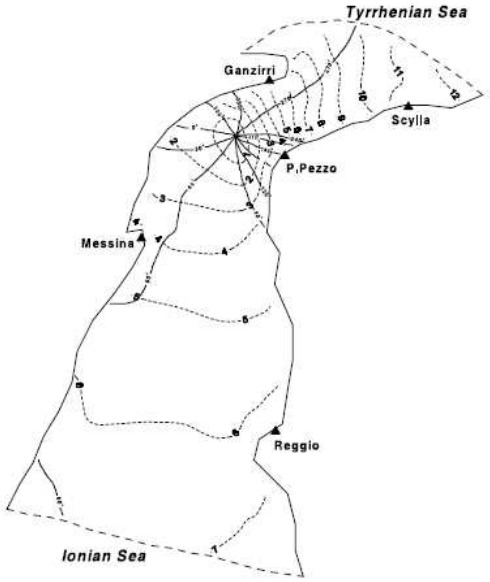

Figure 5.2: Tidal map of the M_2-tidal wave in the Strait of Messina ___ iso-phases (degrees) and ----- iso-amplitudes (cm) [280]

Locality	M_2				χ (cm)
	Amplitudes (cm)		Phases (°)		
	Record	Calculate	Record	Calculate	
Ganzirri	3.2	2.3	316	303	0.77
Faro	5.5	7.5	269	281	1.70
P. Pezzo	0.9	4.5	143	146	2.55
Reggio	6.2	6.6	95	75	1.60
Villa S.G.	3.3	3.8	116	124	0.50
Messina	5.3	4.2	31	38	0.89
Scylla	10.2	10.2	271	267	0.50

Table 5.2: Observed and computed M_2-wave amplitudes and phases [280]

5.3 The Tidal Flow Development (TFD) numerical model

5.3.1. Aim of using the TFD numerical model

The target of the previous models applied in the Strait of Messina was mainly to understand the dynamics of tides in the Strait. The energy extraction process using these strong currents and the identification of the locations of excess energy within the Strait are not present in any of these research except in that of Androssov *et al.* [280]. Even in the later, just an estimation of the energy dissipation over a tidal cycle was given without identifying the place of excess energy in the Strait. In the present work the process simulation to configure the tidal flow within the Strait of Messina will be given in order to determine the locations of excess energy in this strong flow where tidal turbines can be deployed for the energy extraction process. This is carried out using the Tidal Flow Development (TFD) numerical model. This model differs than that of Androssov *et al.* [280] in two points: the applied coordinate system which is Cartesian and not curvilinear system and in that its code has a specific routine able to calculate and simulate the energy extraction process from a tidal current resource. Hence, examining changes in the hydrodynamical environment before and after the energy extraction process can be simulated.

Applying the TFD model to the tidal environment of the Strait of Messina shows some shortfalls in the suitability of using the model to a complex domain like that of Messina. That is why in the following discussion the Strait of Messina will be simulated in different cases in which the TFD numerical model is modified to suit each case in order to mimic as closely as possible the Strait in all its complexity.

5.3.2. The structure of the TFD numerical model

The Tidal Flow Development (TFD) model is a numerical model which is based on equations (5.6 - 5.8). The equations are solved numerically using an explicit finite difference approach. The model was developed [237] to specifically simulate estuaries and coastal areas where the tide is the dominant driving force. The model shares a common heritage with other SWE solvers that are typically used in the academic and industrial communities as the standard workhorse in estuarine and coastal modelling applications, e.g. MIKE21, DIVAST [33]. The main code of the

TFD model is written in FORTRAN77. The appropriate outputs are based on the initial, input and boundary conditions specified when using the model. The bathymetry and the grid domain are additional important factors that affect the resultant outputs and have to be initially determined for each case study. Several files must be prepared before running the TFD model. Firstly, a parameter data file, in which the following parameter information must be defined: the bathymetry file from which to read, the output file names and their paths, the Manning parameter value and the latitudes and longitudes. Appendix (1) is an example of the parameter file used in the present study.

Secondly, the following initial files are built:

1. The grid selection

i.e. the cell size of the basic grid that represents the morphological, bathymetric and topographic configurations in the model. This selection is related to the CFL condition (5.9). It is found by experiments and trials that it is strongly recommended to restrict the value of the CFL condition not to exceed half, i.e. CFL<0.5. This is to avoid problems arising from the stability requirement and to guarantee a stable solution. The TFD model automatically checks whether the CFL condition is satisfied before calculating any parameter. If the condition is satisfied, the simulation process proceeds normally, otherwise the model stops until the required condition is satisfied.

2. Determination of the model boundaries

The boundaries in the TFD numerical model may be defined either as open or closed. For an open boundary, the flow parameters are allowed to move in/out of the domain, while a closed boundary denotes a dry/interference cell.

3. Determination of the driving boundaries

The TFD model uses only one conditional boundary driving force. This may either be the fluid elevation or the fluid velocity. The latter is thought to difficult to apply due to difficulty in describing the interaction between velocity filed as a driving force and the domain. The former, however, is preferred since the solution obtained close to the boundary in this case will be able to interact with the local bathymetry and topography.

4. The radiating boundaries

This is the data file of the physical/numerical conditions in the neighbourhood of the domain boundaries. It is important to explore these surrounding conditions and to examine their effects inside and outside the main domain of interest. The recommended mathematical expression (Sommerfeld condition) of the radiating boundary condition [283-285] is:

$$\frac{\partial \phi}{\partial t} + C_v \frac{\partial \phi}{\partial x} = 0 \qquad (5.10)$$

where, φ is the propagating variable; and C_v is the phase velocity

In the TFD numerical model, the propagating variable is the flow discharge per unit width (qu) and the phase velocity is that of the shallow long tidal wave ($\sqrt{gh}$). Accordingly, the radiation boundary condition in the model is given by the following equation:

$$\frac{\partial qu}{\partial t} + \sqrt{gh} \frac{\partial qu}{\partial x} = 0 \qquad (5.11)$$

The outputs of the TFD model are mainly hydrodynamical data values for the velocity and the sea-free surface elevation. These outputs may be graphically displayed using the WOLF model, developed in Strathclyde University, or the SURFER surface mapping program. The data output from WOLF can also be adapted to create .avi streaming animations for presentation purposes [237]. The hydrodynamic results from the TFD model may be further used in other applications such as examination of pollutant dispersion.

Upon the development of the TFD model, and as a new numerical tool, the three step approach for model testing [286] was attempted. This includes [237]:

1. Verification, which is a procedure to ensure that the program solves the modelled equations correctly.
2. Validation, which is a procedure to validate numerical models to complex flows, i.e. testing of the models predictive capabilities against detailed test data.
3. Calibration, which is a procedure to calibrate code from a particular model in its ability to predict global quantities for realistic geometries of design interest.

The simulation procedures through which the TFD model runs and proceeds to simulate tidal flows is presented in appendix (2).

It is not possible to verify the complete set of governing equations in one test model. Hence, the verification process for the TFD numerical model was done for each individual term separately in simple model tests. The TFD model was verified through 8 test-cases. The verification exercises have validated the running of the program code. The validation of the model was then carried out by applying four validation tests: the steady flow eddy circulation (physical model), the wind-induced circulation model in a circular basin, the 2-D partial dam-break steady case model and the estimation of the numerical diffusion inherent to the TFD model case. Finally the calibration exercise of the TFD model was carried out using Flamborough Head, northeast of England.

Subsequently, the model has been extensively applied and proved to be an effective simulation-tool for the examination of the tidal phenomena in different cases, e.g. [11, 33, 43, 225, 287, 288]

5.4 Simulation of the tidal-flow regime in the Strait of Messina

First of all, two points, Capo Peloro (38° 16.00’ N; 15° 39.00’ E) and Reggio Calabria (38° 06.00’ N; 15° 38.72’ E) to the north and to the south of the Strait of Messina, respectively, are chosen to represent the extremities of the domain of simulation. The two points are used to examine the tidal out-of-phase characteristic along the Strait. The tidal harmonic constituents are computed using a parameter data file (Appendix 3) for each point using Admiralty Tide Tables [289]. The tidal out-of-phase behaviour of 180º between the two chosen extremities is confirmed and the maximum difference between the M_2-tidal amplitudes, of 0.27 m, is verified. Figures 5.3 and 5.4 represent the M_2-tidal elevations at each extremity, while Figure 5.5 represents the tidal out-of-phase behaviour between them.

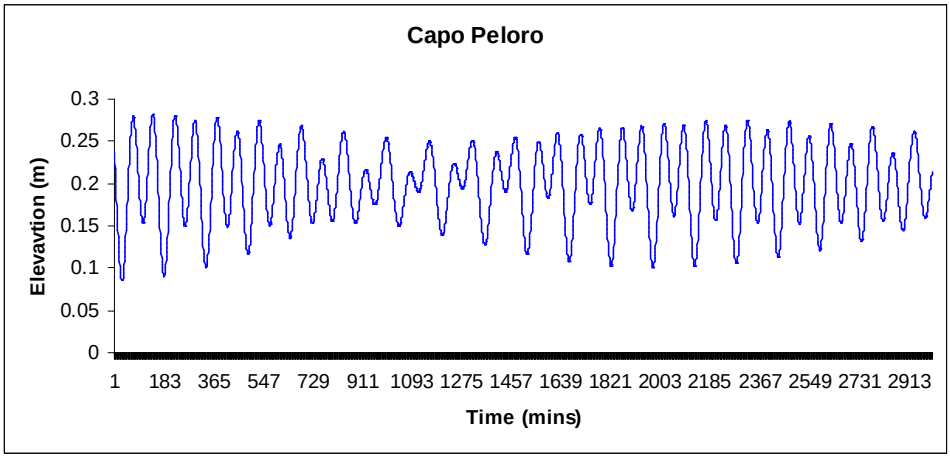

Figure 5.3: M_2-tidal elevation at Capo Peloro (northern tip)

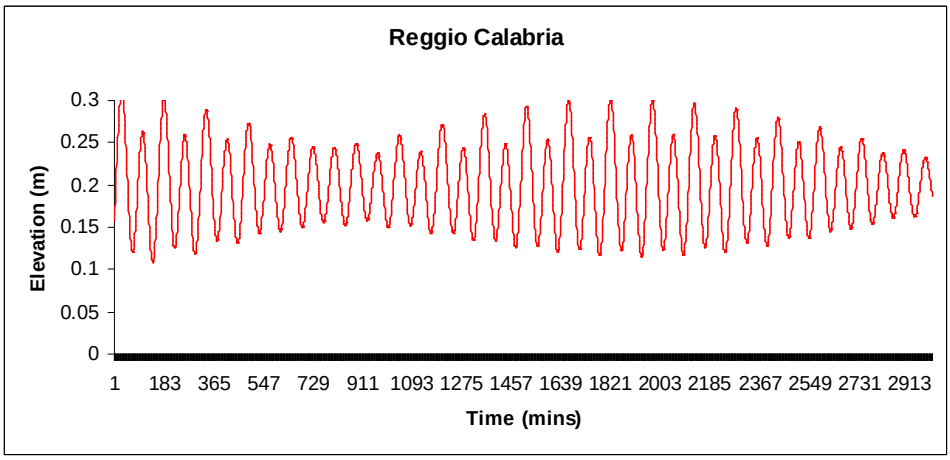

Figure 5.4: M_2-tidal elevation at Reggio Calabria (southern tip)

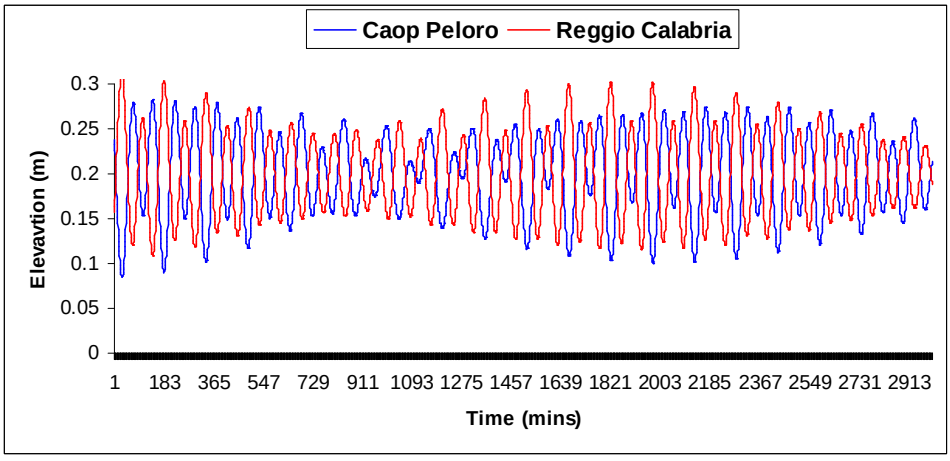

Figure 5.5: The 180º out-of-phase tidal behaviour between the two chosen extremities of the Strait of Messina associated with 0.27 m M_2 amplitude difference

5.4.1. The Strait of Messina as a simple tidal channel

In this case of numerical simulation, the Strait of Messina is represented in the form of a simple tidal channel extending horizontally in a west-east direction (Fig. 5.6). The Tyrrhenian Sea basin represents the outer western boundary of the specified domain while the Ionian Sea basin represents its outer eastern boundary. The fluid domain (i x j = 186 x 40 cells) extends for 18600 x 4000 m based on a cell grid size of 100 m, i.e. $\Delta x = \Delta y = 100$ m. The land represents the upper and lower edges of the domain of simulation. The water depth gradually increases from 0 m at the land-sea interaction on both upper and lower domain limits to a maximum depth of 80 m seaward within the domain itself. Figure (5.7) is a schematic representation of a transverse section in the specified domain.

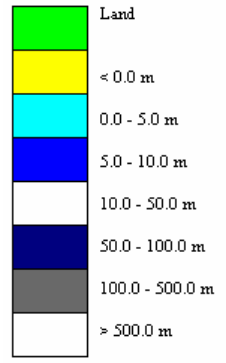

Applied 2D depth-averaged bathymetric scale for the simulation process of the Strait of Messina as a simple tidal channel case

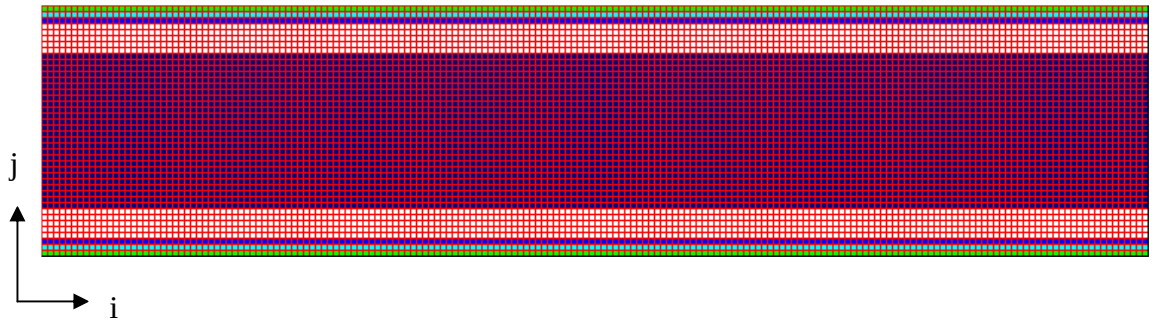

Figure 5.6: The simple tidal channel domain of simulation

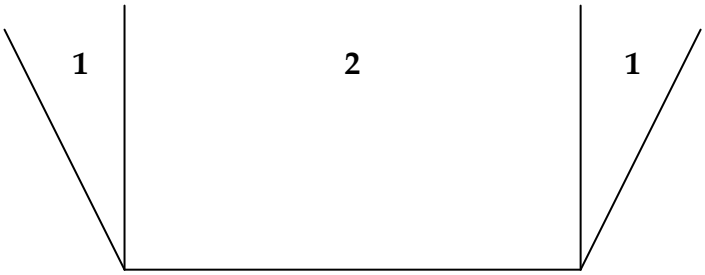

Figure 5.7: A transverse section in the simple tidal channel domain of simulation

Additionally, for the present domain of simulation the Tyrrhenian Sea represents the input boundary side, while the Ionian Sea represents the radiating boundary side (Fig. 5.8). The domain satisfies the CFL stability condition. The total time of the simulation process is 190000 s, i.e. four complete tidal cycles, with dt = 1.0 s. The resultant accumulated output is given every 1800 s, i.e. every half an hour.

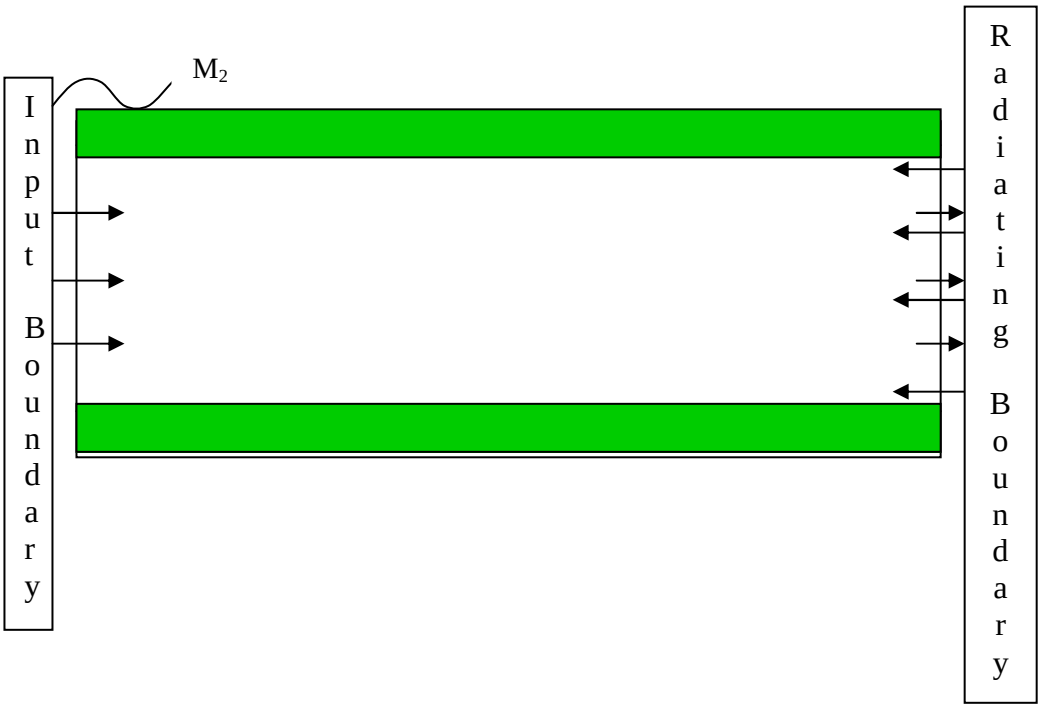

Figure 5.8: Schematic presentation of the domain of simulation showing the input and the radiating boundaries

In addition to the conditional assumptions applied to the Shallow Water Equations (section 5.1.1), the following assumptions are proposed in the present case of simulation:

1. The M_2-sine wave tidal oscillation (amplitude = 0.135 m, period = 44640 s) is the main driving force of flow within the domain from both input and radiating sides.
2. A constant Manning seabed friction coefficient is chosen (n = 2.5 x 10^{-2} s/m^3).
3. The Coriolis force effect is neglected.
4. The following cells (i, j) = (5, 20), (90, 20) and (180, 20) are considered within the output scheme to represent the western, central and eastern zones of the domain of simulation, respectively.

Figures (5.9 - 5.11) represents the simulation outputs of the tidal behaviour (velocity and elevations) of the Strait of Messina as a simple tidal channel at the specified chosen cells.

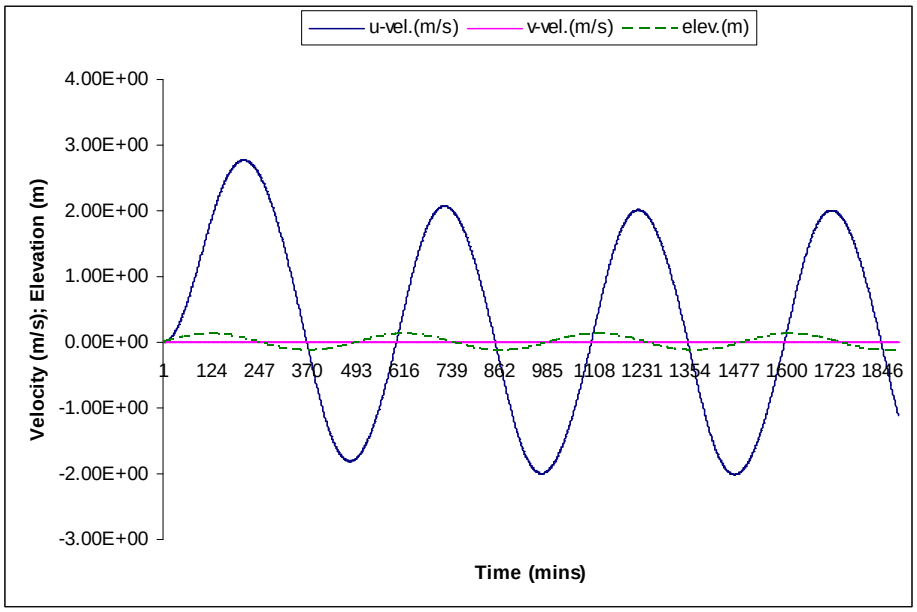

Figure 5.9: Tidal behaviour of the Strait of Messina simulated as a simple tidal channel (western region (5, 20))

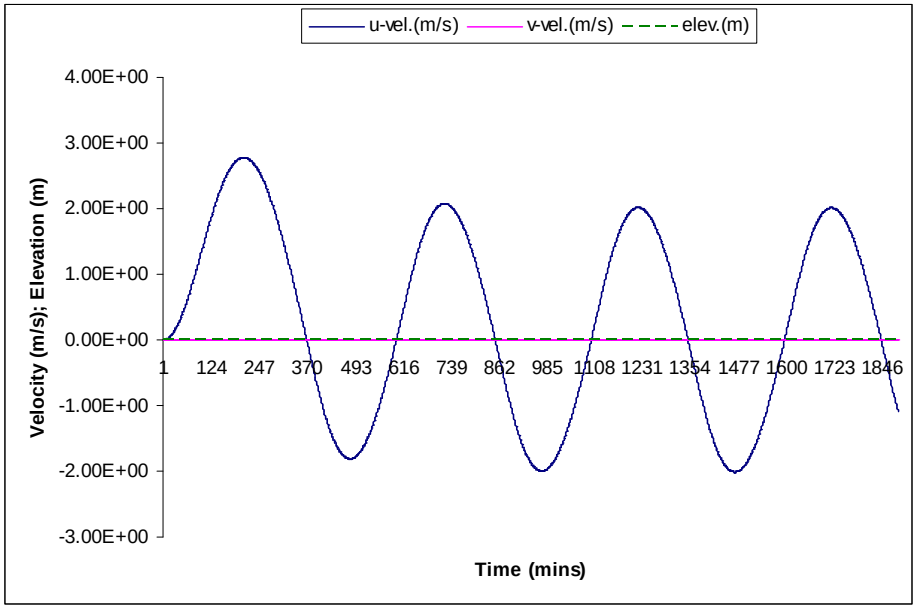

Figure 5.10: Tidal behaviour of the Strait of Messina simulated as a simple tidal channel (central region (90, 20))

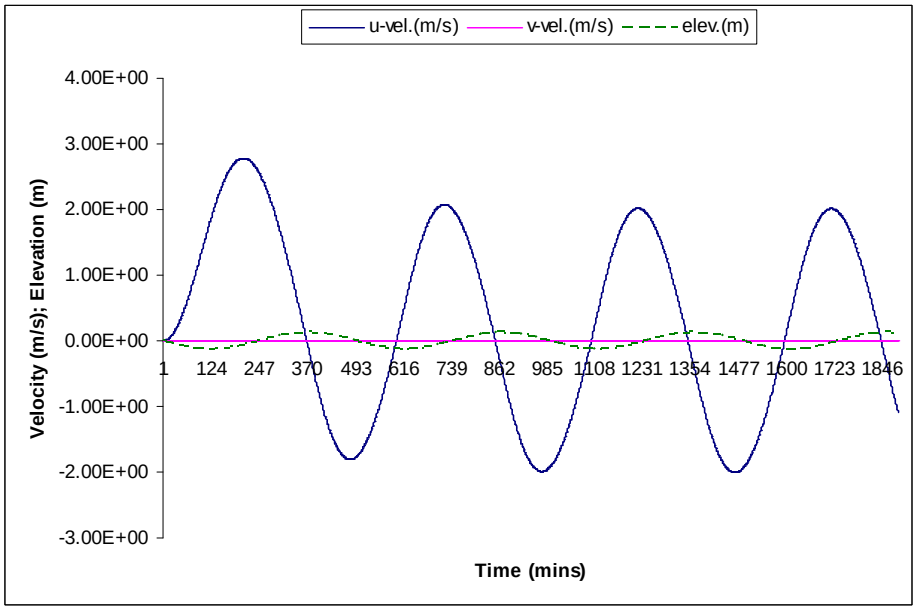

Figure 5.11: Tidal behaviour of the Strait of Messina simulated as a simple tidal channel (eastern region (180, 20))

The dominant maximum simulated tidal velocity in this case is 2 m/s for the whole domain, while the minimum is 0 m/s for the central zone of the domain, 9.30×10^{-3} m/s and 9.14×10^{-3} m/s for the western and eastern areas, respectively.

Meanwhile, the simulated tidal amplitudes are 0.129 m and 0.126 m for the western and eastern zones, respectively and 0.005 m for the central area. The minimum simulated tidal elevations, on the other hand, are 4.8 x 10^{-5} m and 1.88 x 10^{-6} m for the western and the eastern domains, respectively and 0 m for the central domain.

The zero values for both tidal velocity and amplitude in the chosen central cell (90, 20) of the domain of simulation mainly result from the interaction between the two opposite M_2-tidal waves (input and radiating). This may be regarded as a good representation of the amphidromic point within the real Strait of Messina. Additionally, the transverse tidal velocity component along the whole domain of simulation is too small to be considered. This agrees with the field records [139, 140, 188].

Examining the simulation outputs, flood and ebb have the westward and eastward direction, respectively. Figure 5.12 represents twelve successive hours of simulation output showing these movements. This is in good agreement with the real field records, where flood moves from the Ionian Sea towards the Tyrrhenian Sea, and the ebb moves southward in an opposite direction [161, 167, 188].

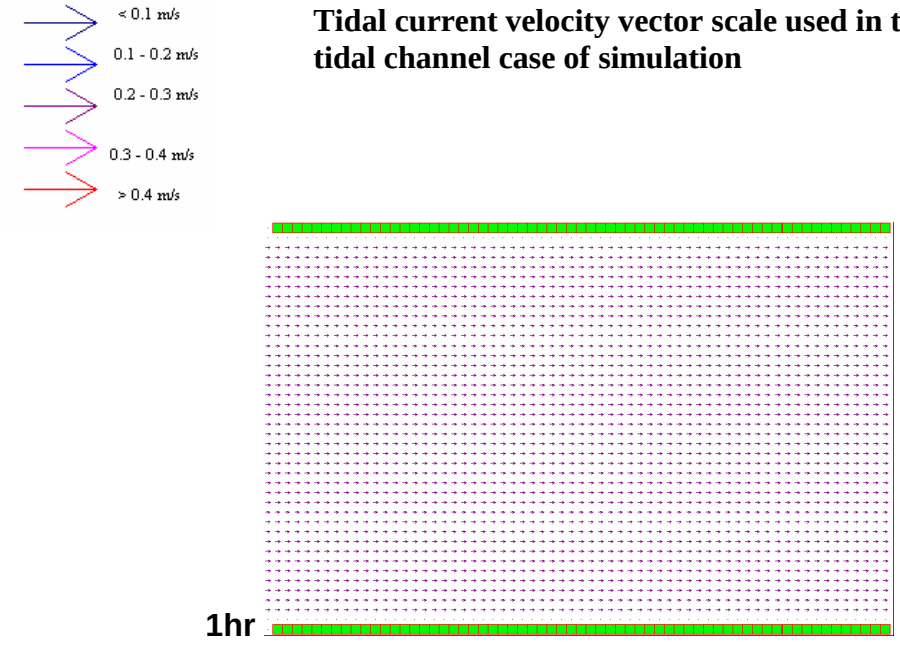

Figure 5.12: Simulated flood and ebb during 12 hours of simulation within the simple tidal channel using the TFD model

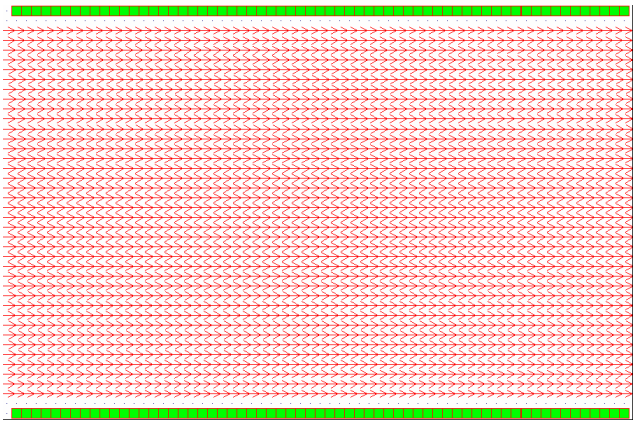

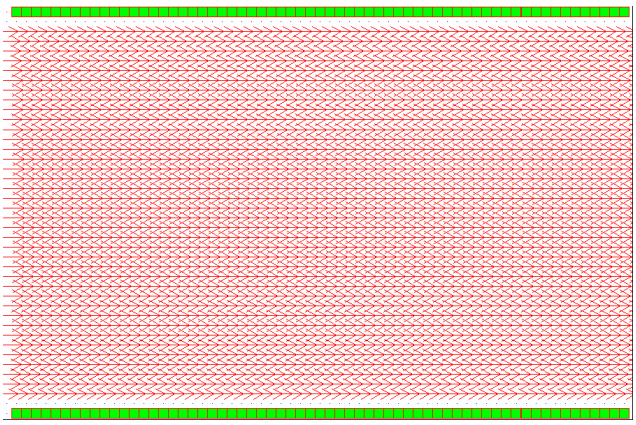

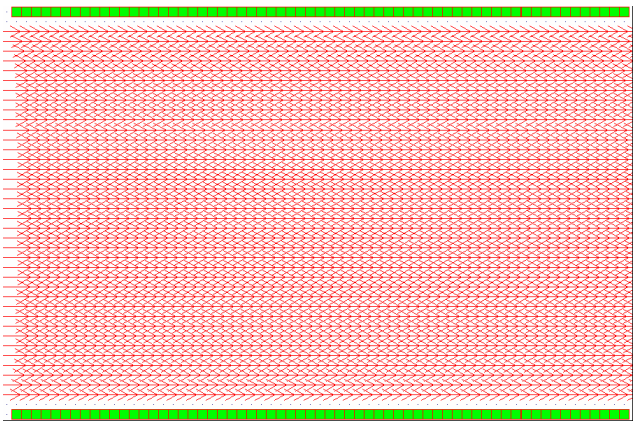

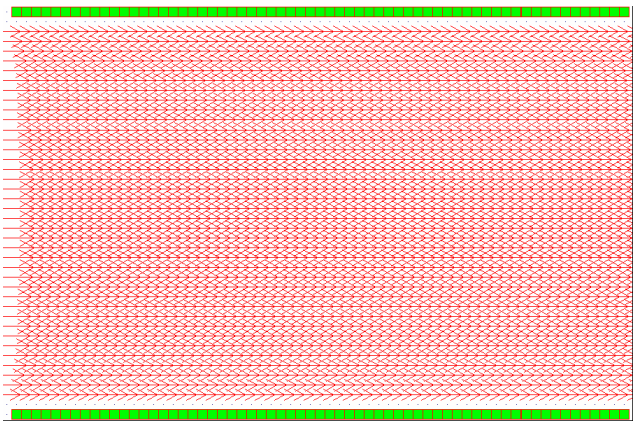

Figure 5.12 (Continued)

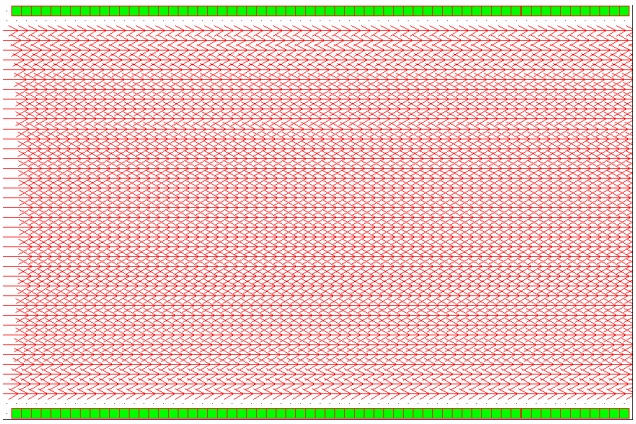

6hr

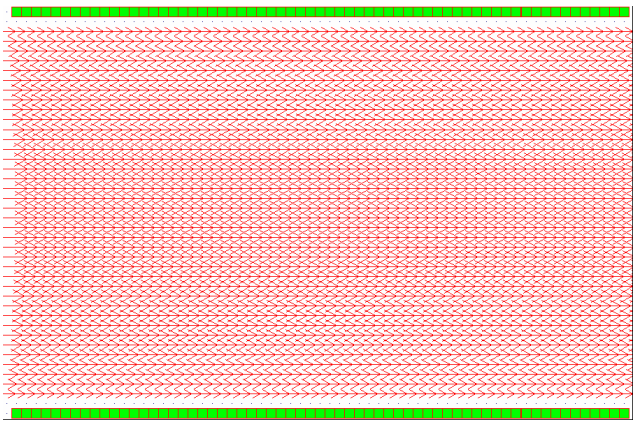

7hr

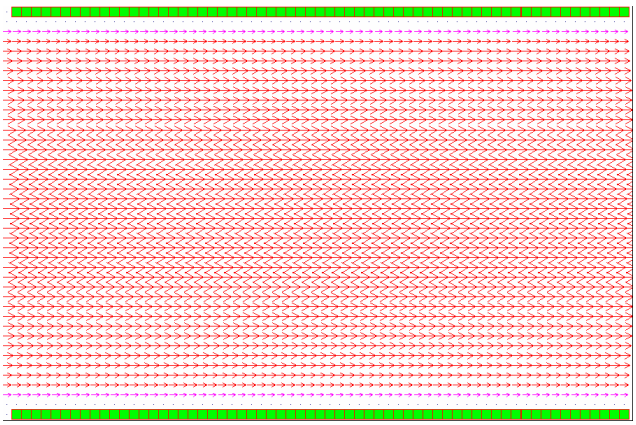

8hr

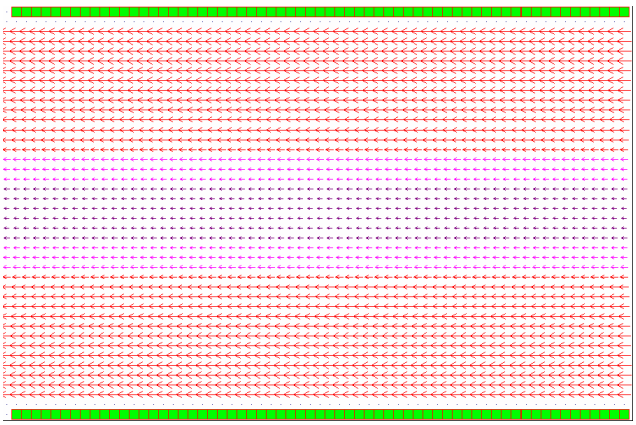

9hr

Figure 5.12 (Continued)

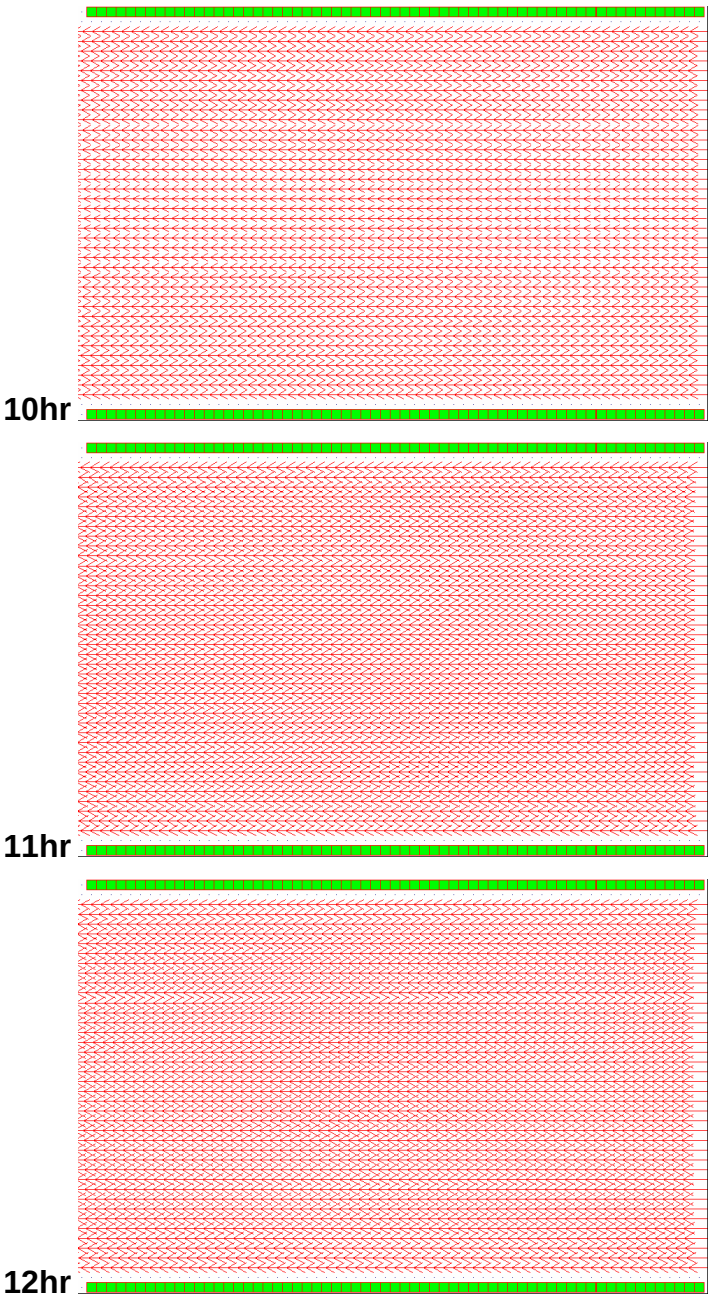

Figure 5.12 (Continued)

Tidal behaviour (velocity and elevations) within the Strait of Messina during the examination of the two most well-developed tidal phases: spring and neap tides, is important. For each chosen extremity, Capo Peloro in the north and Reggio Calabria in the south, four successive days for each tidal phase are chosen and the tidal constituents are examined from Admiralty Tide Tables [289]. Appendix (4) is the parameter file used to examine the spring tidal constituents for the northern tip, Capo Peloro. The M_2 constituent during both phases is important as it represents the

input/radiating boundaries for this simple tidal channel case of simulation. The Capo Peloro M_2-tidal wave represents the input boundary, while the Reggio Calabria M_2-tidal wave represents the radiating boundary for both spring and neap tides. The particular importance of the M_2-tidal wave is proved and applied to simulate the Strait of Messina in some previous studies, e.g. [140, 141, 191, 280]. Figures 5.13 (a, b) and 5.14 (a, b) are graphical representations of the M_2 constituent during spring and neap tides at the two extremities of the Strait.

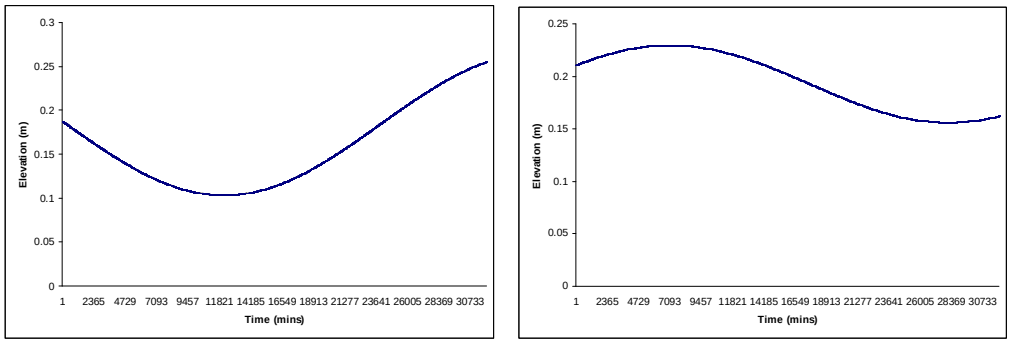

(a) **(b)**

Figure 5.13: The M_2-tidal constituent during (a) spring and (b) neap tides for the northern extremity of the Strait of Messina (Capo Peloro)

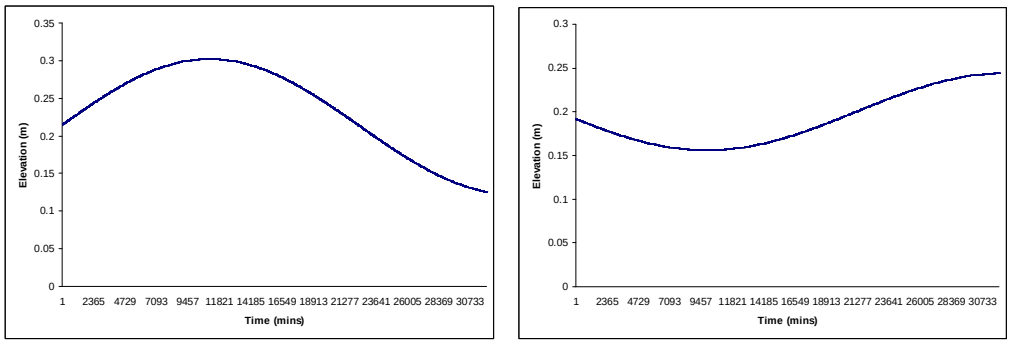

(a) **(b)**

Figure 5.14: The M_2-tidal constituent during (a) spring and (b) neap tides for the southern extremity of the Strait of Messina (Reggio Calabria)

12 successive hours of tidal velocity along the specified domain are represented in Figures 5.15 and 5.16 during spring and neap tides, respectively. Figures 5.17 (a, b and c) are the graphical representation of the tidal behaviour within the Strait during spring tide at the chosen western, central and eastern cells of the domain, respectively, while Figures 5.18 (a, b and c) represent the tidal behaviour during neap tide. During spring tide, the maximum simulated tidal velocity is 1.0 m/s at the western zone of the domain of simulation, while it is 0.61 m/s during neap tide for

the three chosen regions. The minimum simulated tidal velocity for the western and eastern zones within the domain of simulation are 6.78 x 10^{-4} m/s, 9.66 x 10^{-3} m/s, 9.95 x 10^{-4} m/s and 4.76 x 10^{-4} m/s during spring and neap tides, respectively. Again, the minimum simulated velocity for the central zone (cell (90, 20)) within the domain is 0 m/s during both spring and neap tides. The maximum simulated tidal amplitude is always recorded at the chosen eastern part of the domain with a value of 0.14 m during spring tide and 0.12 m during neap tide. The minimum simulated tidal elevation in the central zone of the domain of simulation is 0.07 m and 0.08 m during spring and neap tides, respectively. Meanwhile the western and eastern zones are identical in their minimum amplitudes during both phases. These are 0.05 m during spring and 0.07 m during neap. The very noticeable fluctuations (noise) which appear at the beginning of the graphical representation of the output might be referable to the interaction between the input and radiating M_2-tidal waves.

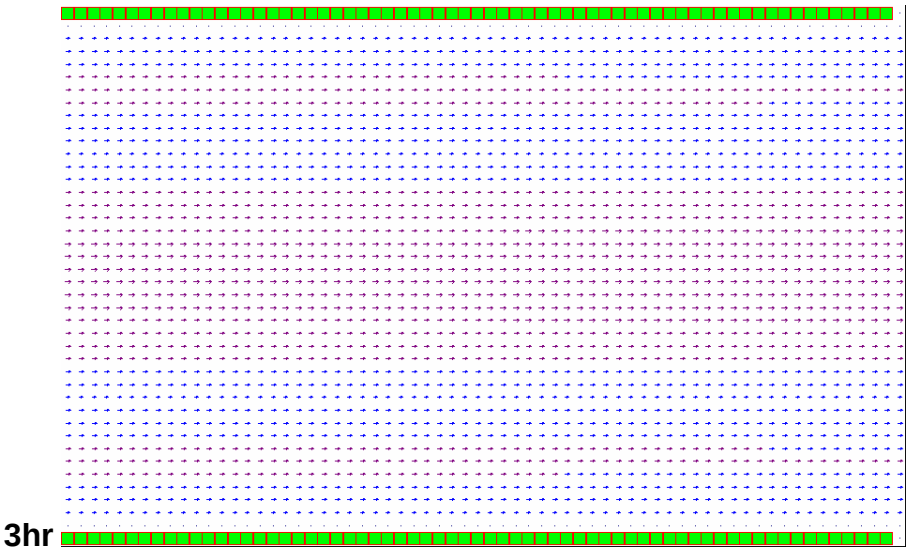

Figure 5.15: The simulated spring tide velocity for the Strait of Messina as a simple tidal channel using the TFD model

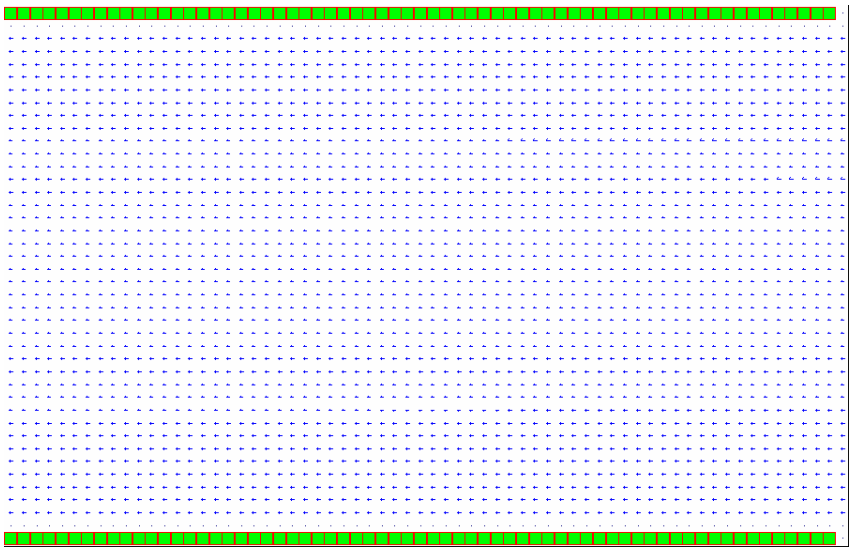

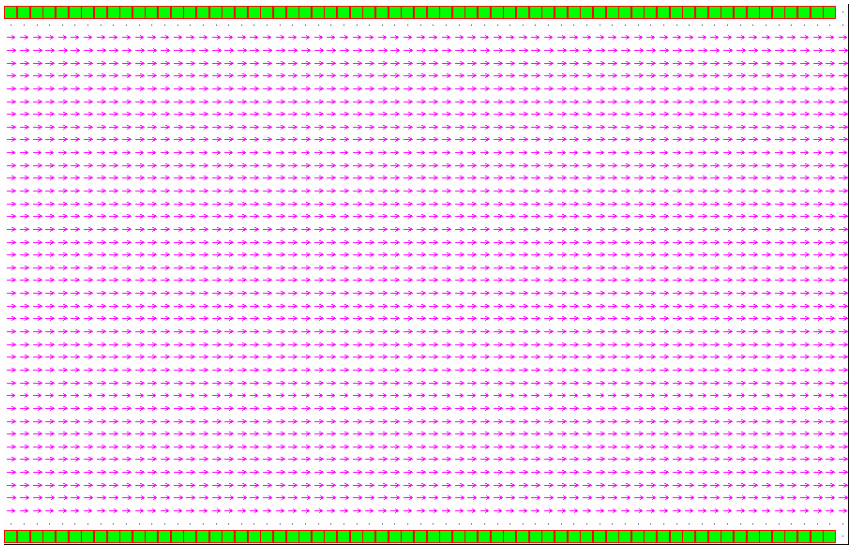

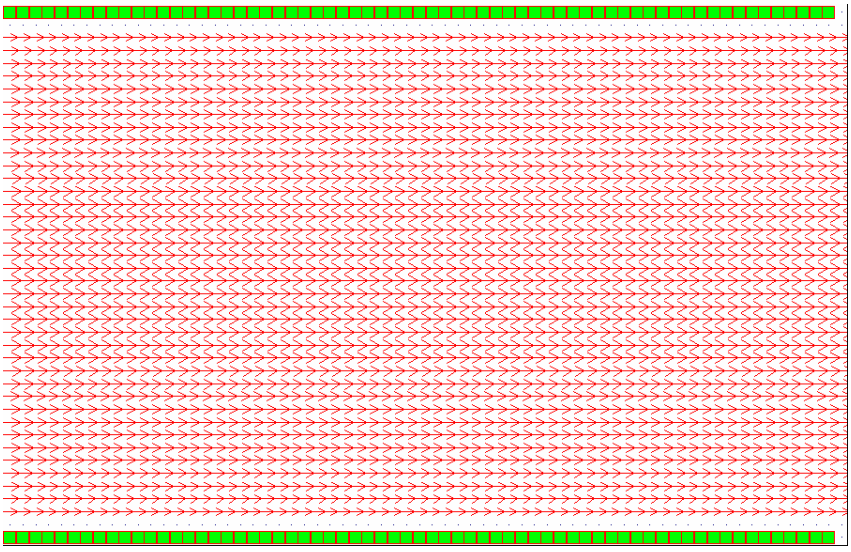

Figure 5.15 (Continued)

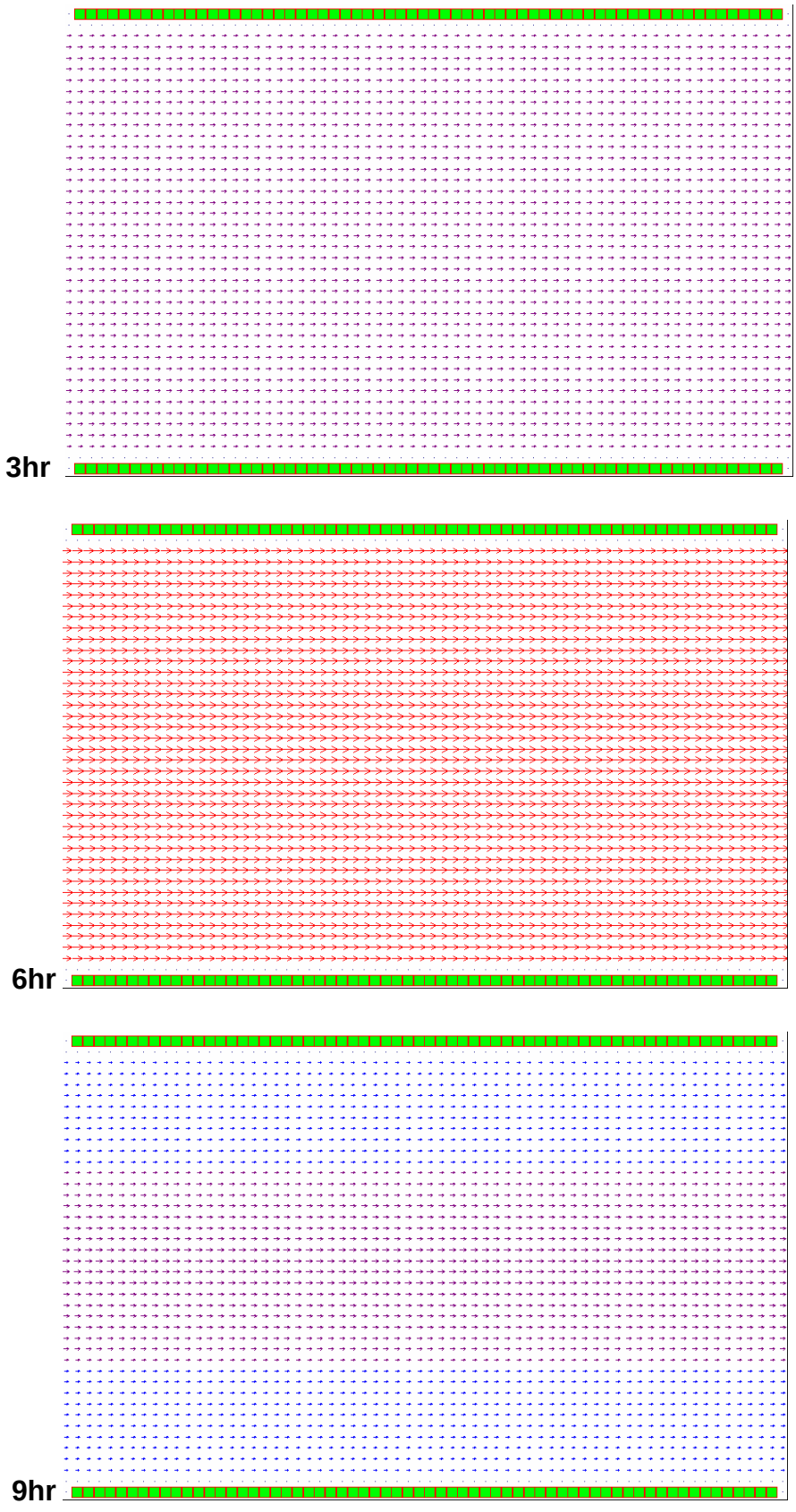

Figure 5.16: The simulated neap tide velocity for the Strait of Messina as a simple tidal channel using the TFD model

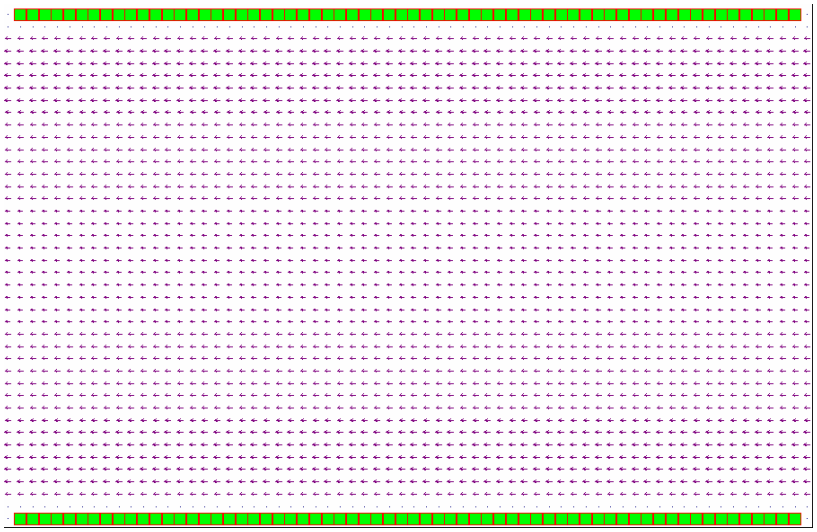

Figure 5.16 (Continued)

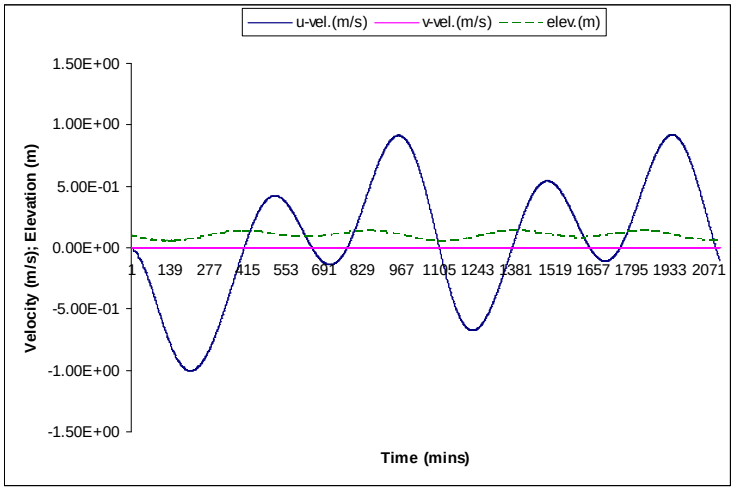

(a)

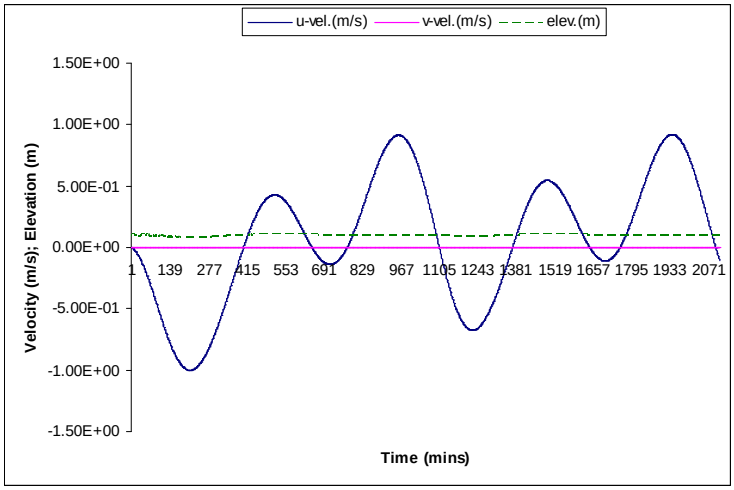

(b)

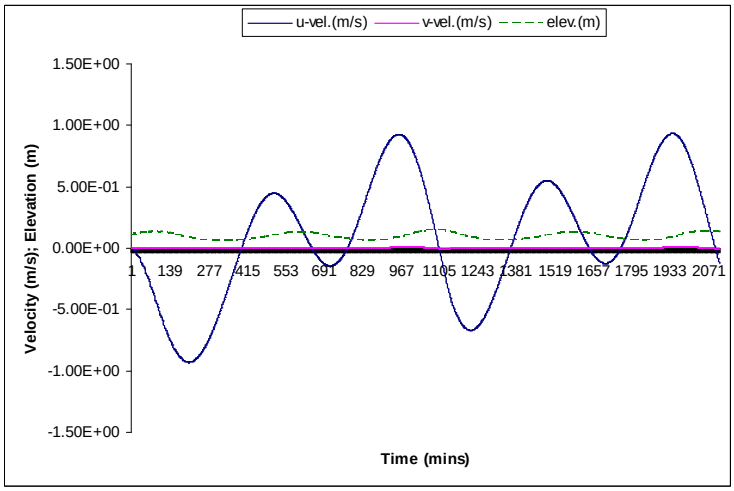

(c)

Figure 5.17: Tidal behaviour of the Strait of Messina simulated as a simple tidal channel during spring tide at (a) western, (b) central and (c) eastern chosen cells

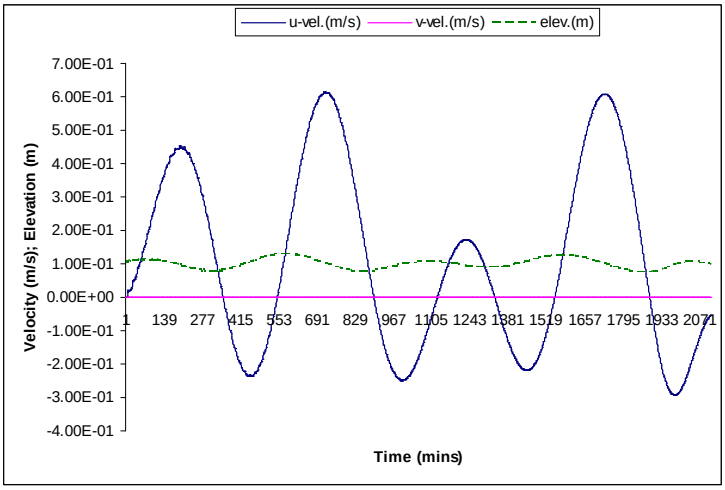

(a)

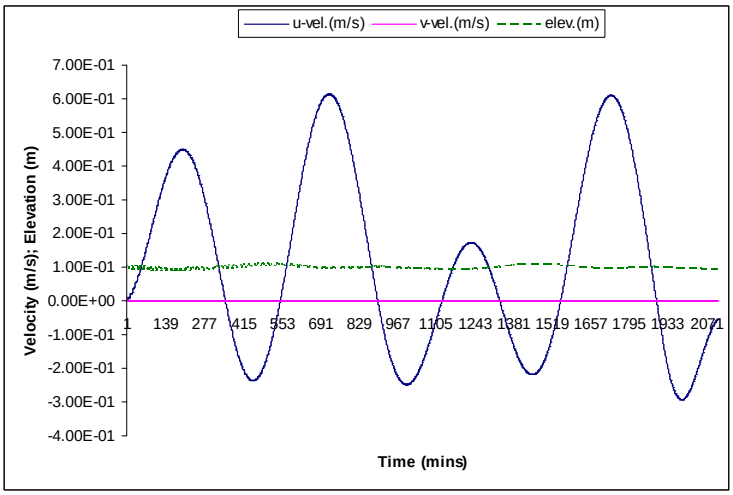

(b)

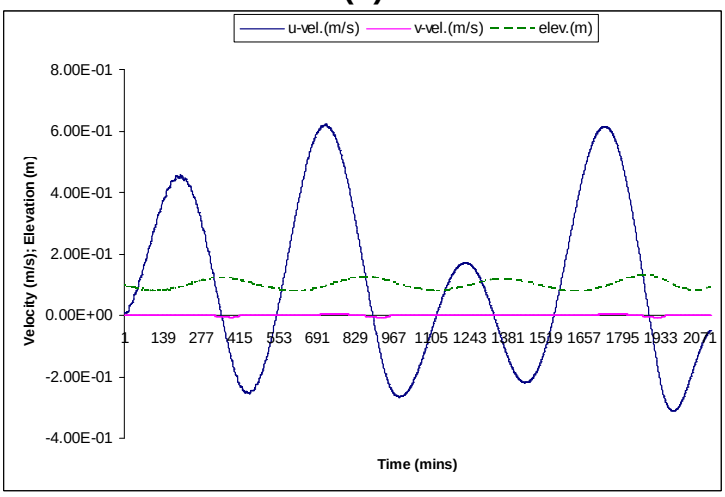

(c)

Figure 5.18: Tidal behaviour of the Strait of Messina simulated as a simple tidal channel during neap tide at (a) western, (b) central and (c) eastern chosen cells

5.4.2. The Strait of Messina as a real tidal domain

The numerical simulation process attempting to simulate the real Strait of Messina comprises of three different case studies. This is mainly due to the changes required in the TFD main code to mimic the complex morphometry and bathymetry of the Strait to a reasonable degree. The cases vary from an exact full real domain to a Level of No Motion (LNM) domain to a final case in which a flat constant depth is considered. The changes made in the TFD code as well as the shortness of the model used to mimic the Strait of Messina with the real conditions are discussed in detail hereunder. Step-by-step moves from one simulation case to the next are justified.

Eight positions were located along the domain of simulation which represents the real morphometry of the Strait of Messina, in the three examined cases, to present the checkpoints of the outputs. These locations are set in Table (5.3) and shown in Figure 5.19. Care is taken to represent red-spot points to check the final outputs. Thus the set of points includes the two chosen extremities Capo Peloro and Reggio Calabria, the sill section boundary cities Ganzirri (Sicilian coast) and Punta Pezzo (Calabrian coast), and a point close to Messina harbour, in addition to three other points that represent northern, central and southern locations within the domain. Ganzirri, Central Point and Punta Pezzo together represent the important section of the region of the sill in the Strait (Fig. 5.20). This will be the main area of interest for which the examined simulated tidal velocities will be schematically displayed for different cases of simulation in the present study.

Location	Latitude (38º xx.xx N)	Longitude (15º xx.xx E)
Capo Peloro	16.00	39.00
Reggio Calabria	06.00	39.61
Ganzirri	15.00	36.20
Punta Pezzo	13.00	37.91
Messina (Harbour)	10.80	33.60
Northern point	15.06	38.70
Central Point	14.16	37.43
Southern Point	10.03	35.10

Table 5.3: Names and locations of the checkpoints in the Strait of Messina

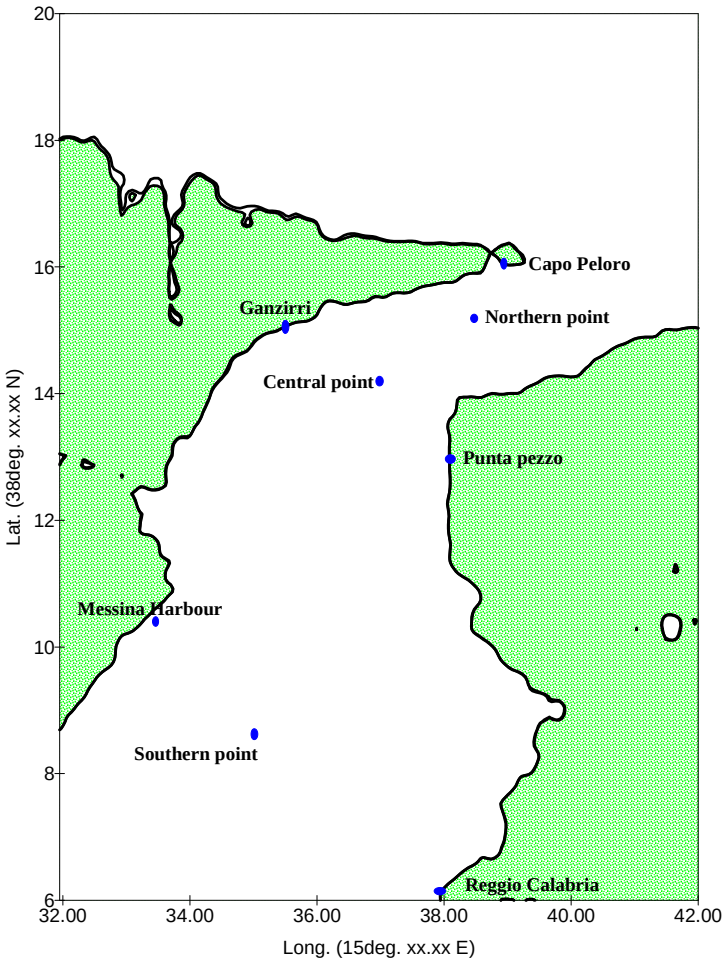

Figure 5.19: The simulation checkpoints in the Strait of Messina

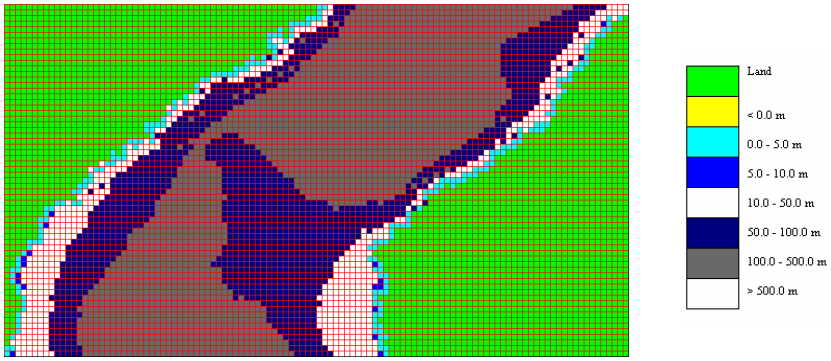

Figure 5.20: The grid of the area of interest (sill region) comprises the Ganzirri, Central Point and Punta Pezzo checkpoints

5.4.2.1. Real Strait of Messina case study

The constructed grid to simulate the Strait of Messina with its real morphometry and topographic features is shown in Figure 5.21. This grid is based on a cell grid of $\Delta x = \Delta y = 75$ m covering a domain of 150 x 260 cells.

Figure 5.21: The domain used to simulate the real Strait of Messina

The isodepth within the domain of simulation are interpolated based on real depth data extracted from Admiralty Charts [165, 290].

Three modifications take place along this constructed domain, which differ from the natural configuration of the Strait of Messina:

1- A smooth land-sea transition by applying a constant 2.5 m isodepth along the coastline within the whole domain.

2- Maintaining a uniform input entry for the applied driving force by a uniform extension at the northern domain boundary. This extension is of 750 m (10 cells x 75 m).
3- General depth degradation within the extended domain from the coastline seaward. The depth increases from 2.5 m close to the coastline to 202.7 m at the deepest point.

These modifications are required to control the driving input force to the domain from its northern boundary in order to obtain stable and realistic outputs. This is due to the interaction boundary between the Strait of Messina and the Tyrrhenian Sea that naturally represents a wide open boundary, which is difficult to simulate numerically and which will affect the resultant output. The difficulty in this open boundary stems from the fact this natural opening leads to having three affecting input driving forces to the main body of the Strait. This is mainly due to the natural morphometry of the Strait and its borders. The TFD model, as a 2D numerical model, deals only with one file of driving force to the target domain. Having three multidirectional forces the model will not respond to perform the simulation process. Moreover, if positively responded, a mess in the outputs may result giving meaningless results.

Having constructed the domain of simulation, the examination of the simulation process of the tidal flow regime within the Strait of Messina can then be processed. Two boundary files, driving and radiating, are built based on an M_2-sinusoidal uniform tidal wave of 0.135 m amplitude. This will satisfy the 0.27 m natural tidal range between the two extremities of the real Strait of Messina. Also, the two waves propagate in opposite directions, as shown in Figures 5.22 and 5.23, to fulfil the out-of-phase tidal behaviour between the real northern and southern tips of the Strait. The applied coefficients in this simulation process are set to be 9.81 m/s^2 for the acceleration due to gravity, 0.025 s/m^3 for the Manning coefficient and with the effect of the Coriolis force ignored.

Starting the simulation process using the previously mentioned driving/radiating tidal wave files and coefficients, the domain is checked to satisfy the CFL stability condition. The total period of simulation is 170000 s, i.e. 3.8 tidal cycles with time step dt = 0.25 s. The resultant accumulated output is given every 1800 s, i.e. every half an hour. Figure 5.24 represents the output of this simulation process. Figure 5.25

is a schematic representation of the simulated tidal velocity at the area of interest: the sill region, where tidal currents are expected to be enhanced to reach its maximum values and where tidal turbines may be deployed close to the eastern or western coasts.

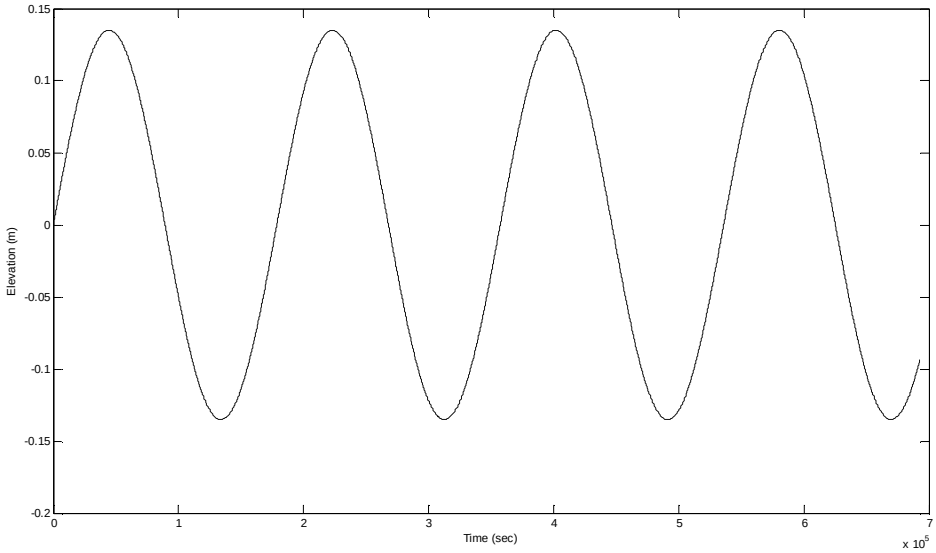

Figure 5.22: The M_2-tidal wave of 0.135 m amplitude used as input file

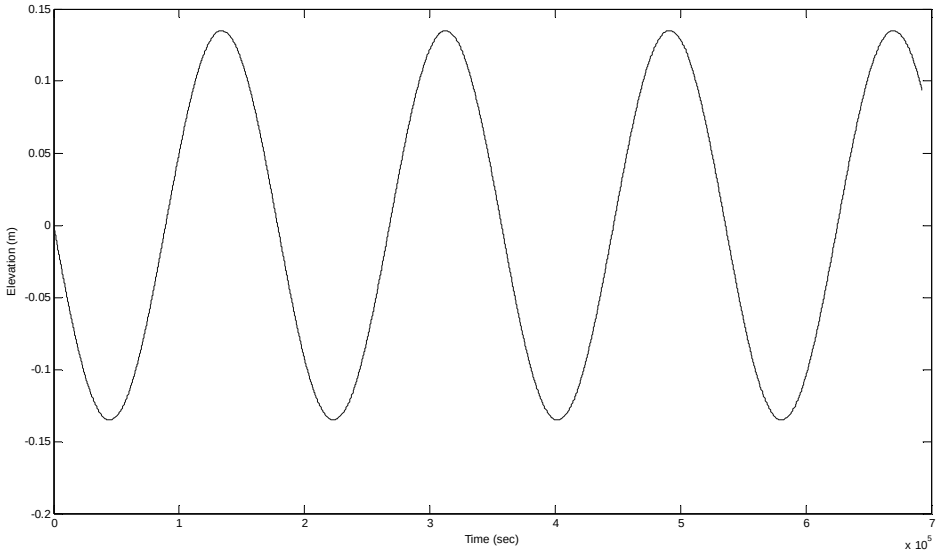

Figure 5.23: The M_2-tidal wave of 0.135 m amplitude used as radiating file

The simulated tidal velocity at the sill section is presented for 24 successive hours based on 6 hours interval, i.e. for two complete semidiurnal tidal periods. As may be

clearly observed, the resultant outputs do not reflect any feature of the natural behaviour for the real Strait of Messina, except the presence of the gyre north to Punta Pezzo, which was previously simulated [280] at the same place. The following points can be concluded:

1. The simulated tidal current velocities are very high exceeding 20 m/s, which never exist in the real field.
2. Extremely high and unstable amplitude distribution all over the domain, with no evidence of true tidal range or out-of-phase behaviour.
3. No tidal periodicity. As tides in the Strait of Messina are semidiurnal, it is to be expected that the flow changes direction every 6 hours, which is not fulfilled in this case.

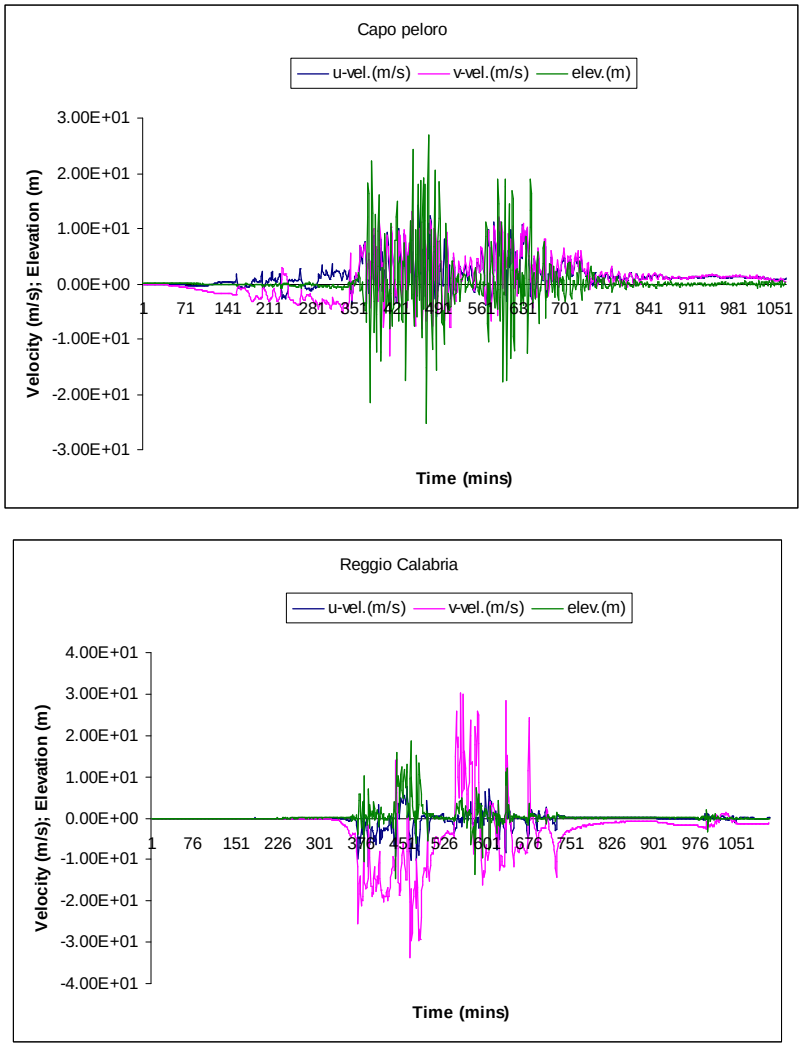

Figure 5.24: Tidal behaviour of the simulated real Strait of Messina

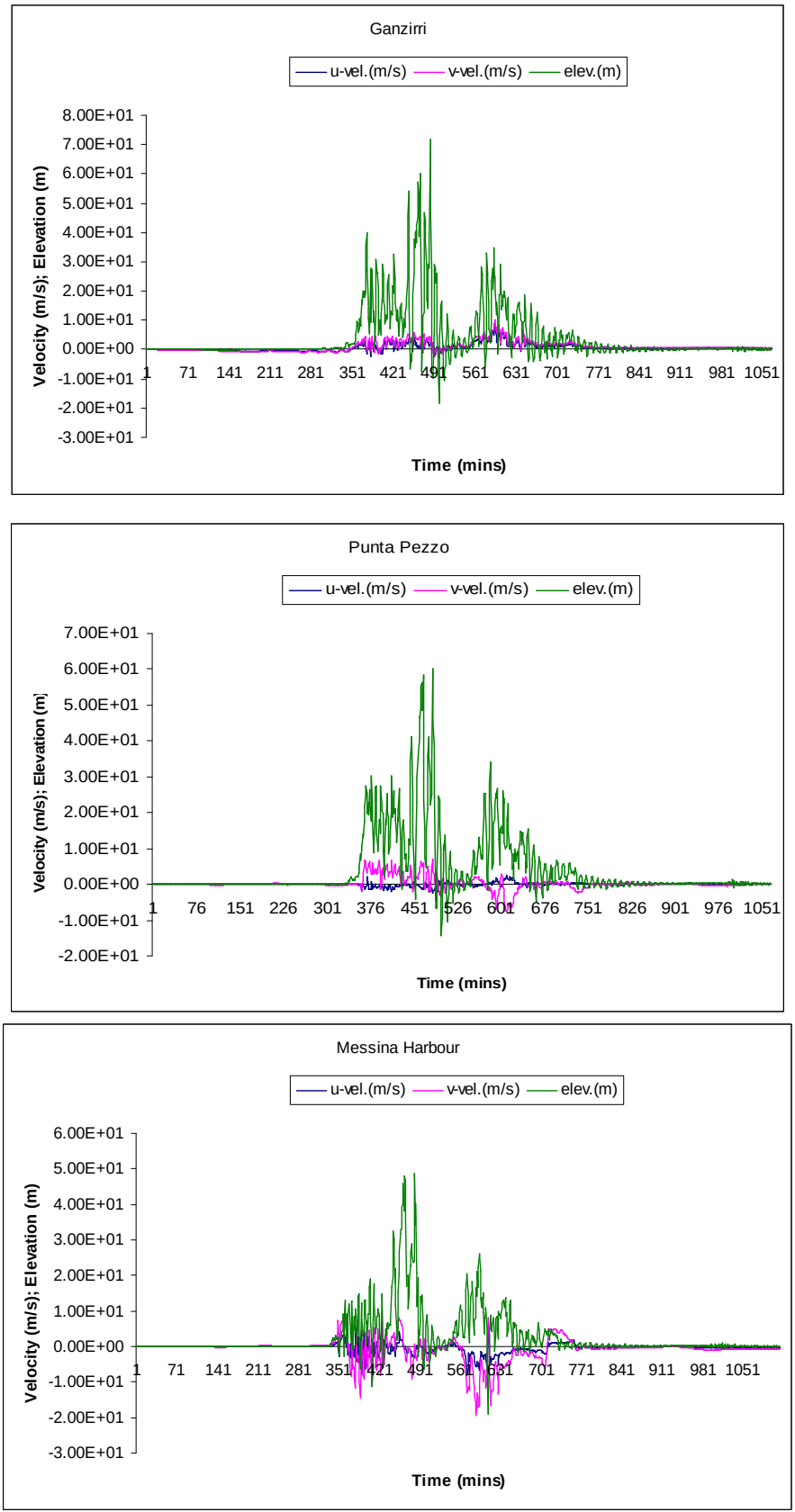

Figure 5.24 (Continued)

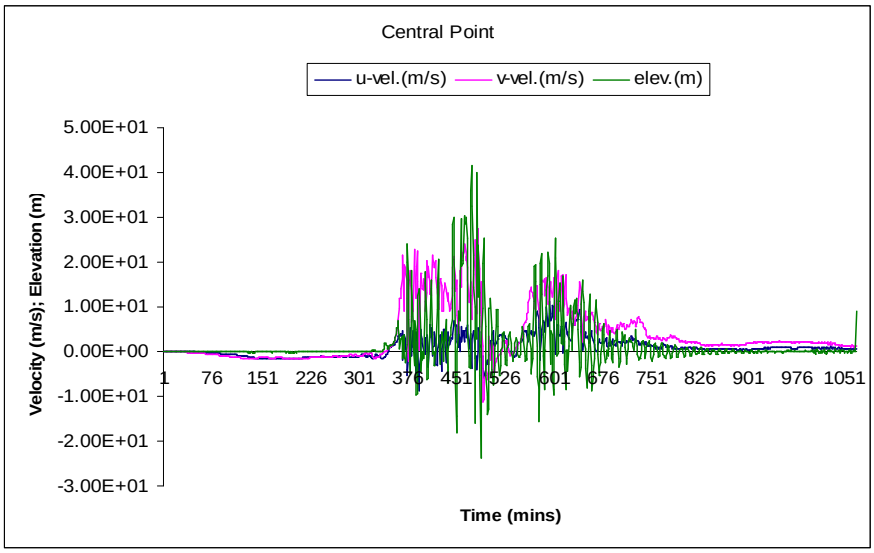

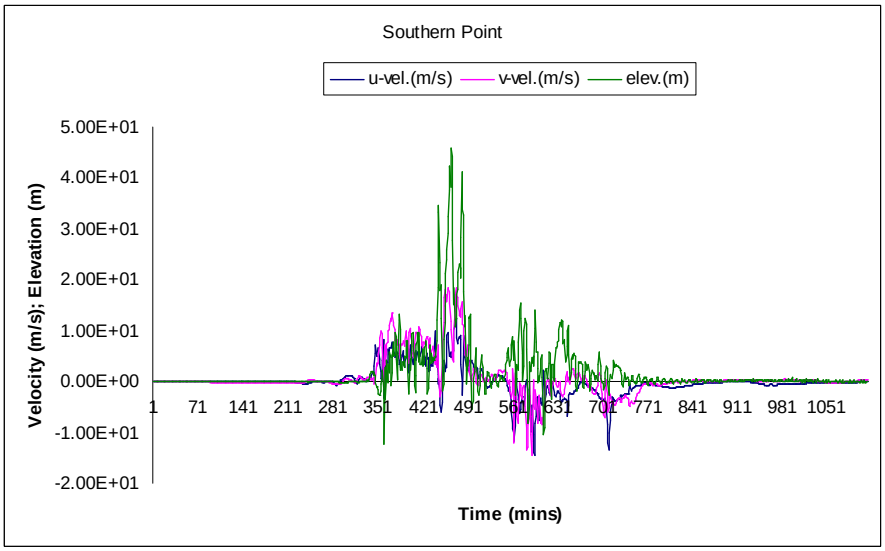

Figure 5.24 (Continued)

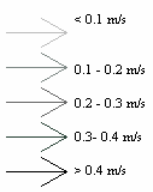

Tidal current velocity vector scale used in the different domains of the simulated real Strait of Messina

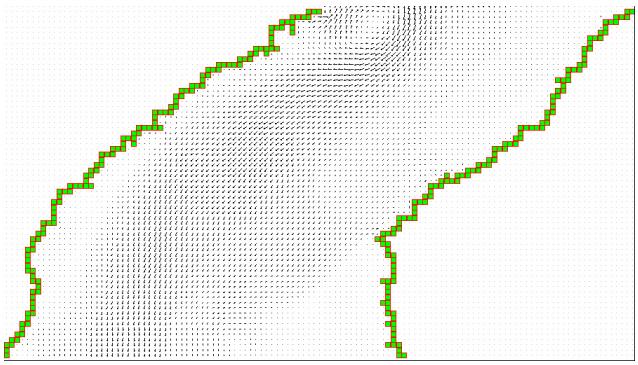

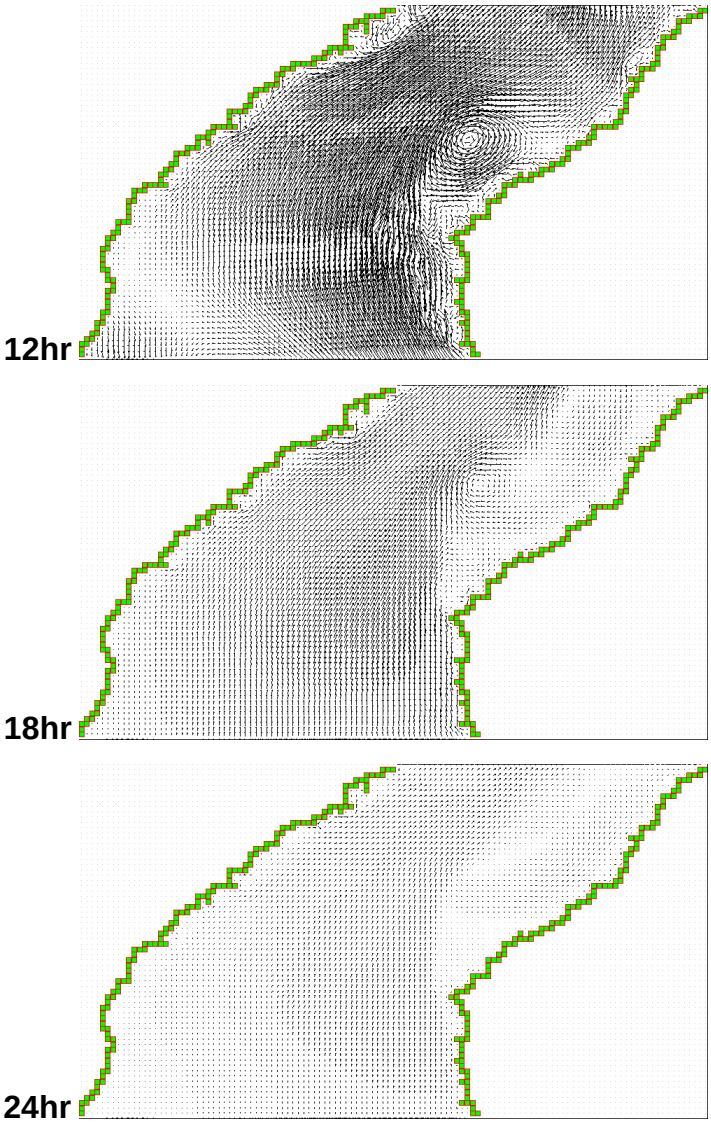

Figure 5.25: Initial simulated tidal velocities at the Ganzirri - Punta Pezzo section (sill region)

As a result of these unreasonable outputs, the effect of Coriolis force is therefore included in the calculations in order to check whether this may adjust the results of the simulation process. Looking at the specified domain, the mid-way latitude of the Strait is used to calculate the Coriolis parameter to be applied. This is the Lat. 38º 12' 00''N, i.e. 38.2º N. Consequently the Coriolis parameter is 9.02 x 10^{-5} s^{-1} ($f = 2\ \Omega \sin \varphi$; where Ω is the angular speed of Earth rotation = 7.2921159 × 10^{-5} rad/s and φ is the latitude). The simulation process is then carried out using the same driving/radiating boundaries and coefficients. The graphical presentations of the simulation process in this case are shown in Figure 5.26. It seems that the Coriolis

force does not result in more regular and stable outputs. Once more, the outputs are unrealistic, having a tidal current velocity exceeding 20 m/s and a tidal amplitude exceeding 50 m. In addition, the semidiurnal tidal periodicity is still not predicted by the flow regime. Moreover, examination of the simulated velocities shows some errors in the predicted direction of flow (Fig. 5.27). It is supposed that under the Coriolis Effect the input flow directed from the north southward will be driven to accumulate to the western coast of the Strait, which does not happen in the obtained results. This poses a question as to the validity of the effect of the Coriolis force in the TFD model. To get an answer, a simple domain made up of 20 x 20 cells of extent $\Delta x = \Delta y = 150$ m is constructed. The domain of simulation is an open 2D coastal area of uniform depth of 30 m and the effect the Coriolis force is checked at the same latitude (38.2º N). Using a driving simple sinusoidal wave of 1.0 m amplitude directed from north to south for 45000 s (i.e. one complete tidal cycle), the hourly results show unreasonable outputs applying the effect of the Coriolis force (Fig. 5.28).

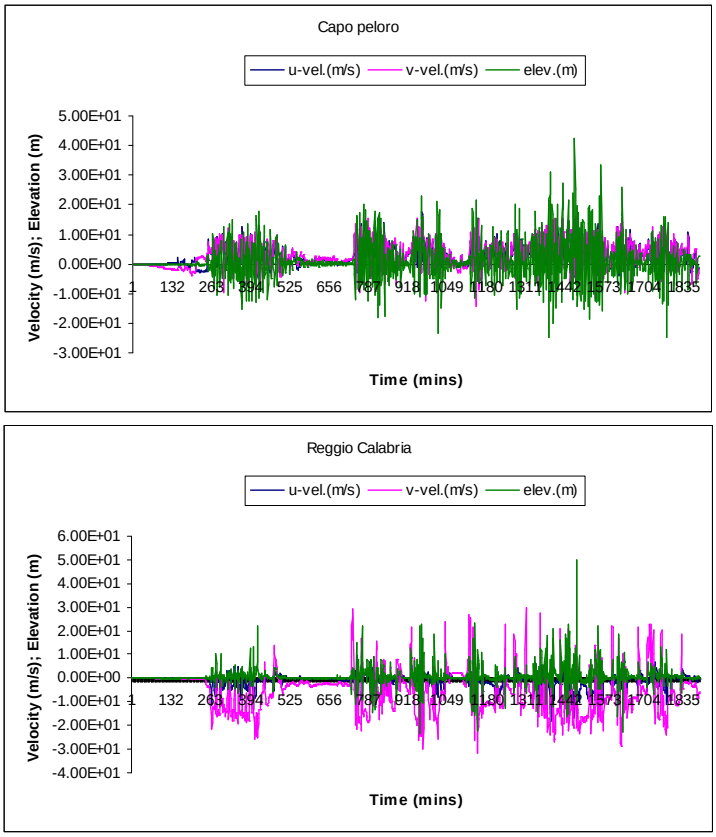

Figure 5.26: Tidal behaviour of the simulated real Strait of Messina applying the Coriolis force effect

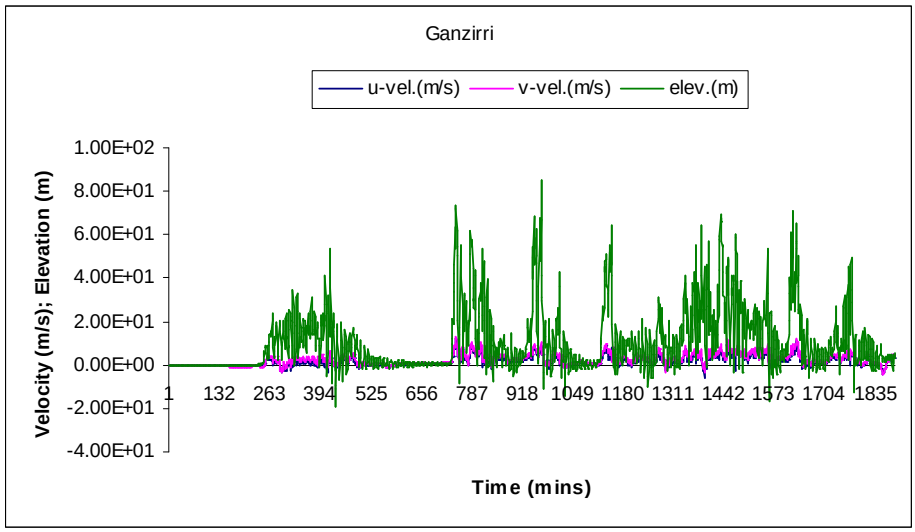

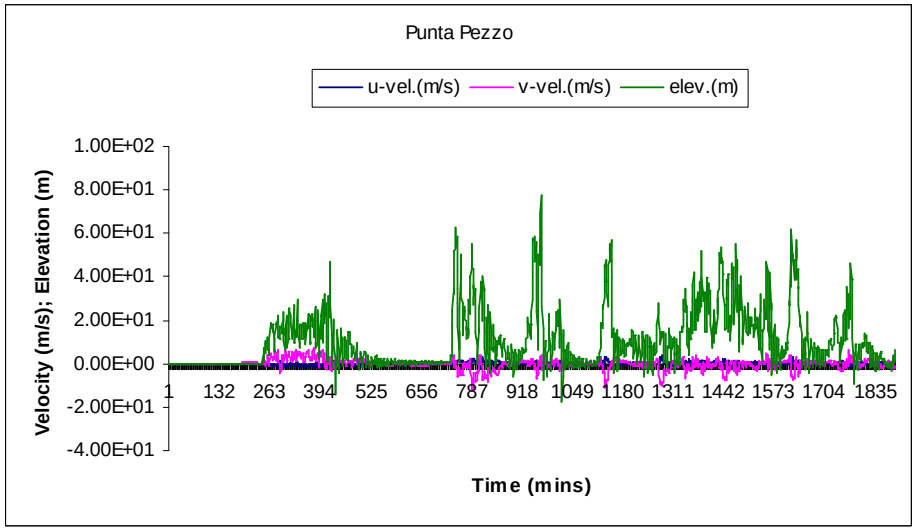

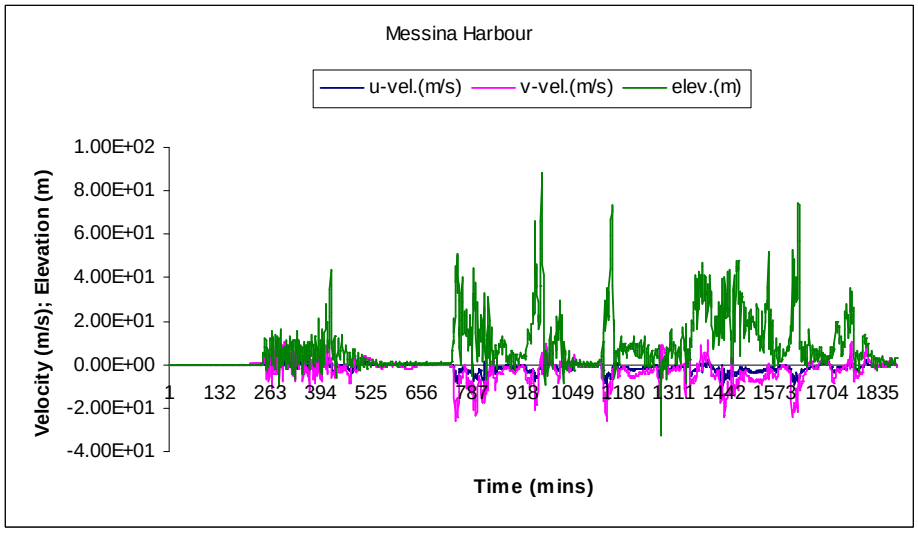

Figure 5.26 (Continued)

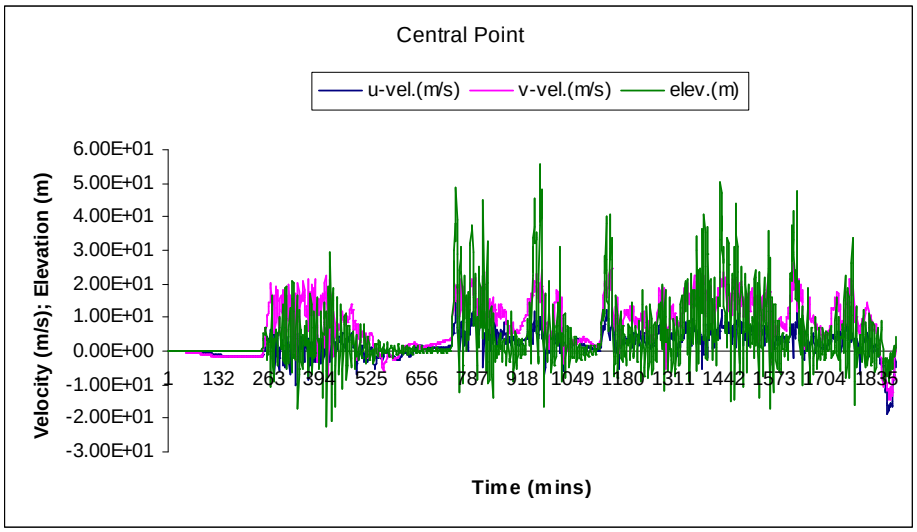

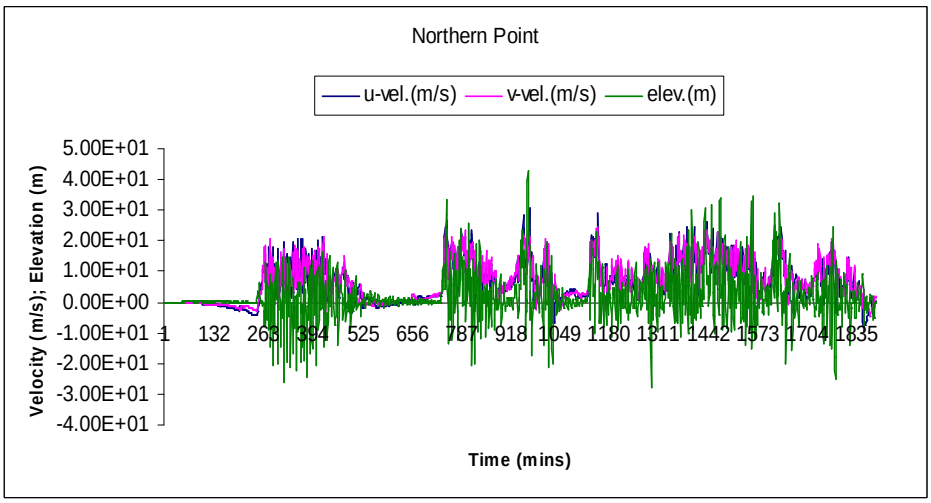

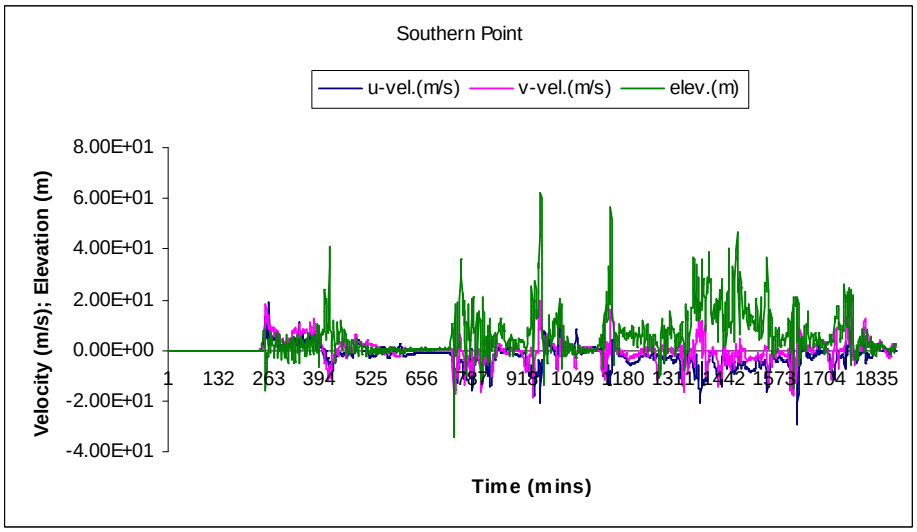

Figure 5.26 (Continued)

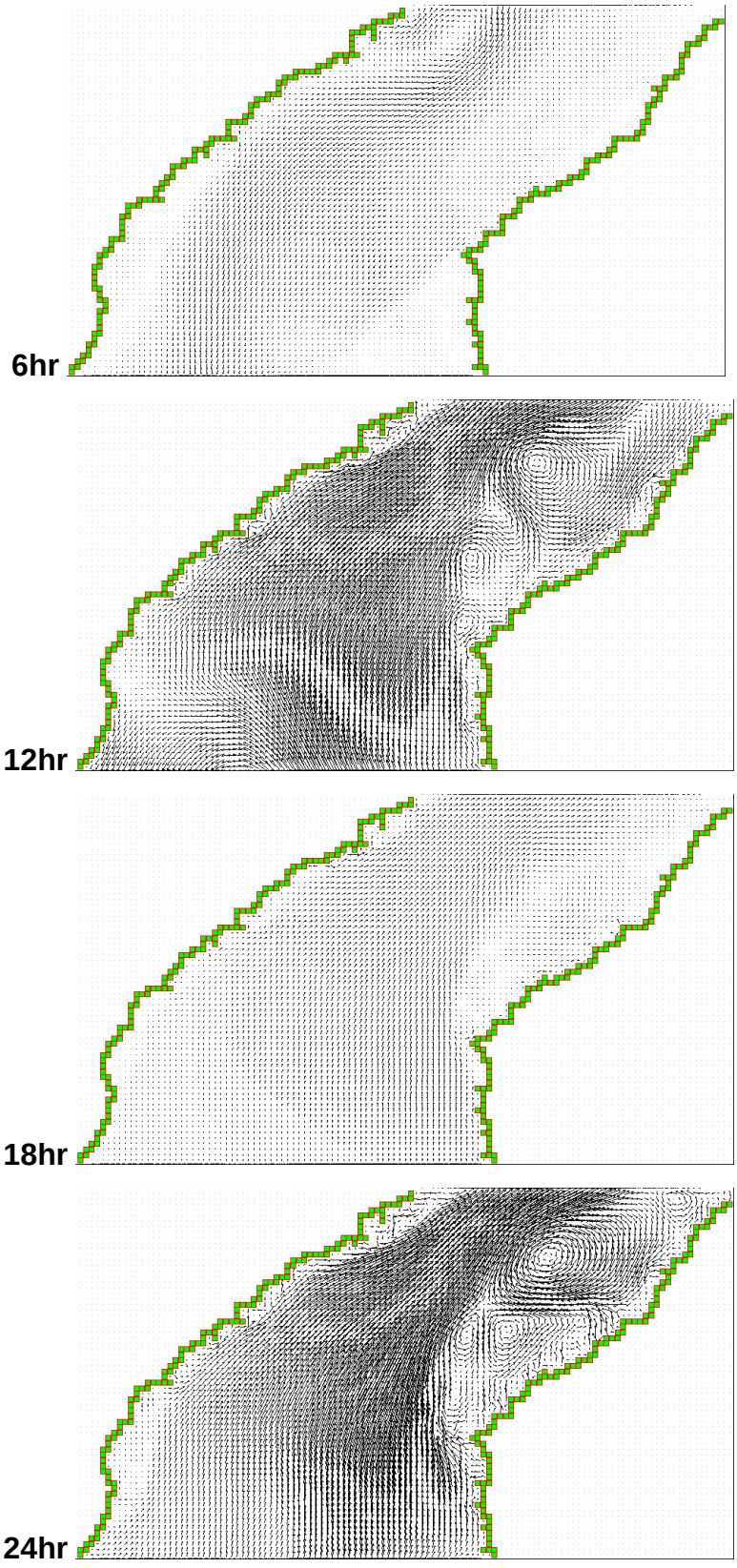

Figure 5.27: Second simulated tidal velocities at the Ganzirri - Punta Pezzo section (sill region)

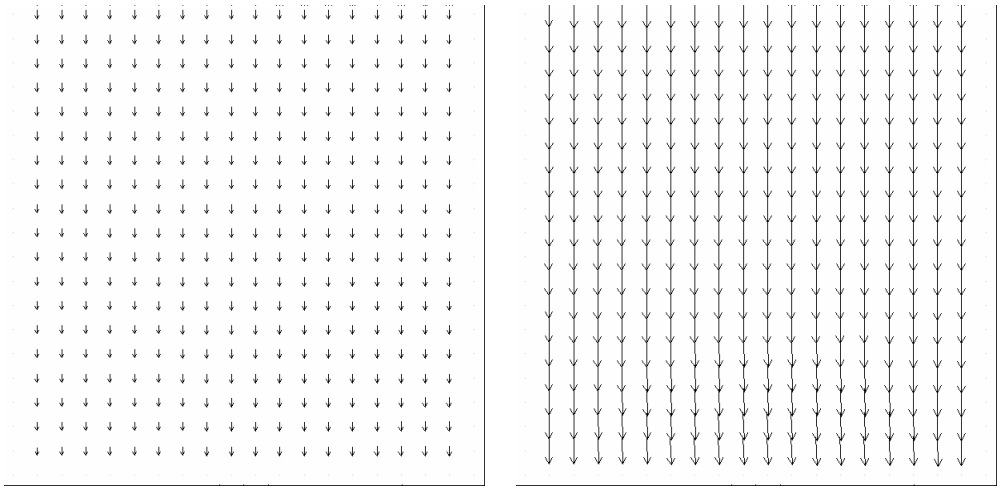

1hr **2hr**

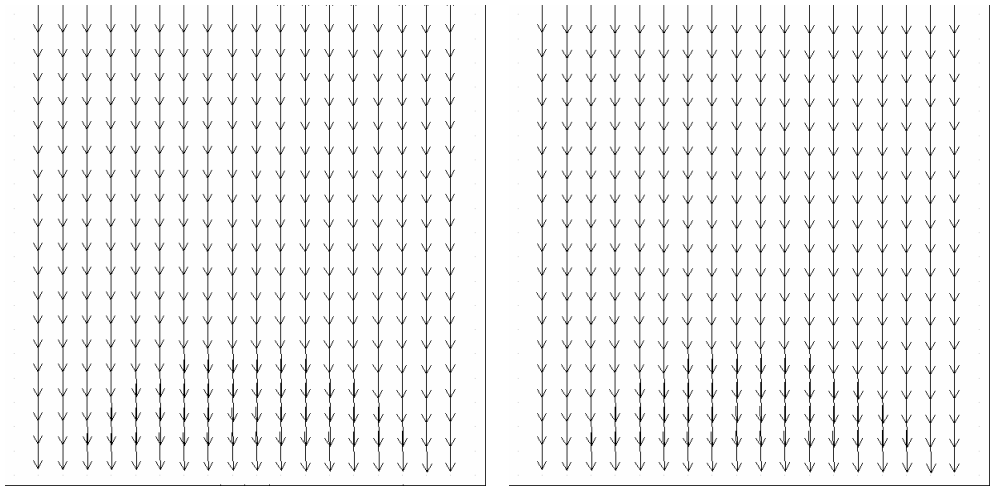

3hr **4hr**

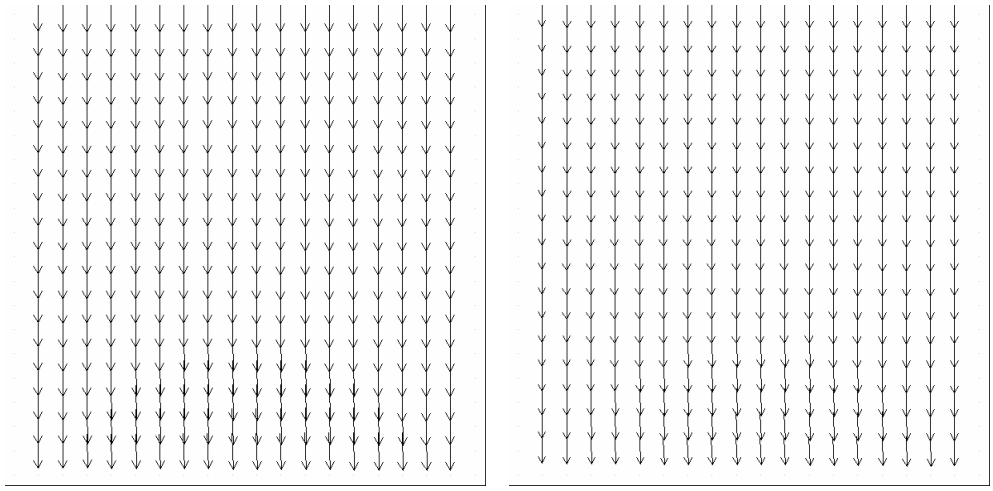

5hr **6hr**

Figure 5.28: A simple domain to check the validity of the Coriolis force in an unsteady domain using the TFD model

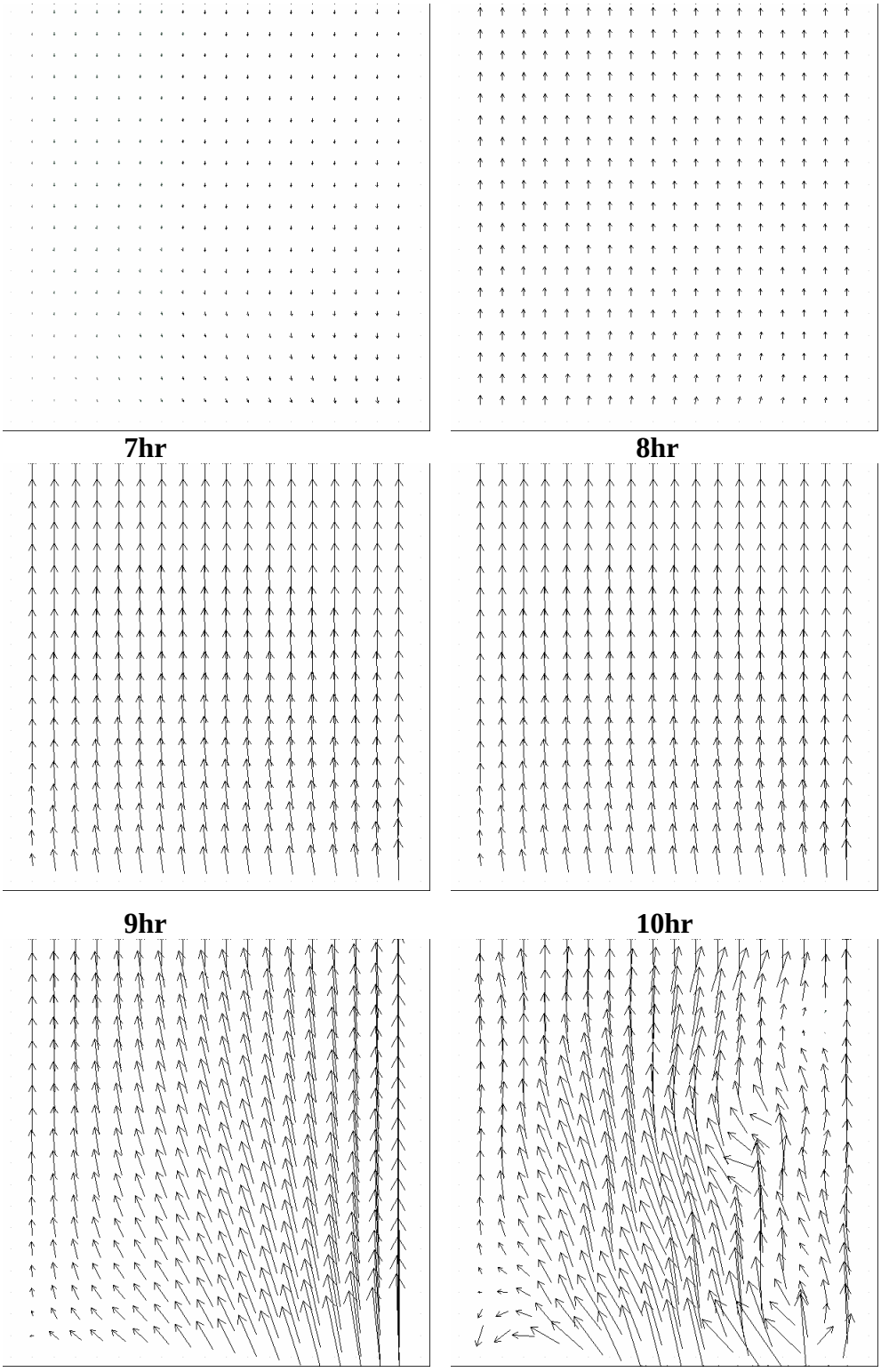

Figure 5.28 (Continued)

Hence, the Coriolis force does not have the expected effect of smoothening the simulated velocities and amplitudes and, additionally, does not mimic the real Coriolis field. Accordingly, the Coriolis force will be ignored in the all forthcoming cases of simulation.

The next assumption made to obtain stable outputs from the model was to increase the effect of the eddy viscosity term within the main code. This was done to increase the affecting frictional forces acting on the moving flow in order to reduce the resultant extreme velocities and amplitudes. The effect of the eddy viscosity term is multiplied by 10. For the new simulation process, the main driving/radiating files of M_2-tidal wave (0.135 m amplitude), Manning factor = 0.025 s/m^3, and a ten times eddy viscosity effect are applied for 170000 s total simulation time, i.e. more than 3 complete tidal cycles, based on dt = 0.25 s. The graphical presentation of this simulation process is given in Figure 5.29, while the results of 24 successive hours of simulation representing the area of interest (sill region) are shown in Figure 5.30.

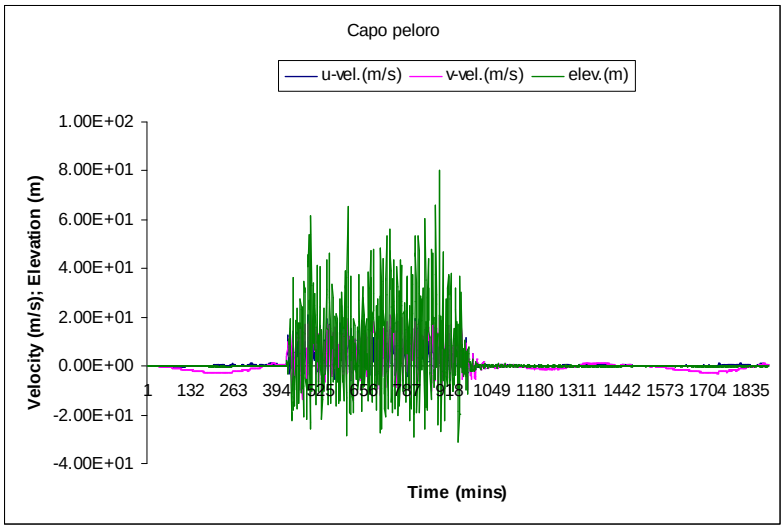

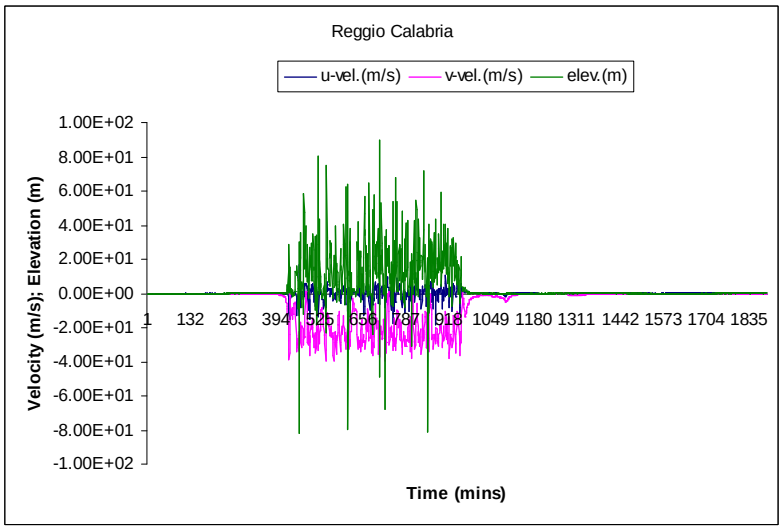

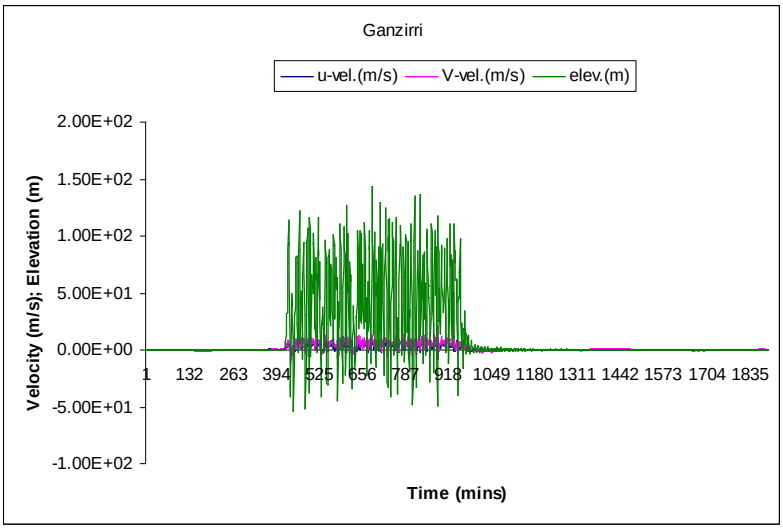

Figure 5.29: Tidal behaviour of the simulated real Strait of Messina using high eddy viscosity effect

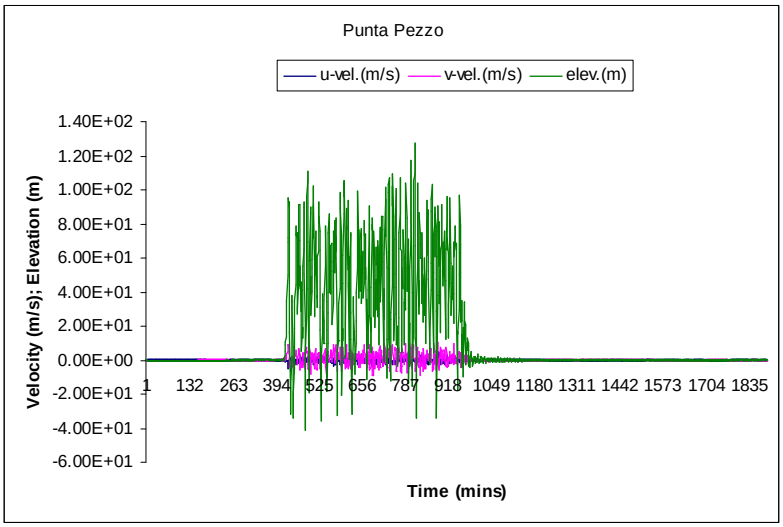

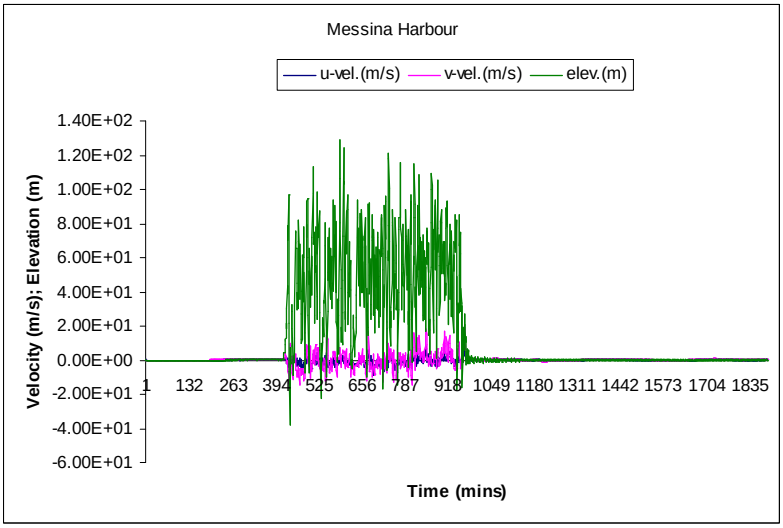

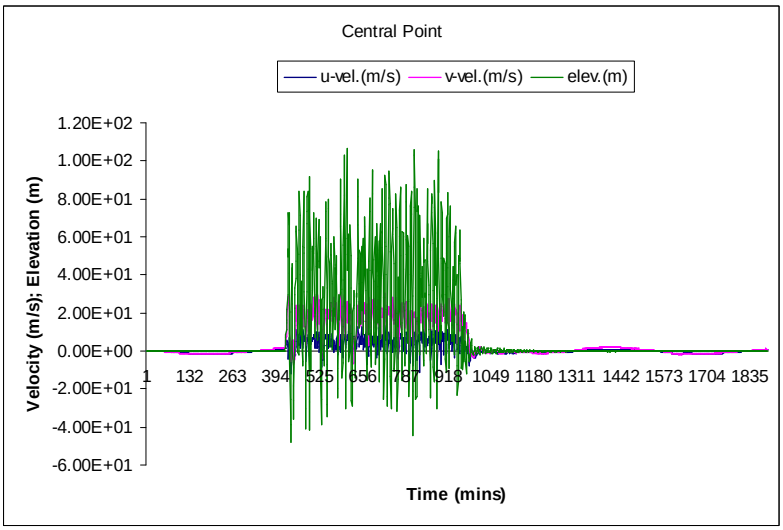

Figure 5.29 (Continued)

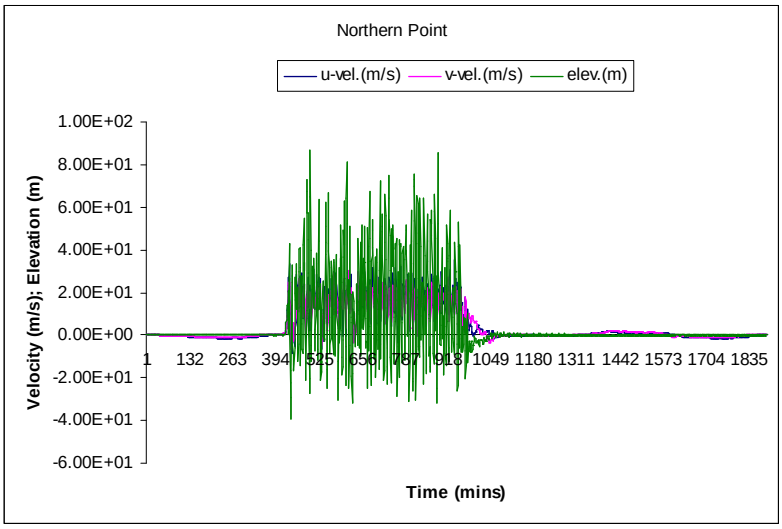

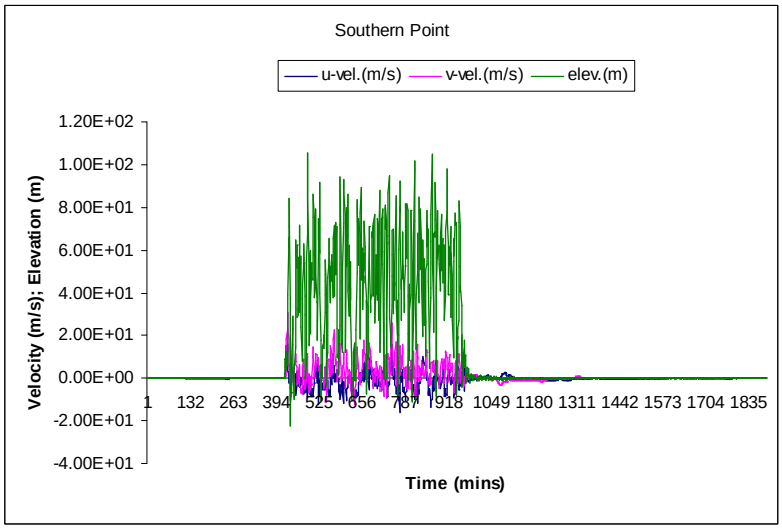

Figure 5.29 (Continued)

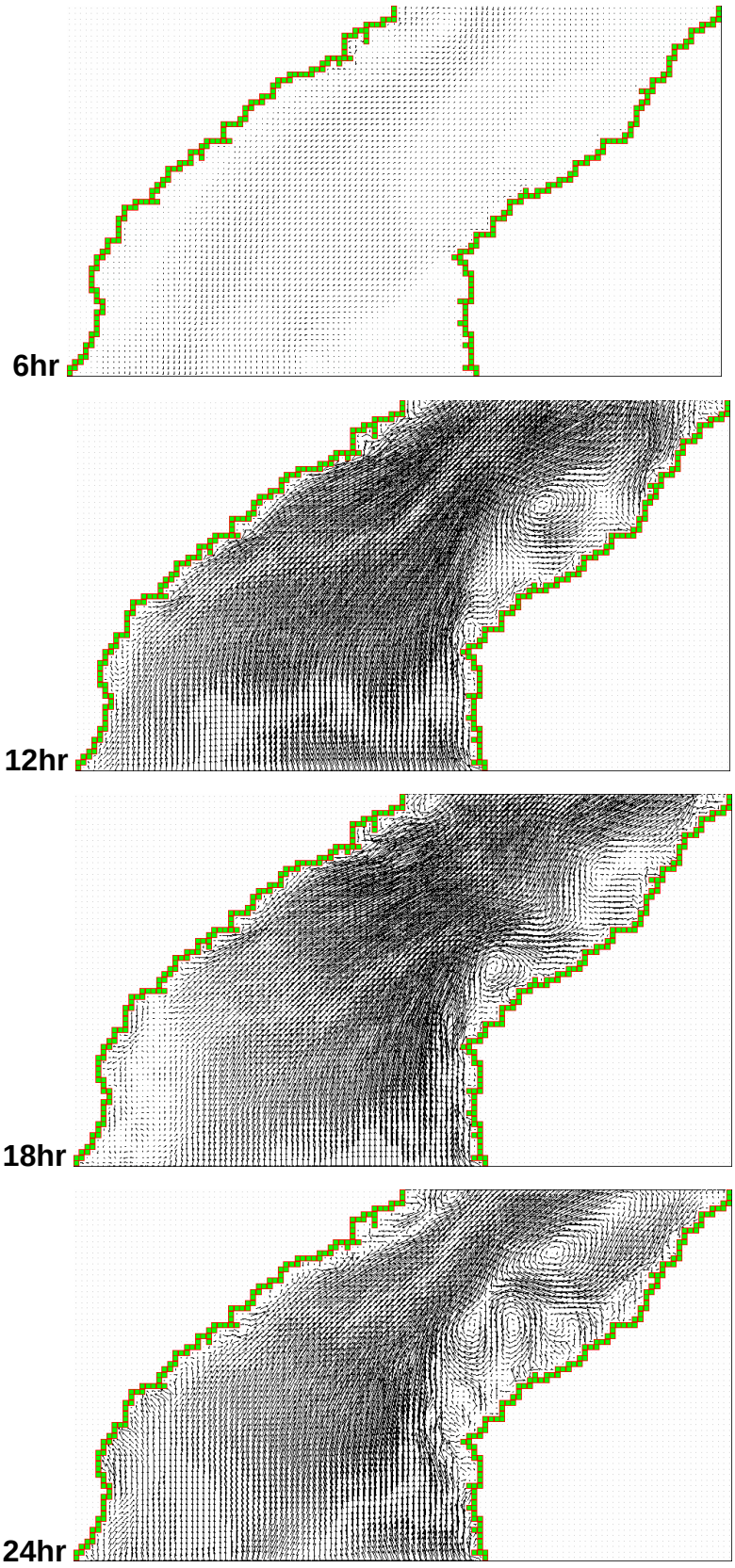

Figure 5.30: Third simulated tidal velocities at the Ganzirri - Punta Pezzo section (sill region)

It is still obvious that the outputs of the simulation process of the real Strait of Messina are still unstable and do not resemble the simulated area of study. The problem now is how to obtain realistic tidal velocities and amplitudes and to simulate the semidiurnal tidal cycle in the Strait of Messina. This is again made by increasing the effect of the frictional forces acting on the tidal flow within the domain of simulation. Having increased the effect of the eddy viscosity term to ten times its original value, the seabed frictional force is now dealt with by increasing the value of the roughness Manning coefficient. By gradually increasing this coefficient to twice (0.05 s/m^3) and three times (0.075 s/m^3) its original value, this failed to change the unstable simulated tidal behaviour. Raising the roughness Manning coefficient to 0.1, i.e. to four times its original normal value, and applying the normal effect of the eddy viscosity term, the resultant tidal behaviour are shown in Figure 5.31. It seems that raising the Manning coefficient, which means increasing the value of seabed friction parameter, has its effect on the simulated tidal outputs, velocity and amplitudes, as noticed from the figures. At the start of the simulation process (385 mins), the tidal out-of-phase behaviour between the northern and southern boundaries (Capo Peloro and Reggio Calabria; northern and southern points) is confirmed. Throughout the simulation period, the velocity values are reduced to reach values not exceeding 4 m/s and amplitudes do not exceed 2 m. However, the simulated outputs still suffer from instability that does not reasonably reflect the real tidal flow regime within the Strait of Messina. Accordingly, making a decision to allocate the place of excess energy where tidal turbines may be deployed is still distant. Moreover, the semidiurnal tidal behaviour is still missed in the present simulation outputs. Figure 5.32 shows the simulated velocity outputs for the sill region section.

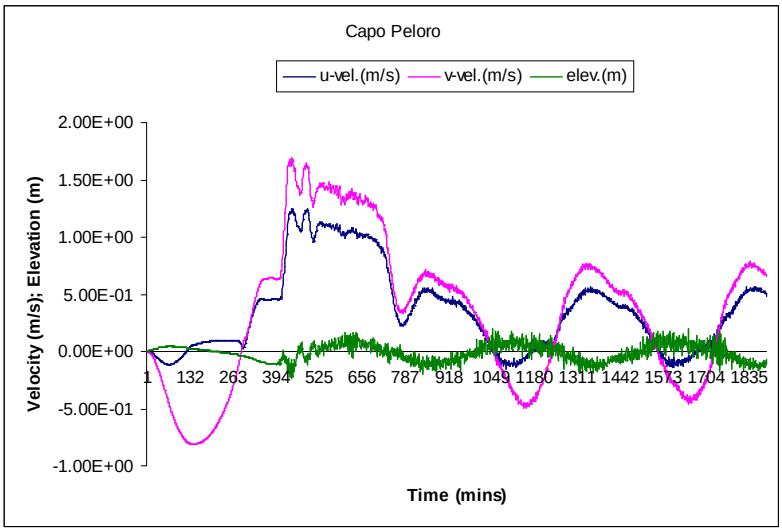

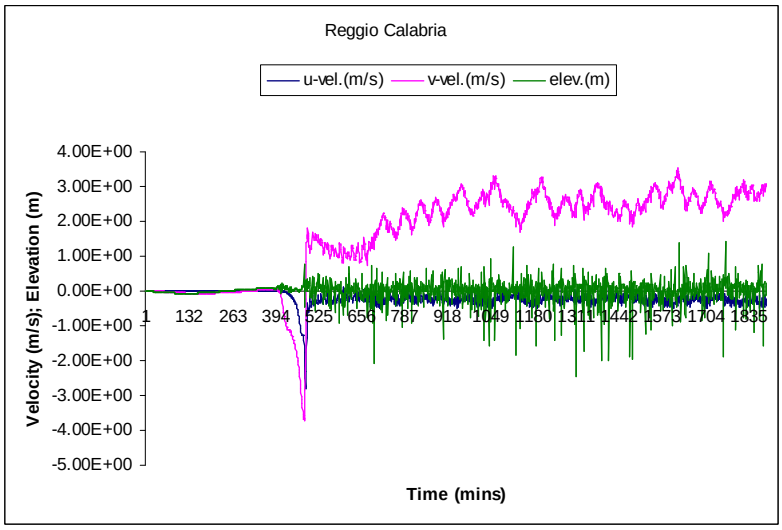

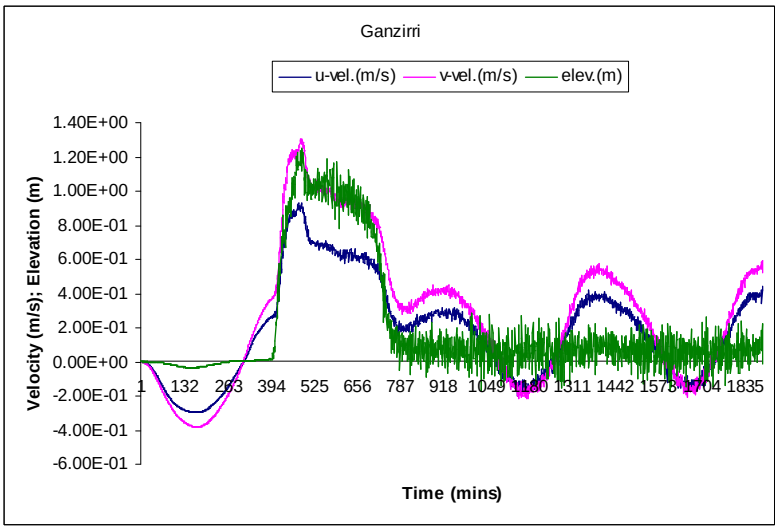

Figure 5.31: Tidal behaviour of the simulated real Strait of Messina using high Manning coefficient

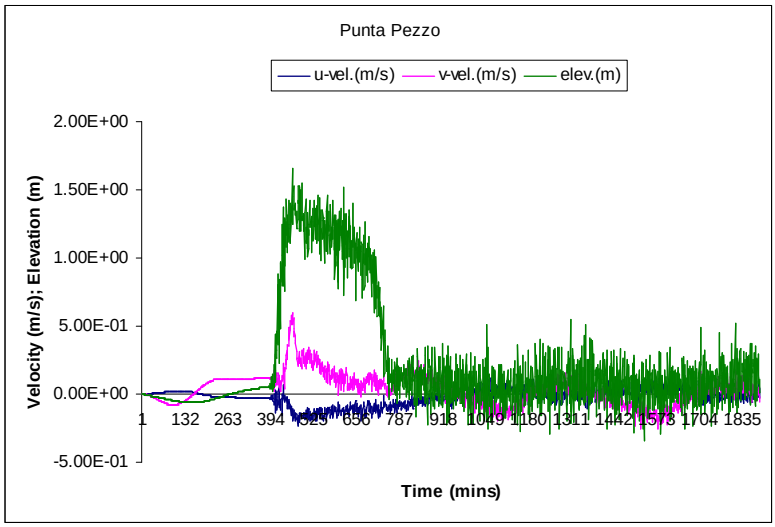

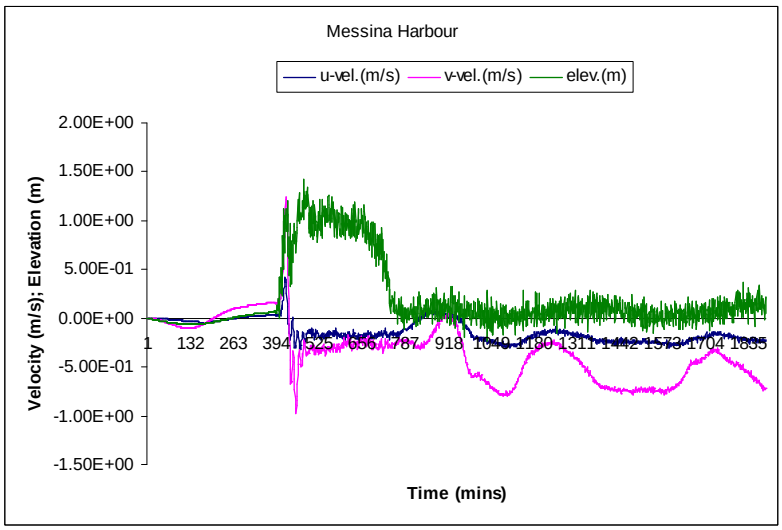

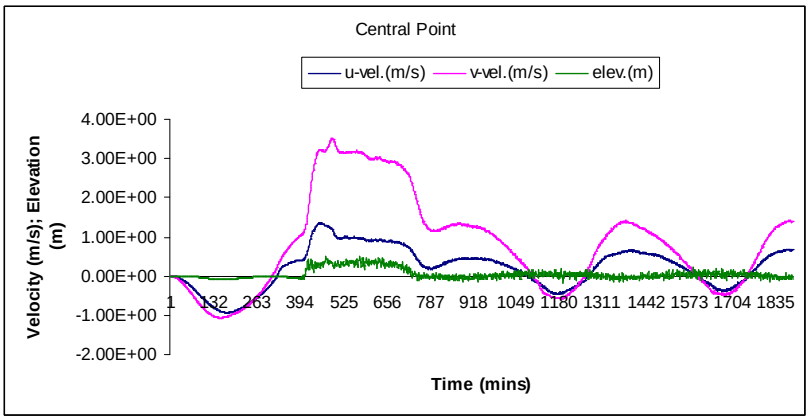

Figure 5.31 (Continued)

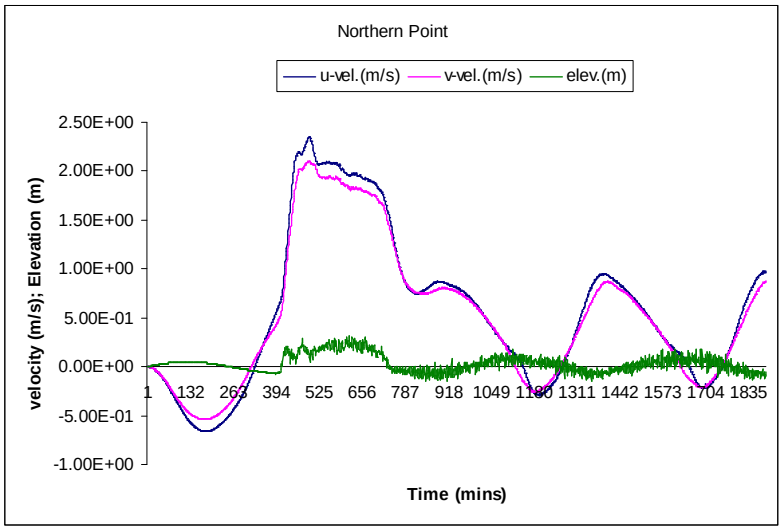

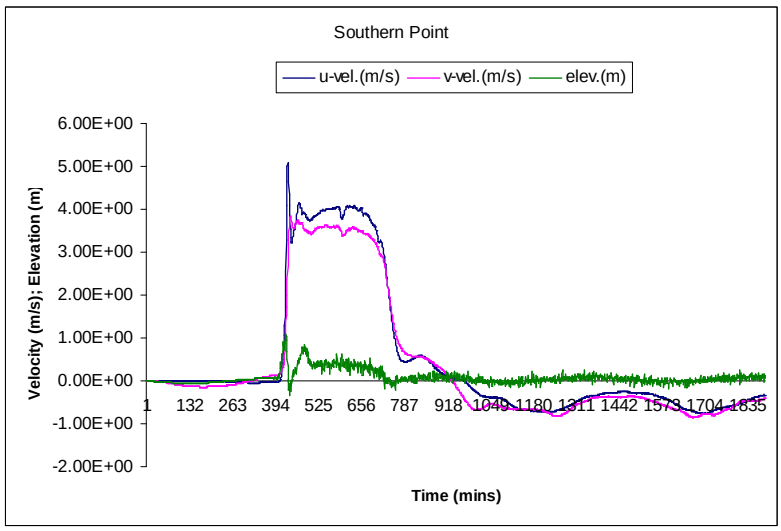

Figure 5.31 (Continued)

Figure 5.32: Fourth simulated tidal velocities at the Ganzirri - Punta Pezzo section (sill region)

Based on the conditions applied in the previous cases, it can be concluded that the simulation process may give the most appropriate results by using a high Manning coefficient (n = 0.1 s/m^3) combined with a high eddy viscosity effect (edvisc. x 10). Accordingly, using the high frictional forces with the same driving/radiating boundary files (opposite M_2-tidal waves of 0.135 m amplitude) for a total time of 170000 s with a time interval dt = 0.25 s will be the conditions for the fifth examined simulation process, the results of which are graphically displayed in Figure 5.33.

This graphical representation of this fifth numerical simulation process is more appropriate than the all previous ones. Tidal behaviour (velocity and elevations) are stable and show the main tidal characteristics of the Strait of Messina in a very clear manner. The out-of-phase behaviour is clear between the extremities of the Strait (Capo Peloro and Reggio Calabria; northern and southern points) by comparing the tidal elevation graph between the specified locations. The periodicity of the tidal flow of the semidiurnal type is also satisfied. Both velocities and elevations are smoother in the southern investigated location points. This is reasonable and refers to the wider cross sectional area of the Strait of Messina, which enables smoother propagation for the tidal flow within the Strait. The figures also confirm the minor effect of the transverse velocity component along the whole domain of simulation at all chosen locations. The non-uniform sinusoidal configuration of the propagating M_2-tidal wave along the domain may refer to the interaction between the two propagating waves having a 180º phase difference but with the same period.

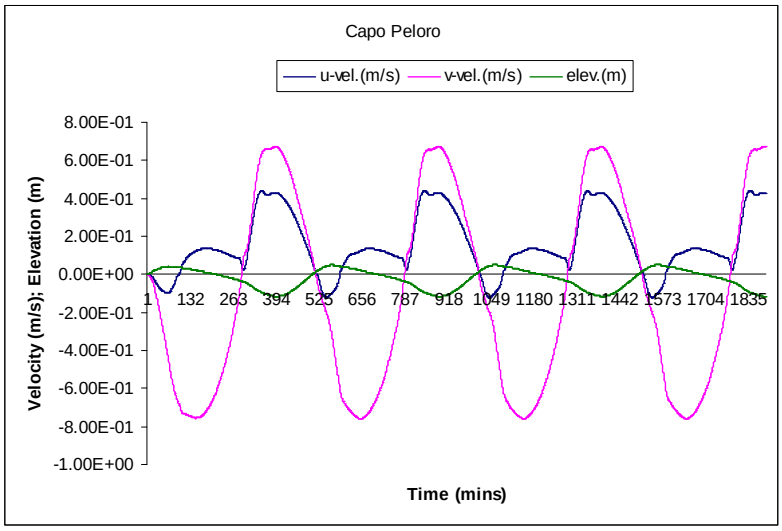

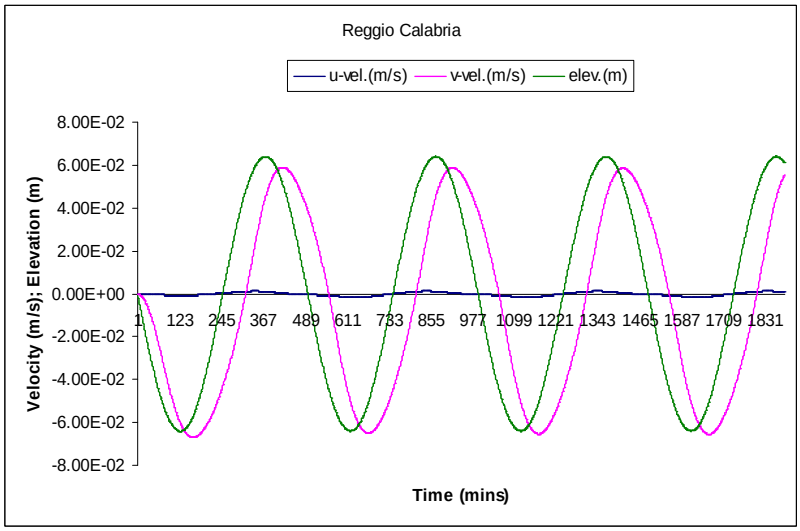

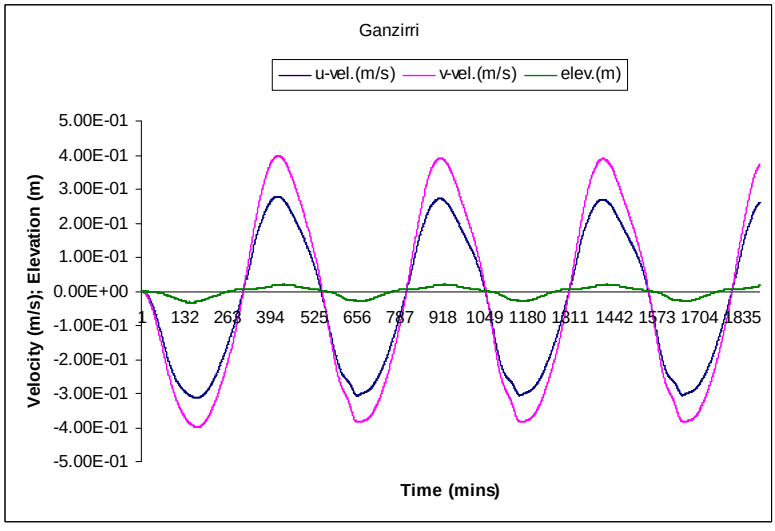

Figure 5.33: Tidal behaviour of the simulated real Strait of Messina using a high Manning coefficient and high eddy viscosity effect

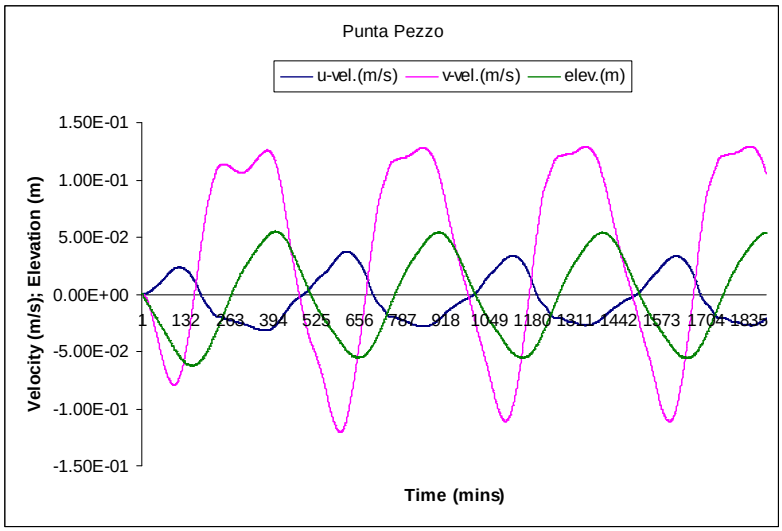

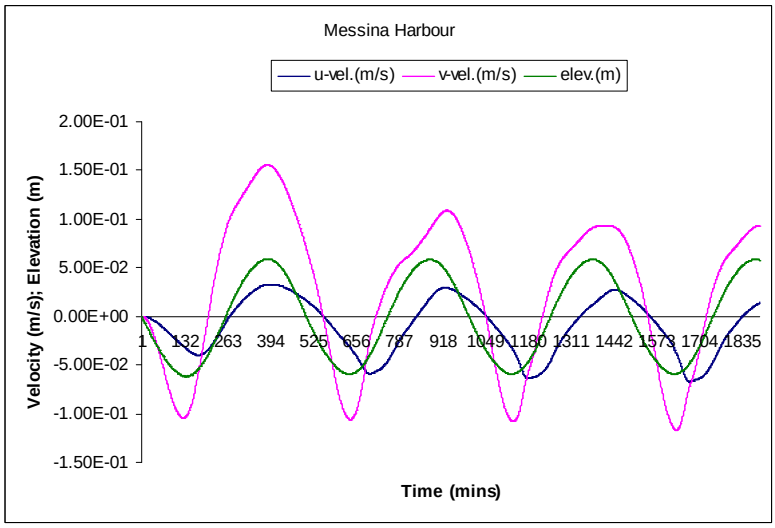

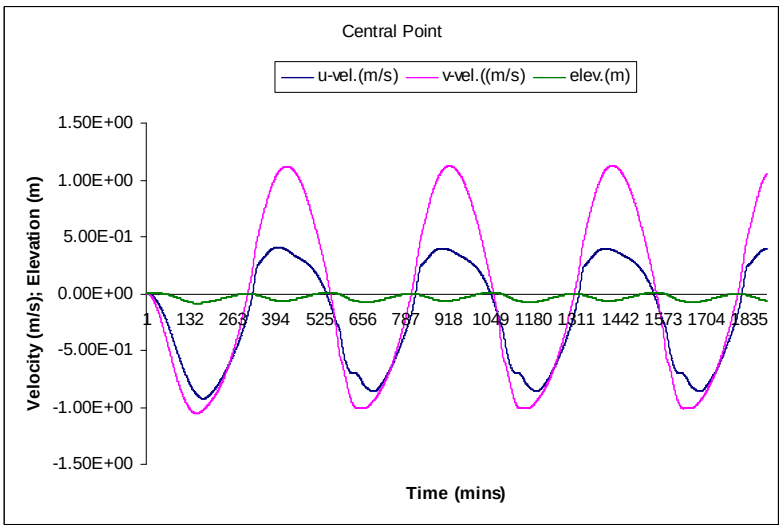

Figure 5.33 (Continued)

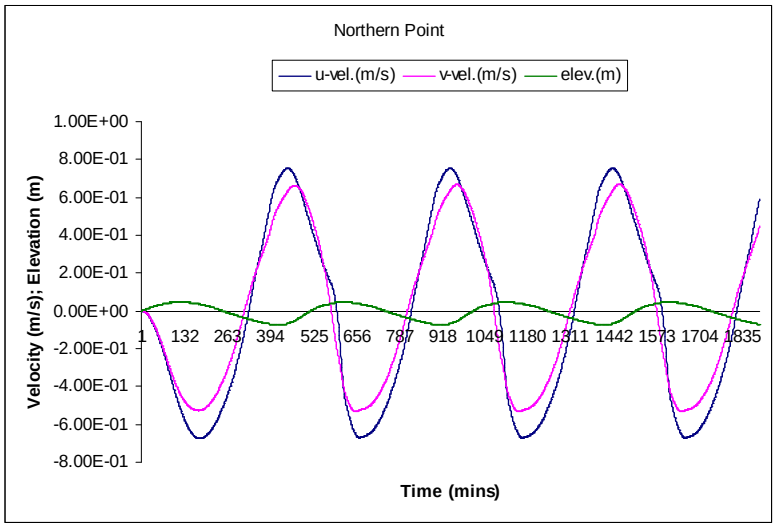

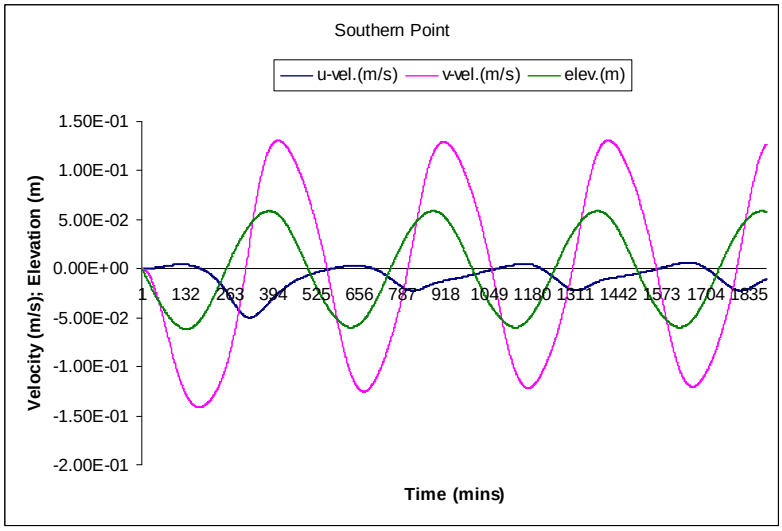

Figure 5.33 (Continued)

The following table (Table 5.4) summarises the maximum and minimum values of the simulated tidal current velocities and elevations at the chosen checkpoints. According to these results, the current velocity is maximum (1.22 m/s) at the central point. This is associated with a moderate tidal elevation of 0.09 m. The minimum velocity occurs at Punta Pezzo (0.10 m/s) with an elevation of 0.06 m.

	Max. Vel. (m/s)	**Min. Vel. (m/s)**	**Max. Elev. (m)**	**Min. Elev. (m)**
Capo Peloro	0.68	8.14×10^{-4}	0.11	5.47×10^{-5}
Reggio Calabria	0.97	4.93×10^{-5}	0.06	9.02×10^{-4}
Ganzirri	0.40	8.85×10^{-3}	0.03	2.94×10^{-6}
Punta Pezzo	0.10	2.50×10^{-9}	0.06	9.60×10^{-4}
Messina Harbour	0.18	5.65×10^{-9}	0.06	9.80×10^{-4}
Central Point	1.22	$5.2\ 0x\ 10^{-8}$	0.09	2.98×10^{-6}
Northern Point	0.67	6.50×10^{-7}	0.08	8.50×10^{-6}
Southern Point	0.95	2.25×10^{-6}	0.06	9.42×10^{-6}

Table 5.4: Maximum and minimum simulated tidal velocities and elevations at the chosen checkpoints along the domain of simulation

The results of the simulated tidal elevations at Reggio Calabria, Ganzirri, Punta Pezzo and Messina Harbour, in the present study for this case of simulation are in very good agreement with both the recorded [141] and the simulated [280]. As anticipated prior to the simulation process, and according to literature reviews [139-141, 280] the maximum tidal velocity occurs at the central area of the domain where the effect of morphometrical constriction and the sill take place. Figure 5.34 represents the simulated tidal velocity at the sill region (Ganzirri - Central Point - Punta Pezzo section). It appears that tidal currents are more intensive in the central flow path, just over the sill, and along the eastern coasts of the Strait, near Punta Pezzo. This is in good agreement with the observations [139], the analysis [141,188] and the simulation results [280]. The gyre associated with the northward tidal flow north to Punta Pezzo is presented. Additionally, contrary to all previous simulation cases in this section, the simulated flow satisfies the semidiurnal behaviour of tides

in the Strait of Messina. However, the use of these exceptional parameter values, high Manning coefficient and high eddy viscosity effect, restricts the simulated tidal current velocity to less than 1.23 m/s, which is less than half the real velocity of 3.0 m/s [139, 140, 188] and also less than the recorded [141] and simulated [280] tidal velocities of 2.85 m/s and of 2.8 m/s, respectively.

The tidal amplitudes at Reggio Calabria, Ganzirri, Punta Pezzo and Messina Harbour in the present case study of the real Strait of Messina, with these exceptional coefficients values, are in a very good agreement with the recorded results [141] and simulated outputs [280] as shown in Table (5.5).

	Recorded (m) [141]	**Simulated (m) [280]**	**Present case-study (m)**
Reggio Calabria	0.06	0.06	0.06
Ganzirri	0.03	0.02	0.03
Punta Pezzo	0.009	0.04	0.06
Messina Harbour	0.05	0.04	0.06

Table 5.5: Comparison between the simulated tidal elevations in the present case-study and those previously recorded and simulated at four common checkpoints

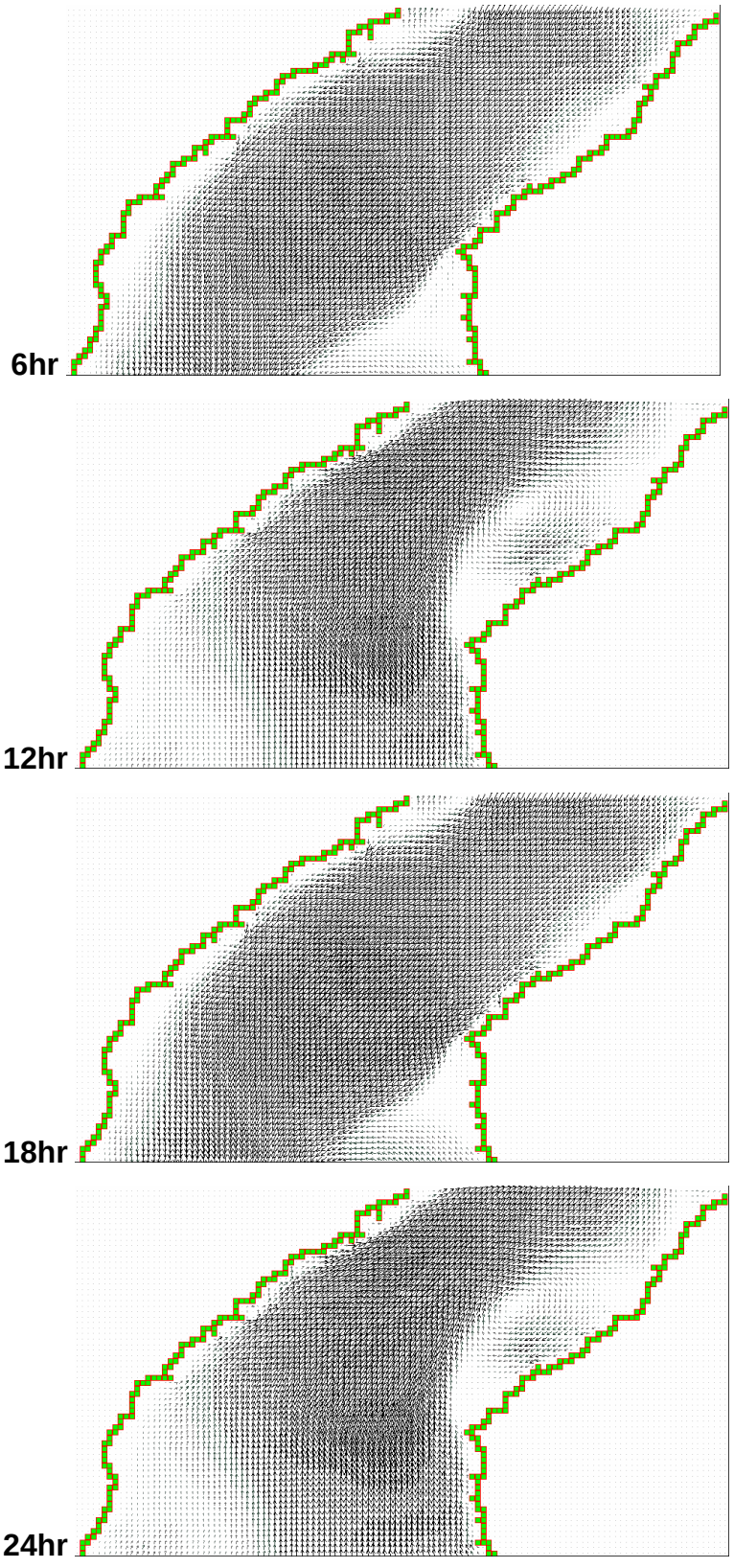

Figure 5.34: Fifth simulated tidal velocities at the Ganzirri - Punta Pezzo section (sill region)

Examination of the tidal flow pattern during the spring and the neap tides is important. This examination helps to identify the areas of excess energy within the Strait during these two important tidal phases and, hence, helps to make a decision about the most suitable place to deploy tidal turbines. Using the constructed files for four successive days for each phase (Fig. 5.13 and 5.14) for the two extremities of the Strait: Capo Peloro (north) and Reggio Calabria (south), the northern tip represents the input driving boundary file while the southern represents the radiating boundary file. The conditions of higher Manning coefficient ($n = 0.1\ s/m^3$) and eddy viscosity effect, which enable stable outputs from TFD model, will be applied. The total simulation time is 170000 s with dt = 0.25 s and the outputs are given every 1800 s, i.e. every half an hour. The graphical representations of the spring and neap tidal behaviour for the simulated real Strait of Messina are shown in Figures 5.35 and 5.36, respectively. The simulated tidal velocity along the Ganzirri – Punta Pezzo section, during spring tide is given in Figure 5.37, while Figure 5.38 shows the same data during neap tide.

Tables (5.6 and 5.7) summarise the maximum and minimum velocities and elevations at the eight chosen locations within the real domain of simulation during spring and neap tides, respectively. The maximum velocity is 1.36 m/s simulated at the chosen Central Point during both phases. This confirms the effect of the sill and the morphometry in enhancing the tidal flow. The graphical figures suffer from a lot of instability and noisy distributions. This appears to be less frequent at the southern checkpoints (Reggio Calabria, Messina Harbour and Southern Point) due to the wider cross-sectional areas which enable smoother propagation of the tidal flow. The simulated tidal behaviour is nearly identical during the two tidal phases, which, in turn, does not reflect any real situation in the Strait of Messina. The simulated velocity during the spring tide phase reflects no periodical motion after 12 hours of simulation and the flow continues to have the southward direction throughout the remainder of the simulation. This does not reflect the semidiurnal type of tides within the Strait of Messina. The same flow scheme appears during the neap tide phase. All these unexpected results impose exclamation points for the simulation process for these two important tidal phases as the applied boundary files are constructed using Admiralty Tide Tables [289] data, assessed and assured to satisfy the out-of-phase

behaviour, the semidiurnal scheme within the Strait and the natural normal variations between spring and neap tides. What is, again, confirmed during these tidal phases from the simulated velocities examined at the sill region is the intensity of tidal currents close to the eastern coast of the Strait, near Punta Pezzo, and the existence of an eddy north of this checkpoint.

	Max. Vel. (m/s)	**Min. Vel. (m/s)**	**Max. Elev. (m)**	**Min. Elev. (m)**
Capo Peloro	1.0	8.5×10^{-4}	0.38	9.0×10^{-2}
Reggio Calabria	0.50	9.7×10^{-4}	0.36	8.7×10^{-6}
Ganzirri	0.47	7.3×10^{-4}	0.36	9.8×10^{-4}
Punta Pezzo	0.98	6.0×10^{-5}	0.35	8.3×10^{-6}
Messina Harbour	0.20	8.9×10^{-5}	0.40	7.6×10^{-8}
Central Point	1.36	3.4×10^{-3}	0.27	8.8×10^{-6}
Northern Point	0.67	4.9×10^{-4}	0.47	6.8×10^{-3}
Southern Point	0.48	9.2×10^{-5}	0.37	5.1×10^{-6}

Table 5.6: Maximum and minimum simulated tidal velocities and elevations along the domain of simulation during spring tide phase

	Max. Vel. (m/s)	**Min. Vel. (m/s)**	**Max. Elev. (m)**	**Min. Elev. (m)**
Capo Peloro	1.10	8.1×10^{-4}	0.46	9.0×10^{-3}
Reggio Calabria	0.48	5.5×10^{-5}	0.28	8.2×10^{-6}
Ganzirri	0.50	8.0×10^{-4}	0.48	3.4×10^{-4}
Punta Pezzo	0.96	3.0×10^{-5}	0.37	8.2×10^{-7}
Messina Harbour	0.20	9.2×10^{-4}	0.30	3.7×10^{-6}
Central Point	1.36	7.2×10^{-4}	0.40	7.1×10^{-5}
Northern Point	0.67	9.0×10^{-4}	0.57	7.5×10^{-3}
Southern Point	0.23	9.1×10^{-5}	0.26	2.5×10^{-6}

Table 5.7: Maximum and minimum simulated tidal velocities and elevations along the domain of simulation during neap tide phase

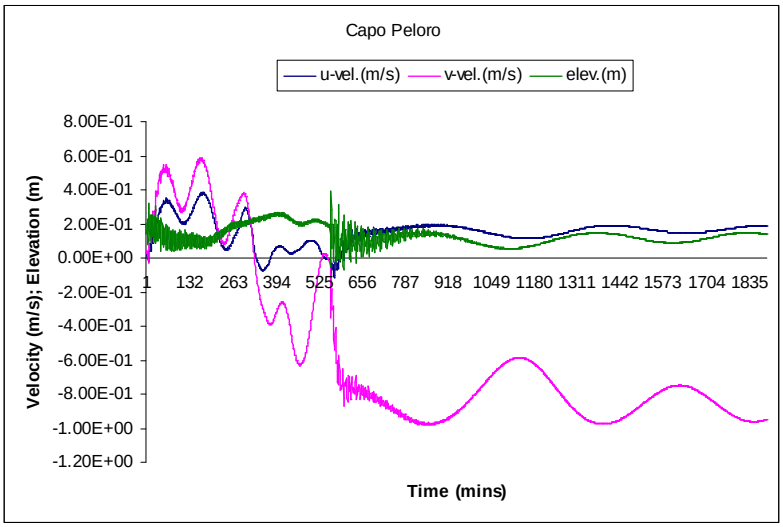

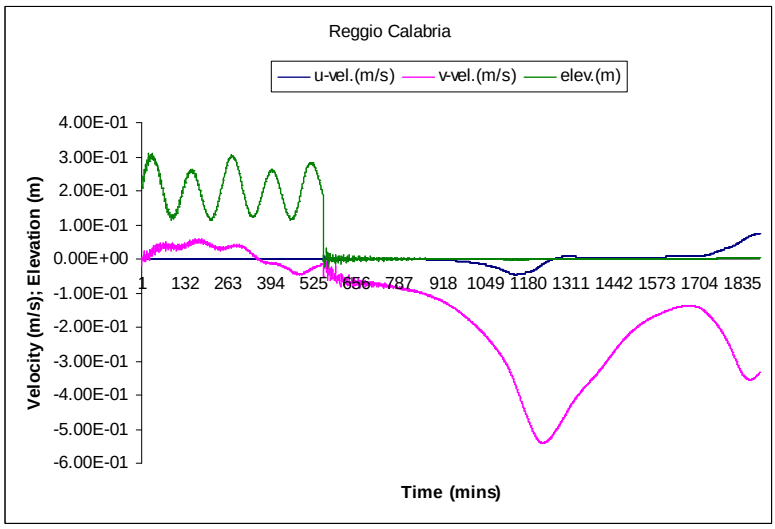

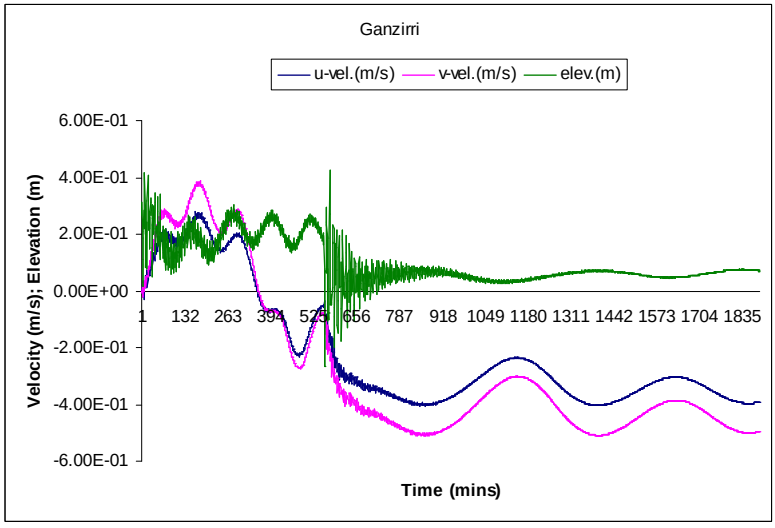

Figure 5.35: Tidal behaviour of the real Strait of Messina during the spring tide phase

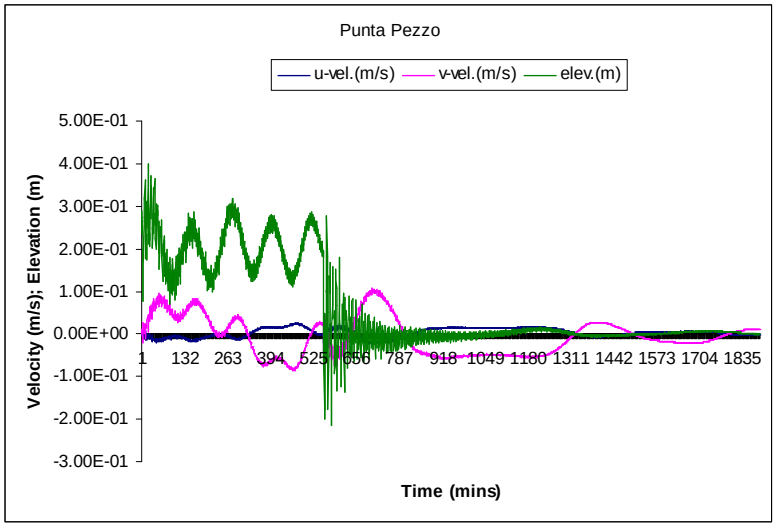

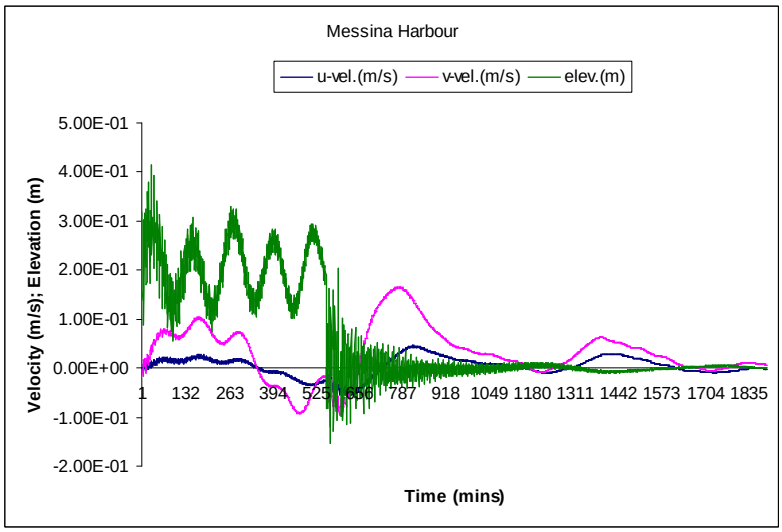

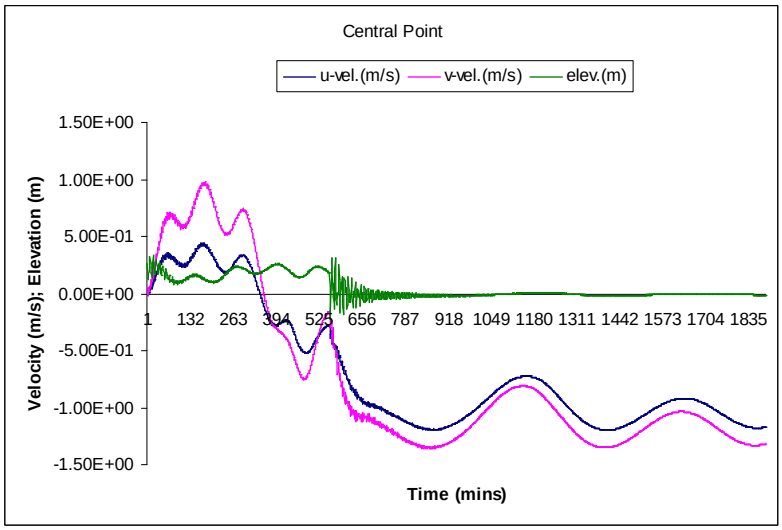

Figure 5.35 (Continued)

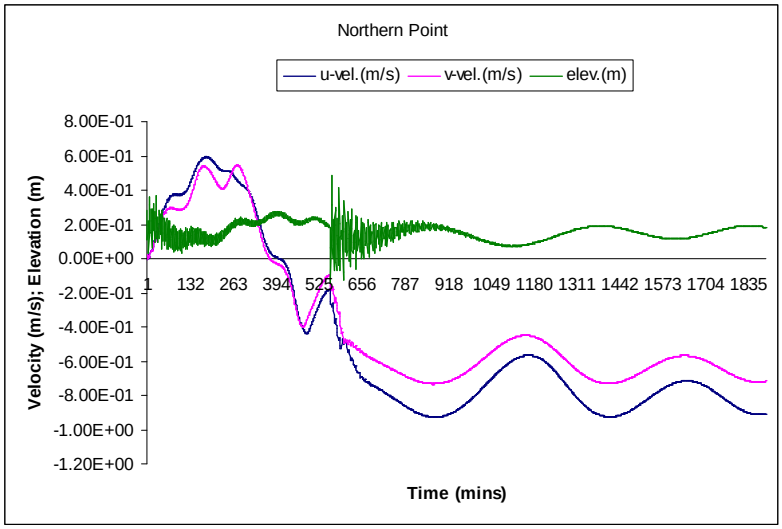

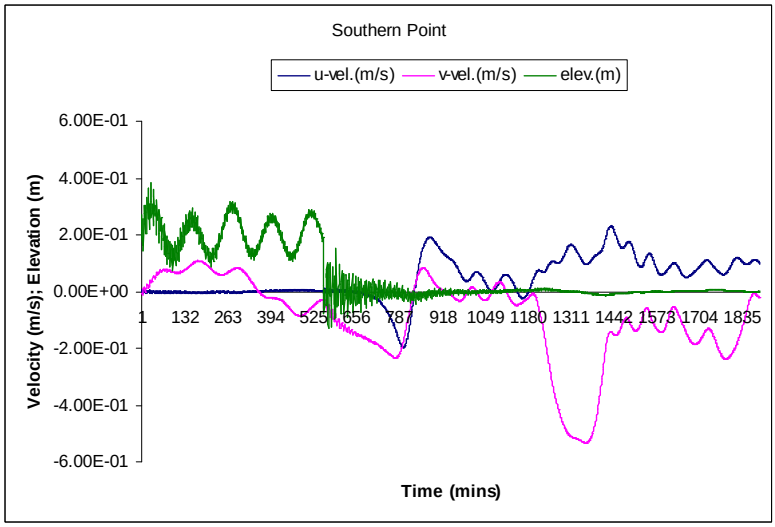

Figure 5.35 (Continued)

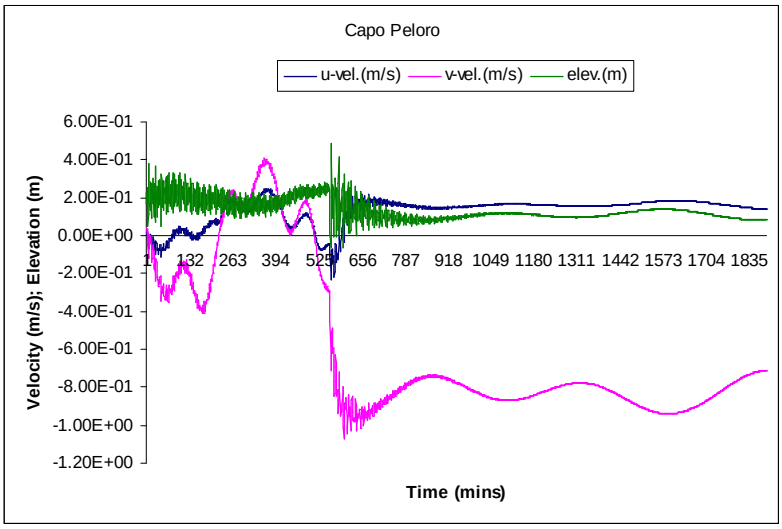

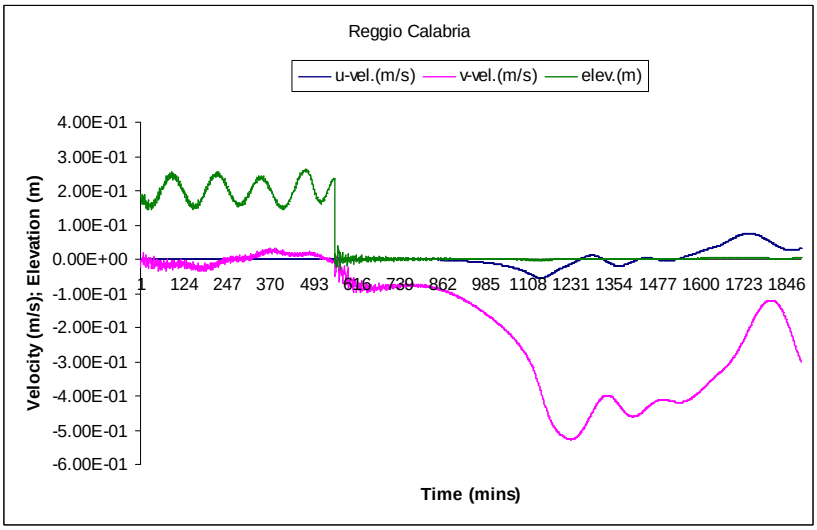

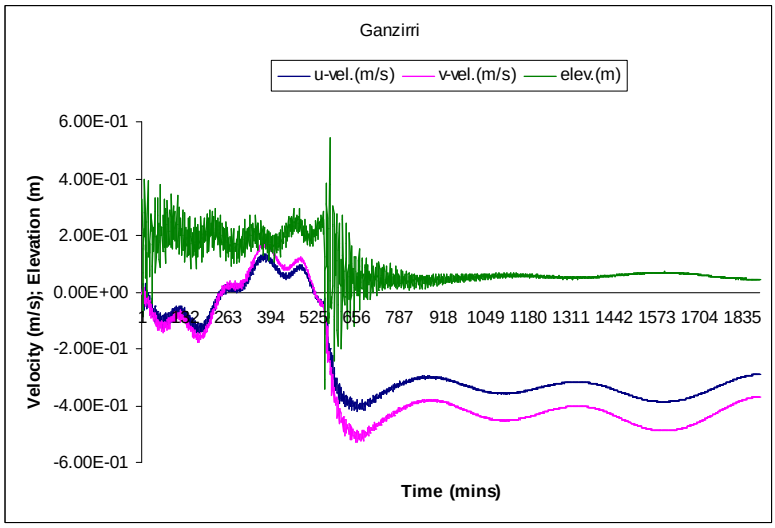

Figure 5.36: Tidal behaviour of the real Strait of Messina during the neap tide phase

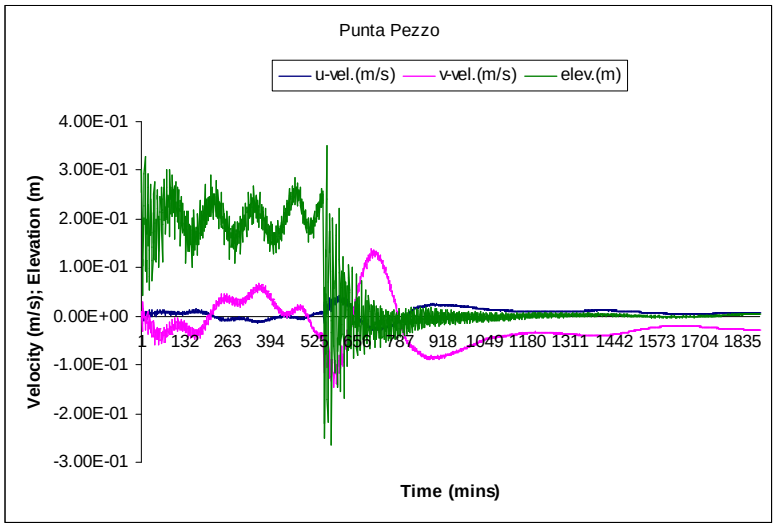

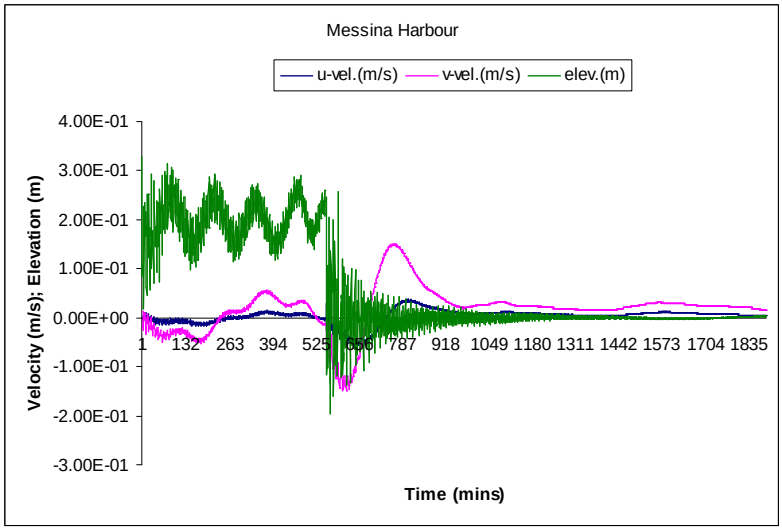

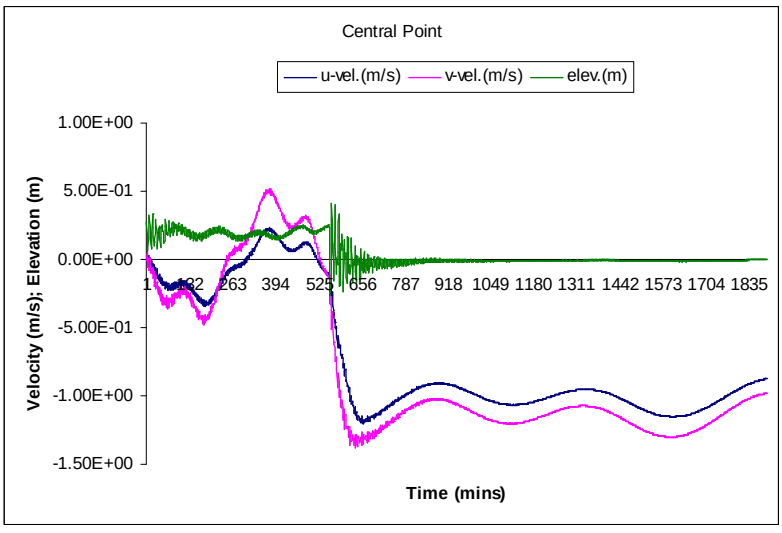

Figure 5.36 (Continued)

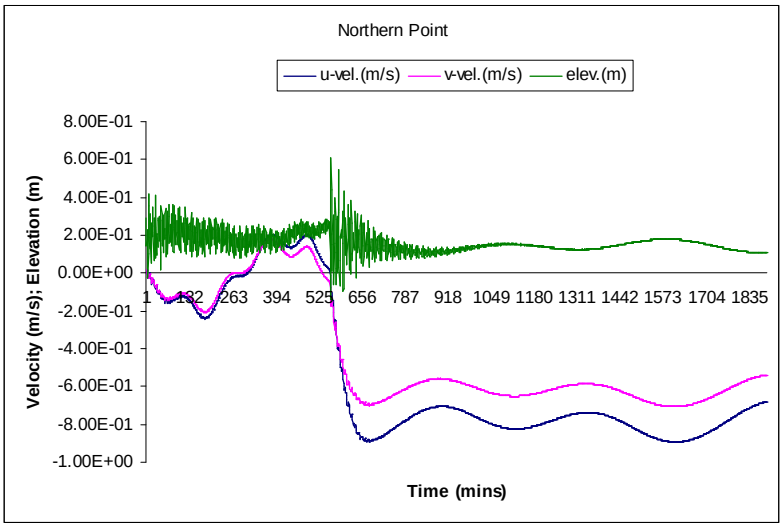

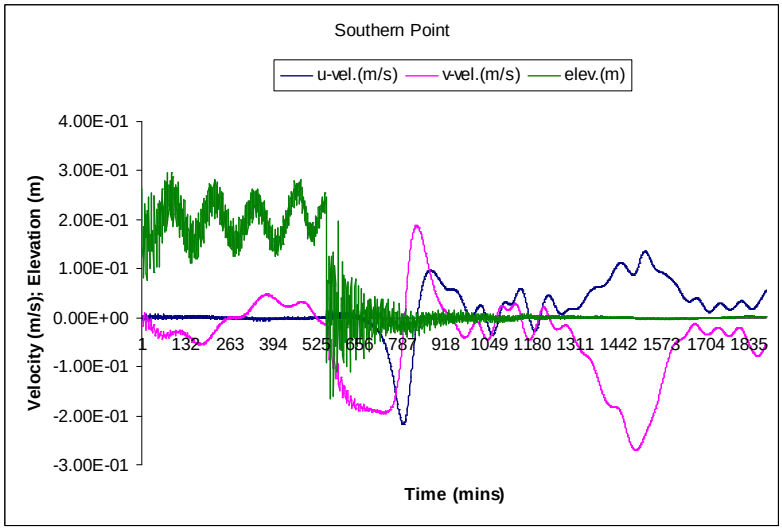

Figure 5.36 (Continued)

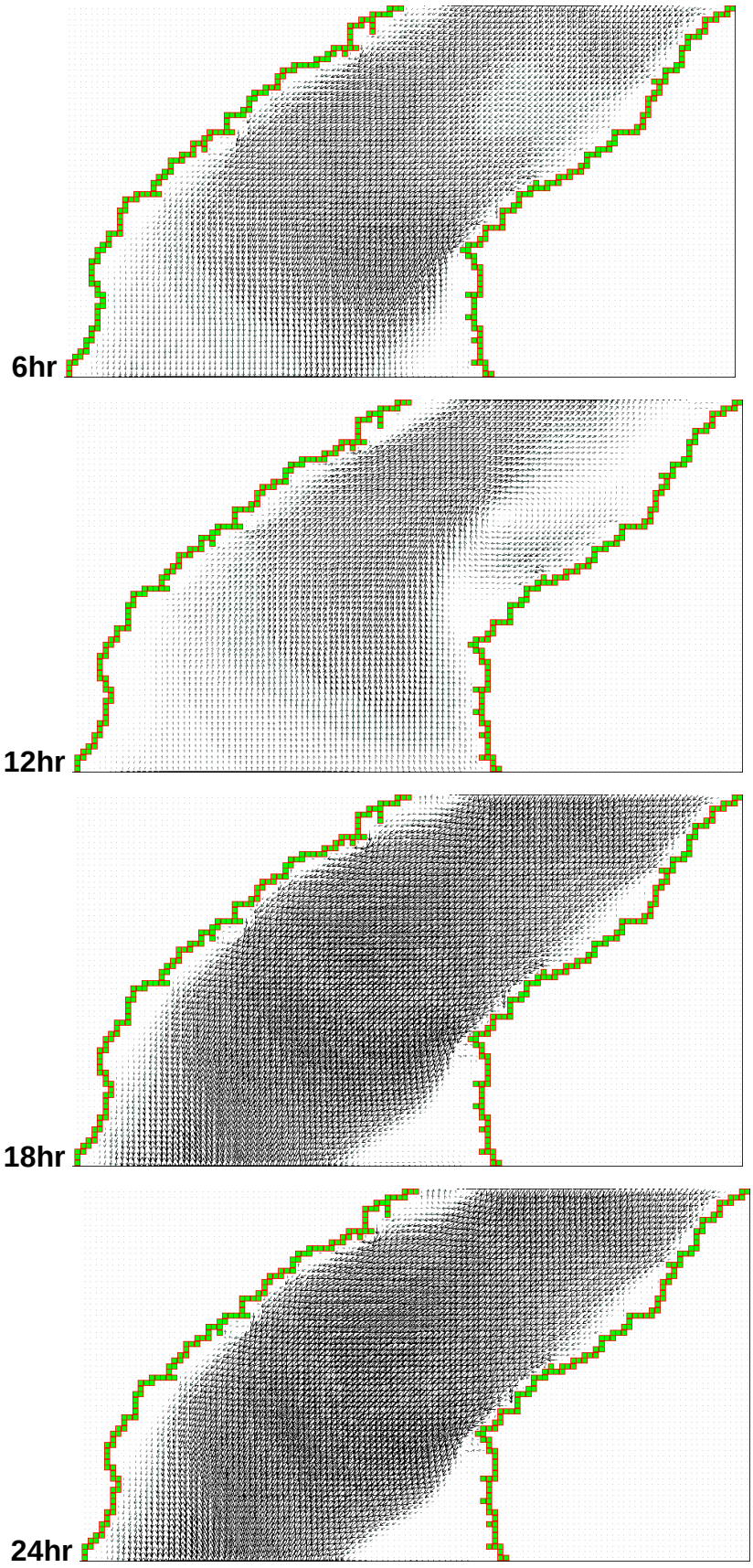

Figure 5.37: Simulated tidal velocities during spring tide

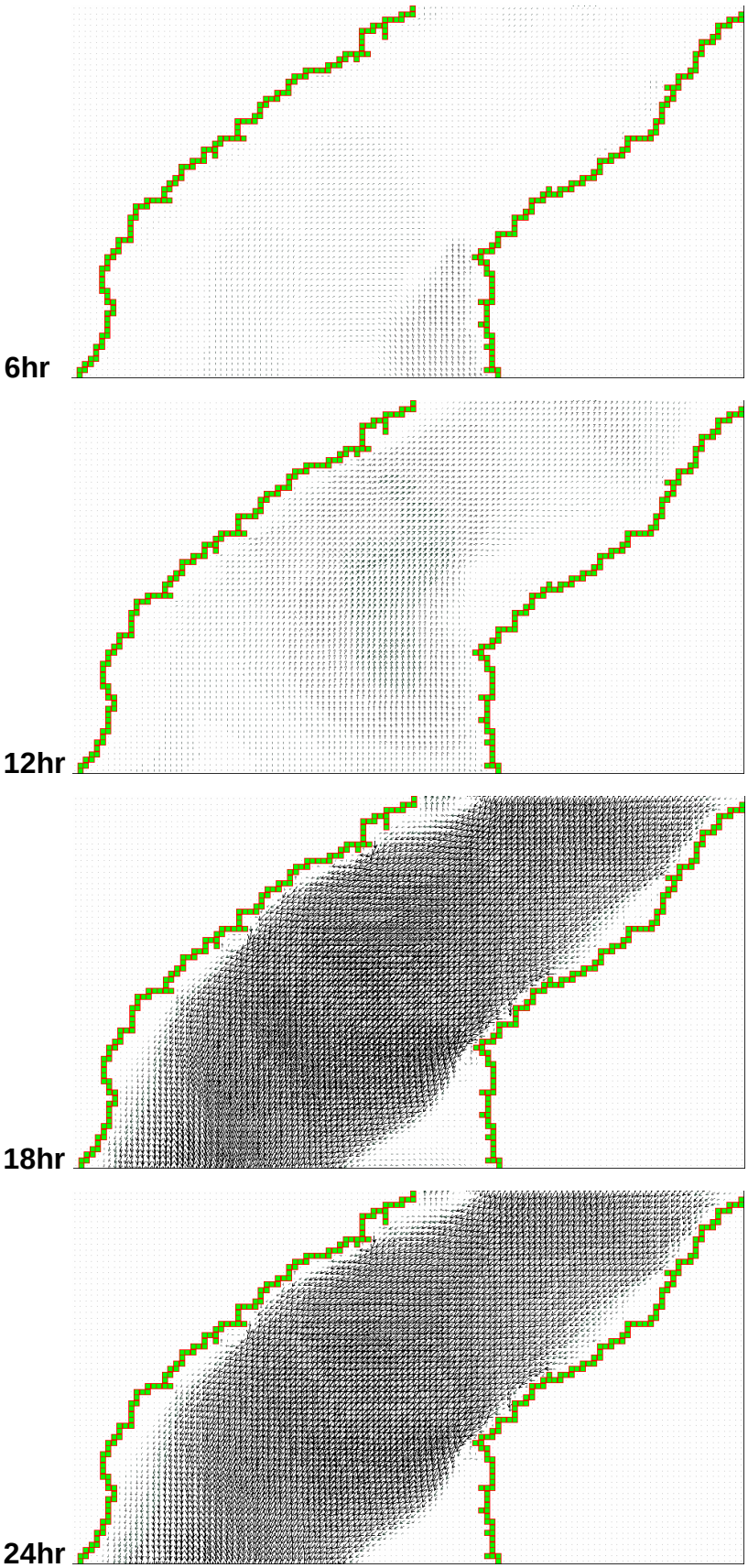

Figure 5.38: Simulated tidal velocities during neap tide

5.4.2.2. 80 m Level of No Motion (LNM) case study

Bearing in mind the following four facts:

1. Tidal currents are surface currents and found only in the surface layer.
2. The superficial Tyrrhenian current in the Strait occupies the first 30 m depth [140, 141] and the Ionian current in the opposite direction occupies the layer below that right to the bottom of the Strait.
3. The present conditional tidal technology that allows tidal turbines to be deployed between 25-45 m depth [33].
4. The sill region in the Strait of Messina has a depth of 80 m.

The following assumption is proposed in a trial to mimic the Strait of Messina to a closer degree than the previous trials (section 5.4.2.1). This assumption is to use the Level of No Motion (LNM) concept in which current velocity is assumed to vanish below a certain depth [291]. The depth of 80 m is assumed in the present case study. The domain for this simulation process is similar to that previously applied, but with all the depths greater than 80 m reduced to 80 m while the shallower depths are left unchanged. The real morphometry of the Strait is maintained and the 2.5 m land-sea isodepth is also maintained. Figure 5.39 is the 80 m LNM simulation domain. Variations, as may be seen, appear along the domain only close to the shelf area while the whole domain has a fixed depth of 80 m. Once more a simulation process applying a normal Manning coefficient ($n = 0.025\ s/m^3$) and a normal eddy viscosity effect gave unreasonable outputs in which the main tidal behaviour of the Strait are not mimiced even to a close degree. The same results occur when using both normal and higher ($n = 0.1\ s/m^3$) Manning coefficients with both a higher and a normal eddy viscosity effects, respectively. Accordingly, the main simulation process, even for a LNM case, is carried out applying a high Manning coefficient ($n = 0.1\ s/m^3$) with a high eddy viscosity effect (edvisc. x 10). The driving and radiating tidal amplitude are those expressed in Figures 5.22 and 5.23. The total duration of the simulation is 170000 s with dt = 0.25 s.

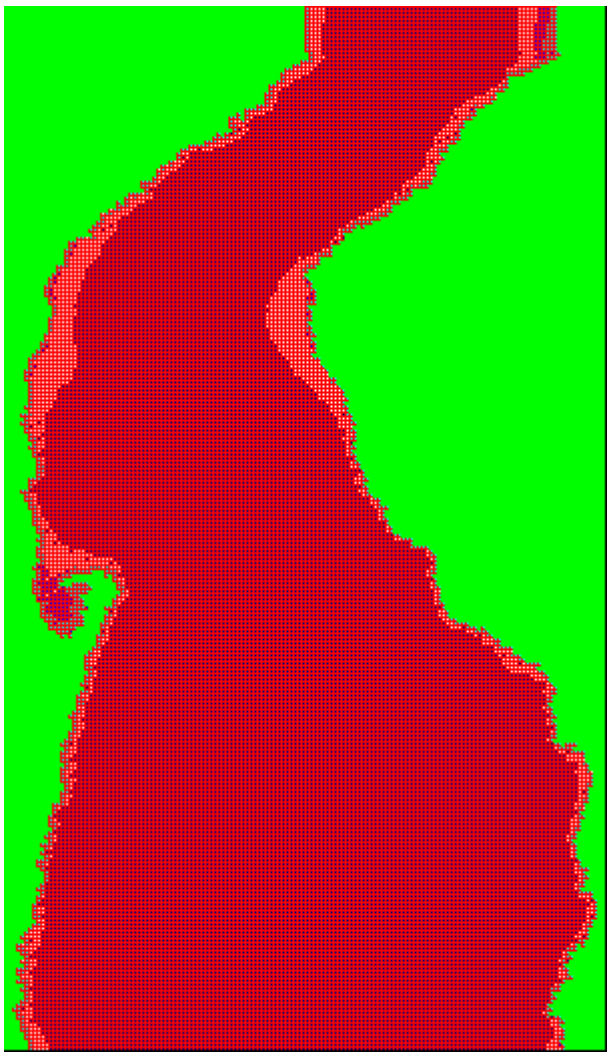

Figure 5.39: The 80 m Level of No Motion (LNM) domain for the Strait of Messina

The graphical representation of the simulated tidal velocities and elevations at the chosen eight locations along the domain is presented in Figure 5.40, while the simulated domain at the Ganzirri to Punta Pezzo section is shown for 24 successive hours, every 6 hours, in Figure 5.41.

Table (5.8) summarises the maximum and minimum tidal current velocities and amplitudes at the chosen eight locations for the 80 m LNM simulation case. The outputs of this simulation case appear to be smoother and more stable than the previous case for the full real domain (section 5.4.2.1); however, it is obvious that both the velocities and the amplitudes are much lower. This spotlights the effect of the whole domain bathymetry on the tidal flow within the Strait as, although the

depths are maintained at the sill region at the 80 m, it appears that the whole system is affected by the complete bathymetric variations.

	Max. Vel. (m/s)	**Min. Vel. (m/s) x 10^{-8}**	**Max. Elev. (m) x 10^{-2}**	**Min. Elev. (m) x 10^{-6}**
Capo Peloro	0.22	2.80	5.3	3.0
Reggio Calabria	0.20	0.08	6.4	0.3
Ganzirri	0.20	1.00	5.7	3.0
Punta Pezzo	0.20	3.26	5.4	3.0
Messina Harbour	0.18	0.08	6.0	5.5
Central point	0.22	2.20	5.6	9.3
Northern point	0.22	1.70	5.7	2.6
Southern point	0.18	0.04	6.0	3.2

Table 5.8: Maximum and minimum tidal current velocities and elevations in the 80 m LNM case

The simulated tidal elevations in this 80 m LNM case at Reggio Calabria and at Messina Harbour are still in good agreement with the previously recorded and simulated elevations, while those at Ganzirri and Punta Pezzo (> 0.05 m) are much higher than those previously mentioned (< 0.05 m). The outputs of this 80 m LNM simulation process conserve the main tidal characteristic of the Strait of Messina: the out-of-phase behaviour between the northern and southern extremities, the intensive currents at the sill region due to the natural morphometrical constriction combined with the bathymetric effect (sill rise) and the low transverse flow velocities, compared to the longitudinal components, along the domain of simulation. Additionally, the semidiurnal type of the tidal currents in the Strait is well represented in the simulated velocity outputs. Moreover, the increased intensity of tidal currents near to Punta Pezzo is well represented. However, the TFD model in this case failed to give any near-to-real values for the tidal velocity. In addition, the model failed to simulate the gyre north to Punta Pezzo with the northward flow.

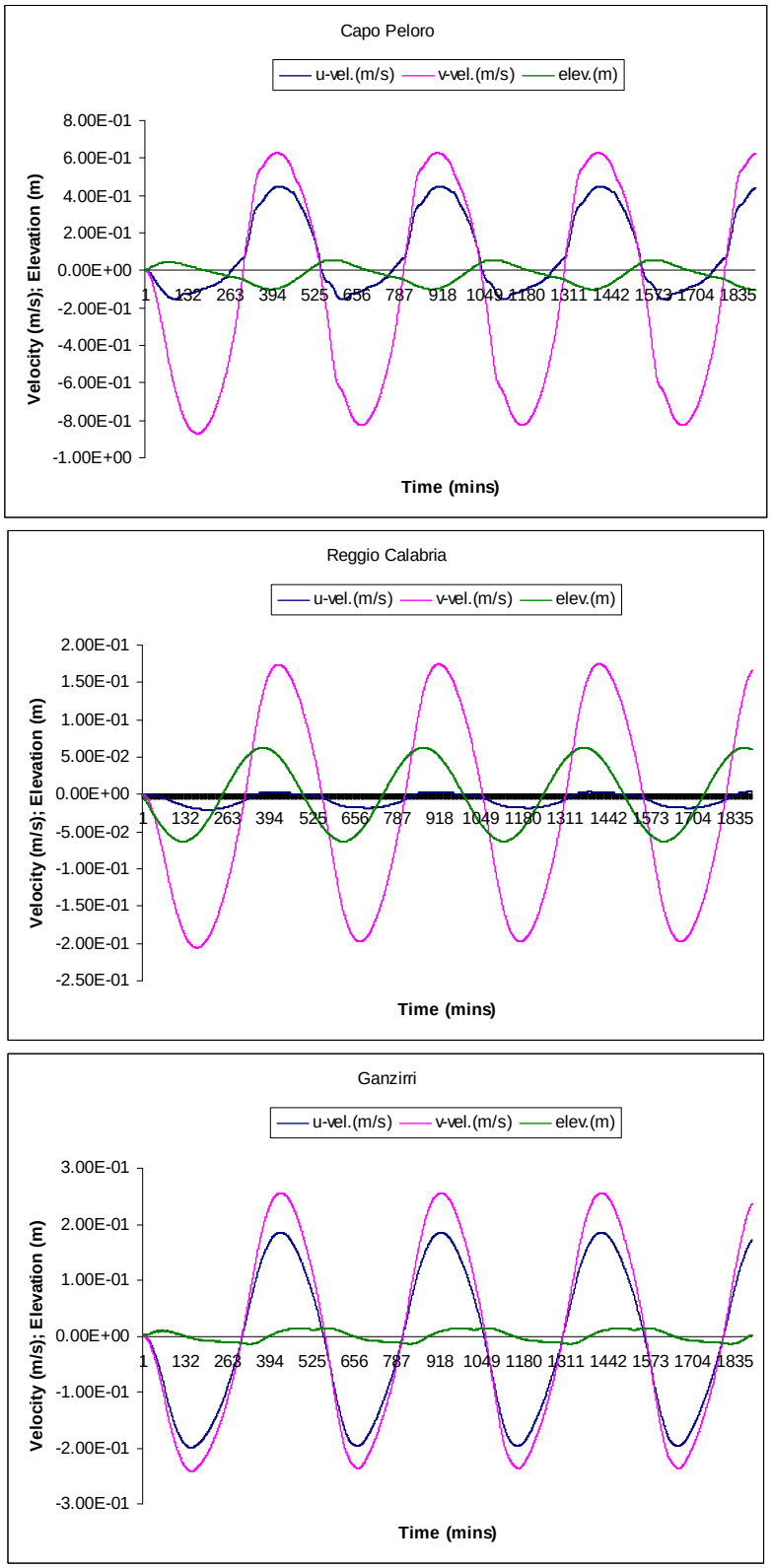

Figure 5.40: Tidal behaviour of the simulated 80 m LNM Strait of Messina using a high Manning coefficient and a high eddy viscosity effect

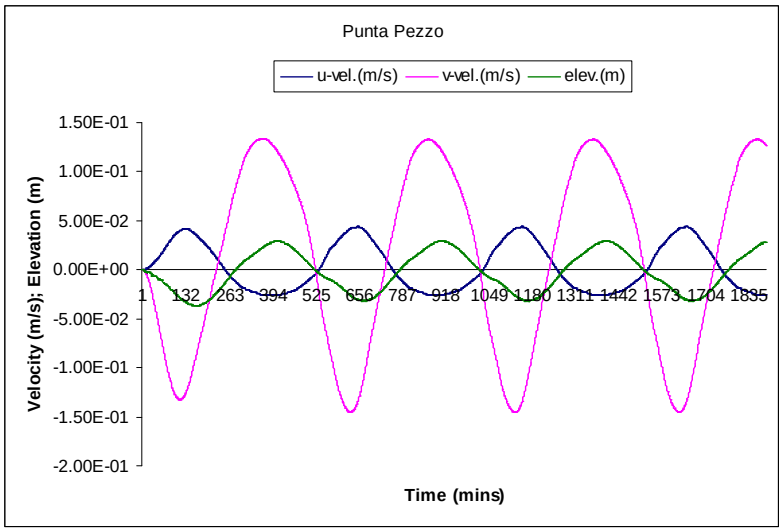

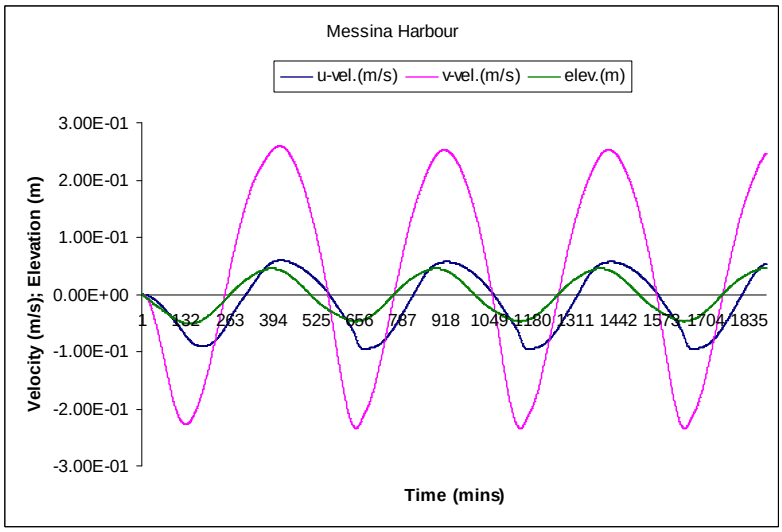

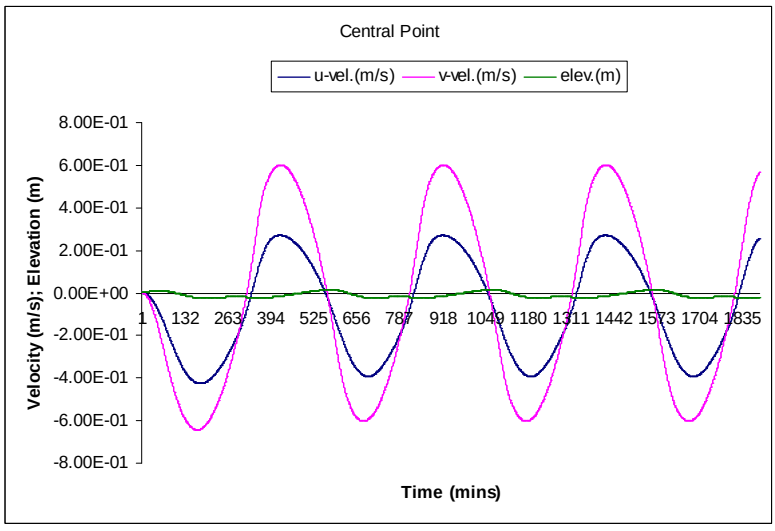

Figure 5.40 (Continued)

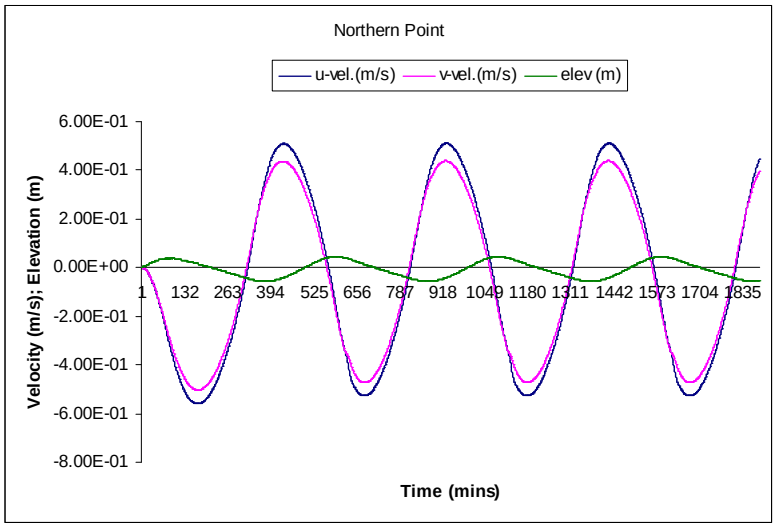

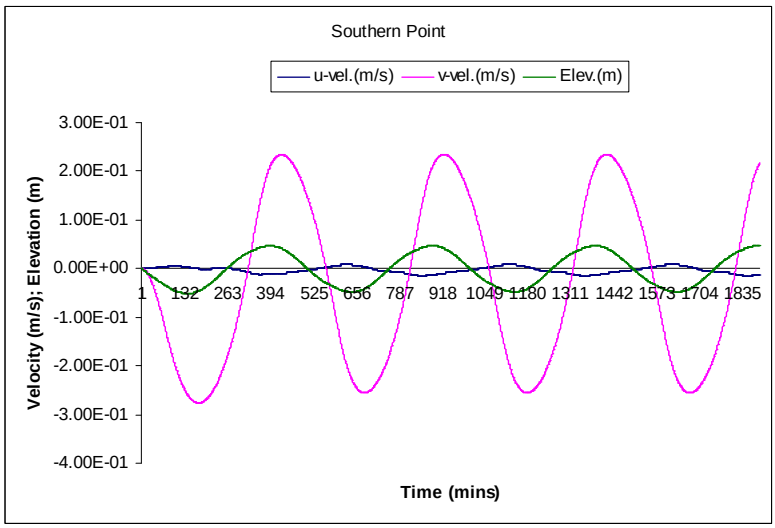

Figure 5.40 (Continued)

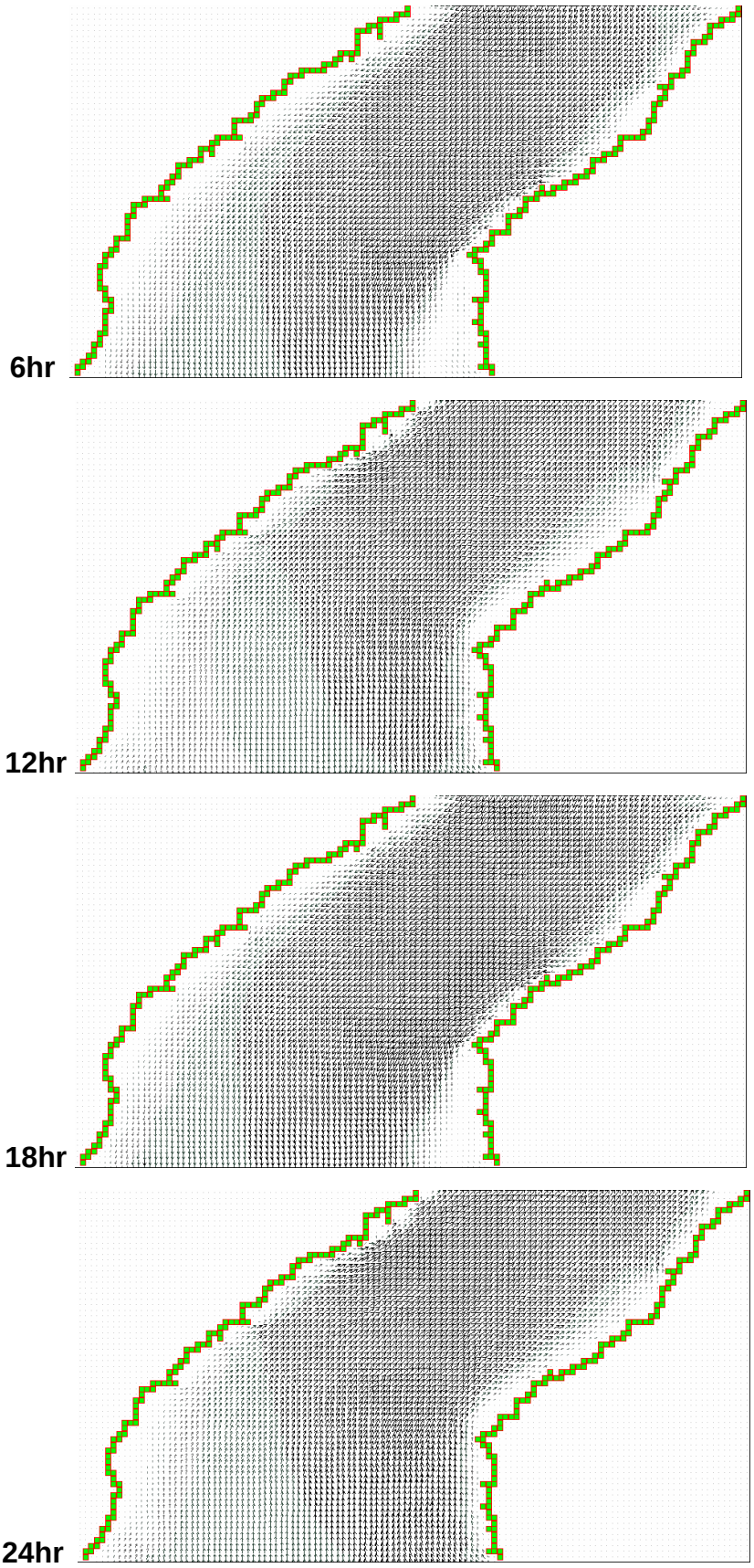

Figure 5.41: Simulated tidal velocities of the 80 m LNM simulation case

The examination of the tidal flow regime during spring and neap tides in this case of simulation is carried out using the same driving and radiating boundary files used in the previous cases. These boundary files are constructed using Admiralty Tide Tables [289]. The driving force is directed from the north southwards while the radiating force acts in the opposite direction. Figures 5.42 and 5.43 are, respectively, the graphical presentations of the spring and neap tidal behaviour at the eight chosen checkpoint locations within the Strait of Messina. Figures 5.44 and 5.45 are the simulated velocity outputs during spring and neap tides, respectively; at the sill region the section comprises Ganzirri, Central Point and Punta Pezzo as checkpoints. Comparing the figures for both the tidal behaviour and the simulated velocities at the sill region with those obtained in the real domain of the Strait of Messina, the only difference is in the smoother propagation of tidal elevation at the different locations, with lower results for tidal velocities. Otherwise, the configurations are nearly identical: phase and tidal periodicity are totally missed. These unrealistic results reflect a greater effect of morphometry than that of the bathymetry on the applied boundary files. The Proceeding to reduce the observed disturbance and instability in the resultant outputs means to increase either the Manning coefficient to exceed 0.1 s/m^3, or to increase the eddy viscosity effect to more than 10 times its original value. Both suggestions cannot in any way be accepted as this leads the situation to be totally imaginary and unrealistic. The maximum and minimum velocities and elevations during spring and neap tides for the present 80 m LNM simulation case are given in Tables (5.9) and (5.10), respectively. An important point to notice is that the central point records, for the first time, the second highest velocity (0.90 m/s) after the northern tip, Capo Peloro (1.2 m/s) during the two tidal phases. Additionally, as for the case of examining the tidal regime of the 80 m LNM domain, the simulation process fails to simulate the gyres north to Punta Pezzo during spring and neap tides.

	Max. Vel. (m/s)	Min. Vel. (m/s)	Max. Elev. (m)	Min. Elev. (m)
Capo Peloro	1.20	1.6×10^{-2}	0.30	4.8×10^{-3}
Reggio Calabria	0.30	7.3×10^{-4}	0.33	2.5×10^{-5}
Ganzirri	0.23	9.0×10^{-4}	0.40	5.8×10^{-4}
Punta Pezzo	0.12	1.8×10^{-4}	0.42	2.8×10^{-4}
Messina Harbour	0.23	7.0×10^{-5}	0.40	8.1×10^{-5}
Central point	0.90	1.9×10^{-4}	0.34	1.4×10^{-2}
Northern point	0.71	2.7×10^{-3}	0.32	3.1×10^{-3}
Southern point	0.42	1.1×10^{-4}	0.38	1.3×10^{-4}

Table 5.9: Maximum and minimum tidal current velocities and elevations during spring tide in the 80 m LNM case

	Max. Vel. (m/s)	Min. Vel. (m/s)	Max. Elev. (m)	Min. Elev. (m)
Capo Peloro	1.20	3.8×10^{-3}	0.32	9.5×10^{-3}
Reggio Calabria	0.30	3.0×10^{-4}	0.26	3.3×10^{-6}
Ganzirri	0.30	1.0×10^{-4}	0.41	3.2×10^{-4}
Punta Pezzo	0.20	3.0×10^{-5}	0.41	1.8×10^{-4}
Messina Harbour	0.32	2.6×10^{-5}	0.35	2.8×10^{-5}
Central point	0.90	2.5×10^{-4}	0.37	6.0×10^{-3}
Northern point	0.70	1.5×10^{-4}	0.37	1.4×10^{-3}
Southern point	0.41	3.3×10^{-5}	0.33	7.2×10^{-5}

Table 5.10: Maximum and minimum tidal current velocities and elevations during neap tide in the 80 m LNM case

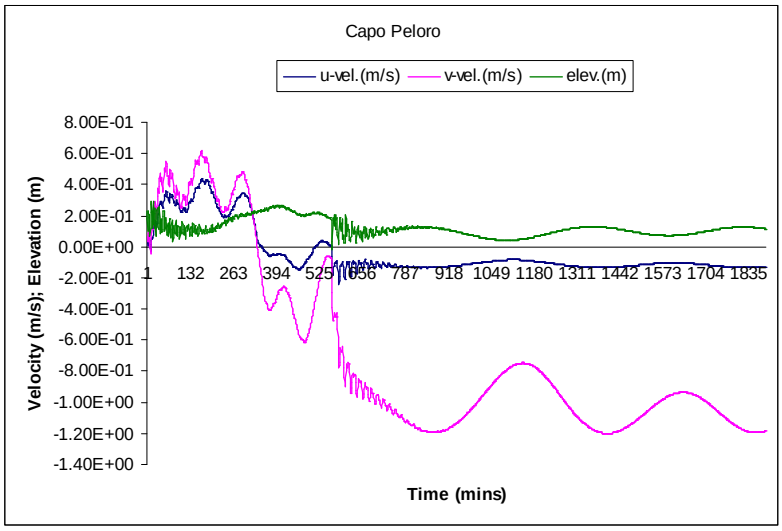

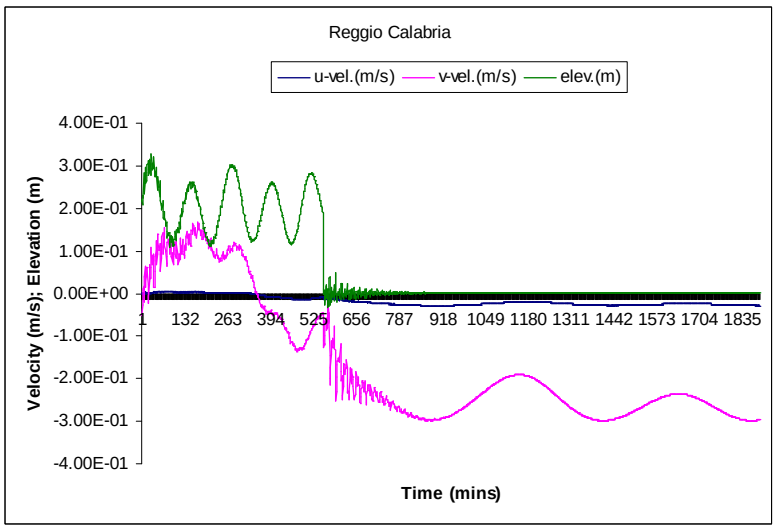

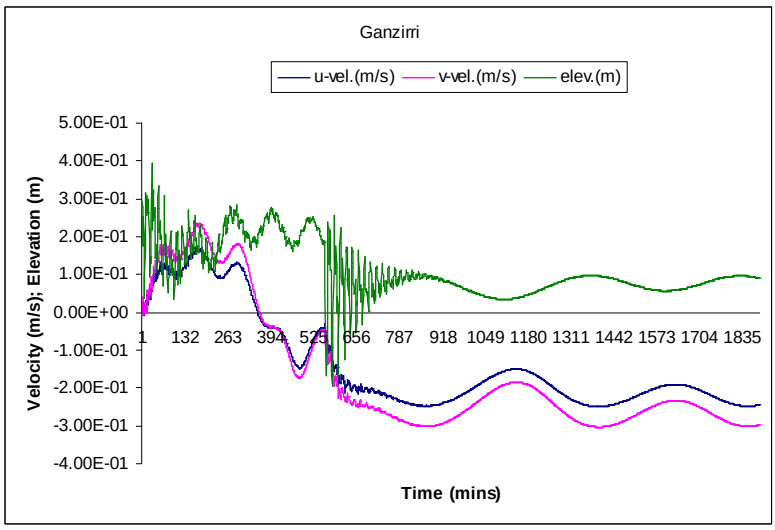

Figure 5.42: Tidal behaviour of the 80 m LNM domain of the Strait of Messina during the spring phase

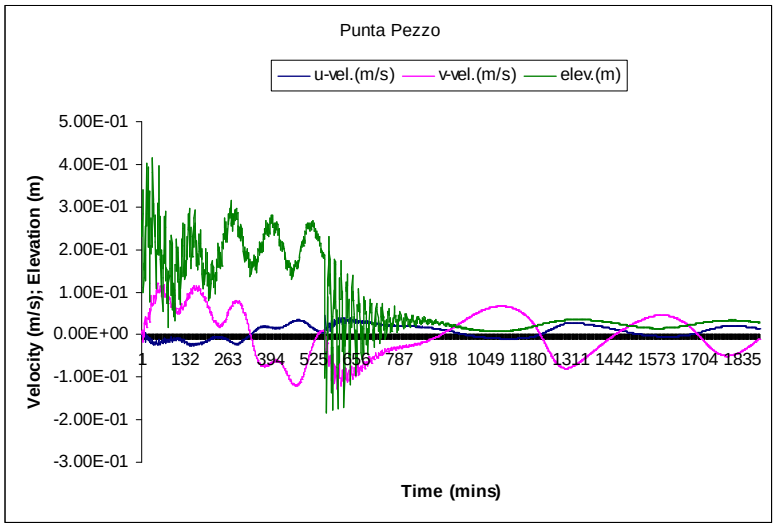

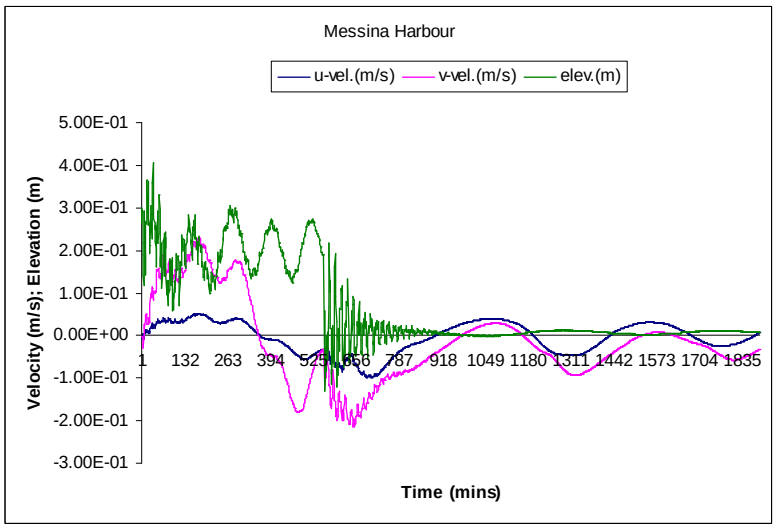

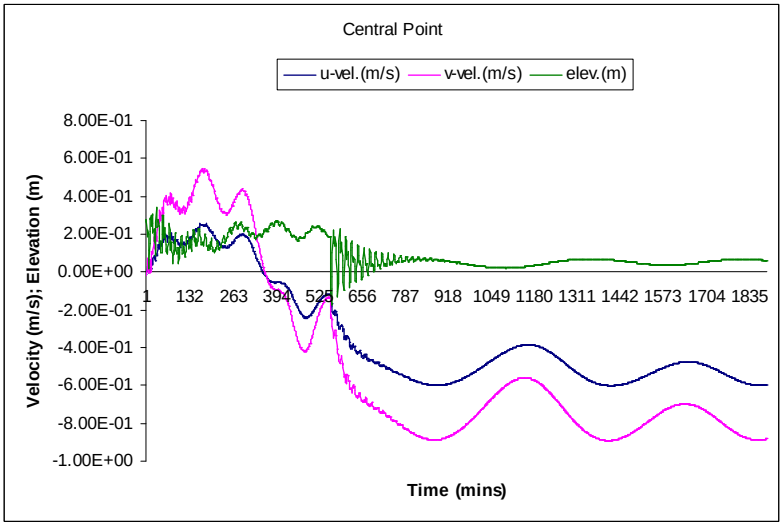

Figure 5.42 (Continued)

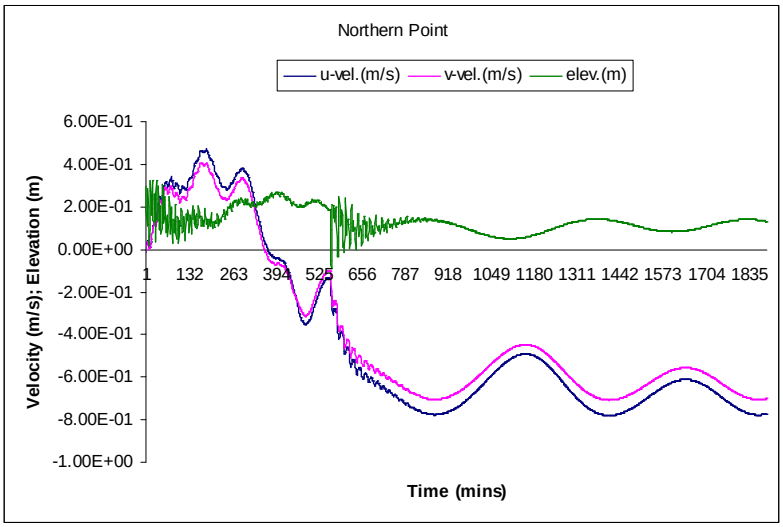

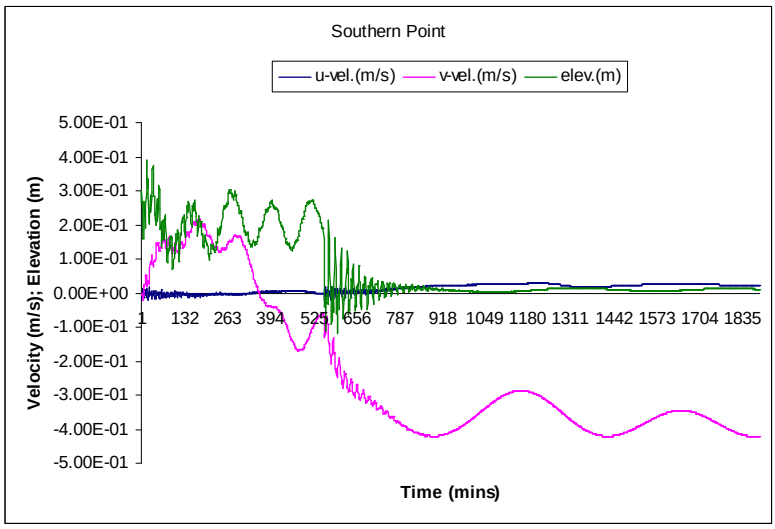

Figure 5.42 (Continued)

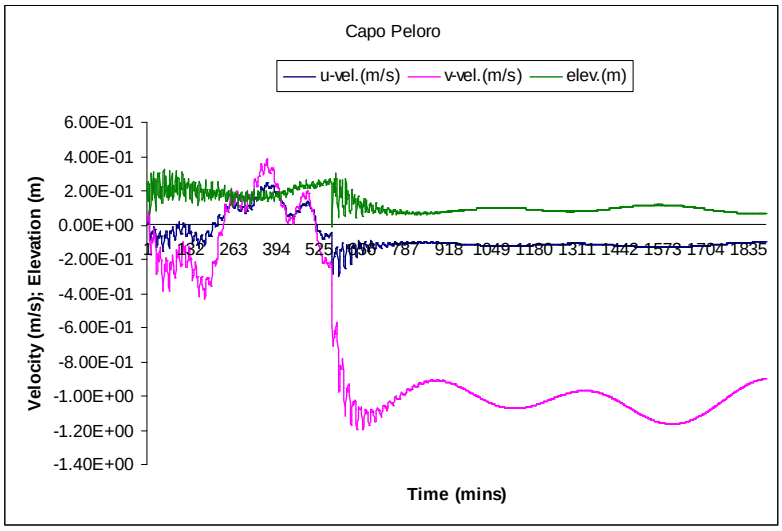

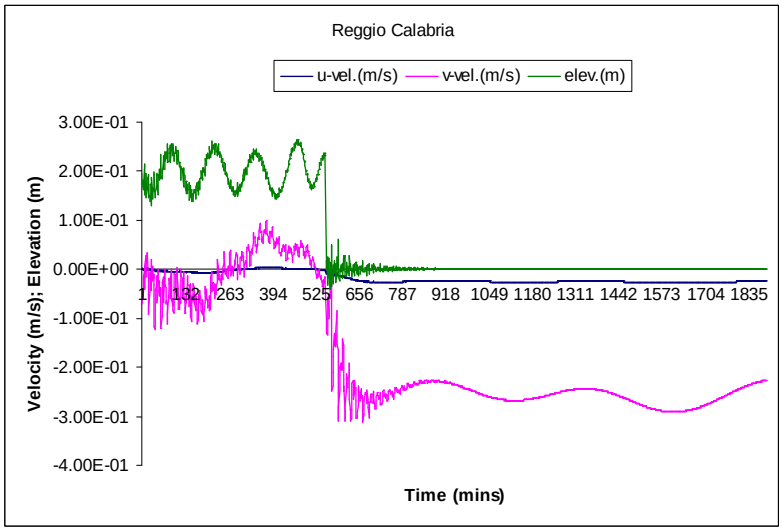

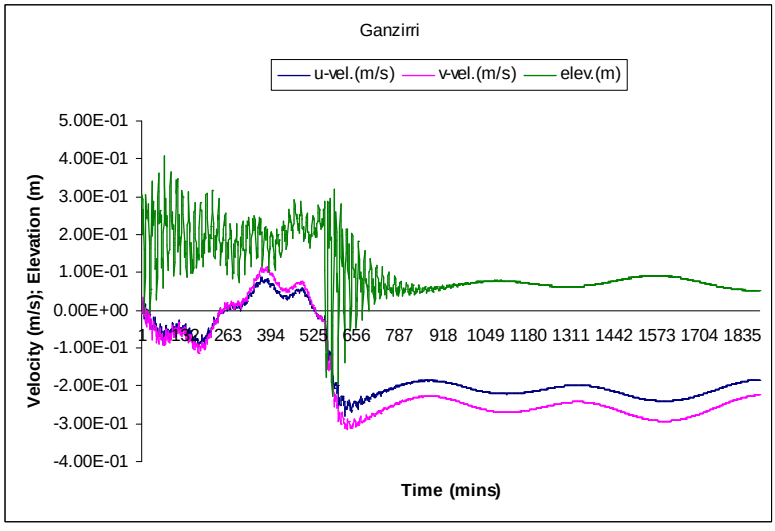

Figure 5.43: Tidal behaviour of the 80 m LNM domain of the Strait of Messina during the neap phase

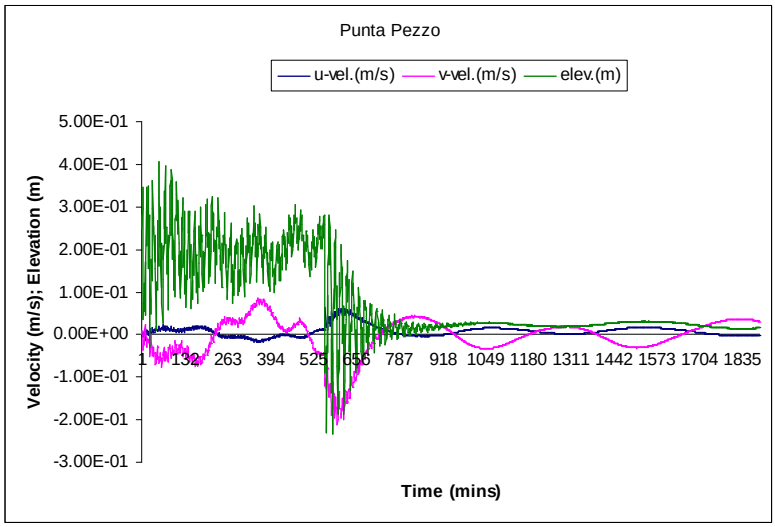

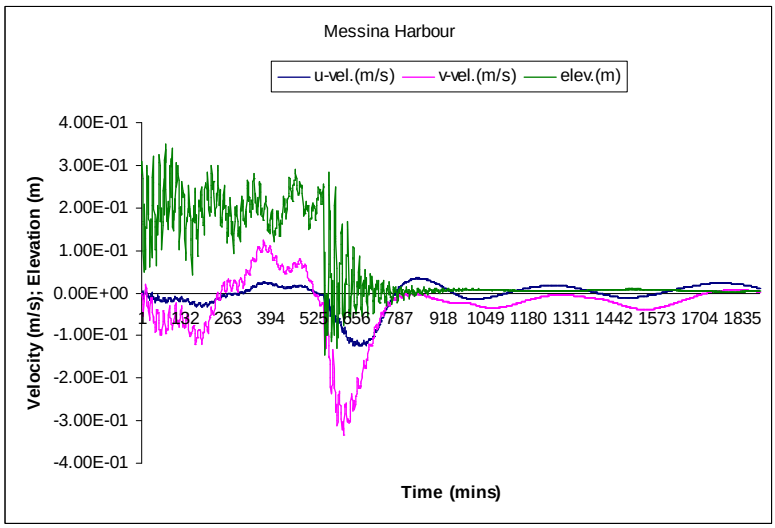

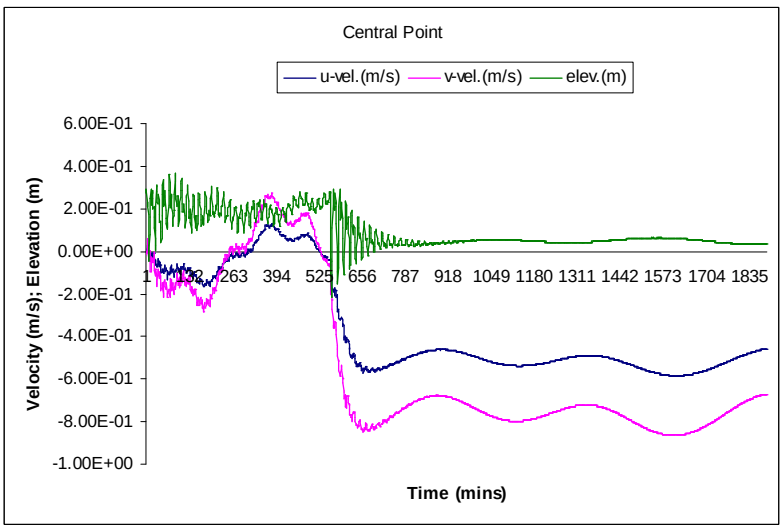

Figure 5.43 (Continued)

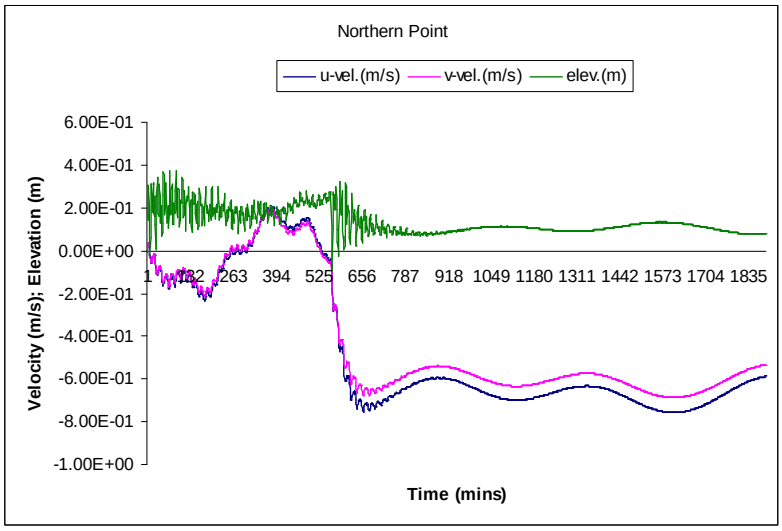

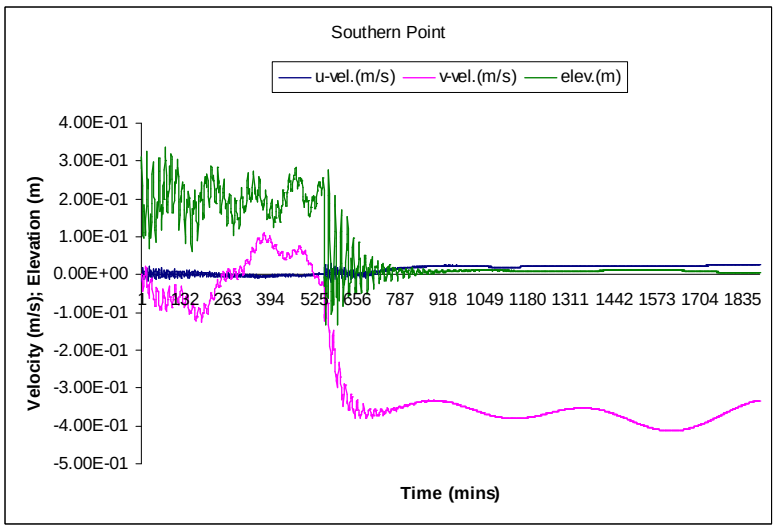

Figure 5.43 (Continued)

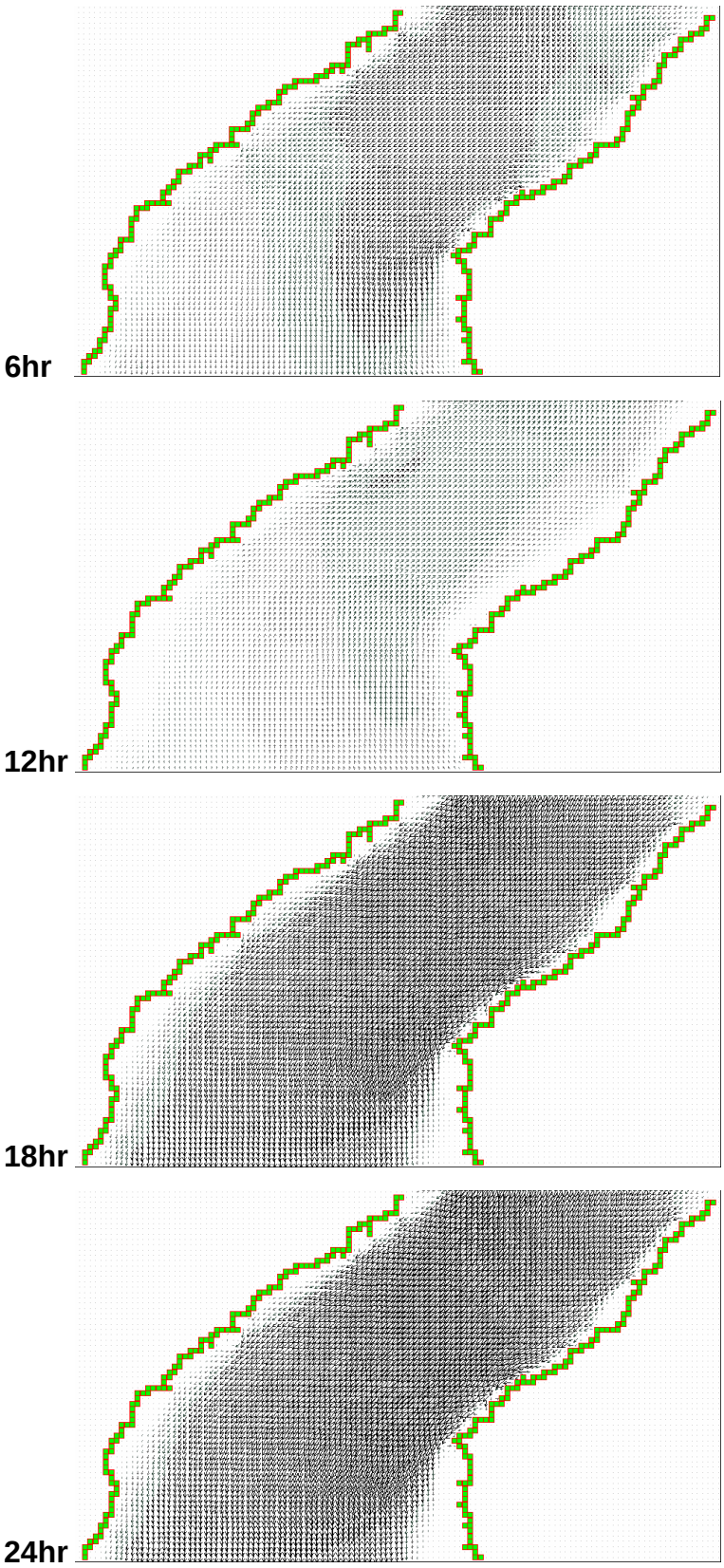

Figure 5.44: Simulated tidal velocities of the 80 m LNM domain of the Strait of Messina during the spring phase

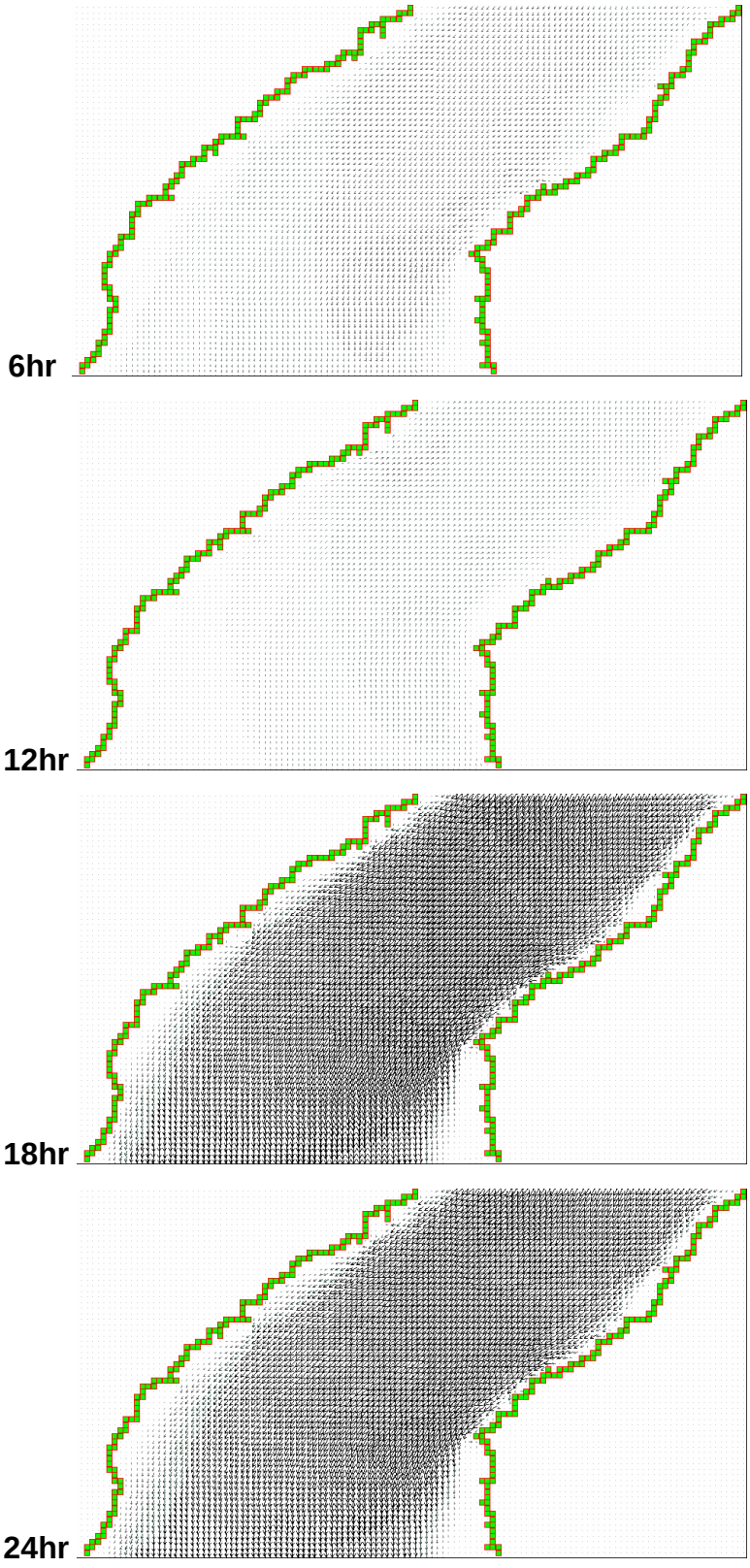

Figure 5.45: Simulated tidal velocities of the 80 m LNM domain of the Strait of Messina during the neap phase

5.4.2.3. 80 m flat depth case of simulation

This is the last numerical simulation case examined in the present study, in which the domain of simulation has a flat depth of 80 m (Fig. 5.46). This means that everywhere in the domain representing the aquatic ecosystem the depth is 80 m. The real morphometry of the Strait of Messina is maintained, the checkpoints and the sill region cross-section to examine the outputs are also the same as in the cases in sections 5.4.2.1 and 5.4.2.2. Again the dimensions of the domain of simulation are 150 x 260 cells with a cell size of $\Delta x = \Delta y = 75$ m. The M_2-tidal wave of 0.135 m amplitude previously applied as input/radiating boundary files will be also applied in this case of simulation.

Figure 5.46: The 80 m flat domain of the Strait of Messina

Having such a shallow depth, compared to the previous cases, the simulation process starts by applying a normal Manning coefficient (n = 0.025 s/m^3) with a normal eddy viscosity term effect. The total period of simulation is 170000 s with a time interval dt = 0.25 s. The effect of the Coriolis force is ignored. The outputs of this simulation case are graphically represented in Figure 5.47 and the simulated tidal velocity at the cross section of interest, Ganzirri to Punta Pezzo, is shown in Figure 5.48. Once again the simulated tidal behaviour (velocity and elevations) of the Strait of Messina using an 80 m flat domain with a normal Manning coefficient and normal eddy viscosity effect are unstable. The configuration of this behaviour shows extreme velocities exceeding 15 m/s as well as extreme elevations exceeding 20 m which is certainly not representative of any real status. In addition, Figure 5.48 shows no periodicity for the semidiurnal type of tides in the Strait of Messina. A still positive schematic presentation is the simulation of the gyres close to the Calabrian Coast north to Punta Pezzo. This, again, is in a good agreement with the simulated outputs [280]. As a consequence of these unreasonable outputs, an assumption is made to increase the effect of the eddy viscosity term and to check the resultant outputs. The initial conditions for the new simulation process will therefore be a flat domain of 80 m depth with a fully-maintained real morphometry of the Strait of Messina. The driving/radiating boundary files are M_2-tidal wave of 0.135 m amplitude. The Manning coefficient is of normal value (n = 0.025 s/m^3). The effect of the Coriolis force is ignored and that of the eddy viscosity is multiplied by 10. The outputs of this simulation case are graphically represented in Figure 5.49, while the simulated tidal velocity at the sill region is represented in Figure 5.50. As may be shown in this case of simulation, the tidal behaviour (velocities and elevations) are reasonable, stable and expressive. Tidal periodicity that expresses the semidiurnal type of tides in the Strait of Messina is well simulated. The simulated tidal velocity exceeds 2.0 m/s and the maximum simulated amplitude exceeds 0.2 m.

Table (5.11) summarises the maximum and minimum simulated tidal velocities and elevations at the eight chosen locations within the domain of simulation. It appears that the results of the present case-study, although being the results of the use of a flat depth with a high eddy viscosity effect, are higher when compared to those recorded [141] and simulated [280] at four common checkpoints as shown in Table

(5.12). This confirms the effect of the bathymetry on the flow regime in the Strait of Messina.

	Max. Vel. (m/s)	**Min. Vel. (m/s)**	**Max. Elev. (m)**	**Min. Elev. (m)**
Capo Peloro	2.4	5.4×10^{-4}	0.12	1.9×10^{-5}
Reggio Calabria	0.85	9.3×10^{-4}	0.12	6.1×10^{-5}
Ganzirri	1.1	8.6×10^{-4}	0.09	5.9×10^{-6}
Punta Pezzo	1.2	2.7×10^{-7}	0.06	6.3×10^{-6}
Messina Harbour	1.1	2.5×10^{-4}	0.10	5.9×10^{-6}
Central Point	2.1	4.9×10^{-8}	0.04	6.0×10^{-6}
Northern Point	2.2	9.3×10^{-3}	0.11	5.4×10^{-6}
Southern Point	1.0	2.2×10^{-7}	0.20	2.2×10^{-7}

Table 5.11: Maximum and minimum tidal current velocities and elevations in the 80 m flat domain case

	Recorded (m) [141]	**Simulated (m) [280]**	**Present case-study (m)**
Reggio Calabria	0.06	0.06	0.12
Ganzirri	0.03	0.02	0.09
Punta Pezzo	0.009	0.04	0.06
Messina Harbour	0.05	0.04	0.10

Table 5.12: Comparison between the simulated tidal elevations in the present-case study and those previously recorded and simulated at four common checkpoints

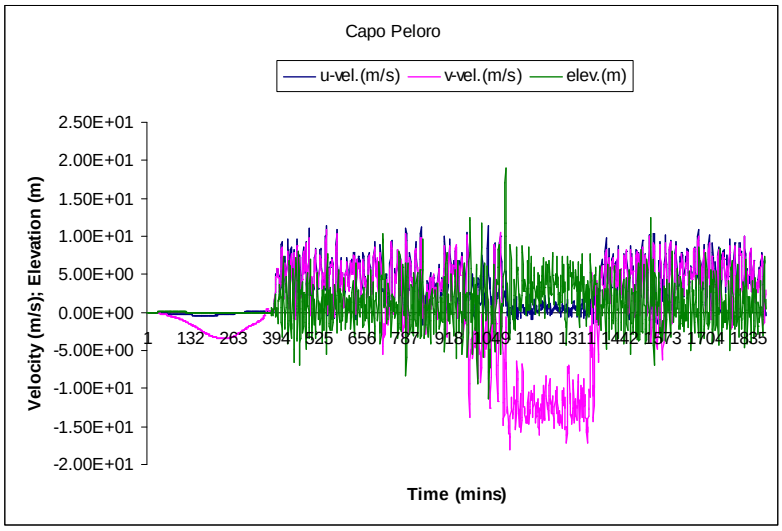

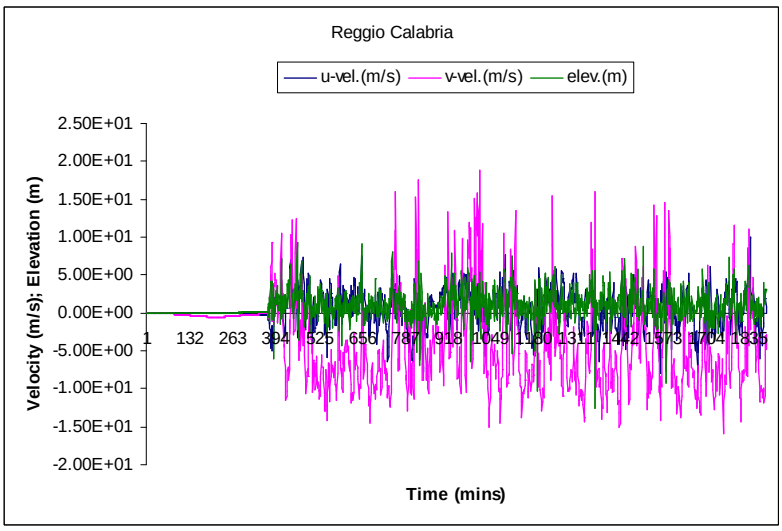

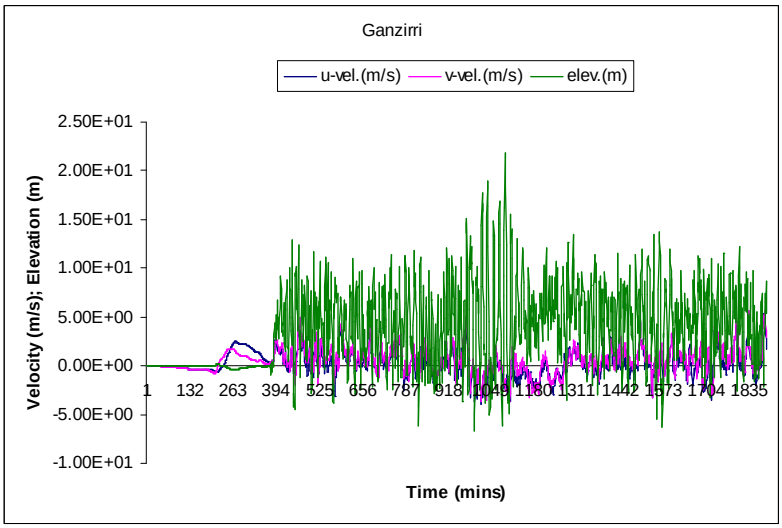

Figure 5.47: Tidal behaviour of the simulated flat 80 m Strait of Messina using a normal Manning coefficient

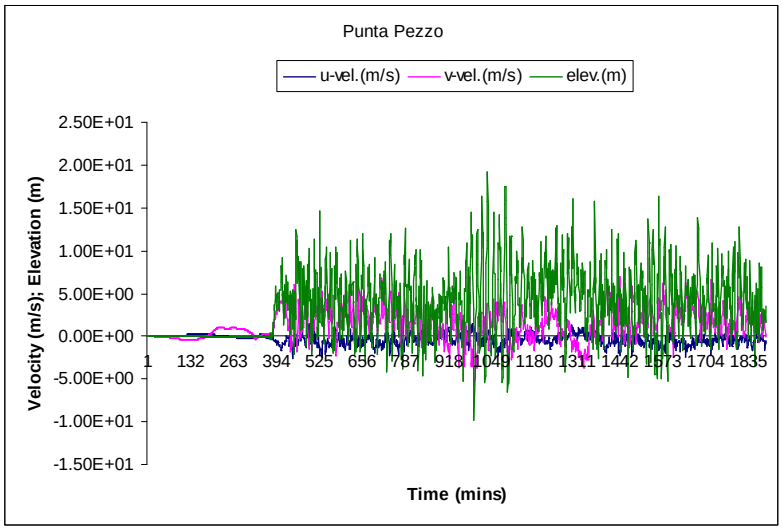

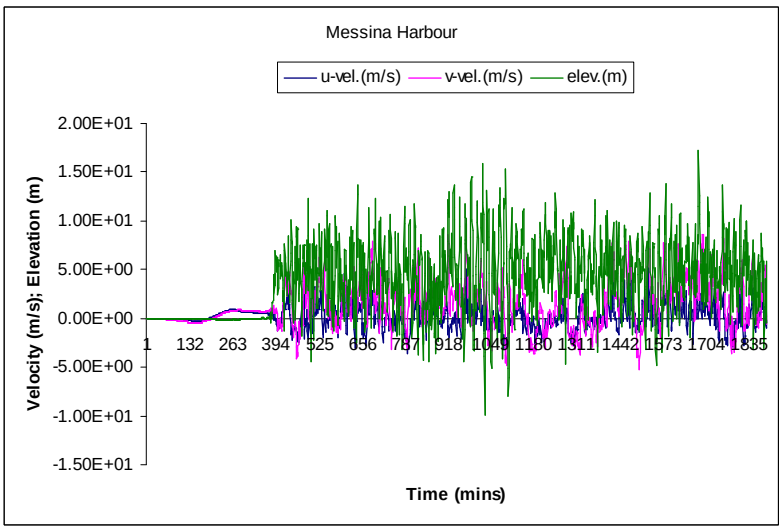

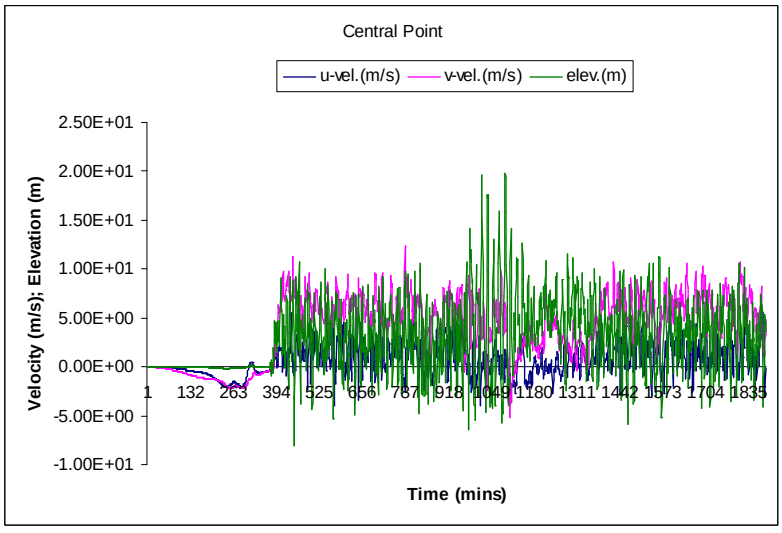

Figure 5.47 (Continued)

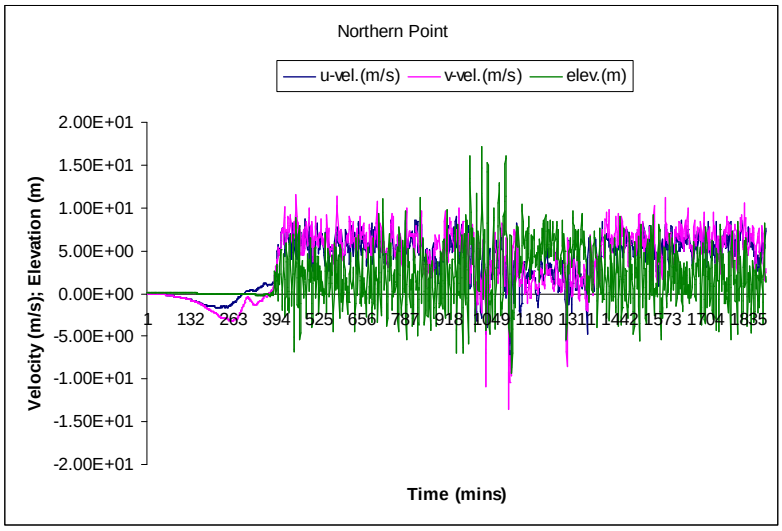

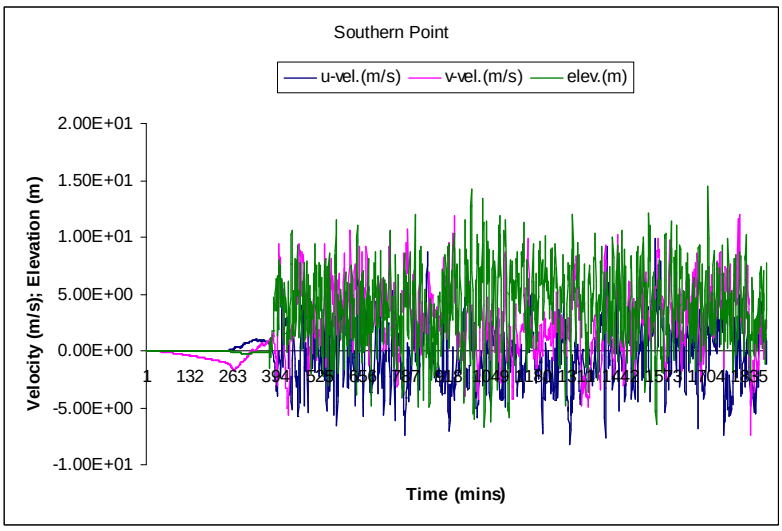

Figure 5.47 (Continued)

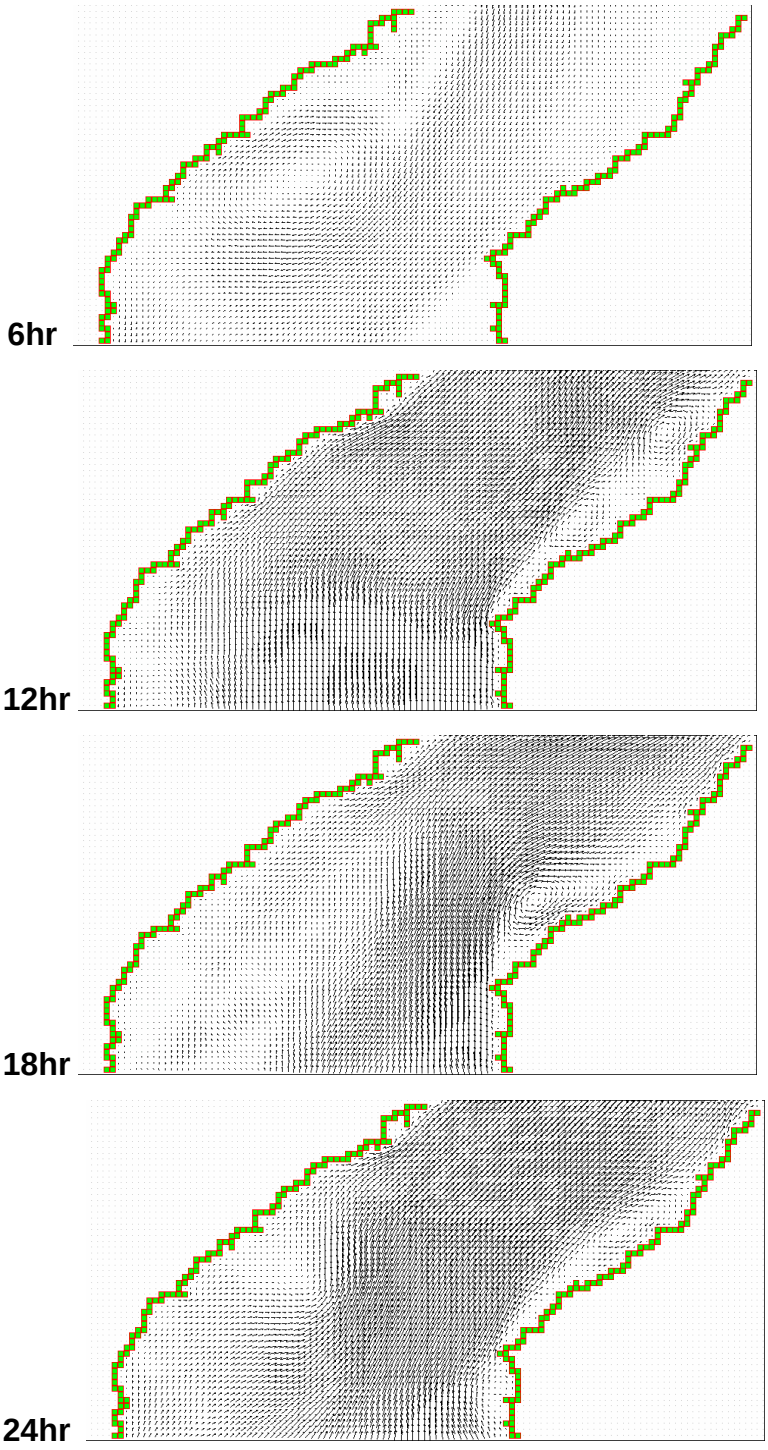

Figure 5.48: Simulated tidal velocities using a normal Manning coefficient and a normal eddy viscosity effect in the 80 m flat Strait of Messina domain

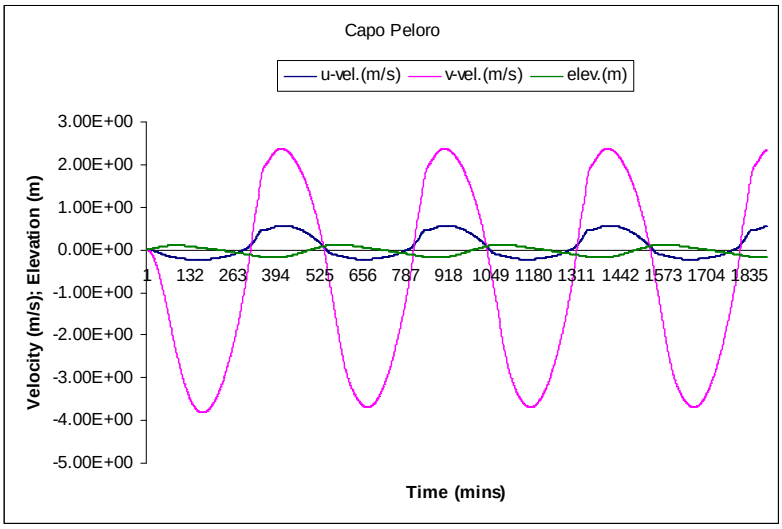

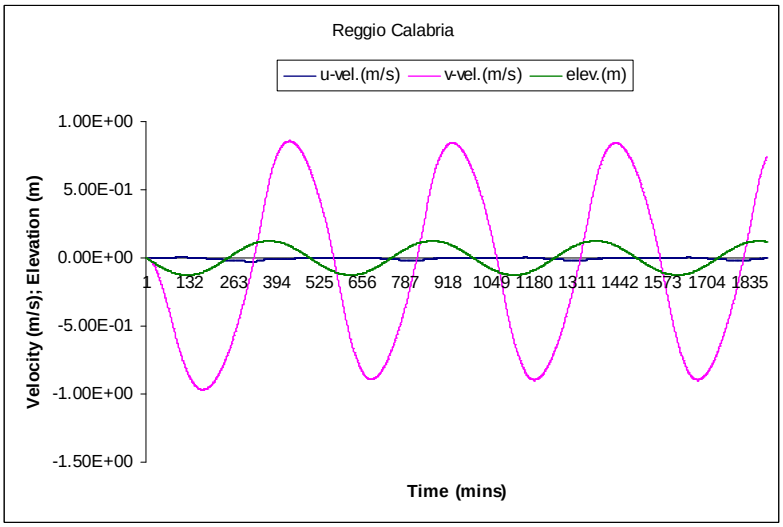

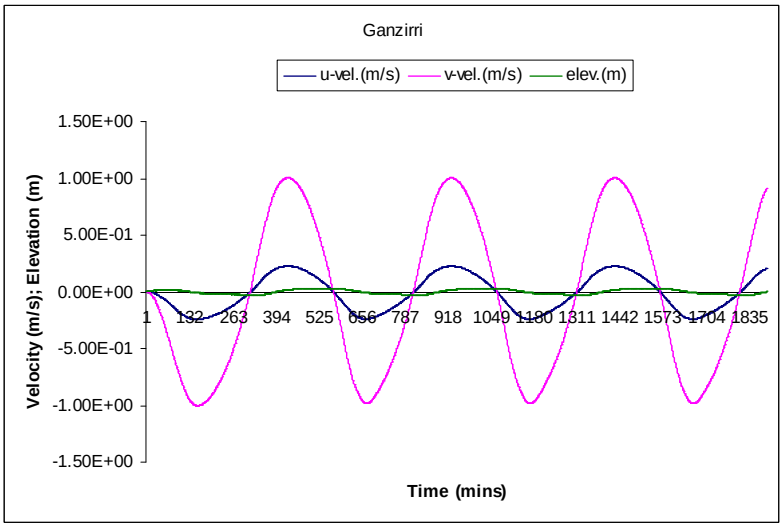

Figure 5.49: Tidal behaviour of the simulated flat 80 m Strait of Messina using a normal Manning coefficient with a high eddy viscosity effect

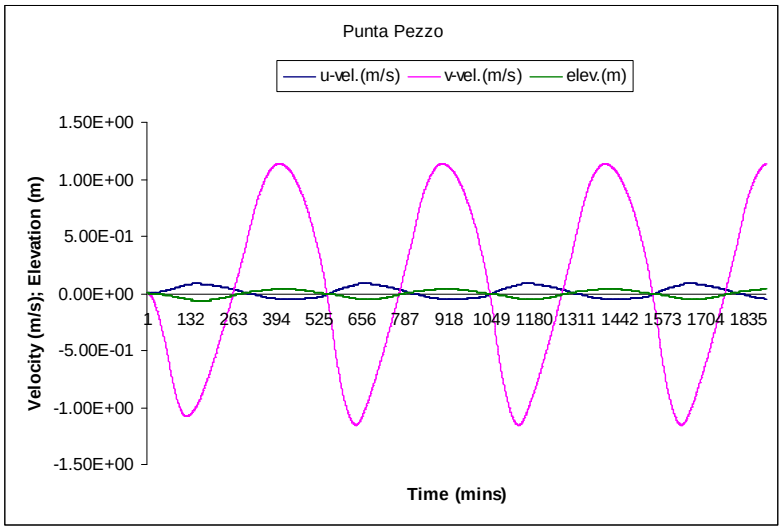

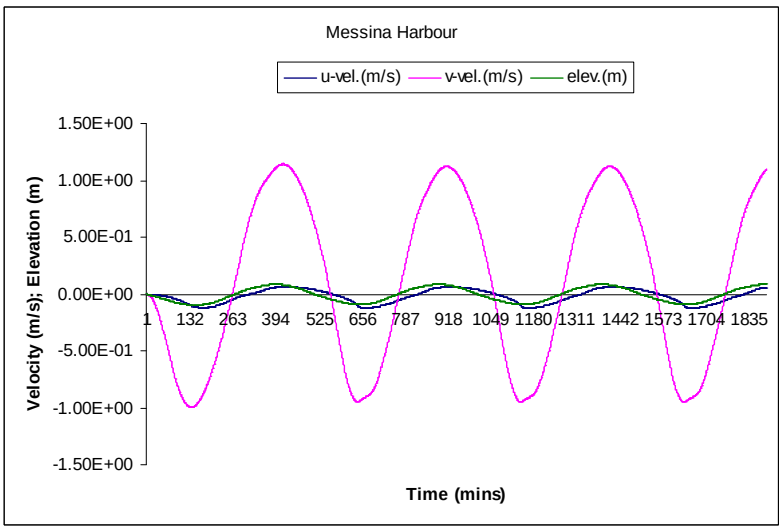

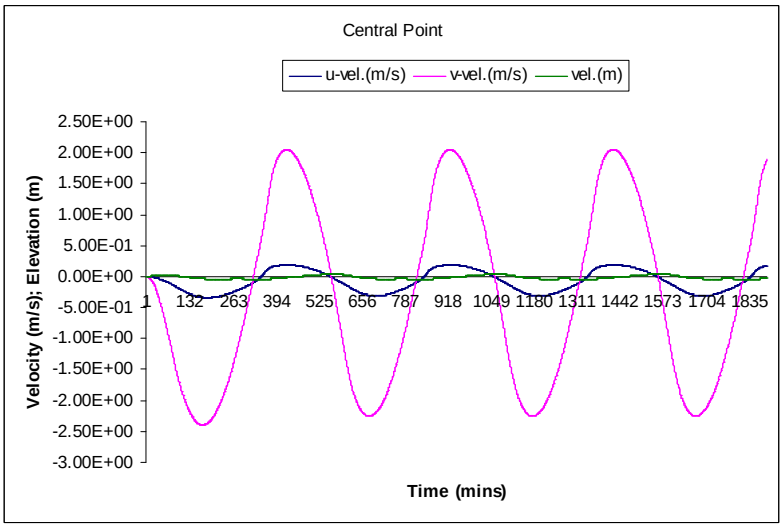

Figure 5.49 (Continued)

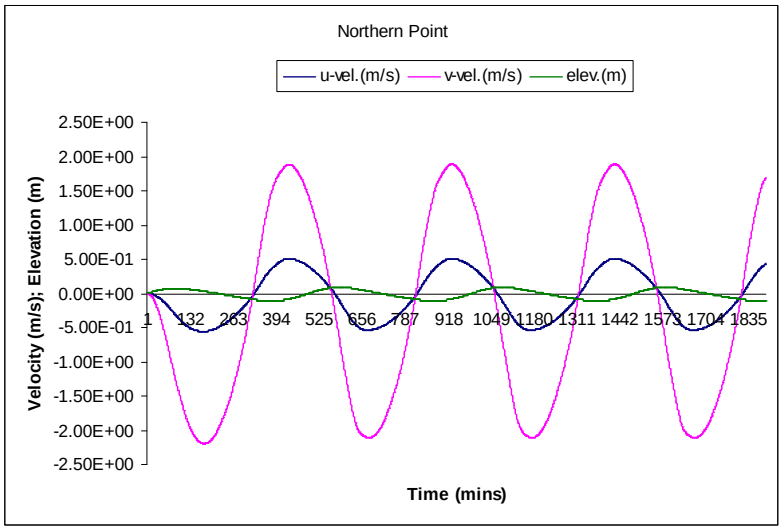

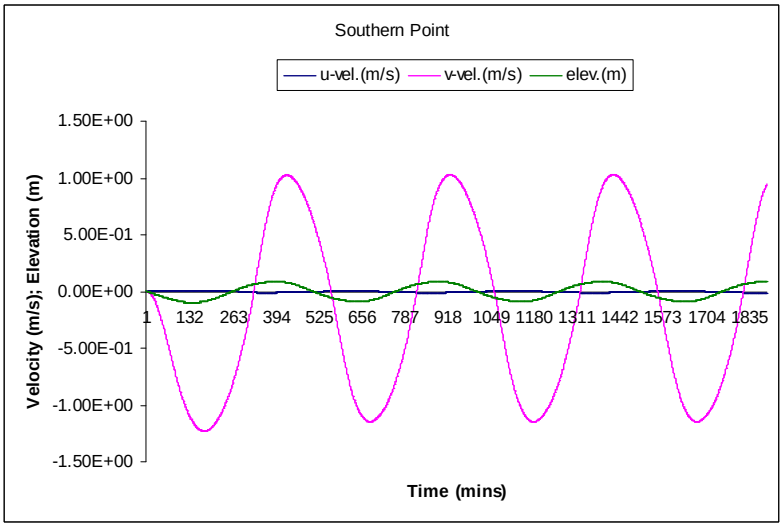

Figure 5.49 (Continued)

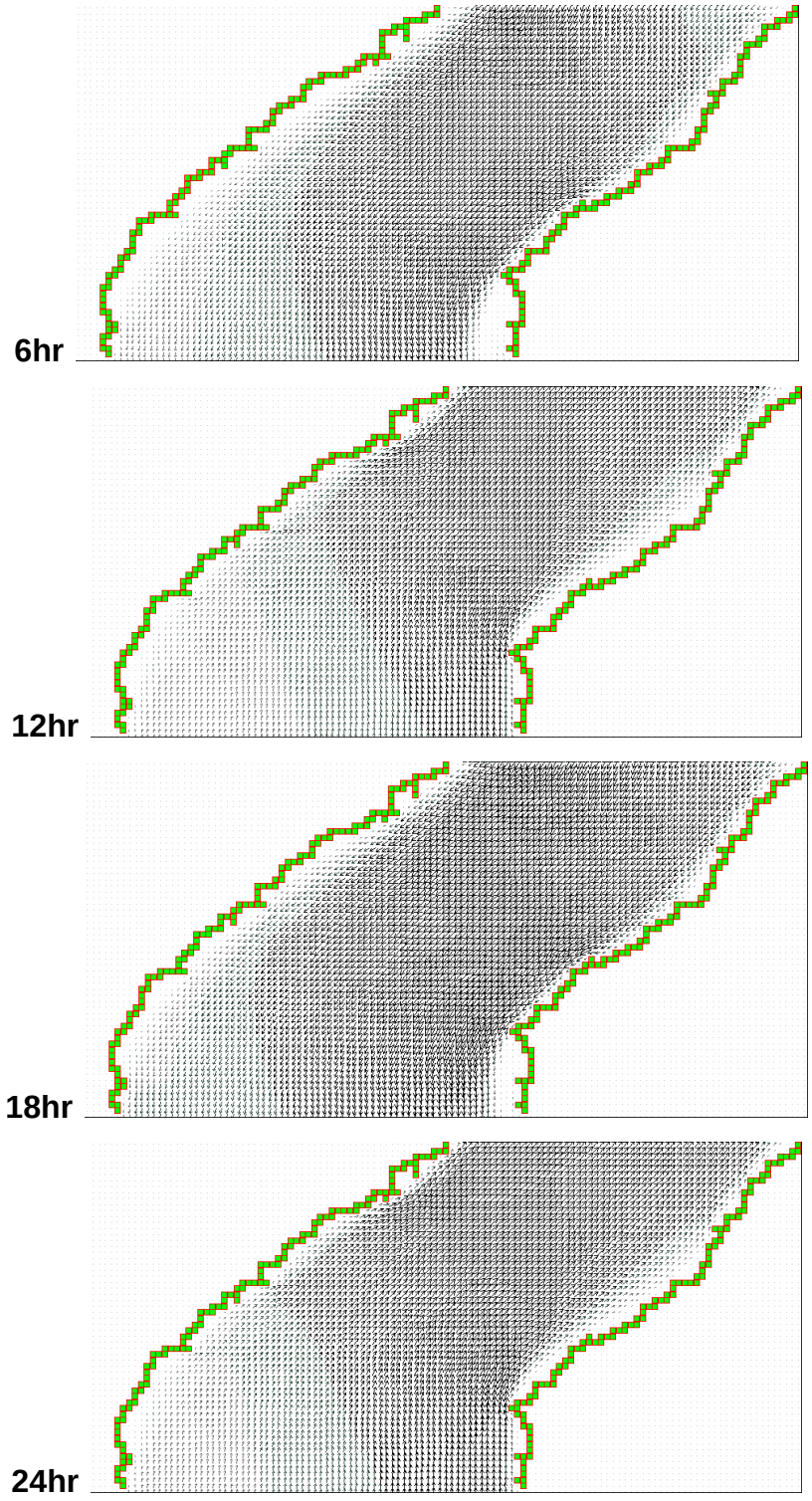

Figure 5.50: Simulated tidal velocities using a normal Manning coefficient and a high eddy viscosity effect in the 80 m flat Strait of Messina domain

It is time now to examine the spring and neap tidal phases whilst applying the 80 m flat domain. The driving and the radiating boundary files are those built for four successive days for each phase (Fig. 5.13 and 5.14). The driving force acts from north to south, while the radiating force acts in the opposite direction. For this domain of simulation a normal Manning coefficient (n = 0.025 s/m^3) with a high eddy viscosity effect (edvisc. x 10) gave stable and reasonable outputs for the examination process of the tidal flow regime within the Strait. These conditions are, accordingly, applied to examine the 80 m flat strait of Messina domain during spring and neap tides. The total period of simulation is 170000 s with dt = 0.25 s. The simulation results are given every 1800 s; i.e. every half an hour. The examination of the numerical simulation process of the Strait of Messina in this case, 80 m flat depth, during spring and neap tides results in the tidal behaviour schematically presented in Figures 5.51 and 5.52, respectively. The simulated tidal velocity during spring tide for the sill section (Ganzirri - Punta Pezzo) of this domain of simulation is shown in Figure 5.53, while that during neap tide is presented in Figure 5.54. The effect of the flat bathymetry with the normal Manning coefficient appears in high tidal velocities exceeding 3 m/s as well as high tidal amplitudes exceeding 0.6 m. The maximum simulated tidal velocity is 3.7 m/s for the chosen Central Point, at the sill region, during the two phases. However, with these appreciated numerical figures, which are the closest to the real situation of the Strait of Messina, three points should be noted:

1. The domain of simulation is, to some extent, imaginary with the flat bathymetry (80 m deep).
2. The graphical representations of the tidal behaviour during the two phases suffer, to a certain extent, from the same instability as the two previous cases of simulation (real Strait of Messina and the 80 m LNM domains).
3. The examined simulated outputs for the sill region during the two tidal phases are still missing the semidiurnal tidal periodicity after the first 12 hours of simulation.

However, the gyre located north to Punta Pezzo appears in these simulation outputs. This feature was completely absent from the previous two simulations.

The resultant maximum and minimum tidal velocities and elevations during spring and neap tides are respectively shown in Tables (5.13) and (5.14).

	Max. Vel. (m/s)	**Min. Vel. (m/s)**	**Max. Elev. (m)**	**Min. Elev. (m)**
Capo Peloro	3.4	8.6×10^{-3}	0.32	5.0×10^{-5}
Reggio Calabria	2.4	7.3×10^{-4}	0.35	5.0×10^{-6}
Ganzirri	1.4	3.9×10^{-4}	0.44	6.5×10^{-5}
Punta Pezzo	1.2	1.8×10^{-4}	0.40	1.9×10^{-5}
Messina Harbour	2.3	1.7×10^{-5}	0.47	7.8×10^{-5}
Central Point	3.7	1.7×10^{-3}	0.37	1.4×10^{-5}
Northern Point	3.4	2.6×10^{-3}	0.37	3.1×10^{-4}
Southern Point	3.2	3.8×10^{-5}	0.48	4.0×10^{-4}

Table 5.13: Maximum and minimum tidal current velocities and elevations in the 80 m flat domain during the spring phase

	Max. Vel. (m/s)	**Min. Vel. (m/s)**	**Max. Elev. (m)**	**Min. Elev. (m)**
Capo Peloro	3.6	3.7×10^{-4}	0.38	8.6×10^{-5}
Reggio Calabria	2.7	4.3×10^{-5}	0.29	3.5×10^{-5}
Ganzirri	1.7	8.5×10^{-5}	0.46	4.7×10^{-5}
Punta Pezzo	1.5	2.7×10^{-4}	0.47	7.9×10^{-5}
Messina Harbour	1.8	8.1×10^{-4}	0.49	3.0×10^{-6}
Central Point	3.7	4.6×10^{-4}	0.57	4.7×10^{-5}
Northern Point	3.6	3.8×10^{-4}	0.43	1.1×10^{-4}
Southern Point	2.7	3.3×10^{-5}	0.68	2.4×10^{-4}

Table 5.14: Maximum and minimum tidal current velocities and elevations in the 80 m flat domain during the neap phase

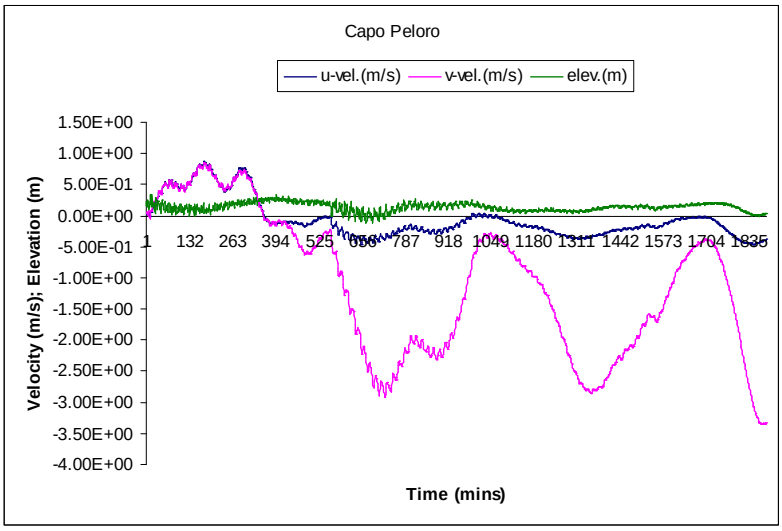

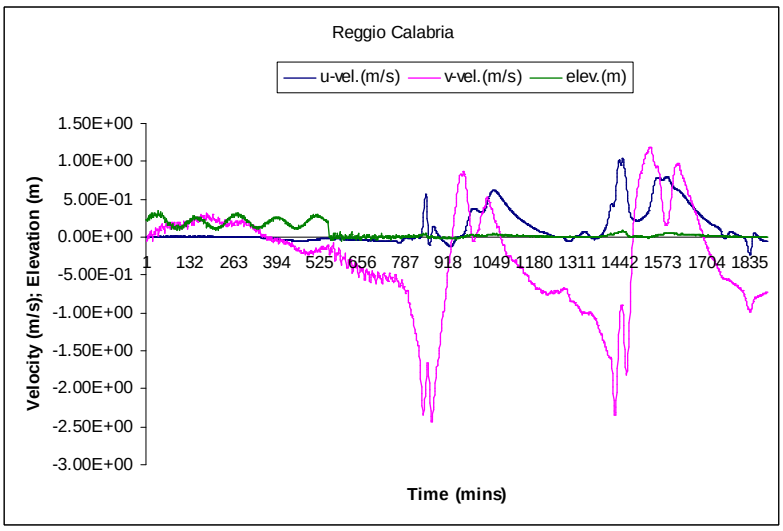

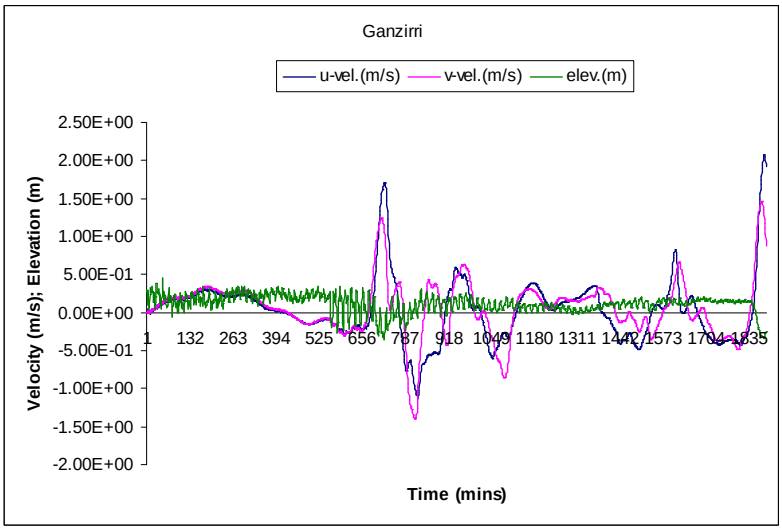

Figure 5.51: Tidal behaviour of the 80 m flat domain of simulation during the spring tide

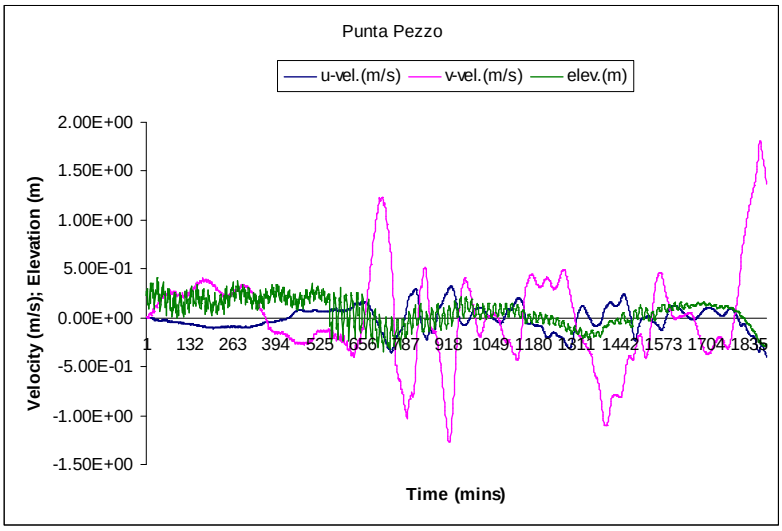

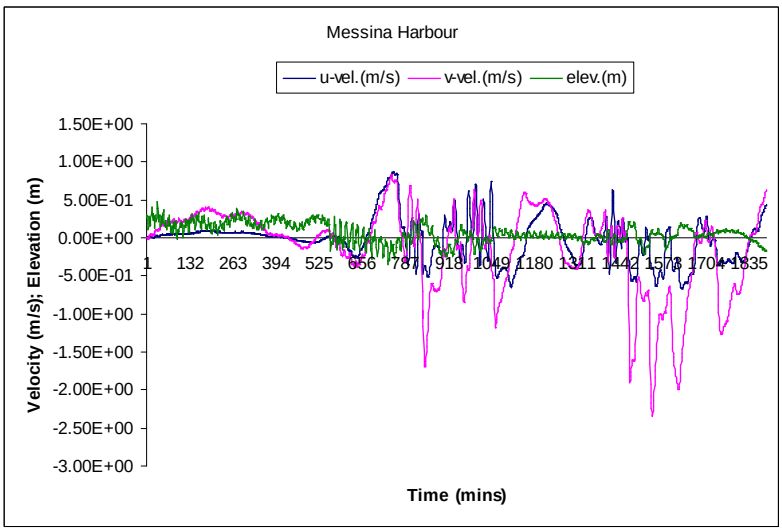

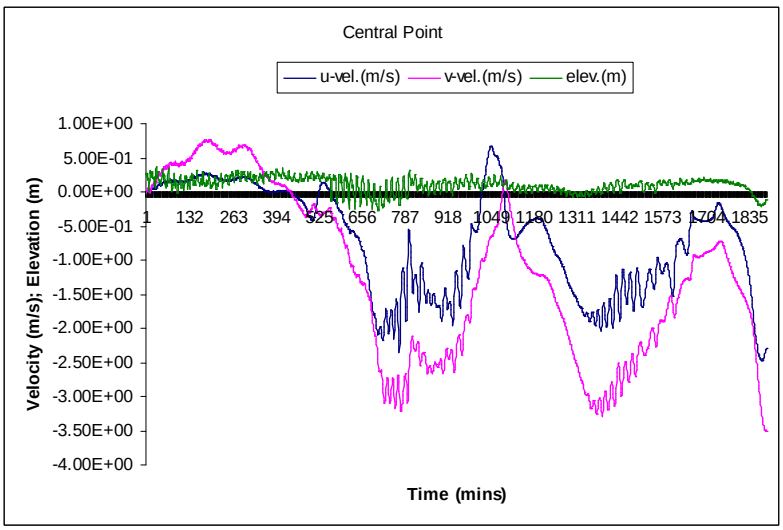

Figure 5.51 (Continued)

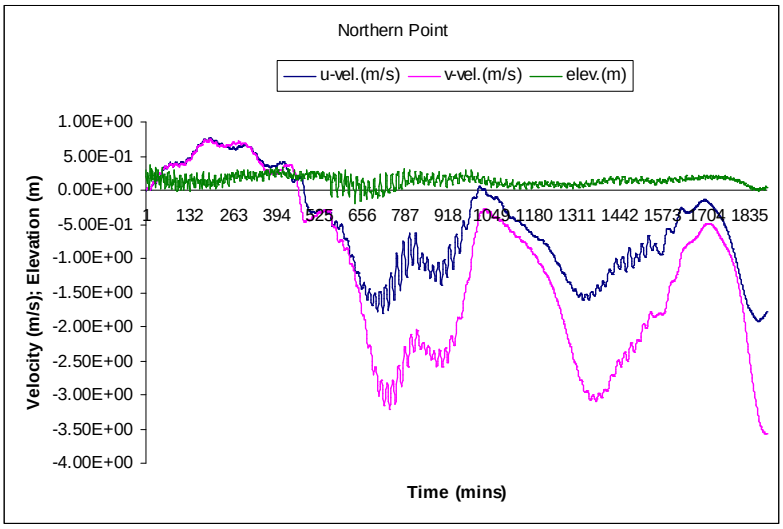

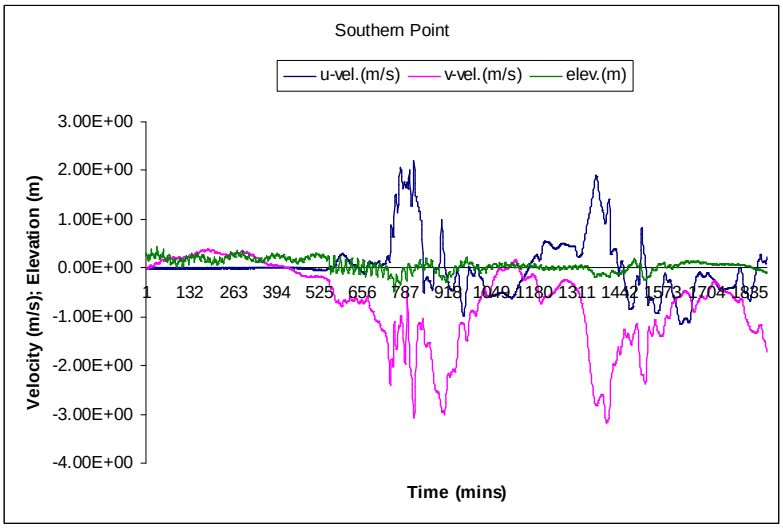

Figure 5.51 (Continued)

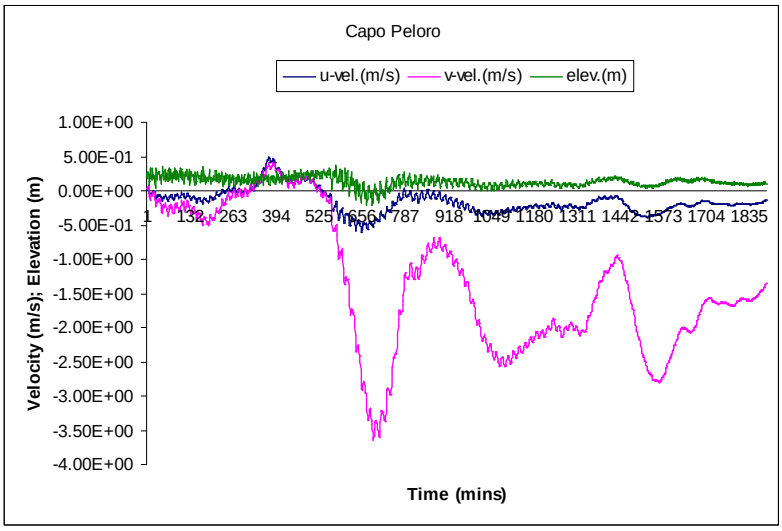

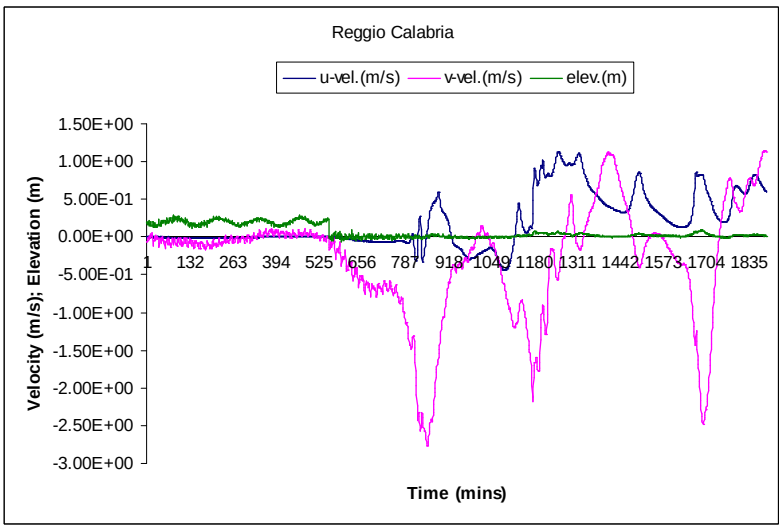

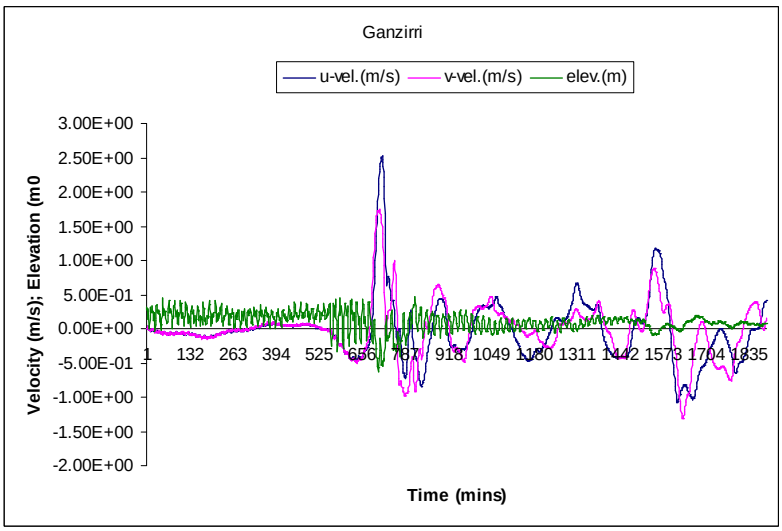

Figure 5.52: Tidal behaviour of the 80 m flat domain of simulation during the neap tide

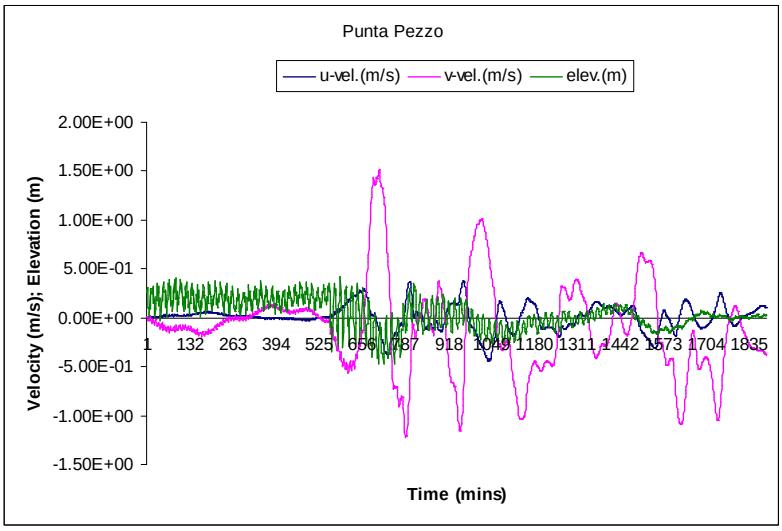

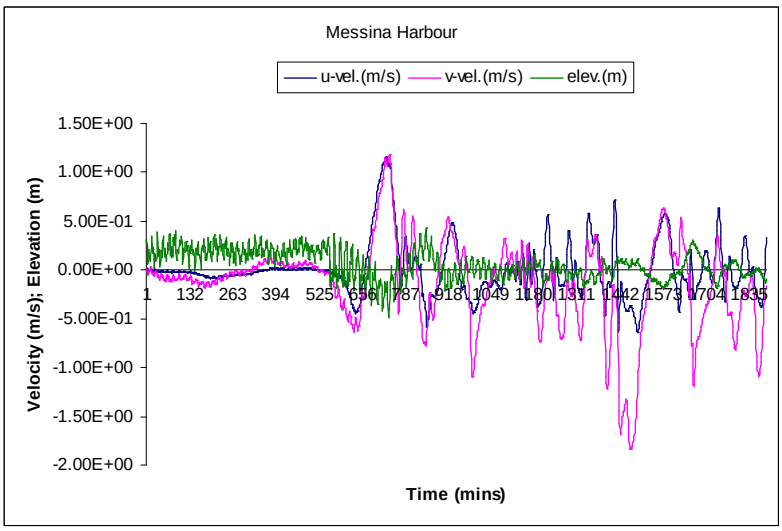

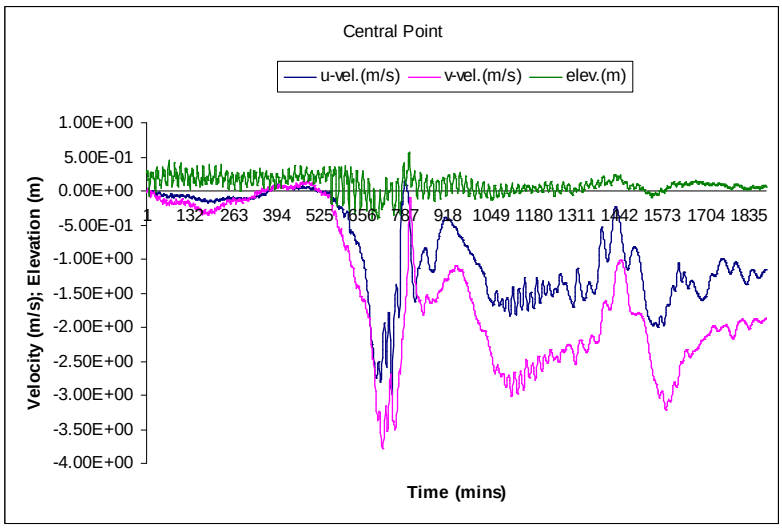

Figure 5.52 (Continued)

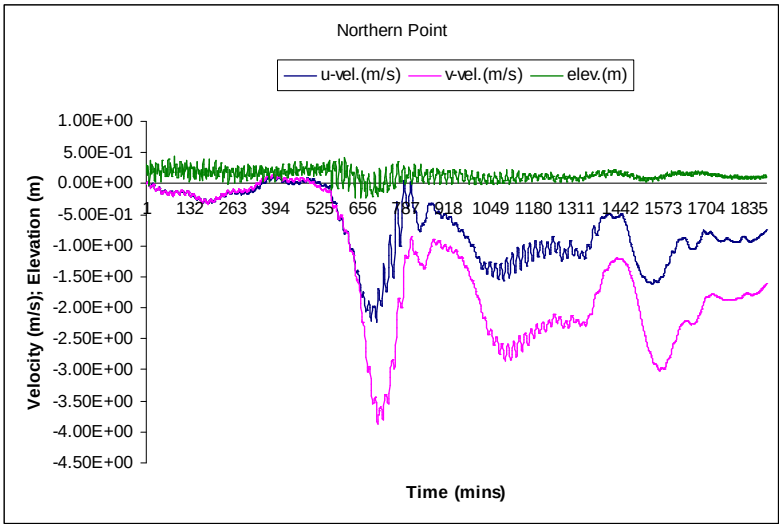

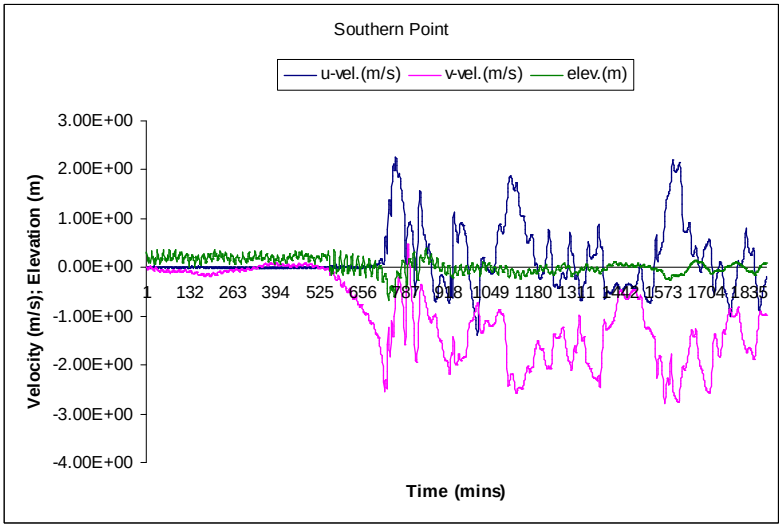

Figure 5.52 (Continued)

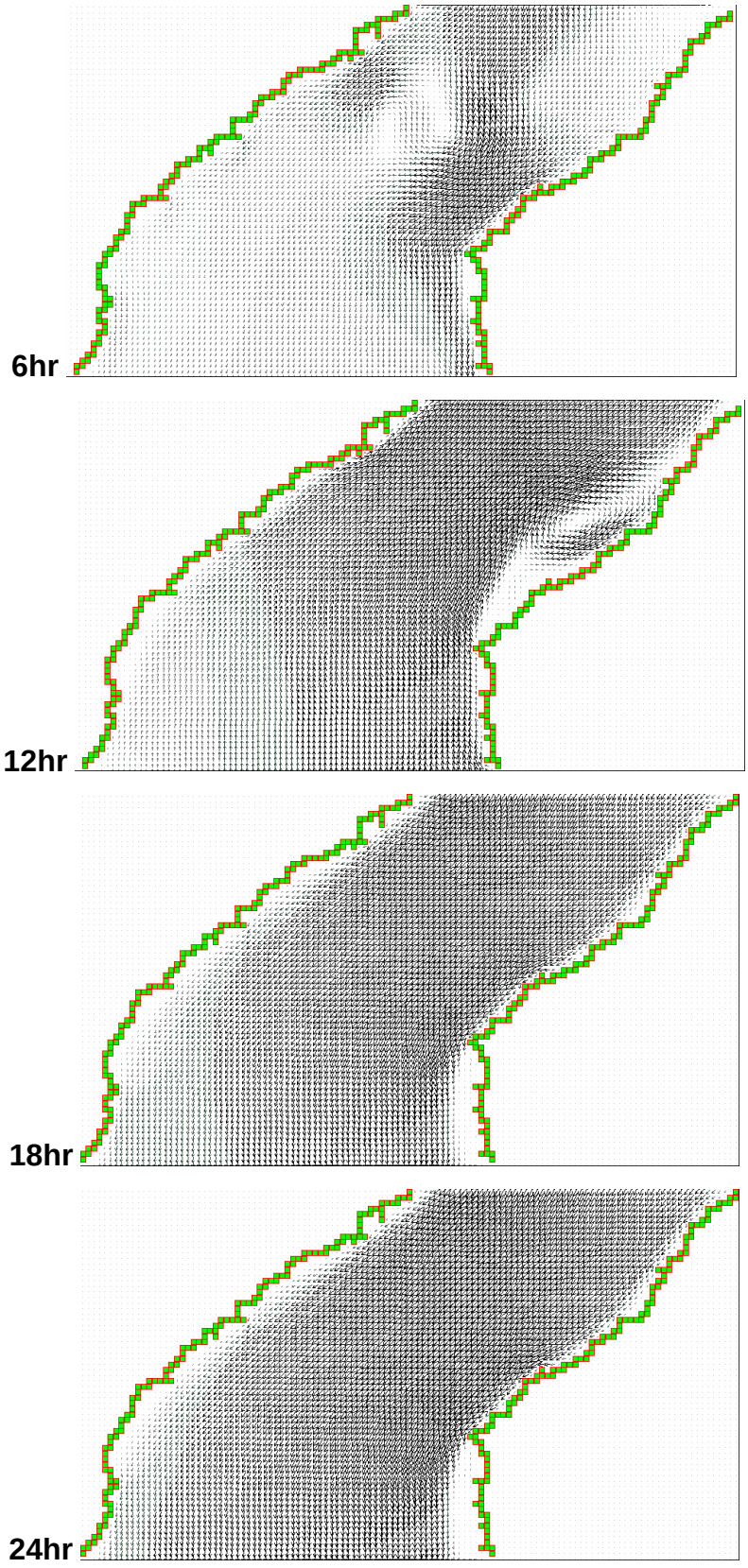

Figure 5.53: Simulated tidal velocities at the sill region for the 80 m flat domain during the spring tide

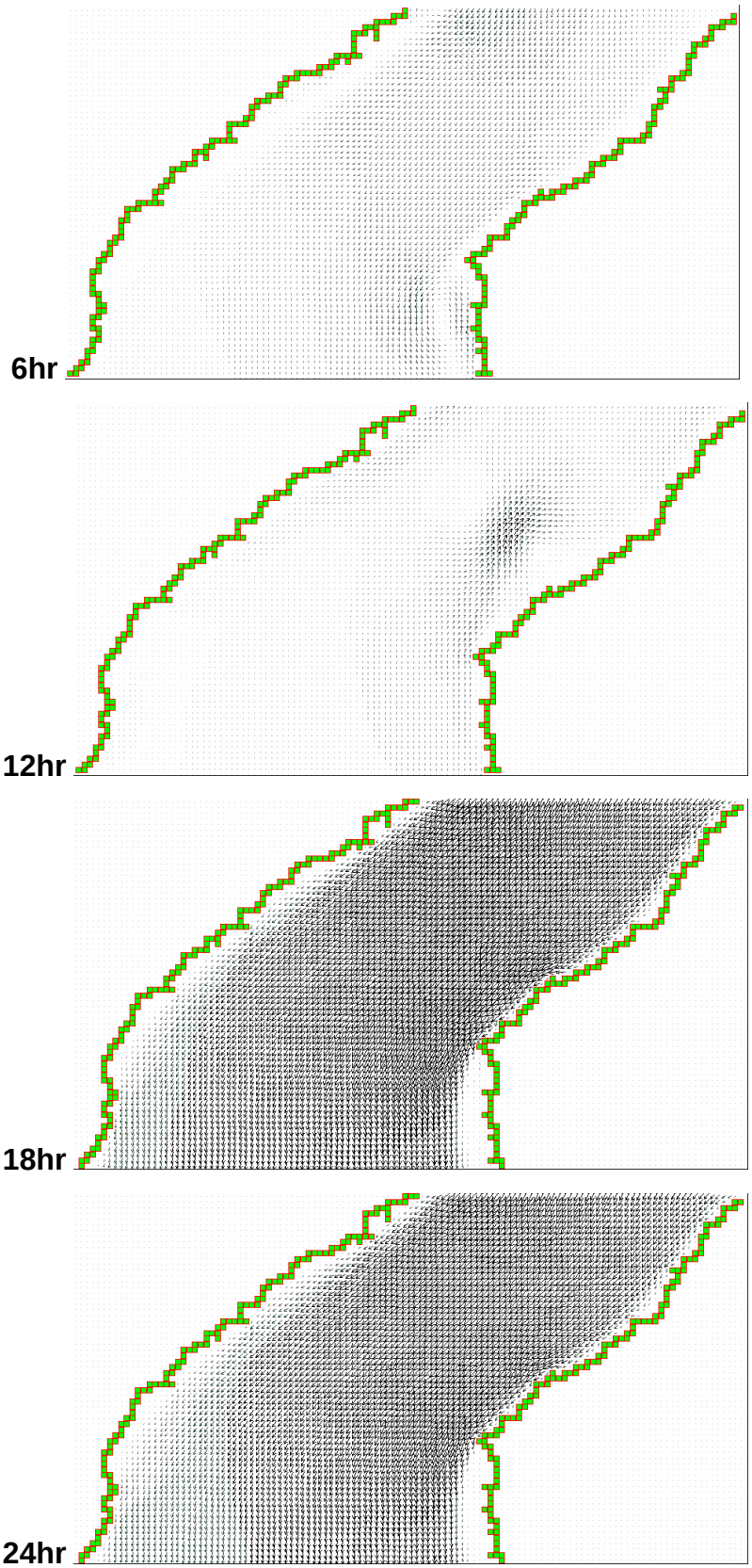

Figure 5.54: Simulated tidal velocities at the sill region of the 80 m flat domain during the neap tide

5.4 Chapter Conclusion

The University of Edinburgh "Tidal Flow Development (TFD)" numerical model is used to simulate the tidal flow regime in the Strait of Messina in different cases. The model is based on the Navier-Stokes system of equations. The model has the advantage of being mainly developed to investigate tidal environments and of being previously applied in different tidal cases. The model differs than those had been previously applied to simulate the Strait of Messina in that it mainly aims at identifying the places of excess energy where tidal turbines can be deployed to extract energy from tidal currents. Moreover, the code of TFD includes a special routine, which can be used to investigate the hydrodynamical changes due to the energy extraction process from a tidal current resource. Two main cases are discussed in the present chapter: the Strait of Messina as a simple tidal channel and the Strait in its real configuration. The simulation in the former case confirms the main tidal features in the Strait of Messina: tidal out-of-phase behaviour and the low importance of the transverse velocity component. However, the simplicity of the domain applied in this case affects the outputs of the model that the maximum tidal velocity does not exceed 1 m/s and for the spring tide does not exceed 0.53 m/s. The latter case of simulation consists of three case studies, in which the morphometry of the Strait of Messina is maintained, while changes are made to the topography. Accordingly, a full-scale Strait of Messina is initially simulated, and then the second and the third cases are simulation of the Strait using Level of No Motion (LNM) and a flat depth of 80 m, respectively. The move from one case to another is made in order to get reasonable outputs with real affecting factors: values of Manning and eddy viscosity coefficients. Unfortunately, these moves did not have the anticipated effect and this lead to conclude that the TFD numerical model does not suit complex domains of simulation like the Strait of Messina. On the other hand, the TFD model successfully simulates the real tidal flow pattern in the Strait of Messina only under these exceptional conditions: a high Manning factor and a high eddy viscosity effect. Reasons and justification for each step are discussed in detail in the present chapter. The simulation process of the real Strait of Messina highlights a shortfall in the application of the Coriolis force in the main code of the TFD model in an unsteady case like the Strait of Messina. Even though, the TFD numerical model assures the

effect of morphometry in enhancing tidal current velocities in the Strait of Messina. The model also succeeds in pinpointing locations with an energy excess in tidal currents (near Punta Pezzo) where tidal turbines may be effectively deployed. However, the model cannot be applied in the complex tidal environment of the Strait of Messina to investigate the hydrodynamical environment before and after the energy extraction process. In time, simulation will become available which can handle the wide variations in depth necessary for these environments.

CHAPTER 6
PHYSICAL SIMULATION OF THE TIDAL FLOW REGIME IN THE STRAIT OF MESSINA

An overview

This chapter presents the physical simulation of the tidal current regime in the Strait of Messina. The chapter consists of three sections; the first of which is a general introduction to physical models. The second section focuses on the flow-table tank facility at the University of Edinburgh and on the Particle Image Velocimetry (PIV) technique applied for measurement. Finally, section three discusses the outputs of the experiment.

6.1 Introduction

A physical model, also known as laboratory or experimental model, may be considered as an analogue computer in which the physical processes are reproduced at a reduced scale [292] and in which the major dominant forces acting on the real system are present in correct proportion to the actual case [293]. If the physical model is designed correctly with respect to certain definite scaling rules, then it can give reliable information upon which decisions can be precisely made [294]. If it is designed incorrectly, however, then it will only lead to inaccurate predictions and wrong decisions. An important property of physical models is the ability to closely visualise and observe the processes [295].

Physical models may be broadly classified in two major categories regarding the targeted goal [296]:

1- Validation models. These are used to verify numerical models. They are often idealised and simplified to provide a test case that fits the assumptions applied to the numerical model.
2- Design models. These are used to predict certain behaviour of the tested prototype. In these models all features and forces of an actual prototype are accurately modelled.

From a characteristics point of view, physical models may also be categorised in two groups [293]:

1- Fixed-bed models. These models have solid boundaries that cannot be modified or affected by the hydrodynamic processes taking place in the model. This type of model is used to study waves and currents.
2- Movable-bed models. These models are composed of materials that can react to the applied hydrodynamical forces.

Six reasons are given [297] supporting the use of physical models for studying and solving coastal engineering problems:

1- Once built, physical model technology is cost effective.
2- The development of measuring techniques (e.g. PIV, Doppler Laser) enables better understanding of the fluid mechanic relationships.
3- Physical models allow the monitoring and measurement of physical concepts in a better manner than numerical models and in a controlled environment.
4- Major difficulties in numerical models can be easily overcome using scale models.
5- The visual observations of the tested case are very appropriate to increase understanding of the studied domain.
6- The inherent limits of deterministic fluid mechanics due to turbulence.

Dealing with oceanic tidal features, a well-designed laboratory model may accurately reproduce tidal propagation and tidal currents, including secondary flow characteristics [292].

However, physical models have their disadvantages. The principal disadvantages of a physical model are its cost and its relative inflexibility [292]. In addition, all forcing functions and boundary conditions acting in nature are not included in the physical model, which, in turn, may affect the final judgment [293].

Broadly speaking, a physical model depends on some dimensional quantities. These may be summarised as follow:

- Length (L)
- Time (T)
- Mass (M)
- Velocity ($L\ T^{-1}$)
- Acceleration ($L\ T^{-2}$)
- Density ($M\ L^{-3}$)

- Flow rate ($L^3 T^{-1}$)
- Viscosity ($M L^{-1} T^{-1}$)
- Kinematic Viscosity ($M^2 T^{-1}$)
- Weight ($M L T^{-2}$)
- Work ($M L^2 T^{-2}$)
- Power ($M L^2 T^{-3}$)

Moreover, some dimensionless numbers (e.g. Froude number, Rossby number, Reynolds numbers) should also be considered when dealing with a flow experimental model. These numbers are mainly used in order to investigate the effects of different common forces that act on both model and real field, e.g. gravity, Coriolis force, shear stress, etc. and to scale the laboratory model with the real field of work. For each laboratory model case, there is a specific dimensionless number which must be accurately specified in order to maximise the scaling process.

According to the author's knowledge, the most published hydraulic laboratory simulation research primarily targets the open channel flow systems and only a few are available for studying the tidal phenomena. This might reflect the difficulty of accurately achieving flow stability in large moving water channels under laboratory conditions, and also the fact that the laboratory testing of scale model tidal devices is still in its early developing stages [298]. The present laboratory-modelling case study aims to simulate the tidal current regime of the Strait of Messina in the laboratory.

6.2 Tidal Flow-table

6.2.1. Tidal Flow-table set-up and scaling procedures

The tool for physical simulation in the present study is the closed tidal flow-table tank system located in the wet-mechanical laboratory of the Sanderson Building at the University of Edinburgh.

The system consists of a tidal flow-table tank of horizontal dimensions 5 m x 2 m (Fig. 6.1) with two openings: a flow inlet and outlet (Fig. 6.2). These are connected through underlying pipes and the flow within the tank is controlled by a motor pump shown in Figure 6.3. The pump itself is controlled by a digital control box (Fig. 6.4), which allows the rotational speed of the motor to be specified in revolutions per

minute (rpm). In order to generate a steady (uniform) flow along the width of the tank between its two ends, two stilling rooms with diffusers are located at the extremities of the tank (Fig. 6.5). The holes, which are located along each diffuser, are identical and have increasing diameters from the centre outwards to maintain a constant pressure gradient during the operation. A water-proofed plywood frame (Fig. 6.6) has been used to represent the northern, central and southern widths of the real Strait of Messina. These actual Strait widths are: 5 km for the northern boundary, 3 km for the sill region 10 km for the southern boundary. Accordingly, the three widths in the flow-table tank are proportionally scaled as 1: 0.6: 2, respectively, as shown in Figure 6.6. The frame has equal dimensions for its two parts. It is settled symmetrically in the tank. The area (1.5 x 0.6 m), which represents the constriction of the sill region, occupies one third of the total frame surface area.

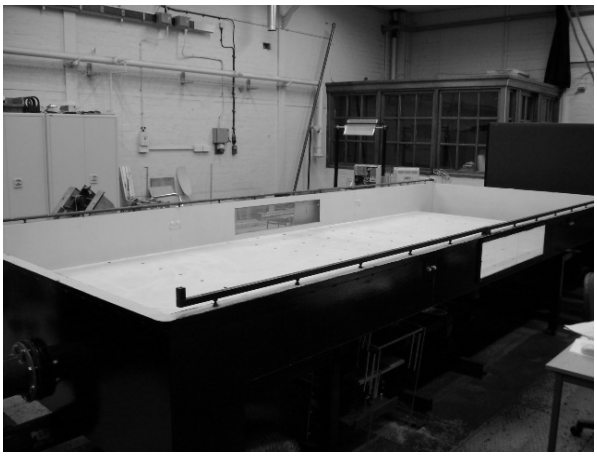

Figure 6.1: The flow-table tank facility in the wet laboratory at the University of Edinburgh

Figure 6.2: The inlet pipe to the flow-table tank

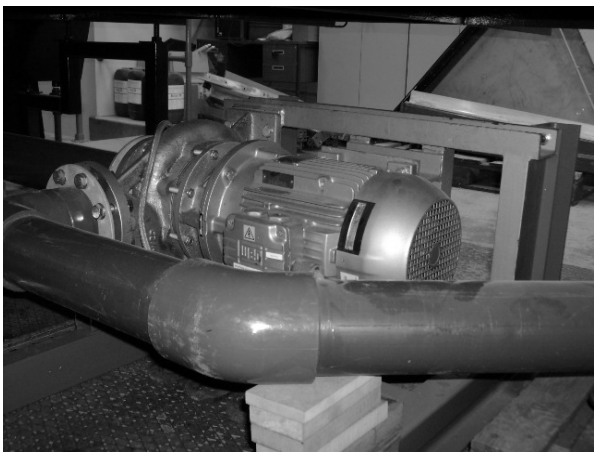

Figure 6.3: The underlying connecting pipes and the controlling motor pump

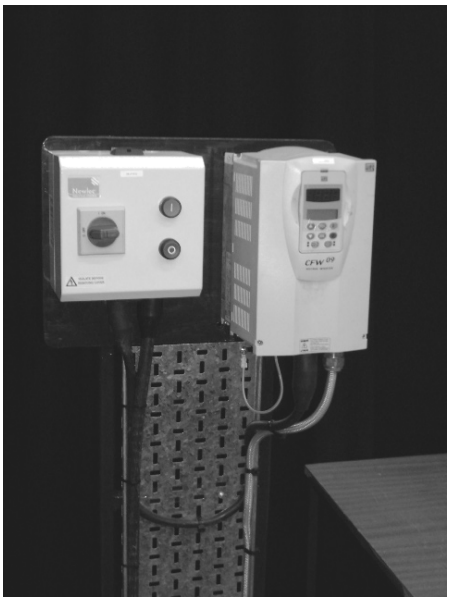

Figure 6.4: The digital control On/Off driving motor pump system

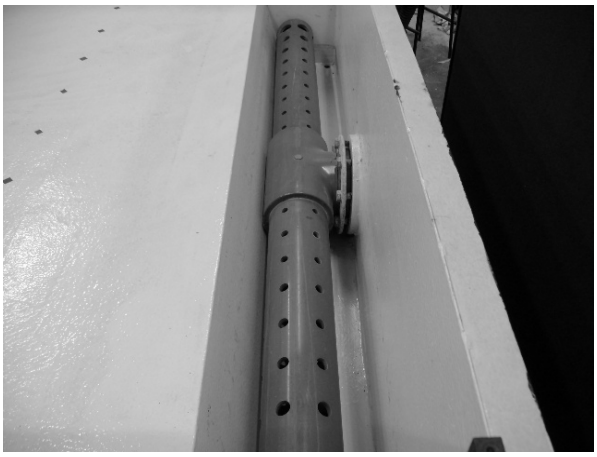

Figure 6.5: One of the stilling rooms and diffusers in the flow-table system

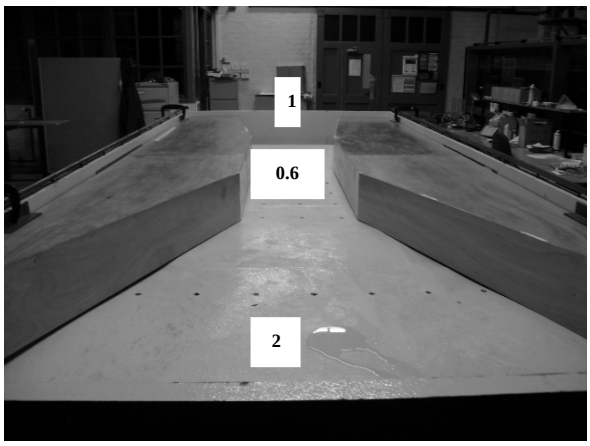

Figure 6.6: The inner plywood frame representing the three scaled widths (1: 0.6:2) of the Strait of Messina

In order to simplify the present experimental work, the following assumptions are made:

- The Coriolis force parameter (f) and the wind-shear stress are both negligible.
- Only three forces affect the present physical experiment: gravity, the inertial force and the viscosity.
- The scale of acceleration due to gravity is equal to unity.
- The inertial balance between the simulated and the real fields is calculated by the Froude number.

Before starting the simulation process in the present laboratory experiment, scaling calculations have been done to ensure the ratio between the simulated and the real fields. Scaling depends upon two dimensionless numbers: the Froude and Reynolds numbers.

The Froude number is given by the following equation:

$$F_r = \frac{u}{\sqrt{g\,L}} \qquad (6.1)$$

where,

u is the flow velocity (m/s); g is the gravitational acceleration (equals to 9.81 m/s^2); and L is a characteristic length (m)

As water depth is more significant for tidal technology than length, the characteristic length in equation (6.1) may be replaced by the water depth (h). Hence, the above equation takes the form

$$F_r = \frac{u}{\sqrt{g\,h}} \qquad (6.2)$$

where, h (m) is the total water depth of area of interest.

To ensure accurate results, the flow-velocity within the flow-table tank must be scaled to the full-scale. This depends mainly on the gravitational-inertial forces relationship derived from the Froude number, which, in turn, should be unique for both real field and laboratory. Accordingly, the flow velocity within the flow table may be given by the following equation

$$u_m = u_f \sqrt{\frac{h_m}{h_f}} \qquad (6.3)$$

where,

u_m and u_f are the model and the real field flow velocities (m/s), respectively; and

h_m and h_f are the water depths in the model and the real field (m), respectively.

In the present study, the sill region, with a depth of 80 m, is the main area of interest and where the tidal peak current-velocity is 3 m/s. Consequently, the corresponding Froude number is 0.107. The depth of water within the laboratory tank, which satisfies the Froude number equality between full-scale and laboratory environments, is 0.20 m. Consequently, the applied flow velocity in the experiment using the Froude number scaling is 0.15 m/s.

The balance between advective and viscous forces can be quantified using Reynolds number, defined in equation (6.4)

$$R_e = \frac{u\,L}{\upsilon} = \frac{u\,L\,\rho}{\mu} \qquad (6.4)$$

where,

u is the flow velocity (m/s); L is the characteristic length of the flow domain (m), which is interpreted here as fluid depth; υ is the fluid kinematic viscosity (m^2/s); ρ is the fluid density (kg/m^3); and μ is the fluid dynamic viscosity ($N\,s/m^2$)

It is generally impossible to achieve simultaneous Froude and Reynolds similarity, and the Reynolds numbers are 24×10^7 and 3×10^4 for real and laboratory scale, respectively. Both of these represent fully turbulent flow, although there are potential consequences as a result of failing to achieve full Reynolds scaling.

6.2.2. Particle Image Velocimetry (PIV) technique

Particle Image Velocimetry (PIV) is an image-based technique used to determine the flow velocity in a laboratory experiment in a 2D domain scale [299] or in a 3D domain with a very high accuracy [300] and either for laminar flow or turbulent flow of liquids and gases [301]. The term PIV appeared in the 1980s. However, the first attempt to use the technique itself started in the 1970s [3000]. PIV is presently considered as the most accurate quantitative fluid velocity vector measurement technique [300, 302] capable of being applied to physical simulations. The technique is based upon recording the displacement of moving tiny objects, known as tracers, at known times between consecutive image shots and extracting their displacements by a simple comparison process [302]. Flow velocities are subsequently determined by dividing the displacements of these tracer particles by the period between images [299].

A typical PIV system consists of four principal components [301-303]:

1. A transparent flow domain seeded with illuminated tracer particles.
2. A light source, which may be a laser or some other form of illumination.
3. Recording hardware, e.g. digital video camera.
4. Convenient software for image analysis.

A simple diagram illustrating a typical PIV system is shown Figure 6.7.

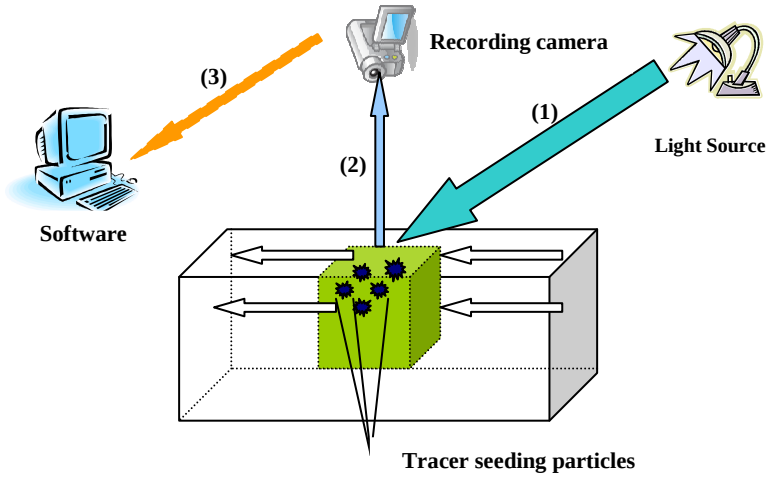

Figure 6.7: A schematic presentation of an ideal PIV system

The applied tracer particles in a PIV experiment must satisfy the following requirements [301, 304]:

1. Tracers should be able to follow the flow streamlines without excessive slip.

2. Their presence should not alter the flow properties.
3. They should be efficient light reflectors and should be homogenously distributed in the flow.

The energy necessary to illuminate the seeding particles (tracers) and produce images of sufficient exposure and clarity is a major issue in PIV [301]. That is why pure white-light sources are recommended for an accurate PIV experiment. A laser may also be used, whenever possible.

There are different types of recording equipment which can be used in a PIV experiment. These include [299]: conventional film photography, Radar imaging systems and direct electronic imaging using a Coupled Charged Device (CCD) such as a digital camera. The last has two main advantages [301]:

1. Large numbers of pictures may be taken which finally lead to more accurate results.
2. Resolution of pictures taken may be easily controlled leading to clearer results.

The two main software techniques used to analyse images from a PIV experiment are: autocorrelation analysis and cross-correlation analysis. In an autocorrelation technique images from two illumination processes are recorded on the same frame, while in a cross-correlation technique images from one illuminating pulse are recorded on two frames [300]. Using the modern sophisticated digital-cameras, cross-correlation analysis is much better than autocorrelation analysis [304]. The two main disadvantages of using the autocorrelation analysis technique in experiments are [305]:

1- Although the particle displacement is known, the flow direction is uncertain.
2- For very small displacements, the side peak can partially overlap with central peak limiting the measurable velocity range.

Three important terms are associated with the application of the Particle Image Velocimetry technique [301, 302]:

Image density (Ni): The mean number of scatterers in an interrogation cell.

Source density (Ns): The mean number of particles in a resolution volume. It is used to express the number of overlapping images in the image plane.

Interrogation cell: It is a square-shaped figure used to trace the displacement of tracers and therefore determine the flow velocity and direction. A set of interrogation cells present a uniform grid.

Readers who look for more understanding, detailed principles, governing laws and information about the Particle Image Velocimetry technique and its applications may refer to many text books, e.g. [295, 301, 306-312].

In the present experiment, the PIV system consists of a MiniDv Sony camcorder (SONY DCR-HC-19E) as a recording tool. The images were recorded on a 60 minute special tape before being uploaded to a PC for analysis. The camcorder was mounted along a bar, perpendicular to the surface of the flow-table tank. The camera-lens was 1.2 m from the water surface (Fig. 6.8) to allow the camera to picture an area of 0.8 x 0.6 m that represents more than the half of the total length of the wooden constriction. This constriction represents the area at the sill region of the Strait of Messina. The light source was white-light from the neon lighting-system in ceiling of the wet-mechanical laboratory normal to the flow-table tank. Polystyrene mini balls of 2-3 mm diameter were used as tracers. These were manually distributed along the inlet diffuser and start from rest with the same flow direction within the tank. The video records were uploaded to a PC and converted to sequences of *.jpg images [313]. The particles in the converted images were followed in consecutive sequences of frames to establish the flow motion within the tank. Some options of the software [314] were applied to increase the accuracy of the flow calculations.

Figure 6.8: Sony DCR-HC-19E camcorder recording tool in the present physical experiment

6.3 Results of the physical experiment

In all the figures, which represent the outputs of the present physical experiment, there is a red circle that works as a guide to express the flow pattern following the polystyrene tracers in the flow-table. Starting the physical experiment to mimic the tidal flow regime in the Strait of Messina, it was first important to apply a scaled flow velocity within the flow-table tank representative of that in the Strait. Using equation (6.3), the peak velocity at the constriction section needs to be 0.15 m/s. The speed of the motor pump was adjusted to give this velocity within the constricted area of the tank. This was verified by using the surface floating polystyrene mini-balls (Fig. 6.9) flowing freely with the flow between two points of known distance at a certain time. The scaled-speed is also confirmed by using a Vectrino plus velocimeter (model 1.29). The device measures the flow-velocity using the Doppler principle. The motor speed, which produces this flow velocity, is 500 rpm. Having the wooden frame with 3 scaled widths 1: 0.6: 2 and using the 500 rpm motor speed to produce 0.15 m /s flow velocity, the velocity at the inlet opening was found to be 0.12 m/s and at the wider width near the outlet of the tank was 0.048 m/s. This is in a very good agreement with the real flow regime within the Strait of Messina and confirms the effect of the Strait morphometry in enhancing the tidal flow to reach its peak velocity at the sill region.

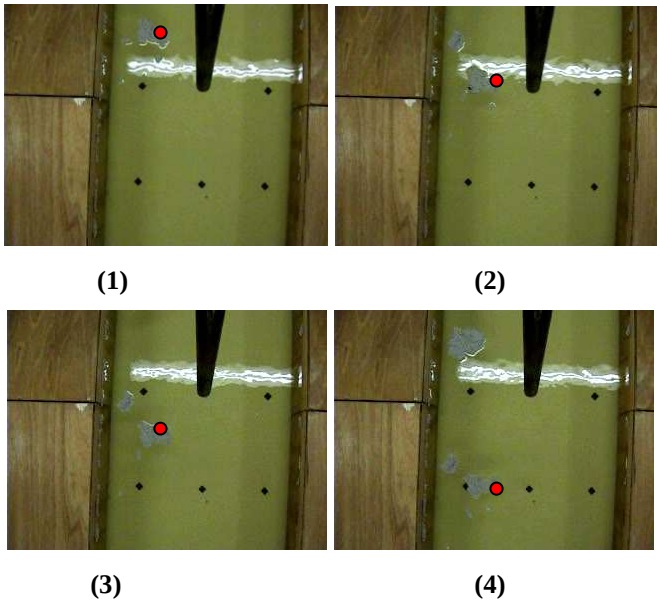

Figure 6.9: Polystyrene mini balls used to measure the surface flow velocity within the flow-table tank

Nine checkpoints, seven of which appear in Figure 6.10, were chosen within the flow-table tank to fix the Vectrino to record an image every 0.005 seconds for 3.3 minutes (i.e. 40000 records per checkpoint). This is in order to check and record the flow velocity within the tank at the three widths representing the real widths of the Strait of Messina. Two checkpoints, at each width, were taken close to the frame and one was taken along the central channel path of the flow. Figures (6.11-6.13) are the graphical presentation of the flow velocity recorded by the Vectrino at the chosen checkpoints. These are arranged from left to right to represent the further width, according to Figure 6.10, then the central and then finally the widest nearest width.

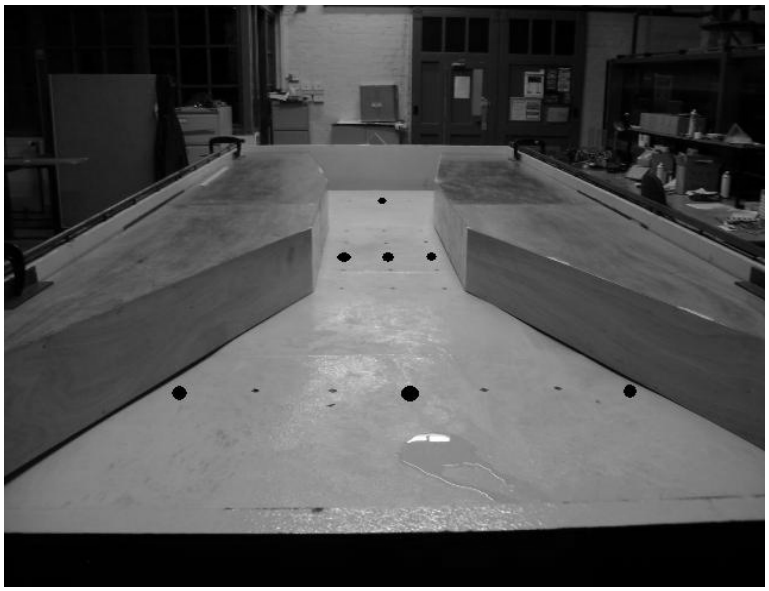

Figure 6.10: Seven of nine checkpoints taken in the flow-table tank to fix the Vectrino

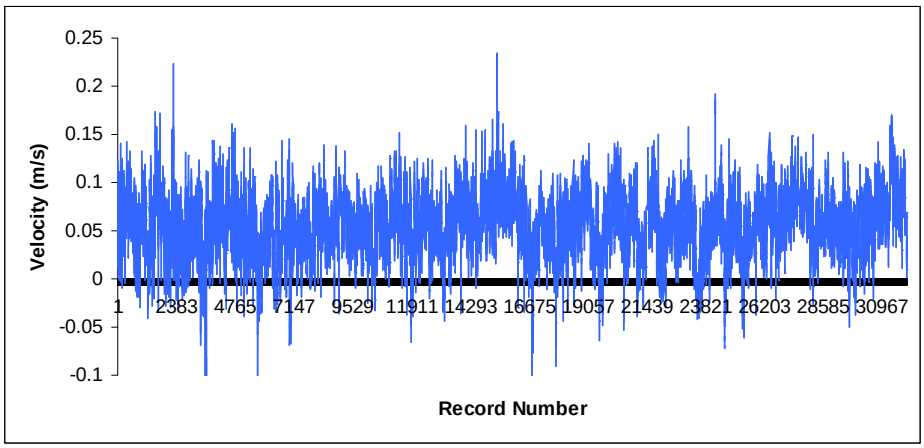

(a)

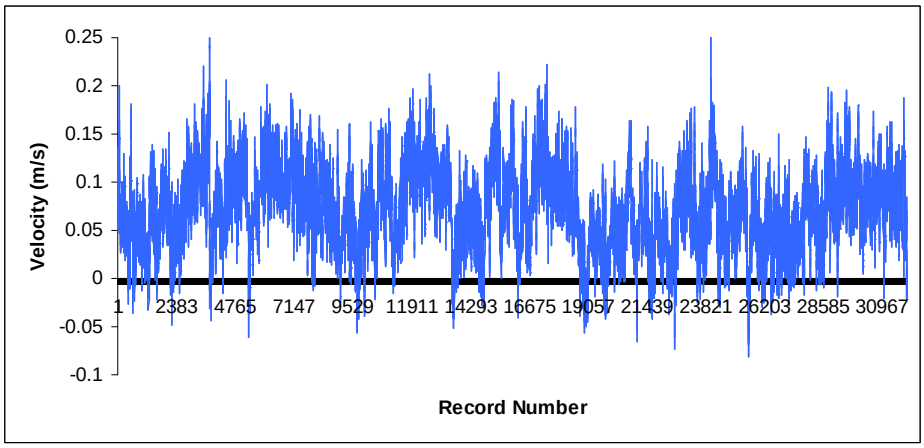

(b)

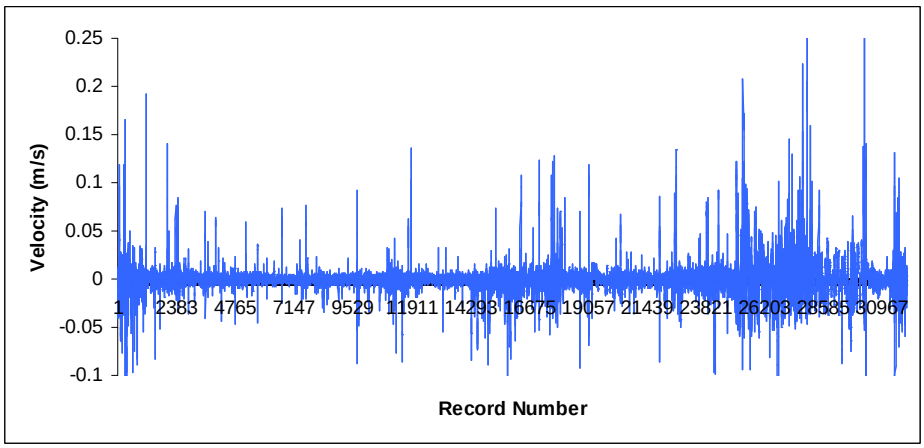

(c)

Figure 6.11: Vectrino records at the further width in the flow-table tank representing the northern boundary of the Strait of Messina (a) left-hand (western) boundary, (b) the central area and (c) the right-hand (eastern) boundary

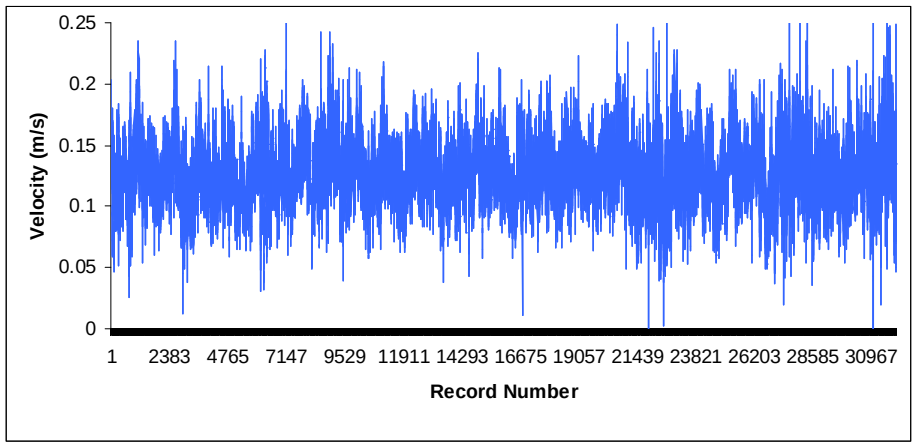

(a)

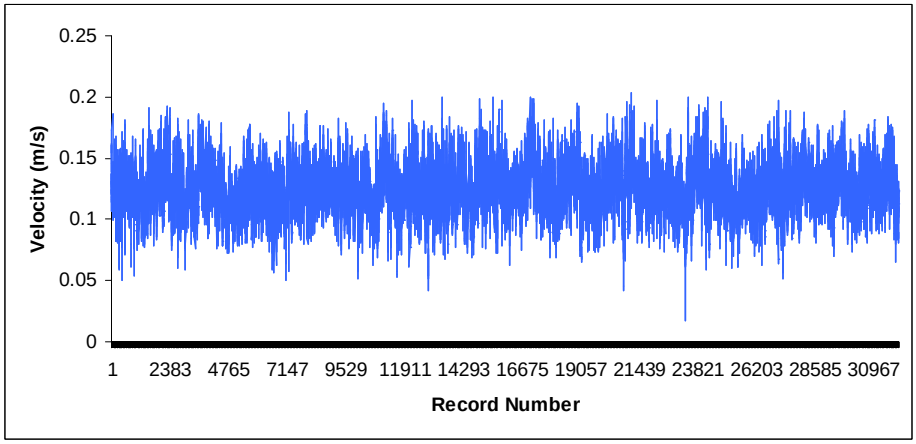

(b)

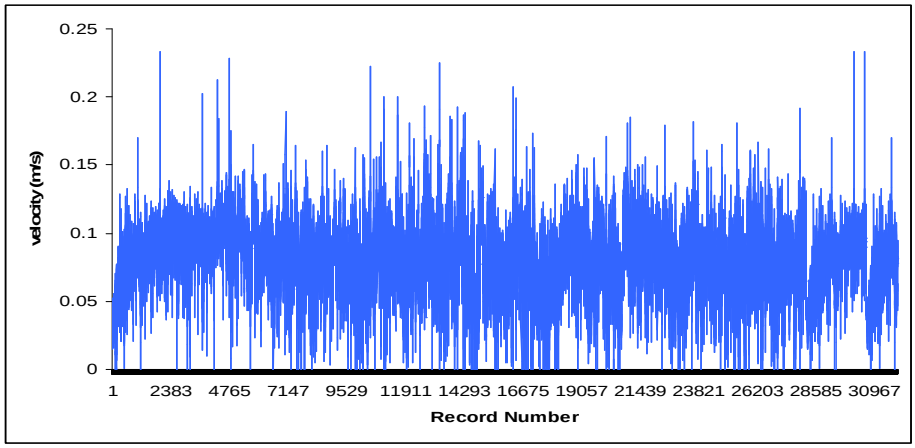

(c)

Figure 6.12: Vectrino records at the central width in the flow-table tank representing the sill region constriction of the Strait of Messina (a) left-hand (western) boundary, (b) the central area and (c) the right-hand (eastern) boundary

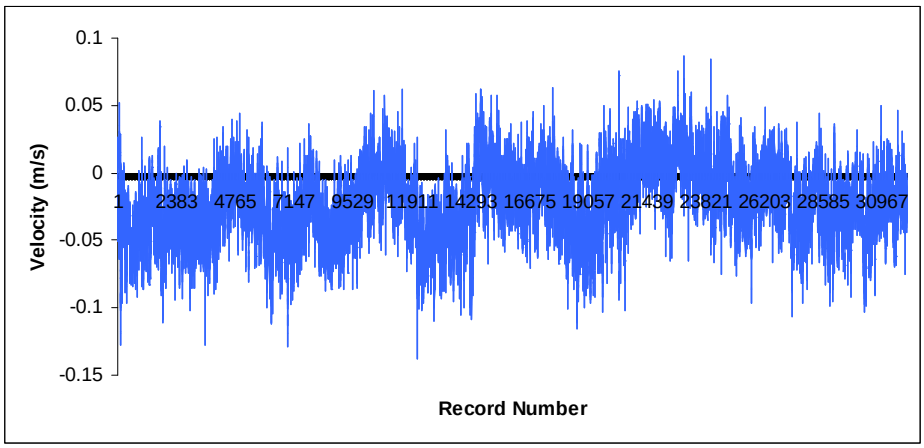

(a)

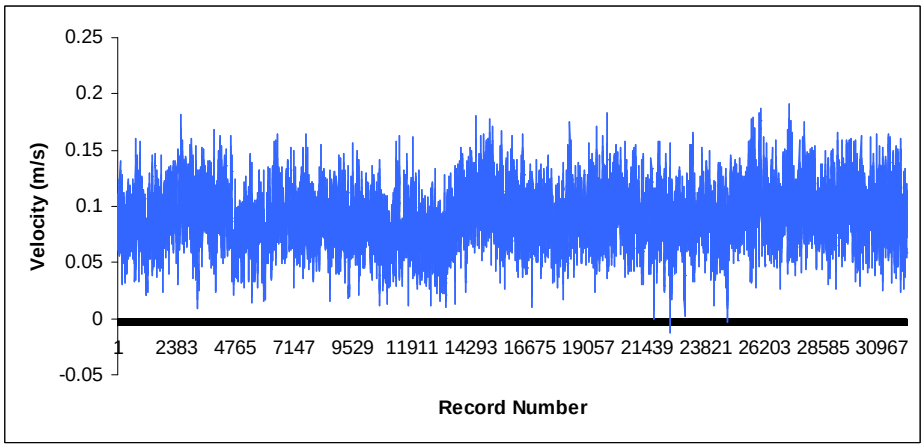

(b)

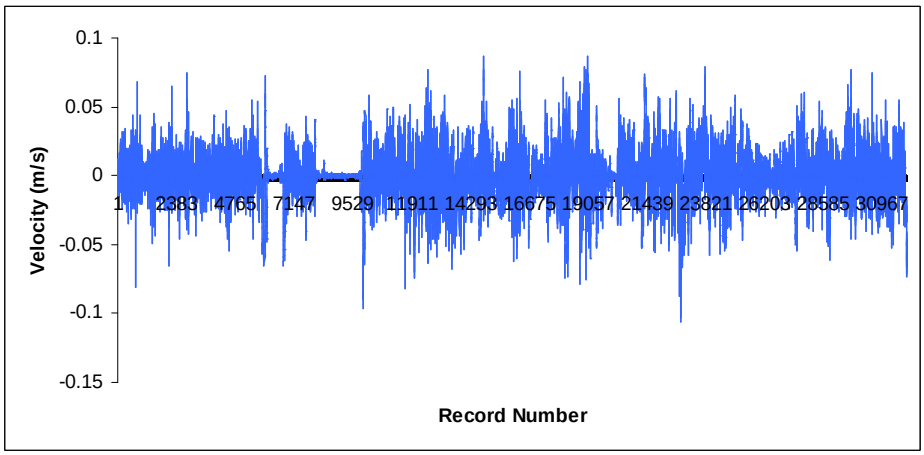

(c)

Figure 6.13: Vectrino records at the nearest widest width in the flow-table tank representing the southern boundary of the Strait of Messina (a) left-hand (western) boundary, (b) the central area and (c) the right-hand (eastern) boundary

From the previous figures it can be deduced that the flow pattern in the flow-table tank closely follows the Tyrrhenian southward flow regime in the real Strait of Messina and is mimicked to a satisfactory degree. At the northern section (Fig. 6.11) the flow velocities are reduced close to the left- and right-hand boundaries with an average velocity of 0.06 m/s and -0.03 m/s, respectively. The flow velocity increases toward the central flow path to reach an average of 0.09 m/s. Negative velocities, indicating turbulent counter flow toward the inlet of the tank, are more intense near the boundary as detected from Figure 6.11. The flow is enhanced due to the effect of the constriction in the frame and velocities are greater in the central width than close to the boundaries. In the channel central zone (Fig. 6.12), the velocities are always of positive values, which mean a uni-directional flow from the inlet of the tank toward its outlet. This is representative of the southward flow in the Strait of Messina. In addition, the recorded velocities at the three checkpoints taken in this central zone of the tank are all close to 0.15 m/s as required by Froude scaling. The average velocities of the flow in the tank are 0.08 m/s and 0.10 m/s. At the widest section which represents the southern border of the Strait of Messina at its opening toward the Ionian Sea the flow velocities drop to their lowest values (Fig. 6.13). The flow velocities at this widest section follow the same pattern of being lowest close to the boundaries, and increasing toward the central path in the flow-table tank. The average velocities are 0.09 m/s and 0.02 m/s at the central flow channel and close to the right-hand boundary, respectively. The average velocity at the left-hand border is negative, -0.02 m/s, which indicates a dominant counter flow at this side. Table (6.1) summarises the minimum, maximum, average and Standard deviation from average measured velocities at the three sections. It can be easily noticed that the central flow velocity (Fig. 6.13 c) is always positive while close to the frame (Fig. 6.13 a and b) the negative values appear to indicate a counter-flow. This is in a good agreement with the observed situation in the Strait of Messina, where eddy motion occurs at its southern borders close to the shores resulting in the well-defined upwelling phenomena in these areas [157, 161, 167, 280]. From Figure 6.13, as well as from the experimental observations, the counter flow velocities are higher on the left-hand side border. This counter flow in the tank, which represents a gyre motion, will be more described by the analysis of the recorded video snaps, as shown hereunder.

		Minimum velocity (m/s)	Maximum velocity (m/s)	Average velocity (m/s)	Standard deviation from average
Northern section in the frame	Left-hand border	-0.001	0.21	0.06	0.03
	Central flow-path	0.0	1.0	0.09	0.07
	Right-hand border	0.009	0.3	-0.03	0.01
Central section in the frame	Left-hand border	0.003	0.23	0.08	0.02
	Central flow-path	0.01	0.18	0.10	0.02
	Right-hand border	0.002	0.25	0.10	0.02
Southern section in the frame	Left-hand border	0.004	-1.1	-0.02	0.02
	Central flow-path	0.007	-1.1	0.09	0.04
	Right-hand border	0.004	-1.1	0.02	0.03

Table 6.1: Summary of velocity records in the present physical experiment

The converted *.jpg snaps of the recorded video are taken for every frame. These frames were recorded at a frequency of 25 frames per second. Figures (6.14-6.16) are 300 consecutive frames representing the northern, the central and the southern boundary widths of the Strait of Messina taken at the scaled widths of the wooden frame in the flow-table tank. The presented snaps are taken on a one second scale time, i.e. 25 frames/photo. From these figures, it can be deduced that the flow pattern in the flow-table tank resembles the southward flow in the real Strait of Messina to a satisfactory degree. The head difference caused by the effect of diffusers in the

stilling rooms at the two ends of the tank enable a steady flow which starts with a relatively moderate velocity (0.12 m/s) and is then enhanced in the constricted section to reach 0.15 m/s. Finally the flow velocity drops to its lowest values (0.04 m/s) at the widest section representing the southern border of the Strait of Messina and splits into two counter-flow circular patterns. The analysis of the snaps taken also reflects the circular motion in the southern section of the Strait of Messina. This consists of two eddies or gyres one of which is anti-cyclonic to the western side of the Strait (Fig. 6.16 a) and the other cyclonic to the eastern side (Fig. 6.16 b). The former occupies about 2/3 of the width while the latter occupies the remaining third of the southern width. In addition, the anti-cyclonic eddy is larger and faster than the cyclonic one. These results are in a good agreement with the observations and numerically simulated investigations of the Strait of Messina, including the case of the 80 m flat depth in the previous chapter of the present study.

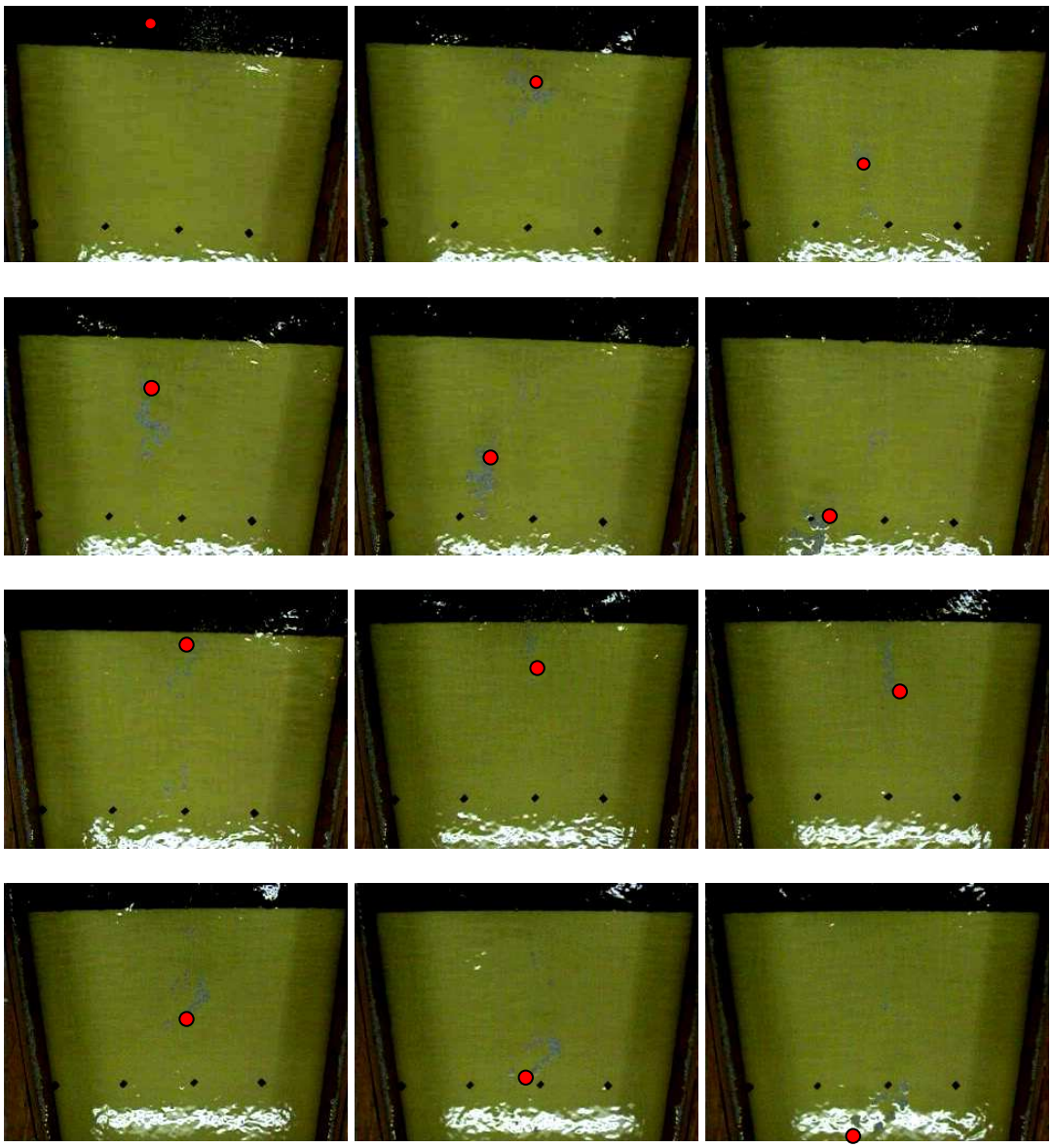

Figure 6.14: 12 consecutive seconds (300 frames) for tracers placed at the simulated northern width to start motion with the flow direction

Figure 6.15: 12 consecutive seconds (300 frames) for tracers placed at the simulated central width

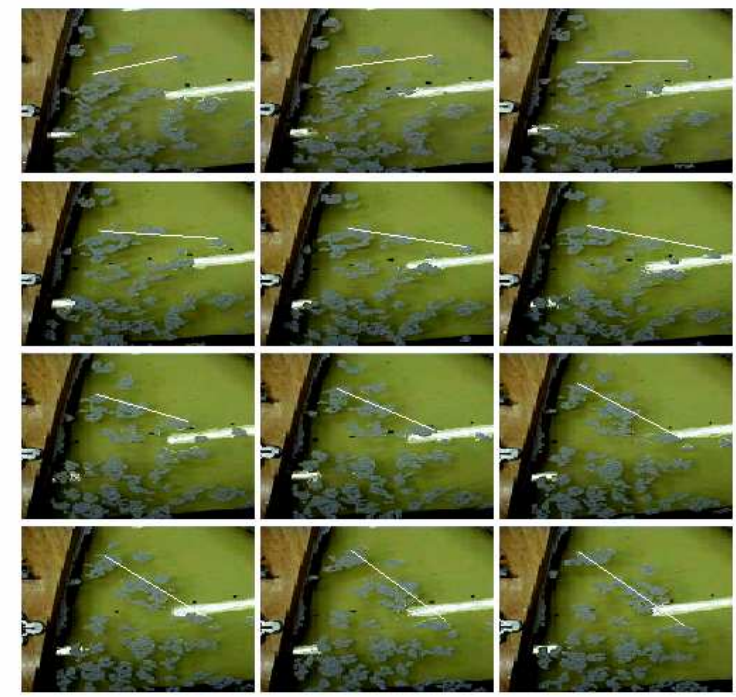

(a)

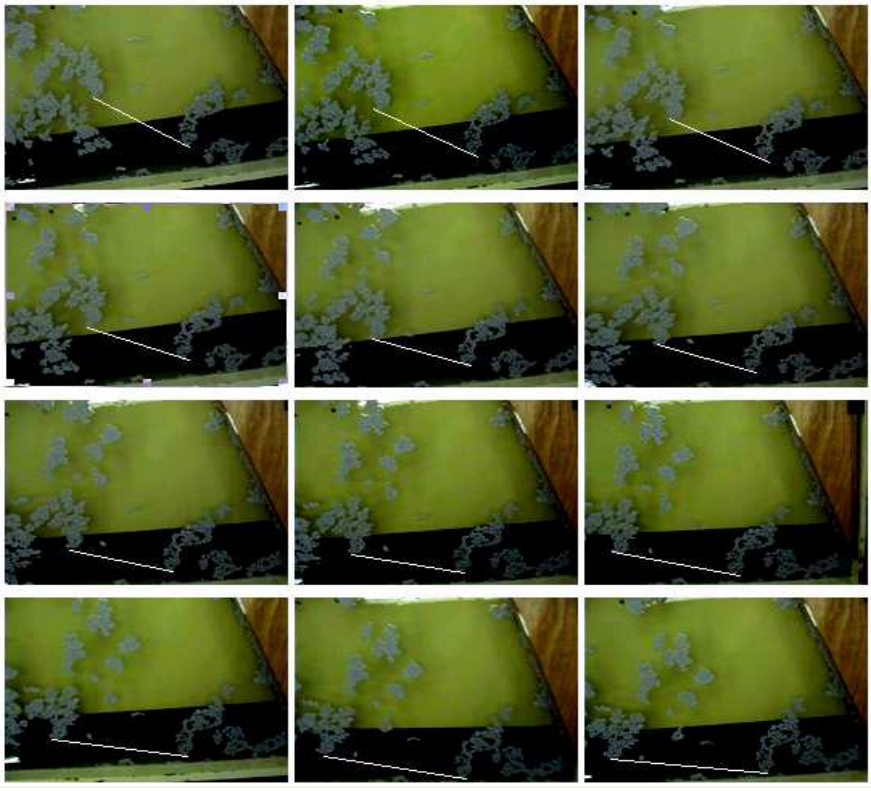

(b)

Figure 6.16: 12 consecutive seconds (300 frames) for tracers placed at the simulated southern width: (a) Anti-cyclonic gyre at the left-hand side border and (b) Cyclonic gyre at the right-hand side border

6.4 Chapter Conclusion

A physical simulation process appears to be a useful tool in order to examine and investigate the tidal-flow environment. The tidal-flow table tank, of horizontal dimension 5 m x 2 m, in the University of Edinburgh is the main tool of physical simulation in the present study. Using a water-proofed marine-plywood frame, the tidal flow regime within the Strait of Messina is physically simulated. A Particle Image Velocimetry (PIV) technique and a Vectrino instrument are used to analyse the simulated flow pattern in the tank. Results from the physical model in the present study confirm the effect of coastline configuration in enhancing tidal current velocity in the Strait of Messina. In addition the model successfully simulates the gyre pattern found in the southern extremity of the Strait of Messina where the well-known upwelling phenomena take place. The latter is caused in the Strait of Messina by the combined effects of tidal displacement and topography [161]. The present physical simulation agrees with the conclusion of Azzaro *et al*. [161] about the existence of a cyclonic motion in the southern area of the Strait of Messina results in enhancing the upwelling at this region.

CHAPTER 7

Discussion and Conclusions

In the course of this thesis I have tried to link my background knowledge and previous studies (B.Sc. and M.Sc. Degrees) in physical oceanography to a mechanical engineering aspect through one common, important topic, which is extracting energy from a marine renewable-resource, namely, tidal currents.

Tides are natural phenomena, which affect many maritime activities and have a special importance for mariners and oceanographers. Tidal currents which are associated with tides greatly contribute to, and affect, the global oceanic current system in a manner that attracts the attention of research oceanographers and investigators. Meanwhile, the kinetic energy in tidal currents, although being conditionally restricted only to a few places around the world, represents a vital renewable energy resource which can be mechanically harnessed to satisfy the current global energy demands in an environmentally-friendly manner. This both attracts and challenges engineers to develop different types of tidal turbines that can be deployed in the marine ecosystem to harness energy from this renewable resource.

Harnessing energy from a tidal current resource, indeed, poses major challenges to both environmentalists and engineers. On one hand, environmentalists care about the marine environment and the global climate. They announce restrictions and mitigations in order to raise environmental awareness; looking for a better global environmental status. It is the environmentalists' responsibility therefore to highlight mitigations, to watch and to follow up projects related to the maritime ecosystems in an applicable way. The challenge is to realise the need and accept the idea that developed environment-friendly tools may safely join the marine ecosystems. On the other hand, engineers are keen to respond to the worldwide energy demands and to provide well-developed technologies to satisfy this requirement. The challenge, however, is to explore possible renewable resources and to develop technologies that are environmentally-friendly to the best possible degree. The important question then is how to benefit from a marine renewable energy resource with the least possible effect on the surrounding environment. Through this PhD research I aimed to find an answer to this question taking tidal currents as the examined marine renewable

resource. This is carried out by, firstly, justifying the choice of the Strait of Messina as the area of investigation and secondly, by drawing attention to the anticipated impacts on the marine environment attributable to harnessing of energy from tidal currents. This is done in order to examine the extent to which the marine ecosystem may be affected by such a process and to suggest how these effects can be minimised and controlled. Finally, I examined both a numerical and a physical model to simulate the tidal-flow regime in the Strait in order to give a clearer picture about the most effective place where excess energy exists, and where tidal turbines may be deployed in a secure manner.

Any applied project must consider the conclusions reached in the present environmental assessment study. In addition, understanding the nature of the tidal-flow pattern may be considered to have a great impact on the choice of a suitable site to deploy tidal turbines as well as on the choice of the applied technology itself, according to the nature of the resource itself.

It is always important to remember the three basic criteria [33] and to ensure that these are fulfilled at any site chosen for a tidal turbine deployment:

1. The local water depth: this should range between 25 and 45 m to suit the installation of the existing device technologies. This depth range requirement may be modified for the new generations of tidal current energy converters and technologies. It is important to bear in mind that the depth will also affect the choice of the rotor-diameter of the tidal turbine.

2. The location of the nearest grid connection: this connection must be easily reached to be economically feasible in order to minimise the capital cost of power generation and, accordingly, to minimise the final kW hour cost to consumers.

3. An energetic and persistent resource: this criterion is the basis of choice as the mean spring and neap tide velocities at the chosen locality must be as high as possible. This velocity should preferably not drop below 3 m/s [23, 33]. Other authors lower this limit to 1 m/s [17] or 2 m/s [6, 15].

The Mediterranean Sea is taken as a vast area of investigation in the present research. Hereunder the results of the present research are discussed. Conclusions and recommended further work are given.

7.1 The environment of the Mediterranean Sea

The Mediterranean Sea extends between latitudes 30º 00.00' and 45˚ 00.00' N, and longitudes 06˚ 00.00' W and 35˚ 00.00' E. The Mediterranean basin is a large semi-closed basin, connected to the Atlantic Ocean through the Strait of Gibraltar in its western extremity. The basin is internally connected to the Black Sea by the Dardanelles/Marmara Sea/Bosphorus system. The Mediterranean Sea covers an approximate surface area of 2.5 x 10^6 km^2 [46]. The greatest measured depth in the Mediterranean Sea is 5.1 km in the Ionian Sea [48]. The Sicilian-Tunisian sill at 400 m depth, divides the Mediterranean basin into the western and the eastern basins. Three main water masses are distinguished within the whole Mediterranean basin:

1. Surface water, originating in the Atlantic inflow through the Strait of Gibraltar and extending from the surface to about 150 m depth.
2. Intermediate water, formed by cooling and evaporation in winter south of Turkey. This layer extends from 150 to 600 m depth, and flows out through the Gibraltar to the Atlantic at this depth.
3. Deep water, found below 600 m depth and formed by strong winter cooling and wind mixing processes south of France and in the Adriatic.

The three water masses are closely related and affect each other's circulation pattern; together they form the general circulation pattern of the Mediterranean Sea.

From a tidal point of view, the Mediterranean tides, mainly of the semidiurnal type, have not been as intensively studied as in other oceans and seas. This is due to the very low tidal amplitudes, which are of the order of a few centimetres except in some places, such as the Adriatic Sea, the Aegean Sea and the Gulf of Gabes off the Tunisian coasts where resonance phenomena act to amplify the tidal amplitude [14, 125]. During this work, the tidal characteristics of five major straits distributed within the Mediterranean basin have been investigated. These include: the Bosphorus, Dardanelles, Messina, Sicily and The Strait of Gibraltar s. The investigations reveal that both tidal-ranges and tidal-currents all over the Sea basin and its straits are weak enough to be excluded from any considered plan to use the tidal phenomenon as a renewable resource to extract energy. There is only one exception, the Strait of Messina, where currents reach reasonably high velocities. This investigation, consequently, justifies the choice of the Strait of Messina as a

potentially a massive tidal current resource that can be exploited to generate electricity.

7.2 The environment of the Strait of Messina

The Strait of Messina extends between latitudes 37˚ 35.00’ and 38˚ 18.00’ N and longitudes 15˚ 06.00’ and 15˚ 42.00’ E. The main axis of the Strait is oriented NE - SW in its northern part and N - S in its southern part. The Tyrrhenian Sea represents the northern boundary of the Strait of Messina, while the Ionian Sea represents its southern extremity. The main width of the Strait generally ranges between 3 km in its narrowest section (Punta Pezzo - Ganzirri) and 4.2 km. The smallest cross-sectional area in the Strait of Messina is of 0.3 km^2 in the sill region where the mean water depth is 80 m [158]. The bathymetry of the main body of the Strait of Messina in the present work is constructed from data extracted from Admiralty Chart [165]. The water circulation system in the Strait of Messina is the result of two dynamical effects that take place in the Strait: hydrological and tidal effects. The former is considered as the usual classical effect observed in any strait due to the vertical haline and density differences between water layers. This results in a two-layer flow regime, where the lighter Tyrrhenian waters occupy the superficial layer flowing from north to south and the denser Ionian waters occupy the lower layer flowing from south to north. The tidal effect, on the other hand, is of special importance in the case of the Strait of Messina. The dominant tidal currents along the Strait are massive and may reach 3 m/s or more at their peak. These massive currents are mainly due to tides in the Tyrrhenian and Ionian Seas whose tidal-phase is almost opposite, approximately 180°, associated with a maximum amplitude range of 0.27 m between the two extremities of the Strait. In general, the flood stream occurs when the current is directed toward the Tyrrhenian Sea, and the ebb stream occurs when the flow is towards the Ionian Sea [167, 188]. Actually, the importance of tides in the Strait of Messina stems not only from being a main driving force for the current there but also from the fact that Messina is an amphidromic point [191, 192] for the tides of the two main basins of the Mediterranean Sea. Because the tidal currents in the Strait of Messina have been shown to be strong enough to be considered for the energy extraction process, the Strait of Messina is selected as an area of investigation

in the present study. It was important to assess this resource environmentally in order to highlight its environmental characteristics and to ensure that the energy extraction process would not have a harmful effect on the marine environment. A desk-based Environmental Impact Assessment (EIA) study is made, in which the EU legislation, the factors affecting the choice of deployment site and the anticipated impacts in every phase of work: installation, maintenance and operation and decommissioning are described. The interactive matrix method is applied in which every environmental parameter of concern (biotic and abiotic) is listed and the degree of anticipated impact is evaluated. The resultant matrix helps in making the right decision and in judging the impact of the project on the marine environment. The expected major impacts in the case of harnessing energy from tidal currents in the Strait of Messina, according to the author's point of view in the present EIA study, does not exceed 10% of the total expected impacts. This may be taken as an encouraging sign to proceed for energy extraction projects using tidal currents within the Strait of Messina. A monitoring programme is proposed at the end of the present EIA study. This programme highlights the main points to be considered during each phase of the energy extraction process from a tidal current resource. It is concluded that the final intention of deploying and operating a clean sustainable renewable energy technology making a sustainable contribution to the future energy mix is significant enough to merit such an intensive monitoring programme.

7.3 Numerical simulation of the tidal current resource in the Strait of Messina

The numerical simulation in the present study is performed using the developed [237] Tidal Flow Development (TFD) numerical model. The TFD is a two-dimensional model based on the main Shallow Water Equations (SWE).

In the present study using the TFD model was an advantage due to the following points:

1. The model has been previously applied to different tidal case studies, e.g. [33, 225, 287, 287, 315].
2. The code is written in a familiar package (FORTRAN77) which enables any required modifications to be easily performed.

3. WOLF, the model interface to show outputs, is easy to apply and express the outputs graphically in a reasonable manner.
4. The model allows the determination of the values of velocities and amplitudes in the domain of simulation in numerical values that can be easily graphically schemed.
5. The calculations of the energy extraction process from the investigated tidal environment are set as subroutines in the main code of TFD.
6. A SWE model was previously applied to the same area [280], the only difference being the coordinate system. In the present study a linear (square grid) system is used while a curvilinear coordinates system and grid are applied [280].
7. The outputs of the model highlight, to a close degree to reality, the interesting and effective zones along the domain, as well as natural phenomenon, to be considered for the energy extraction process.

However, applying the TFD model in the case of the Strait of Messina, in particular, highlights some shortfalls in both the TFD model and the obtained results:

1- The complex bathymetry of the real Strait of Messina, with depths exceeding 700 m, and its complicated morphometry affect the outputs obtained from a SWE model.
2- The effect of the Coriolis force is ignored in the present case studies. This refers to the fact that the effect of the Coriolis force in the TFD is verified for steady cases [237]. In addition, all previous case studies in which the TFD model was applied were made under steady state conditions, while the present case uses dynamic conditions.
3- With the large bathymetry and morphometry variations in the Strait of Messina, the Manning and eddy viscosity coefficients have to be increased to a degree that does not reflect the real world and which, in consequence, affect the final simulation outputs.
4- In the present case of simulation, a critical factor which affected the resultant outputs, and which may be considered as the weak point in the present simulation, is the lack of real field data which can be used as boundary files when applying the TFD model. The applied driving/radiating M_2-tidal waves

are personally driven using both: Admiralty Tide Tables [289] and a comprehensive literature review. In addition, the M_2-spring and neap tidal waves are simulated using data from the Admiralty Tide Tables [289].

The simple channel simulation succeeded in confirming the main tidal features within of the Strait of Messina:

a. The maximum simulated tidal amplitude was 0.11 m. This gives a tidal range of 0.22 m, which is in a good agreement with the real field records (0.27 m).
b. The out-of-phase tidal characteristic between the western and the eastern extremities of the domain of simulation, which represents the northern and southern extremities of the real field of the Strait of Messina, may be detected comparing the elevation graphical presentation in Figures 5.10 and 5.12. This mimics the Strait of Messina and is in good agreement with [140, 160, 188, 280].
c. Using the M_2-tidal wave (a = 0.135 m, T = 44640 s) as input and radiating boundaries results in a dominant maximum simulated tidal velocity along the simple tidal channel case of 2 m/s. This may be considered as a reasonable tidal velocity for the energy extraction process.
d. The transverse velocity component is always too small to detect graphically. This is in a good agreement with the real Strait of Messina, as previously mentioned [187].
e. The simulated flood and ebb directions are in agreement with the real field observations [161, 167, 188].

However, the maximum simulated tidal velocities did not exceed 1.0 m/s during the spring tides nor 0.53 m/s during the neap tides. For these very low velocities, the energy extraction process may appear economically infeasible. This primarily refers to the very simple configuration of the surrounding coastline of the domain of simulation. The simplicity of the domain, which does not reflect any morphometric variations in the case of the Strait of Messina, has its effects on the simulated spring and neap tidal behaviour and the model, in this case, fails to express any significant variations in the hydrodynamical environment.

Generally speaking, the results of this simple tidal-channel case study indicate that such a simple domain may be applied just as an indicator for how a hydrodynamical

environment (flow regime velocity and amplitude) dominate the area of investigation. This was also discussed and concluded [315].

In applying the TFD numerical model to simulate the real Strait of Messina, the domain had to be extended with a straight coastline for 750 m northward in order to adjust the input boundary file. The open boundary with the Tyrrhenian Sea is a complex boundary that challenges modellers when developing a numerical model to mimic the real field. The following points may be deduced:

Advantages of using the TFD numerical model in the real domain of simulation:

1. The transverse velocity component along the domain is simulated as observed in the real field: weak and of minor importance.

2. Tidal currents are enhanced in the sill region in the Ganzirri – Punta Pezzo cross section. This is confirmed in the three different cases of simulation: real, LNM and flat domain. This reflects the real situation in the Strait.

3. Intensive currents are predicted close to the eastern coasts of the Strait of Messina near to Punta Pezzo in the three cases of simulation, and also during the spring and neap phases. This is in good agreement with previous simulation studies. These results support the comments [315, 317] that the location of the Kobold turbine (ENERMAR project) deployed near Ganzirri is not the most intensive tidal current path within the Strait of Messina.

4. Eddies to the north of and near to Punta Pezzo are predicted at their locations within the northward tidal flow. This is in good agreement with real field [141] and simulation results [280].

5. The TFD model confirms the combined effect of bathymetry and morphometry in enhancing tidal current velocities and in simulating featured eddies within the Strait in the three simulation cases.

Disadvantages of using TFD numerical model in the real domain of simulation:

1. The wrong effect of Coriolis force in the main code, which does not reflect the real Coriolis Effect. This is a point of concern for the TFD model as the Coriolis Effect was successfully applied in another SWE model [280]. For the TFD model this might be a direct result of the unsteady-state case in the present study.

2. The model failed to mimic the real Strait of Messina and the 80 m LNM domain with normal Manning coefficient and normal eddy viscosity effects. These

had to be increased by a factor of four and ten, respectively. However, a Manning coefficient of 0.026 and normal eddy viscosity effect have been applied [280]. This again imposes the question about the suitability of applying the TFD model to areas with complex configuration in both bathymetry and morphometry such as the Strait of Messina.

2. From the simulation outputs in the three cases (real, LNM and flat domains) it appears that the TFD model does not suit a wide domain with widely varying depths. Morphometry and bathymetry affect the results of the model to a very noticeable extent. The application of the model in previous case studies is limited to more regular-shaped shallow areas, e.g. [11, 33, 225, 288, 315].

3. The TFD model does not respond properly to the constructed boundary files made using Admiralty Tide Tables [289] for spring and neap tides. The model reflects neither the out-of-phase behaviour of the Strait nor the opposite flow pattern during these phases.

4. Applying the 80 m LNM domain smoothes the simulation results but, at the same time, reduces the predicted velocity to less than 1 m/s which does not reflect any reality. This would also suggest that the site is unsuitable as a tidal current resource.

5. Using the 80 m LNM and the 80 m flat depth domains results in the disappearance of one important feature from the simulated domain: gyres north to Punta Pezzo with the northward tidal flow, except for spring tides. This might refer to the flatness of the domain in these two cases and, meanwhile, confirms the effect of bathymetry on the flow motion.

6. The normal periodicity of the semidiurnal tide which dominates the Strait of Messina is fulfilled only when applying high Manning coefficient and high eddy viscosity effect.

7. The TFD model failed to simulate the tidal flow regime in the real Strait of Messina during spring and neap tidal phases (identical outputs), even when using an exceptionally high Manning coefficient and eddy viscosity effect. This is not useful in examining these important phases to the degree that helps to make a decision about tidal turbine deployment.

8. The TFD model in the present study failed to simulate any of the higher lunar tidal harmonics (M_4, M_6 and M_8) other than the applied lunar M_2-tidal component. The latter itself is not simulated as found in the real field due to the exceptional frictional coefficients which had to be applied in order to obtain stable outputs from the model. However, these higher harmonics in addition to the main Solar and Luni-solar tidal components (S_2, K_1 and O_1) have been successfully simulated [280] and the effect of the bathymetry of the Strait on the simulation procedure, especially at the sill region between Ganzirri and Punta Pezzo, has been explained. This again questions the suitability of applying the TFD model for a complex domain like the Strait of Messina.

9. The results of the numerical simulation process in the present work are not suitable for any further hydrodynamical investigation. The model cannot be applied to investigate changes in the hydrodynamical environment prior and after any energy extraction process. This is mainly due to the use of unrealistic conditions: a high Manning coefficient and a high eddy viscosity effect.

7.4 Physical simulation of the Strait of Messina

The physical simulation process in the present study is performed using the flow-table tank located in the wet-mechanical laboratory at the University of Edinburgh. The tank has horizontal dimension of 5 m x 2 m. A water-proofed marine-plywood frame representing the northern, central and southern widths of the real Strait of Messina is placed in the tank scaled to 1: 0.6: 2, according to the full-scaled ratios. A 500 rpm water pump is used to drive a steady flow with a maximum velocity of 0.15 m/s in the tank in a closed system. A Particle Image Velocimetry (PIV) technique is used for image analysis. In addition, a Vectrino plus velocimeter is used to measure three sectional flow velocities in the tank.

The results of the physical model in the present study reflect the real tidal flow regime in the Strait of Messina in a satisfactory fashion:

a. The applied velocity has been scaled using the dimensionless Froude number and is representative of the velocity in the Strait.
b. The effect of the constriction at the sill region in enhancing the currents is confirmed.

c. The model reflects the observed southern circular motion in the Strait of Messina, which agrees with the conclusion of Azzaro *et al*. [161].
d. The cross-sectional flow velocities measured by the Vectrino are in acceptable agreement with the published field observations and measurements.

7.5 Conclusions and Recommendations

1. Tidal currents and ranges in the Mediterranean Sea basin, from a tidal energy perspective, are generally low.
2. The narrows through the Strait of Messina are an exception, exhibiting reasonably intensive tidal currents that have the potential for economic exploitation.
3. Maximum current velocities at spring peak tides through the Strait of Messina vary between 1.8 m/s to more than 3 m/s. This is due to the effect of morphometry, topography and the out-of-phase characteristic between the Northern and Southern extremities of the Strait.
4. The performed EIA study highlights the effect of waves, either surface or internal, on the tidal current resource. This point has to be taken in consideration as a further research point in order to get a clearer picture of these effects.
5. A monitoring programme is a must for any energy extraction project from a tidal environment. This is necessary in order to maintain the safety of the surrounding ecosystem.
6. We should not let our care and environmental concern hold back promising technologies and the possibility of obtaining sustainable and clean energy.
7. Numerical simulation processes using numerical models may be applied to simulate the tidal energy resource in the Strait of Messina.
8. The Tidal Flow Development (TFD) numerical model is most convenient for simulating steady-state hydrodynamical cases, and is more successful for areas with regular domains.
9. In the present study, the TFD model has always required exaggerated frictional effects: a high Manning coefficient (0.1 s/m^3) and a high eddy

viscosity effect (edvisc. x 10) to be applied in order to give stable results. This may be due to the complexity of the domain (morphometry and topography) with the misuse of Coriolis Effect in the main code.

10. Unfortunately, the final simulated output using the TFD numerical model to mimic the tidal current energy resource in the Strait of Messina does not reflect the real field to the anticipated/required degree.
11. The Tidal Flow Development model cannot be used for further simulation processes for the Strait of Messina.
12. The results obtained from the present study may be regarded as primary guide results for further, more accurate numerical simulation studies.
13. The main conclusion suggested by the simulation process of the real Strait of Messina is that the excess energy location within the tidal flow is found close to the eastern coasts of the Strait near the City of Punta Pezzo. This is confirmed in the three distinctive cases-studies made using the real morphometry and bathymetry of the Strait.
14. A physical simulation process for a tidal energy resource is a good means of examining and investigating the tidal environment.
15. The present physical model confirms the effect of morphometry in enhancing tidal currents within the Strait of Messina.
16. In addition, the physical model in the present study predicts the circular motion of the surface water in the southern area of the Strait to a very reasonable degree.
17. It is recommended that the effect of the Coriolis force in the main code of the TFD model should be re-examined and adjusted. This may allow the model to be applied in both steady-state and dynamic-state cases.
18. According to the real case of simulation results it is recommended that tidal turbines be placed close to the eastern coats of the Strait of Messina near to Punta Pezzo. This area has excess tidal current energy and, additionally, is clear of any navigational/maritime route within the Strait of Messina.
19. It is recommended to deploy vertical tidal turbines in order to explore tidal currents in this area of excess energy. This is mainly due to the advantageous free-moving criterion of these turbines; regardless the flow direction.

20. It is highly recommended to apply an adaptive monitoring programme for tidal-current energy projects in order to conserve and assure the safety of the marine ecosystem to a high standard precaution level.
21. It is recommended to apply advanced 3D numerical models, whenever possible, in order to get a more accurate idea about the tidal energy environment.
22. The present study did not investigate the changes, due to the energy extraction process, in the hydrodynamical environment. This is mainly due to the exceptional conditions applied in the numerical model. However, the study strongly recommends applying more convenient models to predict these changes in order to be minimised to the minimal limits.
23. The recommended 10% limit of energy extraction recommended in previous researches should be appreciated to secure the marine ecosystem both environmentally and hydrodynamically.
24. The present study confirms that the issue of choosing a location for tidal turbine deployment still presents great challenges for tidal turbine designers.

7.6 Further work

The present study can be considered as a base for any further research on the tidal current energy resource in the Strait of Messina. The further recommended work includes:

1. A more accurate simulation of the flow regime that depends on real field data and accurate frictional coefficients, using more appropriate numerical model.
2. Investigation of hydrodynamic changes in the resource due to the energy extraction process is the most urgent research requirement, if we are to keep the hydrodynamic environment safe, so that the extraction process as well as the marine ecosystem can both be positively controlled.
3. This also includes real field measurements of the physical parameters in the Strait in order to give a more accurate picture on the hydrography of the Strait.

4. Moreover, research on the effect of surface and internal waves, highlighted in the present EIA study, on the energy extraction process from a tidal current resource needs to be more investigated and adequately carried out.
5. Although simulating tidal channels on a laboratory scale is still hard to some extent, further physical experiment research is required to examine and assess the exploration of a tidal current energy resource. This will help to make a right decision for any proposed project and to choose the best place and structure to deploy tidal turbines. The present study may serve as a base for further work in this domain.

References

[1] Creswell, L., R.T., Wigg and J. Buchdahl, 2002. Energy: Fact Sheet Series for Key Stage 4 and A-level. Atmosphere, Climate and Environment (ACE), Information Program, Manchester Metropolitan University, 30p. http://www.ace.mmu.ac.uk/Resources/Fact_Sheets/Key_Stage_4/Energy/pdf/Energy.pdf

[2] REN21, 2008. Renewables 2007: Global Status Report. Paris: REN21 Secretariat and Washington DC: Worldwatch Institute, 51p.

[3] Pelc, R. and R.M. Fujita, 2002. Renewable energy from the ocean. *Marine Policy*, Vol. 26(6): 471-479.

[4] Hodge, N., 2007. Enough electricity for five times World demand. Energy and Capital. http://www.energyandcapital.com/articles/tidal-marine-energy/416.

[5] Hicks, S.D., R.L. Sillcox, C.R. Nichols, B. Via and E.C. McCray, 2000. *Tide and Current Glossary*. National Ocean service, US Department of Commerce, 29p.

[6] Anonymous. 1997. Waves, tides and shallow water processes. Butterworth-Heinemann in association with the Open University, 187p.

[7] Pugh, D.T., 1987. Tides, surges and mean sea level. John Wiley and Sons Ltd., 472p.

[8] Pugh, D.T., 2004. Changing sea levels: Effects of tides, weather and climate. Cambridge University Press, 280p.

[9] Militello, A. and A.K. Zundel, 1999. Surface water modelling system - Tidal constituents toolbox for ADCIRC. *Coastal Engineering Technical Notes*, Vol. 4(21): 1-8.

[10] Doodson, A.T., 1922. The harmonic development of the tide generation potential. *Proceedings of the Royal Society A*, Vol. 100: 305-329.

[11] Bryden, I.G., S.J. Couch and G.T. Melville, 2007. Tidal current resource assessment. *Proceedings of the Institution of Mechanical Engineers, Part A: Journal of Power and Energy*, Vol. 221: 125-135.

[12] Shum, C.K., P.L. Woodworth, O.B. Andersen, G.D. Egbert, O. Francis, C. King, S.M. Klosko, C. Le Provost, X. Li, J-M. Molines, R.D. Ray, M.G. Schlax, D. Stammer, C.C. Tierney, P. Vincent and C.I. Wunsch, 1997. Accuracy assessment of recent ocean tide models. *Journal of Geophysical Research*, Vol. 102(C11): 25173-25194.

[13] Kowalik, Z., 2004. Tide distribution and tapping into tidal energy. *Oceanologia*, Vol. 46(3): 291-331.

[14] Defant, A., 1961a. *Physical Oceanography*. Pergamon Press, Vol. I: 729p.

[15] Fraenkel, P.L., 2002. Power from marine currents. *Proceedings of the Institution of Mechanical Engineers, Part A: Journal of Power and Energy,* Vol. 216(1): 1-14.

[16] World energy Council (WEC), 1993. Renewable energy resources: opportunities and constraints 1990-2020. London, UK: WEC.

[17] Buigues, G., I. Zamora, A.J. Mazon, V. Valverde and F.J. Perez, 2006. Sea energy conversion: Problems and Possibilities. International Conference on Renewable Energies and Power Quality (ICREPQ'06), 8p.

[18] Anonymous. 2001. Electricity from waves: The revival of wave power. The Economist:
http://www.economist.com/science/displaystory.cfm?story_id=E1_GNPRRP

[19] Thorpe, B.C., M.K. Mary O'Malley and D. Herbert, 2006. Can we shift from the petroleum economy to the bio-based and solar future? Talk given to Conamara Island Sea Week Conference, October 28, 2006, 13p.

[20] Holmes, R. and S. Edwards, 2003. Primer on the technologies of renewable energy. In: Pollution Probe (Ed.), ISNB-0919764-52-5: 81p.

[21] Thorpe, T.W., 2001. The UK market for marine renewables. All Energy Future Conference, Aberdeen, UK, February 2001: 1-10.

[22] Pontes, M.T. and A. Falcao, 2001. Ocean energies: Resources and Utilisation. World Energy Council, 18th Congress, Buenos Aires, October 2001, 16p.

[23] Bryden, I.G., 2006. The marine energy resource, constraints and opportunities. *Maritime Engineering,* Vol. 159(MA2): 55-65.

[24] Centre of Renewable Energy Sources (CRES), 2002. Wave energy utilization in Europe: current status and perspectives, 28p.

[25] Ocean Energy report, 2003. Rep. No. 1. ABS Energy Research.

[26] Takahashi, P. and A. Trenka, 1996. Ocean Thermal Energy Conversion. 1st ed. John Wiley & Sons Ltd., 96p.

[27] Crews, R., 1997. Ocean sites.
http://library.greenocean.org/oteclibrary/otecpapers/otec_sites.pdf/view?searchterm=crews

[28] Takahashi, P., 2003. Energy from the sea: the Potential and Realities of Ocean Thermal Energy Conversion (OTEC). IOC Technical Series, Rep. No. 66, UNESCO, 42p.

[29] Bryden, I.G., 2004. Tidal energy. *Encyclopedia Energy,* Vol. 6: 139-150.

[30] Hammons, T.J., 1993. Tidal Power. *Proceedings of the IEEE,* Vol. 8(3): 419-433.

[31] Gorlov, A.M., 2001. Tidal energy. In: James Trefil (Ed.), *Encyclopedia of Science and Technology:* 2955-2960. Rutledge, UK.

[32] Fraenkel, P.L., 1999. Tidal currents: A major new source of energy for the Millennium. *Sustainable Developments International:* 107-112.

[33] Couch, S.J. and I.G. Bryden, 2006. Tidal current energy extraction: hydrodynamic resource characteristics. *Proceedings of the Institution of Mechanical Engineers, Part M: Journal of Engineering for the Maritime Environment,* Vol. 220(4): 185-194.

[34] Bryden, I.G., S. Naik, P. Fraenkel and C.R. Bullen, 1998. Matching tidal current plants to local flow conditions. *Energy,* Vol. 23(9): 699-709.

[35] Bryden, I.G. and G.T. Melville, 2004. Choosing and evaluating sites for tidal current development. *Proceedings of the Institution of Mechanical Engineers, Part A: Journal of Power and Energy,* Vol. 218(8): 567-577.

[36] Garrett, C. and P. Cummins, 2004. Generating power from tidal currents. *Journal of Waterway, Port, Coastal, and Ocean Engineering,* Vol. 130(3): 114-118.

[37] Barthelmie, R.J., I. Bryden, J.P. Coelingh and S.C. Pryor, 2000. Energy from the Oceans: Wind, Wave and Tidal. In: C. Sheppard (Ed.), *Seas at the Millennium: An Environmental Evaluation:* 303-322. Elsevier Science Ltd.

[38] Bryden, I.G., S.J. Couch and G. Harrison, 2006. Overview of the issues associated with energy extraction from tidal currents. World Renewable Energy Congress IX and Exhibition, 19-25 August 2006, Florence. Invited paper.

[39] Guena, F., J. Daviau, H. Majastre, V. Bischoff, J. Ruer and C. Tartivel, 2006. Design and operational features of a tidal stream turbine. European Seminar on Offshore Wind and Other Marine Renewable Energies in Mediterranean and European Seas, OWEMES, Civitavecchia, Italy, 22nd April 2006, 8p.

[40] Mason, K., 2010. Composite tidal turbine to harness ocean energy. Article from CompositeWorld.com, posted on 5th February 2010.

[41] Engineering Business Ltd. 2008. www.engb.com.

[42] Department of Trade and Industry (DTI), 2002. Research and development of a 150 kW tidal stream generator. Rep. No. 02/1400, 45p.

[43] Bryden, I.G. and S.J. Couch, 2006. Marine energy extraction: tidal resource analysis. *Journal of Renewable Energy,* Vol. 32(1): 133-139.

[44] Department of Trade and Industry (DTI), 2003. Stingray tidal stream energy device - Phase 2. Rep. No. 03/1433, 67p.

[45] Millot, C. and I. Taupier-Letage, 2005. Circulation in the Mediterranean Sea. In: Saliot, A. (Ed.), *Handbook of Environmental Chemistry: The Natural Environment and the Biogeochemical Cycles, Vol. 5 (K):* 29-66. Springer-Verlag, Germany.

[46] Pinet, P.R., 2003. *Invitation to Oceanography*. 3rd ed. Jones & Bartlett Publishers, 202p.

[47] Bianchi, C.N. and C. Morri, 2000. Marine biodiversity of the Mediterranean Sea: Situation, Problems and Prospects for Future Research. *Marine Pollution Bulletin*, Vol. 40(5): 367-376.

[48] Defant, A., 1961b. *Physical Oceanography*. Pergamon Press, Vol. II: 598p.

[49] Zenetos, A., I. Siouko-Frangou and O. Gotsis-Skretas, 2001. Seas around Europe: The Mediterranean Sea. European Environmental Agency (EEA), 22p.

[50] UNEP, 1996. State of the Marine and Coastal Environment in the Mediterranean Sea. Rep. No. 100. United Nation Environmental Programme (UNEP), Athens.

[51] Horvat, M., J. Kotnik, M. Logar, V. Fajon, T. Zvonaric and N. Pirrone, 2003. Speciation of mercury in surface and deep-sea waters in the Mediterranean Sea. *Atmospheric Environment*, Vol. 37(1): 93-108.

[52] Zavatarelli, M. and G.L. Mellor, 1995. A numerical study of the Mediterranean Sea circulation. *Journal of Physical Oceanography*, Vol. 25(6): 1384-1414.

[53] Kourafalou, V.H. and K.A. Barbopoulos, 2003. High resolution simulations on the North Aegean Sea seasonal circulation. *Annales Geophysicae,* Vol. 21(1): 251-265.

[54] Russo, A. and A. Artegiani, 1996. Adriatic Sea hydrography. *Scientia Marina,* Vol. 60(2): 33-43.

[55] Bellan-Santini, D., J.C. Lacaza and C. Poizat, 1994. Les biocénoses marines et littorales de Méditerranée, synthèse, menaces et perspectives. *Collection patrimoines naturels,* Vol. 19: 246p.

[56] European Union Environmental Report, 1993. Fifth European Community Environmental Programme: towards sustainability. Rep. No. C138/5, 93p.

[57] European Environmental Affairs (EEA), 1999. State and pressures of the marine and coastal Mediterranean environment, 37p.

[58] Saliot, A., 2005. The Mediterranean Sea. In: *Handbook of Environmental Chemistry: The Natural Environment and the Biologeochemical Cycles, Vol. 5 (K).* Springer-Verlag, Germany, 414p.

[59] Fredj, G., D. Bellan-Santini and M. Menardi, 1992. Etat des connaissances sur la faune marine Mediterranée. *Bulletin de l'Institut océanographique,* Vol. 9: 133-145.

[60] Frid, C., C. Hammer, R. Law, H. Loeng, J.F. Pawlak, Ph.C. Reid and M. Tasker, 2003. Environmental Status of the European Seas. International Council for the Exploration of the Sea (ICES), 75p.

[61] Pascoe, S., J.E. Kirkley, D. Gréboval and C.J. Morrison-Paul, 2003. *Measuring and assessing capacity in fisheries*. Food and Agriculture Organisation (FAO), Rome, Rep. No. 433/2, 130p.

[62] International Fund for Animal Welfare. 2008. www.ifaw.org

[63] Notarbartolo di Sciara, G., M.C. Venturino, M. Zanardelli, G. Bearzi, F.J. Borsani and B. Cavalloni, 1993. Cetaceans in the central Mediterranean Sea: distribution and sighting frequencies. *Bolletino di Zoologia,* Vol. 1(131): 138.

[64] Notarbartolo di Sciara, G. and G. Bearzi, 2002. Cetacean direct killing and live capture in the Mediterranean Sea. In: G. Notarbartolo di Sciara (Ed.), *Cetaceans of the Mediterranean and Black Seas: State of knowledge and conservation strategies*, section 5, 4p.

[65] Reeves, R.R. and G. Notarbartolo di Sciara, 2006. The Status and Distribution of Cetaceans in the Black Sea and Mediterranean Sea. IUCN Centre for Mediterranean Cooperation, Malaga, Spain, 137p.

[66] Podesta, M., A. D'Amico, G. Pavan, A. Drougas, A. Komnenou and N. Portunato, 2006. A review of Curvier's beaked whale strandings in the Mediterranean Sea. *Journal of Cetcean Research and Management*, Vol. 7(3): 251-261.

[67] Margaritoulis, D., 2001. The status of marine turtles in the Mediterranean. Proceedings of the First Mediterranean Conference on Marine Turtles, Rome: 51-61.

[68] UNEP-RAC, 1995. Future for the Mediterranean basin. The Blue Plan.

[69] Caddy, J.F., 1997. Review of the State of World Fishery Resources: Marine Fisheries. Regional reviews: 5.Mediterranean and Black Seas. Rep. No. 920 FIRM/C920. FAO, ISSN 0429-9329, Rome.

[70] UNEP, 1994. Technical report on the state of cetaceans in the Mediterranean. Rep. No. 82. United Nation Environmental Programme (UNEP), Tunis.

[71] Demetropoulos, A. and M. Hadjichristophorou, 1995. Manual on Marine Turtle Conservation in the Mediterranean. UNEP-SPA/IUCN / CWS/Fisheries Department, Cyprus, 64p.

[72] UNEP-RAC/SPA, 1997b. Protected areas in the Mediterranean, from Geneva 1982 to Barcelona 1995, Tunisia.

[73] UNEP-RAC/SPA, 1998a. Cetacean populations in the Mediterranean Sea: Evaluation of the knowledge on the status of the species, UNEP (OCA) MED WG 146.3, Arta, Greece.

[74] UNEP-RAC/SPA, 1998b. Interaction of fishing activities with cetacean populations in the Mediterranean Sea, UNEP (OCA) MED WG 146.4, Arta, Greece.

[75] UNEP-RAC/SPA, 1999d. Draft action plan for the conservation of marine vegetation in the Mediterranean Sea, CIESM, Monaco.

[76] Sharaf El-Din, S.H. and A. El-Gindy, 1987. Characteristics, spreading and mixing of the intermediate water masses and their seasonal variations in the Eastern Mediterranean. *Acta Adriatica,* Vol. 28(1): 45-58.

[77] Said, M.A., 1990. Horizontal circulation of the Eastern Mediterranean waters during winter and summer seasons. *Acta Adriatica,* Vol. 31(1-2): 5-21.

[78] Millot, C., 2005. Circulation in the Mediterranean Sea: evidences, debates and unanswered questions. *Scientia Marina,* Vol. 69(1): 5-21.

[79] Fusco, G., G.M.R. Manzella, A. Cruzado, M. Gacic, G.P. Gasparini, V. Kovacevic, C. Millot, C. Tziavos, Z.R. Velasquez, A. Walne, V. Zervakis and G. Zodiatis, 2003. Variability of mesoscale features in the Mediterranean Sea from XBT data analysis. *Annales Geophysicae,* Vol. 21: 21-32.

[80] Marullo, S., R. Santoleri, M. Guarracino, B.B. Nardelli and V. Artale, 2007. Sea surface temperature trends in the Mediterranean Sea: from interannual to decadal variations. *Geophysical Research Abstract,* Vol. 9: 03578.

[81] Poulain, P. and R. Barbanti, 2007. Thermohaline properties of the Mediterranean Sea as measured by profiling floats between 2000 and 2006. *Rapp.Comm.Int.Mer Medit.,* p38.

[82] Said, M.A., 1985. The sources of formation of the intermediate water masses in the Mediterranean Sea. *Acta Adriatica,* Vol. 26(2): 191-201.

[83] Astraldi, M., G.P. Gasparini, A. Vetrano and S. Vignudelli, 2002. Hydrographic characteristics and interannual variability of water masses in the central Mediterranean: a sensitivity test for long-term changes in the Mediterranean Sea. *Deep-Sea Research,* Vol. 49: 661-680.

[84] Wu, P. and K. Haines, 1996. Modelling the dispersal of Levantine Intermediate Water and its role in Mediterranean deep water formation. *Journal of Geophysical Research,* Vol. 101(C3): 6591-6607.

[85] Reid, J.L., 1979. On the contribution of the Mediterranean Sea outflow to the Norwagean-Greenland Sea. *Deep-Sea Research,* Vol. 26: 1199-1223.

[86] Fernandez, V., D.E. Dietrich, R.L. Haney and J. Tintore, 2005. Mesoscale, seasonal and interannual variability in the Mediterranean Sea using a numerical ocean model. *Progress in Oceanography,* Vol. 66: 321-340.

[87] Alvarez, A., J. Tintore, G. Holloway, M. Eby and J. Beckers, 1994. Effect of topographic stress on circulation in the Western Mediterranean. *Journal of Geophysical Research,* Vol. 99(C8): 16053-16064.

[88] Roussenov, V., E. Stanev, V. Artale and N. Pinardi, 1995. A seasonal model of the Mediterranean Sea general circulation. *Journal of Geophysical Research,* Vol. 100(C7): 13515-13528.

[89] Nielsen, J.N., 1912. Hydrography of the Mediterranean and adjacent waters. In: *Report of the Danish Oceanographic Expedition 1908-1910 to the Mediterranean and Adjacent Waters:* 77-192. A.F. Host and Son.

[90] Wust, G., 1961. On the vertical circulation of the Mediterranean Sea. *Journal of Geophysical Research,* Vol. 66(10): 3261-3271.

[91] Ovchinnikov, I.M., 1966. Circulation in the surface and intermediate layers of the Mediterranean. *Oceanology,* Vol. 6: 48-59.

[92] Lacombe, H., 1975. Apercus sur l'apport a l'oceanographie physique des recherches recent en Mediterranée. *Bulletin de l'étude en commun de la Méditerranée,* Vol. 7: 5-23.

[93] Millot, C., 1985. Some features of the Algerian current. *Journal of Geophysical Research,* Vol. 90(C4): 7169-7176.

[94] Millot, C., 1987. Circulation in the Western Mediterranean. *Oceanologica Acta,* Vol. 10(2): 143-149.

[95] Millot, C., 1991. Mesoscale and seasonal variabilities of the circulation in the Western Mediterranean. *Dynamics of Atmospheres and Oceans,* Vol. 15(3-5): 179-214.

[96] Millot, C., 1999. Circulation in the Western Mediterranean Sea. *Journal of Marine Systems,* Vol. 20(1-4): 423-442.

[97] El-Gindy, A.A.H. and S.H. Sharaf El-Din, 1986. Water masses and circulation patterns in the deep layer of the Eastern Mediterranean. *Oceanologica Acta,* Vol. 9(3): 239-248.

[98] Taupier-Letage, I. and C. Millot, 1988. Surface circulation in the Algerian Basin during 1984. *Oceanologica Acta,* Vol. 9: 119-131.

[99] El-Gindy, A.A.H. and F.M. Eid, 1990. Long-term variations of monthly mean sea level and its relation to atmospheric pressure in the Mediterranean Sea. *International Hydrographic Review,* Vol. 67(1): 147-159.

[100] Malanotte-Rizzoli, P. and A. Bergamasco, 1991. The wind and thermally driven circulation of the Estern Mediterranean Sea. Part II: the baroclinic case. *Dynamics of Atmospheres and Oceans,* Vol. 15(3-5): 355-419.

[101] Alberola, C., C. Millot and J. Font, 1995. On the seasonal and mesoscale variabilities of the northern current during the PRIMO-0 experiment in the Western Mediterranean Sea. *Oceanologica Acta,* Vol. 18(2): 163-192.

[102] Malanotte-Rizzoli, P., B.B. Manca, M.R. d'Alcala, A. Theocharis, A. Bergamasco, D. Bregant, G. Budillon, G. Civitarse, A. Michelato, E. Sansone, P. Scarazzato and E. Souvermezoglou, 1997. A synthesis of the Ionian Sea hydrography, circulation and water mass pathways during POEM-Phase 1. *Progress in Oceanography,* Vol. 39(3): 153-204.

[103] Fuda, J.L., C. Millot, I. Taupier-Letage, U. Send and J.M. Bocognano, 2000. XBT monitoring of a meridian section across the Western Mediterranean. *Deep-Sea Research,* Vol. 47(11): 2191-2218.

[104] Manca, B.B., L. Ursella and P. Scarazzato, 2002. New development of Eastern Mediterranean circulation based on hydrological observations and current measurements. *Marine Ecology,* Vol. 23(1): 237-257.

[105] Puillat, I., I. Taupier-Letage and C. Millot, 2002. Algerian eddies lifetime can near 3 years. *Journal of Marine Systems,* Vol. 31(4): 245-259.

[106] Ruiz, S., J. Font, M. Emelianov, J. Isern-Fontanet, C. Millot, J. Salas and I. Taupier-Letage, 2002. Deep structure of an open sea eddy in the Algerian Basin. *Journal of Marine Systems,* Vol. 33-34: 179-195.

[107] Sorgente, R., A.F. Drago and A. Ribotti, 2003. Seasonal variability in the central Mediterranean Sea circulation. *Annales Geophysicae,* Vol. 21: 299-322.

[108] Zervakis, V., G. Papadoniou, C. Tziavos and A. Lascaratos, 2003. Seasonal variability and geostrophic circulation in the Estern Mediterranean as revealed through a repeated XBT transect. *Annales Geophysicae,* Vol. 21: 33-47.

[109] Testor, P., U. Send, J.C. Gascard, C. Millot, I. Taupier-Letage and K. Beranger, 2005. The mean circulation of the south-western Mediterranean Sea: Algerian Gyres. *Journal of Geophysical Research,* Vol. 110(C11): C11017.

[110] Hamad, N., C. Millot and I. Taupier-Letage, 2006. The surface circulation in the eastern basin of the Mediterranean Sea. *Scientia Marina,* Vol. 70(3): 457-503.

[111] Bethoux, J.P., 1980. Mean water fluxes across sections in the Mediterranean Sea, evaluated on the basis of water and salt budgets and observed salinities. *Oceanologica Acta,* Vol. 3: 79-88.

[112] Drakopoulos, P.G. and A. Lascaratos, 1999. Modelling the Mediterranean Sea: climatological forcing. *Journal of Marine Systems,* Vol. 20(1-4): 157-173.

[113] Astraldi, M., G.P. Gasparini, L. Gervasio and E. Salusti, 2001. Dense water dynamics along the Strait of Sicily (Mediterranean Sea). *Journal of Physical Oceanography,* Vol. 31(12): 3457-3475.

[114] Manzella, G.M.R., G.P. Gasparini and M. Adtraldi, 1988. Water exchange between the Eastern and Western Mediterranean through the Strait of Sicily. *Deep-Sea Research,* Vol. 35(6): 1021-1035.

[115] Gerin, R. and P.M. Poulain, 2005. Hydrographic structure and circulation outline of the south-eastern Mediterranean off the Egyptian coast. Rep. No. Rel.42/2005/OGA/23, 11p.

[116] Demirov, E. and N. Pinardi, 2002. Simulation of the Mediterranean Sea circulation from 1973 to 1993. Part I: The interannual variability. *Journal of Marine Systems,* Vol. 33/34: 23-50.

[117] Klein, B., W. Roether, B. Manca, D. Bregant, V. Beitzel, V. Kovacevic and A. Luccetta, 1999. The large deep water transient in the Eastern Mediterranean. *Deep-Sea Research,* Vol. 46(3): 371-414.

[118] Roether, W. and R. Schlitzer, 1991. Eastern Mediterranean deep water renewal on the basis of chlorofluoromethane and tritium. *Dynamics of Atmospheres and Oceans,* Vol. 15(3-5): 333-354.

[119] Lozier, M.S., W.B. Owens, and R.G. Curry, 1995. The climatology of the North Atlantic. *Progress in Oceanography,* Vol. 36(1): 1-44.

[120] Johnson, R.G., 1997. Climate control requires a dam at the Strait of Gibraltar. *Eos, Transactions American Geophysical Union,* Vol. 78(27): 277.

[121] Candela, J., C. Winant and A. Ruiz, 1990. Tides in the Strait of Gibraltar. *Journal of Geophysical Research,* Vol. 95(C5): 7313-7335.

[122] Dressler, R., 1980. Hydrodynamish-numerische Untersuchungen der M_2 Gezeit und einiger Tsunamis im europaishen Mittelmer. Rep. No. 23. University of Hamburgh, Germany.

[123] Vincent, P. and P. Cancelli, 1993. Oceanic tides in the Mediterranean Sea. *International Geoid Service Bulletin,* Vol. 2: 84-90.

[124] Tsimplis, M.N., R. Proctor and R.A. Flather, 1995. A two-dimensional tidal model for the Mediterranean Sea. *Journal of Geophysical Research,* Vol. 100(C8): 16223-16239.

[125] Sammari, C., V.K. Koutitonski and M. Moussa, 2006. Sea level variability and tidal resonance in the Gulf of Gabes, Tunisia. *Continental Shelf Research,* Vol. 26(3): 338-350.

[126] Kagan, B.A., 1985. On the relationship between astronomical and geophysical estimates of the tidal energy dissipation. *Okeanologia,* Vol. 25: 373-377.

[127] Birpinar, M.E., G.F. Talu, G. Su and M. Gulbey, 2006. The effect of dense maritime traffic on the Bosphorus Strait and Marmara Sea Pollution. Conference on Water Observation and Information System for Decision Support, 11p.

[128] Oral, N. and B. Ozturk, 2006. The Turkish straits, maritime safety, legal and environmental aspects. Rep. No. 25. Turkish Marine Research Foundation, Istanbul, Turkey, 163p.

[129] Gülter, I., Y. Yuksel, A.C. Yalciner, E. Cevik and C. Ingerslev, 2006. Measurement and evaluation of the hydrodynamics and secondary currents in and near a strait connecting large water bodies - A filed study. *Journal of Ocean Engineering,* Vol. 33(13): 1718-1748.

[130] Ozsoy, E., M.A. Latif and S. Besiktepe, 2002. The current system of the Bosphorus Strait based on recent measurements. In: The 2nd meeting on the Physical Oceanography of Sea Straits: 177-180.

[131] Oguz, T., 2005. Hydraulic adjustments of the Bosphorus exchange flow. *Geophysical Research Letters,* Vol. 32(6): -L06604.

[132] Latif, M.A., E. Ozsoy, T. Oguz, and U. Unluata, 1991. Observations of the Mediterranean inflow into the Black Sea. *Deep-Sea Research,* Vol. 38(2): 711-723.

[133] Gregg, M.C. and E. Ozsoy, 2002. Flow, water mass changes and hydraulics in the Bosphorus. *Journal of Geophysical Research,* Vol. 107(C3): 1-23.

[134] Yuce, H. and B. Alpar, 1994. Investigation of low frequency sea-level changes at the Strait of Istanbul (Bosphorus). *Turkish Journal of Engineering and Environmental Sciences,* Vol. 18: 233-238.

[135] Alpar, B. and H. Yuce, 1998. Sea-level variations and their interactions between the Black Sea and the Aegean Sea. *Estuarine, Coastal and Shelf Science,* Vol. 46(5): 609-619.

[136] Ulutas, B.H., 2005. Determination of the appropriate energy policy for Turkey. *Energy,* Vol. 30(7): 1146-1161.

[137] Stashchuk, N. and K. Hutter, 2001. Modelling of water exchange through the Strait of the Dardanelles. *Continental Shelf Research,* Vol. 21(1361): 1382.

[138] Yuce, H., 1994. Analysis of the water level variations in the Strait of Canakkale. *Turkish Journal of Engineering and Environmental Sciences,* Vol. 18: 397-401.

[139] Vercelli, F., 1925. Il regime delli correnti e dell maree nello Stretto di Messina. Commissione Internazionale del Mediterranea, Venezia, 1925.

[140] Castaldini, M. and L. Franzini, 1979. On the currents in the Strait of Messina: linear and non-linear tidal components on the sill. *Il Nuovo Cimento,* Vol. 5(2): 569-584.

[141] Mosetti, F., 1988. Some news on the currents in the Strait of Messina. *Bolletino di Oceanologia Teorica ed Applicata,* Vol. VI(3): 119-201.

[142] Gasparini, G.P., D.A. Smeed, S. Alderson, S. Sparnocchina, A. Vetrano and S. Mazola, 2004. Tidal and sub-tidal currents in the Strait of Sicily. *Journal of Geophysical Research*, Vol. 109(C2): C02011.

[143] Herbaut, C., F. Cordon and M. Crepon, 1998. Separation of coastal current at a strait level: case of the Strait of Sicily. *Journal of Physical Oceanography*, Vol. 28(1346): 1362.

[144] Lermusiaux, P.F.J. and A.R. Robinson, 2001. Features of dominant mesoscale variability, circulation patterns and dynamics in the Strait of Sicily. *Deep-Sea Research*, Vol. 48(9): 1953-1997.

[145] Mosetti, F. and N. Purga, 1989. The semidiurnal tides in the Sicily Strait. *Il Nuovo Cimento*, Vol. 12(3): 349-356.

[146] Abdennadher, J. and M. Boukthir, 2007. Barotropic and baroclinic tidal energy budget in the Strait of Sicily. *Geophysical Research Abstract*, Vol. 9: 00529.

[147] Stansfield, K., D.A. Smeed and G.P. Gasparini. 2002. The path of the overflows from the sills in the Sicily Strait. In: *The 2nd meeting on the Physical Oceanography of Sea Straits*: 211-214.

[148] Anonymous. 2000. 2nd Workshop on Analysis of Variables and Numerical Simulation of the Water Masses Exchange through the Strait of Gibraltar. University of Cadiz, Spain. http://www2.uca.es/huesped/anasim_gibraltar/english.html

[149] Brandt, P. and W. Alpers, 1994. Validation of a numerical model describing the generation and propagation of internal waves in the Strait of Gibraltar by using ERS-1 SAR data. Proceedings of 2nd ERS-1 Symposium: 225-231

[150] Lacombe, H. and C. Richez, 1982. The regime of the Strait of Gibraltar. In: J. Nihoul (Ed.), *Hydrodynamics of Semi-enclosed Seas:* 13-73. Elsevier.

[151] Send, U. and B. Bascheck, 2001. Intensive shipboard observations of the flow through the Strait of Gibraltar. *Journal of Geophysical Research*, Vol. 106(C12): 31017-31032.

[152] FAO-COPMED Project, G. 1998. Study on the biology and fisheries of Tuna and Tuna-Like species exploited in the Mediterranean Spanish and Moroccan coasts and around the The Strait of Gibraltar . Aim 1: Hydrographic description, 14p.

[153] Bryden, H.L., J. Candela and T.H. Kinder, 1994. Exchange through the Strait of Gibraltar. *Progress in Oceanography*, Vol. 33(3): 201-248.

[154] Alpers, W. and P.E. La Violette, 1993. Tide generated nonlinear internal wave packets in the Strait of Gibraltar observed by the Synthetic Aperture Radar (SAR) aboard the ERS-1 satellite. Proceedings of 1st ERS-1 Symposium-Space at the service of our environment, Paris, 39: 753-758.

[155] Atlas of Oceanic Internal Solitary Waves (AOISW), 2002. *The Strait of Gibraltar*. The Office of Naval Research – Code 322PO: 179-198.

[156] Pillsbury, R., D. Barstow, J. Botero, C. Millero, B. More, G. Pittock, D. Root, J. Simpkins, R. Still and H. Bryden, 1987. Gibraltar experiment: current measurements in the Strait of Gibraltar, October 1985-October 1986. Rep. No. 87-29. College of Oceanography, Oregon State University, 284p.

[166] Azzaro, F., F. Decembrini, F. Raffa and E. Crisafi, 2007. Seasonal variability of phytoplankton fluorescence in relation to the Straits of Messina (Sicily) tidal upwelling. *Ocean Science Discussions,* Vol. 4: 415-440.

[157] Abbate, M., G.A. Dalu and E. Salusti, 1982. Energy-containing eddies in the Strait of Messina. *Il Nuovo Cimento,* Vol. 5(5): 571-585.

[158] Brandt, P., A. Rubino, W. Alpers and J.O. Backhaus, 1997. Internal waves in the Strait of Messina studied by a numerical model and synthetic aperture radar image from the ERS 1/2 Satellites. *Journal of Physical Oceanography,* Vol. 27(5): 648-663.

[159] Brandt, P., A. Rubino, D. Qudfasel, W. Alpers, J. Sellschop and H. Fiekas, 1999. Evidence for the influence of Atlantic-Ionian stream fluctuations on the tidally induced internal dynamics in the Strait of Messina. *Journal of Physical Oceanography,* Vol. 29(5): 1071-1080.

[160] Santoro, V.C., E. Amore, L. Cavallaro, G. Cozzo and E. Foti, 2002. Sand waves in the Messina Strait, Italy. *Journal of Coastal Research,* Vol. 36: 640-653.

[161] Azzaro, F., F. Decembrini, F. Raffa and E. Crisafi, 2007. Seasonal variability of phytoplankton fluorescence in relation to the Straits of Messina (Sicily) tidal upwelling. *Ocean Science Discussions,* Vol. 4: 415-440.

[162] Nesteroff, W.D. and M. Rawson, 1987. Dynamics of modern sediments in the Strait of Messina (Sicily) and south-west of Calabria. Le Detroit de Messina (Italie): Evolution tectono-sedimentaire recente et environment actuel. *Doc.et Trav IGAL, Paris,* 11: 211-223.

[163] Colella, A. and A. d'Alessandro, 1988. Sand waves, Echinocardium traces and their bathyal depositional setting (Monte Torre Palaeostrait, Plio-Pleistocene, southern Italy). *Journal of Sedimentology,* Vol. 35(2): 219-237.

[164] Santoro, V.C., E. Amore, L. Cavallaro and M. De Lauro, 2004. Evolution of sand waves in the Messina Strait, Italy. *Ocean Dynamics,* Vol. 54(3-4): 392-398.

[165] Admirality Charts and Publications, 2005. Stretto di Messina. 3rd edition (Map No. 917).

[166] Bruni, V., 2006. Researches on marine biology in the Straits of Messina: past and present. 2nd Conference of Mediterranean Maritime History Network (MMHN), Messina, Italy, 4p.

[167] Cescon, B., M. Drago, F. Gianfelici and L. Iovenitti, 1998. Environmental Impact Study of projects affecting the quality of marine ecosystems. *Croatica Chemica Acta,* Vol. 71(2): 361-389.

[168] Zagami, G., F. Badalamenti, L. Guglielmo and A. Manganaro, 1996. Short term variations of zooplankton community near the Straits of Messina (northeastern Sicily): relationships with the hydrodynamic regime. *Journal of Estuarine, Coastal and Shelf Science,* Vol. 42(5): 667-681.

[169] Minutoli, R., M.C. Fossi, and L. Guglielmo, 2002. Potential use of biomarkers in zooplankton as early warning signals of ectoxicological risk in the marine food chain. *Journal of Marine Ecology,* Vol. 23(1): 291-269.

[170] Guglielmo, L., G. Costanzo and A. Berdar, 1973. Ulteriore contributo alia conoscenza dei crostacei spiaggiati lungo il litorale messinese dello Stretto. *Atti Soc.Peloritana di Scienze Fisiche Matem.e Naturali Anno,* Vol. 19(129): 156.

[171] Scotto di Carlo, B., G. Costanzo, E. Fresi, L. Guglielmo and A. Ianora, 1982. Feeding ecology and stranding mechanisms in two lanternfishes *Hygophum benoiti* and *Myctophum punctatum* . *Marine Ecology - Progress Series,* Vol. 9: 13-24.

[172] Brancato, G., R. Minutoli, A. Granata, O. Sidoti and L. Guglielmo, 2001. Diversity and vertical migration of euphasiids across the Strait of Messina. In: *Mediterranean Ecosystems: Structures and Processes:* 131-142. Springer-Verlag, Germany.

[173] D'Ancona, U., 1960. The life cycle of the Atlantic eel. *Symp.Zool.Scociety, London,* Vol. 1(61): 77.

[174] Grassi, B., 1896. The reproduction and metamorphosis of the common eel (*Anguilla Vulgaris*). *Proceedings of the IEEE,* Vol. 60: 260-271.

[175] Lintas, C., J. Hirano, and S. Archer, 1998. Genetic variation of the European eel (*Anguilla anguilla*). *Molecular Marine Biology and Biotechnology,* Vol. 7(4): 263-269.

[176] Van Ginneken, V.J.T. and G.E. Maes, 2005. The European eel: its life cycle, evolution and reproduction: a literature review. *Reviews in Fish Biology and Fisheries,* Vol. 15(4): 367-398.

[177] Cavaliere, A., 1962. Studi sulla biologia e pesca di Xiphias gladius L. *Bolletino Pesca Piscioltura e Idrobiologia,* Vol. 17: 123-143.

[178] Castriota, L., M.G. Finoia, S. Campagnuolo, T. romeao, A. Potoschi and f. Andaloro, 2008. Diet of *Tetrapurus belone* (Istiophoridae) in the central Mediterranean Sea. *Journal of Marine Biological Assossiation of the United Kingdom,* Vol. 88(1): 183-187.

[179] Di Natale, A., A. Mangano, A. Asaro, B. Bascone, A. Celona and M. Valastro, 2005. Blue-fin tuna catch composition in the Tyrrhenian Sea and in the Straits of

Sicily in 2002 and 2003. *Collective Volume of Scientific Papers, International Commission for the Conservation of Atlantic Tunas (ICCAT),* Vol. 58(4): 1296-1336.

[180] De Sylva, D., 1975. Synopsis of biological data on the Mediterranean Spearfish, Tetrapturus belone Rafinesque. Proceedings of the International Billfish Symposium, Rep. No. 677 (3): 121-131.

[181] Arocha, F. and M. Ortiz, 2006. Description of Mediterranean Spearfish (MSP). In: *Field Manual:* 1-7. International Commission for the Conservation of Atlantic Tunas (ICCAT).

[182] Baguet, F., J. Piccard, B. Christophe and G. Marechal, 1983. Bioluminescence and luminescent fish in the Strait of Messina from the mesoscaph "Forel". *Journal of Marine Biology,* Vol. 74: 221-229.

[183] Garibaldi, L. and L. Limongelli, 2002. Trends in oceanic captures and clustering of large marine ecosystems. Food and Agriculture Organisation (FAO), *Fisheries Technical Paper*, Rep. No. 435, 71p.

[184] Surfbirds web site. 2008. www.surfbirds.com

[185] Corso, A., 2000. Identification of European Lanner. *Birding World,* Vol. 13(5): 200-213.

[186] EU Joule II Programme CENEX Project, 1995. Tidal and marine current energy exploitation, detailed current analysis. Rep. No. B200, 65p.

[187] Del Ricco, R., 1982. A numerical model of the vertical circulation of tidal strait and its application to Messina Strait. *Il Nuovo Cimento,* Vol. 5(1): 21-45.

[188] Massi, M., E. Salusti and C. Stocchino, 1979. On the currents in the Strait of Messina. *Il Nuovo Cimento,* Vol. 2: 543-548.

[189] Fiorentino, A., 2003. Tidal stream pilot plant at the Straits of Messina. In: *Wave Net Report*: 227-244.

[190] Tomasin, A. and M. Tomasino, 1980. Correnti e livelli marini nello Stretto di Messina: nuovi contributi di misure ed elaborazioni. Proceedings of the 4th Congress (A.I.O.L.), Chiavari: 1-9.

[191] Brandolini, M., L. Franzini and E. Salusti, 1980. On the tides in the Strait of Messina. *Il Nuovo Cimento,* Vol. 6(3): 671-695.

[192] Hopkins, T.S., E. Salusti and D. Settimi, 1984. Tidal forcing of the water mass interface in the Strait of Messina. *Journal of Geophysical Research,* Vol. 89(C2): 2013-2024.

[193] Sterneck, R., 1915. Hydrodynamische Theorie del halbtaegigen Geziten des Mittelmeers. *Wien.: Sitz.Berich.D.K.K.Akad.*

[194] Stocchino, C. and A. Testoni, 1976. Influenza delle correnti di marea sulla circolazione nelle adiacenze tirreniche dello Stretto di Messina. *Istituto Idrografico Della Marina*, Vol. F.C.(3042): 1-18.

[195] Spain, R., 2002. A possible Roman Tide Mill. Paper submitted to the Kent Archaeological Society, 64p. http://www.kentarchaeology.ac/authors/005.pdf

[196] Parker, D.M., 1993. Environmental implications of tidal power generation. *Proceedings of IEEE*, Vol. 140(1): 71-75.

[197] Clean Current Power Systems. 2009. www.cleancurrent.com

[198] Marine Current turbine Ltd. 2009. www.marineturbines.com

[199] Open Hydro. 2009. www.openhydro.com/home.html

[200] Dacre, S.L., 2003. Assessment of the environmental effects specifically related to the use of a ducted turbine. EIA Scoping Study. Final report, 58p.

[201] Calcagno, G., F. Salvatore, L. Greco, A. Moroso and H. Eriksson, 2006. An Experimental Investigation and a Theoretical and Computational Methodology to Study an Innovative Technology for Marine Current Exploitation: the Kobold Turbine. *Bollettino della Comunita' Scientifica in Australasia*, December 2006: 14-24.

[202] Nadur Envieonmental Consultants. http://nadur.biz/eia.html

[203] Abbasi, S.A. and N. Abbasi, 2000. The likely adverse environmental impacts of renewable energy resources. *Applied Energy*, Vol. 65: 121-144.

[204] Mettam, C., 1978. Environmental effects of tidal power generation schemes. *Aquatic Ecology*, Vol. 12(3/4): 307-321.

[205] Shaw, T.L., 1978. Engineering aspects of tidal power barrages, their influence on the environment. *Aquatic Ecology*, Vol. 12(3-4): 299-306.

[206] Department of Trade and Industry (DTI), 2002. A scoping study for an environmental impact field programme in tidal current energy. DTI Publications/URN 02/882, 64p.

[207] National Centre for Technology and Education, Ireland. 2008. www.ncte.ie

[208] Environment Information Brochure, 2002. An introduction to the Directorate-General for the Environment of the European Commission and to sources of information on EU environmental policy. Belgium, 22p.

[209] Official EU Journal, 1975. OJ No L.194. Official Journal of the European Union, 5p. 25-7-1975.

[210] Official EU Journal, 1996. OJ No L.257. Official Journal of the European Union, 26-40. 10-10-1996.

[211] Official EU Journal, 1978. OJ No L.222. Official Journal of the European Union, 1p. 14-8-1978.

[212] Official EU Journal, 1979. OJ No L.281. Official Journal of the European Union, 47-52. 10-11-1979.

[213] Official EU Journal, 2001. Directive 2001/77/EC of the European Parliament and the Council of 27/09/2001. OJL 283/33. Official Journal of the European Union, 8p., 27-10-2001.

[214] Boyes, S., L. Warren and M. Elliot, 2003. Summary of current legislation relevant to Nature Conservation in the Marine Environment in the United Kingdom. Rep. No. ZBB604-F1-2003. Institute of Estuarine and Coastal Studies (IECS), University of Hull, UK, 123p.

[215] European Renewable Energy Council (EREC), 2008. www.erec.org

[216] Proposed EU Directive, 2008. Proposal for a Directive of the European Parliament and the Council on the promotion of energy from renewable resources. COM 2008/30 final report, 60p.

[217] Bryden, I.G., T. Grinsted and G.T. Melville, 2004. Assessing the potential of a simple tidal channel to deliver useful energy. *Applied Ocean Research,* Vol. 26: 198-204.

[218] Supergen-marine Project. 2009. www.supergen-marine.org.uk

[219] Sapia, E. and E. Salusti, 1987. Observation of nonlinear internal solitary wave trains at the northern and southern mouths of the Strait of Messina. *Deep Sea Research*, vol. 34(7): 1081-1092.

[220] Nicolo, L. and E. Salusti, 1991. Field and satellite observations of large amplitude internal tidal wave trains south of the Strait of Messina, Mediterranean Sea. *Annales Geophysicae*, Vol. 9: 534-539.

[221] Dacre, S.L. and C. Bullen, 2001. Pentland Firth tidal current energy feasibility study - Phase 1. Unpublished Report. Robert Gordon University (RGU), Aberdeen and ICIT, Orkney.

[222] Velasco, H.R., J.J. Ayub, M. Belli and U. Sansone, 2006. Interaction matrcies as a first step toward a general model of radionuclide cycling: Application to the $^{137}C_s$ behaviour in grassland ecosystem. *Journal of Radioanalytical and Nuclear Chemistry*, Vol. 268(3): 503-509.

[223] Mavroulido, M., S.J. Hughes and E.E. Hellawell, 2004. A qualitative tool combining an interaction matrix and a GIS to map vulnerability to traffic induced air pollution. *Journal of Environmental Management*, Vol., 70: 283-289.

[224] Mavroulido, M., S.J. Hughes and E.E. Hellawell, 2006. A comparison of two interaction matrix coding techniques used in a GIS-based tool for air quality assessment. Global NEST Journal, Vol. 8(3): 306-314.

[225] Chick, J.P., I.G. Bryden and S.J. Couch, 2007. The influence of energy extraction from open channel flow and its impact on tidal current energy system design. *The International Journal of the Society for Underwater*, Vol. 27(2): 49-56.

[226] Dimla, D.E., I.G. Bryden and K.G. Rados, 2000. Site assessment methodology for offshore tidal current plants: a preliminary investigation. The 10th International Offshore and Polar Engineering Conference, Vol. 1: 478-483.

[227] Boesch, D.F. and N.N. Rabalais, 1987. Long term environmental effects of offshore oil and gas development. Taylor and Francis Group, London, 780p.

[228] Krohn, S., 2002. Offshore wind energy: Full speed ahead. http://www.talentfactory.dk/media(484,1033)/Offshore_Wind_Energy,_Full_speed_ahead.pdf

[229] Salter, S.H., 2003. Research requirments for tidal stream energy. European Community, 20p.

[230] Department of Trade and Industry (DTI), 2005. Development, Installation and Testing of a large scale tidal current turbine. Rep. No. URN 05/1698, 60p.

[231] Department of Trade and Industry (DTI), 2006. Final report on preliminary works associated with 1 MW tidal turbine. Rep. No. URN 06/2046, 35p.

[232] Bearzi, G., G. Notarbartolo di Sciara and S. Bonizzoni, 2005. Scientific literature on Mediterranean Ceatceans: The Italian Contribution. In: B. Cozzi (Ed.), *Marine mammals of the Mediterranean Sea: natural history, biology, anatomy, pathology, parasitology*. Massimo Valdina Editore, Milano: 1-25.

[233] Haidvogel, D.B. and A. Beckmann, 1998. Numerical models of the coastal ocean. In: *The Sea,* Vol.10*:* 457-482.

[234] Semtner, A.J., 1995. Modelling ocean circulation. *Science,* Vol. 269(5229): 1379-1385.

[235] Nihoul, J.C.J., 1999. Seasonal variability of general circulation fields in the Western Mediterranean, Precise of the GHER mathematical visualisation scheme. *Journal of Marine Systems,* Vol. 20(1-4): 415-421.

[236] Falconer, R.A., 1994. An introduction to nearly-horizontal flows. In: *Coastal, Estuarine and Harbour Engineers Reference Book:* 27-36. Chapman & Hall.

[237] Couch, S.J., 2001. *Numerical modelling of tidal flows around headlands and islands*. PhD Thesis, University of Strathclyde, Glasgow, 345p.

[238] Pond, S. and G.L. Pickard, 1983. Introductory Dynamical Oceanography. 2nd ed. Butterworth-Heinemann, 249p.

[239] McWiliams, J.C., 2006. *Fundamentals of Geophysical Fluid Dynamics*. Cambridge University Press, 249p.

[240] Beckers, J.M., 1991. Application of the GHRE 3D general circulation model to the Western Mediterranean. *Journal of Marine Systems,* Vol. 1(4): 315-332.

[241] Delhez, E.J.M., M. Gregorie, J.C.J. Nihoul and J.M. Beckers, 1999. Dissection of the GHRE turbulence closure scheme. *Journal of Marine Systems,* Vol. 21(1-4): 379-397.

[242] Brankart, J.M. and P. Brasseur, 1998. The general circulation in the Mediterranean Sea: a climatological approach. *Journal of Marine Systems,* Vol. 18(1-3): 41-70

[243] Stanev, E.V. and H.J. Friedrich, 1991. On the assimilation of climatological data by means of numerical circulation models, exemplified for the Mediterranean Sea. *Oceanologica Acta,* Vol. 14: 97-114.

[244] Bergamasco, A., P. Malanotte-Rizzoli, W.C. Thacker and R.B. Long, 1993. The seasonal steady circulation of the Eastern Mediterranean determined with the adjoint method. *Deep-Sea Research,* Vol. 40(6): 1269-1298.

[245] Korres, G., N. Pinardi and A. Lascaratos, 2000. The ocean response to low-frequency interannual atmospheric variability in the Mediterranean Sea. Part I: Sensitivity experiments and energy analysis. *Journal of Climate,* Vol. 13(4): 705-731.

[256] Castellari, S., N. Pinardi and K. Leaman, 2000. Simulation of water mass formation processes in the Mediterranean Sea: Influence of the time frequency of the atmospheric forcing. *Journal of Geophysical Research,* Vol. 105(C10): 24157-24181.

[247] Blumberg, A.F. and G.L. Mellor, 1987. A description of a three-dimensional coastal ocean circulation model. In: Norman S. Heaps (Ed.), *Three-Dimensional Coastal Ocean Models (Coastal and Estuarine Sciences):* 1-16. American Geophysical Union, Washington.

[248] Kraus, E.B. and J.S. Turner, 1967. A one-dimensional model of the seasonal thermocline.II: the general theory and its consequences. *Tellus,* Vol. 19: 98-105.

[249] Ahumada, M.A. and A. Cruzado, 2006. Modelling of the circulation in the north-western Mediterranean Sea with the Princeton Ocean Model. *Ocean Science Discussions,* Vol. 3(4): 1255-1292.

[250] Echevin, V., M. Grepon and L. Mortier, 2003. Simulation and analysis of the mesoscale circulation in the north-western Mediterranean Sea. *Annales Geophysicae,* Vol. 21: 281-297.

[251] Lascaratos, A., W. Roether, K. Nittis, and B. Klein, 1999. Recent changes in deep water formation and spreading in the estern Mediterranean Sea: a review. *Progress in Oceanography,* Vol. 44(1-3): 5-36.

[252] Samuel, S., K. Haines, S. Josey and P.G. Myers, 1999. Response of the Mediterranean Sea thermohaline circulation to observed changes in the winter wind stress field in the period 1980-1993. *Journal of Geophysical Research,* Vol. 104(C4): 7771-7784.

[253] Pinardi, N. and E. Masetti, 2000. Variability of the large scale general circulation of the Mediterranean Sea from observations and modelling: A review. *Palaeogeography, Palaeoclimatology, Palaeoecology,* Vol. 158(3): 153-173.

[254] Tonani, M., N. Pinardi, S. Dobricic, I. Pujol and C. Fratianni, 2007. A high resolution free surface model of the Mediterranean Sea. *Ocean Science Discussions,* Vol. 4: 213-244.

[255] Schwiderski, E.W., 1980a. Oceanic tides I: Global ocean tidal equations. *Marine Geodesy,* Vol. 3: 161-217.

[256] Schwiderski, E.W. 1980b. Ocean tides II: A hydrodynamical interpolation model. *Marine Geodesy,* Vol. 3: 219-225.

[257] Schwiderski, E.W., 1980c. On charting global ocean tides. *Reviews of Geophysics and Space Physics,* Vol. 18(1): 243-268.

[258] Vincent, P. and C. Le Provost, 1988. Semidiurnal tides in the northern Atlantic from a finite element numerical model. *Journal of Geophysical Research,* Vol. 93(C1): 543-555.

[259] Le Provost, C., M.L. Genco, and F. Lyard, 1994. Spectroscopy of the world ocean tides from a finite element hydrodynamic model. *Journal of Geophysical Research,* Vol. 99(C12): 24777-24797.

[260] Schrama, E.J.O. and R.D. Ray, 1994. A preliminary tidal analysis of TOPEX/POSEIDON altimetry. *Journal of Geophysical Research,* Vol. 99(C12): 24799-24808.

[261] Cartwright, D.E. and R.D. Ray, 1990. Oceanic tides from geosat altimetry. *Journal of Geophysical Research,* Vol. 95(C3): 3069-3090.

[262] Eanes, R.J., 1994. Diurnal and semidiurnal tides from TOPEX/POSEIDON altimetry. *EOS trans.AGU,* Vol. 75(16): 108.

[263] Matsumoto, K., M. Ooe, T. Sato and J. Segawa, 1995. Ocean tide model obtained from TOPEX/POSEIDON altimetry data. *Journal of Geophysical Research,* Vol. 100(C12): 25319-25330.

[264] Le Provost, C., F. Lyard, J.M. Moulines, M.L. Genco, and F. Rabilloud, 1998. A hydrodynamic ocean tide model improved by assimilating a satellite altimeter derived data. *Journal of Geophysical Research,* Vol. 103(C3): 5513-5529.

[265] Lefevre, F., F. Lyard, and C. Le Provost, 2000. FES98: A new global tide finite element solution independent of altimetry. *Geophysical Reasearch Letters,* Vol. 27(17): 2717-2720.

[266] Matsumoto, K., T. Takanezawa and M. Ooe, 2000. Ocean tide models developed by assimilating TOPEX/POSEIDON altimeter data into hydrodynamical model: A global model and a regional model around Japan. *Journal of Oceanography,* Vol. 56(5): 567-581.

[267] Egbert, G.D. and S.Y. Erofeeva, 2002. Efficient inverse modelling of barotropic ocean tides. *Journal of atmospheric and oceanic technology,* Vol. 19(2): 183-204.

[268] Lefevre, F., F. Lyard, C. Le Provost, and E.J.O. Schrama, 2002. FES99: A Global Tide Finite Element Solution Assimilating Tide Gauge and Altimetric Information. *Journal of atmospheric and oceanic technology,* Vol. 19(9): 1345-1356.

[269] Sanchez, B.V., R.D. Ray and D.E. Cartwright, 1992. A Proudman-function expansion of the M_2-tide in the Mediterranean Sea from satellite altimetry and coastal gauges. *Oceanologica Acta,* Vol. 15(4): 325-337.

[270] Abdallah, M.A., F.M. Eid, I.A. Maiyza and G.F. Soliman, 1993. Numerical investigation of co-oscillating M_2-tide in the Mediterranean with grid size 1x1. *Bulletin of National Institute of Oceanography and Fisheries,* Vol. 19: 37-53.

[271] Soliman, G.F., A.M. Abdallah, F.M. Eid, S.H. Sharaf El-Din and I.A. Maiyza, 1993. Numerical investigation of M_2-tides in the Mediterranean as a closed basin. *Bulletin of National Institute of Oceanography and Fisheries,* Vol. 19: 1-19.

[272] Soliman, G.F., I.A. Maiyza, F.M. Eid and A.M. Abdallah, 1993. Numerical investigation of M_2-tide in the Mediterranean Sea with its real boundaries and of grid size 15' x 15'. *Bulletin of National Institute of Oceanography and Fisheries,* Vol. 19: 55-84.

[273] Soliman, G.F. and I.A. Maiyza, 1994. The influence of depth and friction on the tidal motion in closed rectangular basins. *Bulletin of National Institute of Oceanography and Fisheries,* Vol. 20(1): 1-23.

[274] Dellar, P.J. and R. Salmon, 2005. Shallow water equations with a complete Coriolis force and topography. *Physics of Fluids,* Vol.17: 1-19.

[275] Eagleson, P.S. and R.G. Dean, 1966. Small amplitude wave theory. In: *Estuarine and Coastline Hydrodynamics*. McGraw Hill, New York, 744p.

[276] Weiyan, T., 1992. *Shallow water hydrodynamics*. In: *Elsevier Oceanography series*, No. 55. Elsevier. Amsterdam.

[277] Salmon R., 1998. *Lectures on geophysical fluid dynamics*. Oxford University Press, 372p.

[278] Müller, P., 2006. *The equations of oceanic motions*. Cambridge University press, 302p.

[279] Peyret, R. and T.D. Taylor, 1983. Computational methods for fluid flow. Springer-verlag, New York, 358p.

[280] Androsov, A.A., B.A. Kagan, D.A. Romanenkov and N.E. Voltzinger, 2002. Numerical modelling of barotropic tidal dynamics in the Strait of Messina. *Advances in Water Resources,* Vol. 25(4): 401-415.

[281] Defant, A., 1940. Scilla e Cariddi e le correnti di marea nello Stretto di Messina. *Geofisica Pura e Applicata,* Vol. 2(1): 93-112.

[282] Androsov, A.A., K.A. Kelvanny, E.S. Salusti and N.E. Voltzinger, 1995. Open boundary conditions for horizontal 2D curvilinear-grid long wave dynamics of a strait. *Advances in Water Resources,* Vol. 18(5): 267-276.

[283] Orlanski, I., 1976. A simple boundary condition for unbounded hyperbolic flows. *Journal of Computaional Physics*, Vol. 21: 251-269.

[284] Raymond, W.H. and H.L. Kuo, 1984. A radiation boundary condition for multidimensional flows. *Quarterly Journal of Royal Meteorological Society,* Vol. 110: 535-551.

[285] Oddo, P. and N. Pinardi, 2008. Lateral open boundary conditions for nested limited area models: A scale selective approach. *Ocean modelling*, Vol. 20: 134-156.

[286] Fisher, E. and N. Rhodes, 1994. Uncertainity in Computaional Fluid Dynamics. *Proceedings of the Institution of Mechanical Engineers, Part C: Journal of Mechanical Engineering Science,* Vol. 210: 91-94.

[287] Copeland, G., T. Monteiro, S.J. Couch and A. Borthwick, 2003. A water quality in Spetiba Bay, Brazil. *Marine Environmental Research*, Vol. 55(5): 385-408.

[288] Couch, S.J. and G.J.M. Copeland, 2003. Tidal straining, mixing and Lagrangian flow residuals around headlands. *Journal of Marine Environmental Engineering*, Vol. 7(2): 25-45.

[289] Admiralty Tide Tables, 2002. Admirality Tide Tables for Europe (Excluding UK and Ireland), Mediterranean Sea and Atlantic Ocean. NP 202-02, Vol.2.

[290] Admirality Charts and Publications, 2001. Approaches to Stretto di Messina. 1st edition (Map No. 1018).

[291] Olbers, D.J. and J. Willebrand, 1984. The level of no motion in an ideal fluid. *Journal of Physical Oceanography,* Vol. 14(1): 203-212.

[292] Price, W.A. and M.F.C. Thorn, 1994. Physical models of estuaries. In: *Coastal, Estuarine and Harbour Engineers Reference Book:* 275-288. Chapman & Hall.

[293] Hughes, S.A., 1993. Physical models and laboratory techniques in coastal engineering. World Scientific Publication Co. Ltd., Singapore: 568p.

[294] Yalin, M.S., 1971. Theory of hydraulic models. MacMillan Press Ltd., 266p.

[295] Price, W.A., 1978. Models: Can we learn from the past?. Proceedings of the 16th Coastal Engineering Conference, American Society of Civil Engineering, Vol.1: 25-36.

[296] Dalrymple, R.A., 1989. Physical modelling of littoral processes. In: *Recent advances in Hydraulic physical modelling:* 567-588. Dordrecht, the Netherlands: Kluwer Academic Publishers.

[297] Le Mehaute, B., 1990. Similitude. In: B. Le Mehaute (Ed.), *The Sea, Ocean Engineering Science:* 955-980. New York: John Wiley and Sons.

[298] Sun, X., 2008. Numerical and Experimental Investigation of Tidal Current Energy Extraction. PhD Thesis, University of Edinburgh, Edinburgh, 195p.

[299] Ettema, R., I. Fujita, M. Muste and A. Kruger, 1997. Particle Image Velocimetry for whole field measurment of ice velocities. *Cold Regions Science and Technology,* Vol. 26(2): 97-112.

[300] Prasad, A.J., 2000. Particle image velocimtery. *Current Science,* Vol. 79(1): 51-60.

[301] Adrian, R.J., 2005. Twenty years of particle image velocimetry. *Experiments in Fluids*, Vol. 39(2): 159-169.

[302] Tonddast-Navoei, A., 2005. *Acoustic Particle Image Velocimetry: Development and Applications*. PhD Thesis, Open University, 149p.

[303] Adrian, R.J., 1991. Particle image technique for experimental fluid mechanics. *Annual Review Fluid Mechanics,* Vol. 23: 261-304.

[304] Keane, R.D. and R.J. Adrian, 1992. Theory of cross-correlation analysis of PIV images. *Applied Scientific Research,* Vol. 49: 191-215.

[305] Jensen, K.D., 2004. Flow Measurements. *Journal of the Brazilian Society of Mechanical Sciences and Engineering,* Vol. 26(4): 400-419.

[306] Willert, C.E. and M. Gharib, 1991. Digital Particle Image Velocimetry. *Experiments in Fluids*, Vol. 10(4): 181-193.

[307] Hinsch, K.D., 1993. Particle Image Velocimetry. In: Rajpal S.Sirohi (Ed.), *Speckle Meteorology:* 235-324. Marcel Dekker.

[308] Adrian, R.J., 1996. Bibliography of Particle Velocimetry using imaging methods: 1917-1995. Rep. No. 817. University of Illinois: Department of Theoretical and Applied Mechanics.

[309] Grant, I., 1997. Particle image velocimetry: a review. *Proceedings of the Institution of Mechanical Engineers, Part C: Journal of Mechanical Engineering Science,* Vol. 211(1): 55-76.

[310] Melling, A., 1997. Tracer particles and seeding for particle image velocimetry. *Measurement Science and Technology*, Vol. 8(12): 1406.

[311] Raffel, M., C.E. Willert, S. Wereley and J. Komphehans, 1998. Particle Image Velocimetry: A practical guide. Springer-Verlag, Germany, 253p.

[312] Meinhart, C.D., S.T. Werley and J.G. Santiago, 1999. PIV measurements of a microchannel flow. *Experiments in Fluids*, Vol. 27(5): 414-419.

[313] DVDVideoSoft. 2009. www.dvdvideosoft.com

[314] DigiFlow. 2009. www.damtp.cam.ac.uk/lab/digiflow/

[315] Couch, S.J. and I.G. Bryden, 2007. Large-scale physical response of the tidal system to energy extraction and its significance for informing environmental and ecological impact assessment. IEEE/OES Oceans '07 Marine Challenges: Coastline to Deep Sea, 18-21/06/07, Aberdeen, Scotland, 5p.

[316] Erikson, M.H., A. Moroso and A. Fiorentino, 2006. The vertical axis Kobold turbine in the Strait of Messina - a case study of a full scale marine current prototype. In: World Maritime Technology Conference, London, 14p.

[317] Moroso, A., 2004. ENERMAR marine current exploitation technology. Shenzhen International Workshop on Renewable Energy Technology and Investment: 14-15.10.2004, Shenzhen, P.R.C.

Appendix (1) Example of a parameter file used in the present study

```
Read in bathymetry file   (dname)
C:\programming\Grid\simplechannelgridl.grd
time step (dt). Duration of simulation (time) seconds
          1.0                 190000
tidal period (tidper). (isteady) = 1 for steady flow rampingup over tidper/4
        44640                 0
Do you want to output the residual tide (rt_y_or_n)
n
If so, at what stage(secs) during the simulation should recording start, and end at (simustart, simuend)
          43200  88200
define whether velocity 'v' or elevation 'e' driving boundary at x = 1 'w' or x = ndx+1 'e'
e
w
Do you want to use a pre-defined radiating boundary ? (d = yes, a = no)
d
Input phase difference between input and radiating boundary (seconds)
          0
define driving boundary in currents (Umax) and elev (tamp,z0,theta)
          0.0       0.135   0.00     0
define whether velocity v or elevation driving boundary  at y = 1 (s) or y = ndy+1 (n)
a
r
Do you want to use a pre-defined radiating boundary ? (d = yes, a = no)
a
Input phase difference between input and radiating boundary (seconds)
          0
define driving boundary in currents (Vmax) and elev (tamp,z0, theta)
          0.0       0.135   0.00  0
define land boundary either no-slip (0) or free slip (1)
          0
-Manning nr
          0.025d0
Wind velocity in the x and y direction at z = -10m
          0.0       0.0
latitude in decimal form and hemisphere (n or s)
          0
N
stem of output files (hname)
c:\
nr of iteration steps delay before output and nr steps between output files (io_step)
          42840    1800
switch on/off (1/0) scatter output and gridded output files
          1         0
```

limit below which vorticity in a cell will NOT be output (vortlim)
0.000000001
upper limit of CFL number (<1)
0.40
minimum total depth (m) before cell omitted from computation
0.25
Elevation driving boundary is either (F)ile based or completely(C)alculated
C
If file based, input directory and file name
c:\
Velocity driving boundary is either (F)ile based or completely(C)alculated
C
If file based, input directory and file name
c:\
Radiating boundary is either (F)ile based or completely(C)alculated
C
If file based, input directory and file name
c:\
Record radiating boundary data ?
n
Input directory and file name to store radiating boundary data in
c:\programming\strialrad\trialrad.dat
Do you want to output u and v data 'y' or 'n' - (uvout)
y
Do you want to output elevation data 'y' or 'n' - (nout)
y
Do you want to output vorticity data 'y' or 'n' - (vout)
n

Appendix (2) Tidal Flow Development (TFD) model flowchart [237]

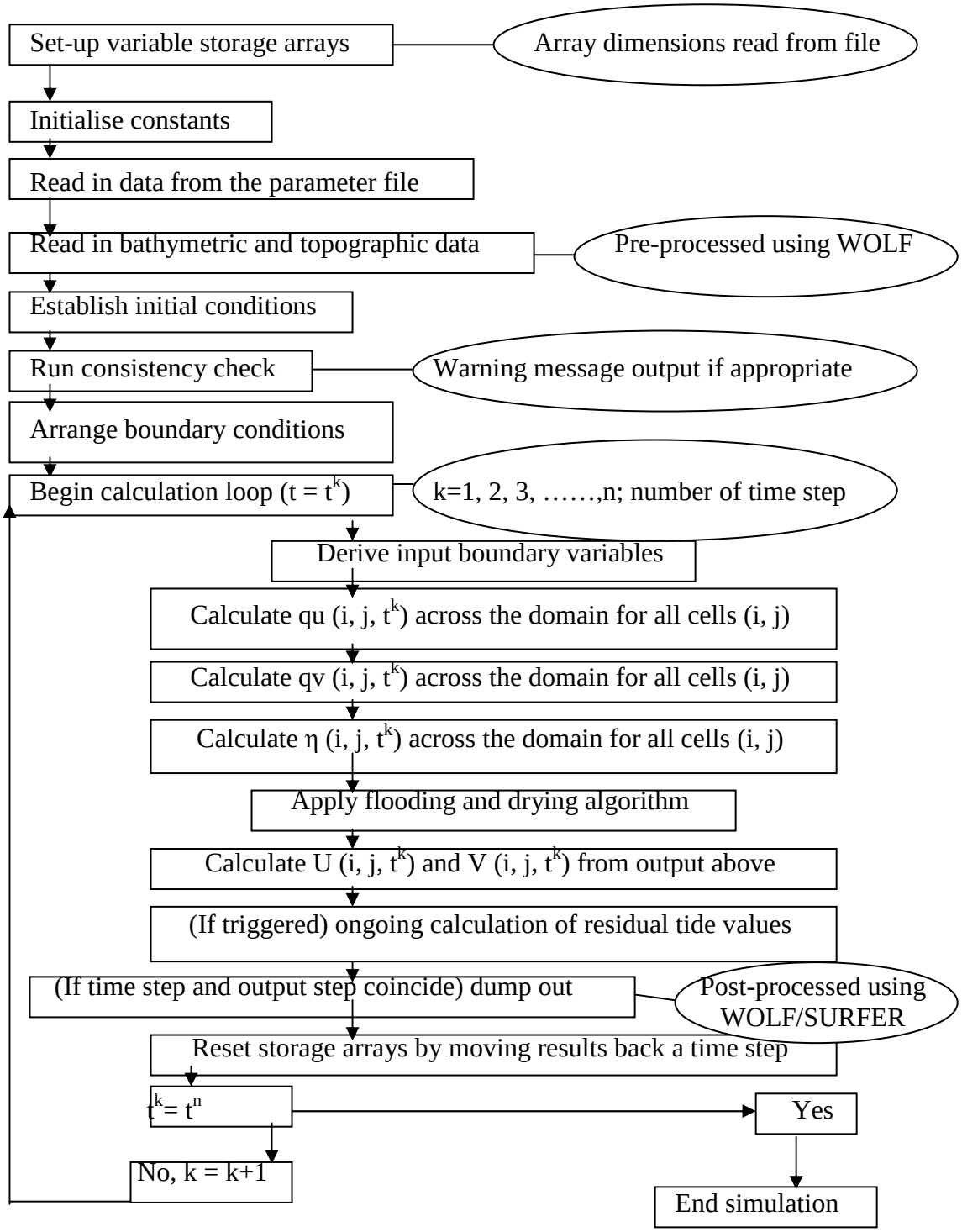

Appendix (3) Example of the parameter file used to compute the tidal constituents at the chosen northen extrimity of the Strait of Messina

```
c       read H(1   to     4), F4,   F6  Messina (Capo Peloro)
        0.05 0.03 0.02 0.01  0.00 0.00
c       read g(1 to 4),       f4, f6
        267  313  231  249   0   0
c       read Zo seas_corr
        0.20 0.0
c       read  nsteps and dt(hrs)
        3000      0.16
c       read A1 F1(1 to 31) from 1 January 2002
        041     1.12    001     0.78    003     1.40    042     1.22
        068     1.15    002     0.78    002     1.40    070     1.23
        095     1.16    003     0.78    001     1.41    097     1.23
        122     1.17    003     0.78    000     1.41    125     1.23
        149     1.16    004     0.78    359     1.40    152     1.21
        176     1.15    005     0.79    358     1.40    180     1.18
        202     1.13    006     0.79    357     1.38    206     1.15
        228     1.10    006     0.79    356     1.37    233     1.11
        254     1.07    007     0.80    356     1.36    259     1.07
        279     1.04    008     0.80    355     1.34    284     1.03
        303     1.01    008     0.81    354     1.32    309     1.00
        327     0.98    009     0.81    354     1.30    334     0.97
        350     0.95    010     0.82    354     1.29    358     0.94
        014     0.93    010     0.82    354     1.27    022     0.92
        037     0.91    011     0.83    354     1.25    047     0.90
        059     0.90    011     0.84    354     1.24    070     0.89
        082     0.88    012     0.84    354     1.23    094     0.87
        104     0.87    013     0.85    354     1.23    117     0.87
        126     0.86    013     0.86    354     1.23    140     0.86
        148     0.85    013     0.87    354     1.23    163     0.87
        170     0.85    014     0.87    354     1.23    186     0.89
        191     0.87    014     0.88    354     1.23    209     0.93
        213     0.89    015     0.89    353     1.24    233     0.97
        236     0.93    015     0.90    353     1.24    257     1.03
        260     0.98    015     0.91    352     1.25    283     1.09
        284     1.02    016     0.92    351     1.25    309     1.14
        309     1.08    016     0.93    350     1.25    336     1.20
        336     1.12    016     0.93    349     1.25    004     1.24
        003     1.16    016     0.94    348     1.25    032     1.27
        030     1.19    017     0.95    347     1.25    060     1.29
        057     1.21    017     0.96    346     1.24    089     1.29
```

Appendix (4) The parameter file used to compute the spring tidal constituents at the chosen northen extrimity of the Strait of Messina

c read H(1 to 4), F4, F6 Messina (Capo Peloro)

0.05 0.03 0.02 0.01 0.00 0.00

c read g(1 to 4), f4, f6

267 313 231 249 0 0

c read Zo seas_corr

0.20 0.0

c read nsteps and dt(hrs)

200000 0.0002778

c read A1 F1(13 to 16) from 13 January 2002

350	0.95	010	0.82	354	1.29	358	0.94
014	0.93	010	0.82	354	1.27	022	0.92
037	0.91	011	0.83	354	1.25	047	0.90
059	0.90	011	0.84	354	1.24	070	0.89

Appendix (5) Published paper during this PhD study

El-Geziry, T.M., I.G. Bryden and S.J. Couch, 2009. Environmental Impact Assessment for tidal energy schemes: an exemplar case study of the Strait of Messina. *Proceedings of IMarEST, Part (A) Journal of Marine Engineering and Technology*, Vol. 2009 (13): 39-48.